NUREG/CR-1562
R4

# Steam Chugging in Pressure Suppression Containment

Final Report
July 1976 — July 1979

Manuscript Completed: August 1979
Date Published: July 1980

Prepared by C. K. B. Lee, C. K. Chan

Chemical, Nuclear, and Thermal Engineering Department
University of California at Los Angeles
Los Angeles, CA 90024

**Prepared for**
**Division of Reactor Safety Research**
**Office of Nuclear Regulatory Research**
**U.S. Nuclear Regulatory Commission**
**Washington, D.C. 20555**
**NRC FIN No. B5875**

8008180637

SUMMARY

The hydrodynamic loads, induced by the steam chugging phenomenon, in a Boiling Water Reactor suppression pool, are studied by a small scale single vent experiment. The experimental effort established an overall physical picture of the phenomenon which enabled the development of a theoretical model intended for the prediction of these loads in the full size containment.

A systematic classification of characteristic interfacial motion patterns is made, based on the steam mass flux and the pool temperature resulting in a condensation regime map. Although the boundaries between various regimes are system dependent, the corresponding characteristic patterns would remain the same. In general, the classification can be divided into three types: the jet at high mass fluxes (>150 $kg/m^2$-sec), the bubble oscillation at intermediate mass fluxes, and the steam chugging at low mass fluxes (<75 $kg/m^2$-sec).

Steam chugging occurs below a steam mass flux of about 75 $kg/m^2$-sec, and below a pool temperature of about 80.°C. Within this condensation regime, three different types of chugs are observed: the internal chug where all condensation occurs within the pipe; the detached bubble chug where the bubble is "cut off" from the vent during bubble formation; and the encapsulating bubble chug where the bubble encapsulates the vent during bubble formation. The first two types of chugs are characterized by high chug heights, high interface velocity but low steam pressures at the interface upon vent clearing. The last type, on the other hand, is characterized by low chug heights, low interface velocity, but high steam pressures at the interface upon vent clearing.

The magnitudes of the pressure overshoot at the pool bottom associated with internal chugs, detached bubble chugs, and encapsulating bubble chugs are: mild (~.1 atm.), moderate (~.3 atm.), and large (~.5 atm.) respectively. For internal chugs, the loads are generated by the collapse and rebound of a bubble within the vent. For the other two types, the loads are generated by the collapse of the bubbles in the pool. Pool bottom pressures data indicate that the pressure oscillations associated with detached bubbles are characterized by two different periods. The first period includes the pressure undershoot and the spike; the second period is the "ring out." For encapsulating bubbles, the pressure oscillations are characterized by three different periods. The first period includes only the pressure undershoot. The second period includes the duration of the pressure spike which consists of a few fine peaks. The third period is the "ring out." Generally, the violent bubble collapse is initiated by the penetration of a liquid jet into the bubble. For detached bubbles the liquid jet penetrates from the side, while for encapsulating bubbles, the liquid jet penetrates from the bottom.

Synchronized movie data and pool bottom pressure measurements show that the rapid pressure undershoot occurs during jet penetration while the sharp pressure overshoot occurs near the completion of a violent collapse. The rapid condensation introduced by the liquid jet causes the rapid decrease in the bubble pressure which initiates the violent collapse. The liquid inertia developed during the violent collapse over-compresses the steam causing the sharp pressure overshoot.

The chug of water up the vent is caused by a pressure undershoot in the vent which is resulted from the rapid condensation occurring at the pipe exit. For internal chugs and detached bubble chugs, the rapid

condensation is caused by the liquid layers draining off the pipe wall and accumulating locally at the exit. For the encapsulating bubble chugs, the liquid jet penetration and atomization phenomenon is responsible for the rapid condensation at the vent exit.

The vent pipe model is developed to predict the chug height in the vent and the bubble behavior at the pipe exit. A one-dimensional pipe flow model for the vent is coupled to a one-volume model for the condensation region at the pipe exit to predict the slug motion in the vent; and, upon vent clearing, the pipe flow equations are coupled to an infinite pool spherical vapor bubble model, to predict the bubble growth in the pool. The condensation heat transfer coefficient in the pipe is determined by comparing the experimental data with the vent pipe model predictions for various values of h. The best value is

$$h = 14. \times h_{Nu}.$$

Comparisons of the vent pipe model predictions with experimental data show that the model is inadequate in predicting the chugging phenomenon; however, the general trends observed in the experiments are predicted. These trends are listed as follows:

(i) The predicted chug height increases as the pool temperature is decreased.

(ii) The predicted maximum bubble size increases with pool temperature.

The bubble collapse model is an infinite pool spherical vapor bubble model with rapid condensation induced by the liquid jet. The condensation caused by the liquid jet penetration and atomization is modelled by an overall heat transfer parameter $UA_c$ determined from the experiments to be 4.37 kw/°C. By assuming that the peak pressure decreases inversely with

distance from the vent exit, the pool bottom pressures are predicted.

Comparisons of the predicted pool bottom pressures with the measured indicate that this model is unable to predict the bubble collapse phenomenon in steam chugging; however, the predicted trends do agree with the general trends observed in the experiments. These trends are listed as follows:

(i) The predicted pool bottom pressure decreases as pool temperature is increased.

(ii) The predicted pool bottom pressure decreases with submergence.

Comparisons of the model predictions with the Japan 1/6-scale data show good agreements in the vent clearing time as well as the bubble growth time. These comparisons are interesting but non-definitive concerning the validity of the present models.

## ACKNOWLEDGMEMTS

The support by the U. S. Nuclear Regulatory Commission through contract No. AT(48-24)-0342 is gratefully acknowledged.

## ABSTRACT

The condensation-induced hydrodynamic loads during low flow vapor injection (steam chugging) is studied experimentally and theoretically. Qualitative visual experiments in a small scale single vent system indicate that the interfacial motion admits certain characteristic patterns in various ranges of pool temperatures and steam mass fluxes. Systematic classification of these characteristic patterns based on these two parameters resulted in a condensation regime map. The basic regimes in the map are: the jet regime at high mass fluxes (>150 $Kg/m^2$-sec); the bubble oscillation regime at intermediate mass fluxes; and the steam chugging regime at low mass fluxes (<75 $Kg/m^2$-sec).

Steam chugging occurs at the low mass flux (below 75 $Kg/m^2$-sec) and low pool temperature (below 80°C) region of the map. Three different modes of chugging are identified: the internal chug where all condensation takes place in the vent; the detached bubble chug where the bubble is detached from the vent during formation; and the encapsulating bubble chug where the bubble grows to encapsulate the vent exit following formation. The hydrodynamic loads measured at the pool bottom show mild oscillations (~0.1 atm.) for internal chugs; moderate oscillations (~.3 atm.) for detached bubble chugs; and large spiky oscillations (~0.5 atm.) for encapsulating bubble chugs.

Two theoretical models are developed to analyze chugging: the vent pipe model which computes the water slug motion in the vent as well as the bubble dynamics at the vent exit after vent clearing; and the bubble collapse model which predicts the pressures associated with the collapse. The predictions of both models are compared to the present data

as well as the Japan 1/6-scale data. The general trends observed in the experiments are predicted.

TABLE OF CONTENTS


| | Page |
|---|---|
| NOMENCLATURE | xii |
| LIST OF FIGURES | xiii |
| LIST OF TABLES | xv |
| CHAPTER 1: INTRODUCTION | 1 |
| 1.0 Introduction | 1 |
| 1.1 Background | 2 |
| 1.2 Past Work | 4 |
| 1.3 Present Work | 16 |
| CHAPTER 2: DESCRIPTION OF THE EXPERIMENT | 18 |
| 2.1 Experimental Apparatus, Instrumentation, and Data Acquisition | 20 |
| 2.2 Experimental Procedure | 27 |
| 2.3 Test Matrix and the Data Reduction | 29 |
| 2.4 Experimental Error Bounds | 32 |
| CHAPTER 3: RESULTS OF THE EXPERIMENTS AND OBSERVATIONS | 35 |
| 3.1 Visual Experiments - Qualitative | 35 |
| 3.1.1 The Criteria for Separating the Condensation Regimes | 36 |
| 3.1.2 The Condensation Regime Map | 38 |
| 3.2 Detailed Experiments on the ydrodynamic Loads on the Pool Structure | 48 |
| 3.2.1 Detailed Results on Interfacial Motion in the Injection Pipe and in the Pool From High-Speed Movies | 48 |
| A. Internal Chug | |
| B. Detached Bubble Chug | |
| C. Encapsulating Bubble Chug | |
| 3.2.2 Detailed Results on the Pressure Spikes Measured at the Pool Solid Boundaries | 66 |
| A. Internal Chug | |
| B. Detached Bubble Chug | |
| C. Encapsulating Bubble Chug | |

Page

3.2.3 Synchronized Movie and Pressure Data . . . . 72

3.2.4 Statistical Data . . . . . 73

3.3 Detailed Experiments on the Dynamics of the Steam Upstream of the Vent Exit . . . . . 79

3.3.1 Vent Pressure Experiments (Runs VP1-4) . . . . 83

3.3.2 Steam Velocity Experiments (Runs FM1-5) . . . 86

3.3.3 Mixed Vent Pressure and Steam Velocity Experiments (Runs MIX1 and MIX2) . . . . . 86
3.3.4 Surge Tank Pressure Experiments (Runs ST1-4) . . . . . 90
3.3.5 Statistical Data . . . . . 90

3.4 Summary of Physical Observations and Discussion . . . 92

CHAPTER 4: THEORETICAL ANALYSES . . . . . 99

4.1 General Description of Theoretical Approach . . . . . 100

4.1.1 Transient Pipe Flow Analysis . . . . . 104

4.1.2 Condensation Model in the Pipe . . . . . 107

4.1.3 Chugging Model for the Water Slug . . . . . 108

4.1.4 Bubble Dynamics Model at Pipe Exit and the Collapse Criteria . . . . . 109

4.1.5 Bubble Collapse Model and the Peak Pressure Developed . . . . . 115

4.1.6 Summary of Physical Phenomena not Included in the Model . . . . . 118

4.2 Determination of System Parameters for the Theoretical Model . . . . . 121

4.2.1 Determination of Condensation Heat Transfer During Bubble Collapse . . . . . 121
4.2.2 Determination of Condensation Heat Transfer in the Pipe . . . . . 122
A. Initial Conditions in the Pipe
B. Determination of h

4.3 Comparison with Experimental Data and Discussion . . 125

4.3.1 Comparison of Experimental Data with Bubble Collapse Model Predictions . . . . . 128

Page

4.3.2 Comparison of Experimental Data with Vent Pipe Model Predictions . . . . . 132

CHAPTER 5: COMPARISON WITH JAPAN 1/6 SCALE DATA . . . . . 139

5.1 Initial Conditions and Scaling (assumed) . . . . . 139

5.2 Comparison of Theory Predictions with the Experiments . . . . . 140

CHAPTER 6: SUMMARY AND CONCLUSION AND RECOMMENDATION . . . . 154

REFERENCES . . . . . 161

GLOSSARY . . . . . 164

APPENDICES . . . . . .

A. Synchronized Movie and Pool Bottom Pressure Data . . . 166

B. Flow Meter Calibration . . . . . 192

C. Vent Pressure Data . . . . . 205

D. Steam Velocity Data . . . . . 224

E. Mixed Vent Pressure and Steam Velocity Data . . . . . 251

F. Surge Tank Pressure Data . . . . . 263

G. The One-Dimensional Bubble Dynamics Equations for a Spherical Bubble in an Infinite Pool . . . . . 270

H. Numerical Study on the Sensitivity of the Solution to Various Parameters in the Theoretical Model . . . . 279

I. Computer Listings of the Programs . . . . . 290

NOMENCLATURE

$A$ = pipe cross-sectional area
$C$ = velocity of sound
$D$ = pipe diameter
$f$ = friction factor
$h$ = heat transfer coefficient
$k$ = specific heat ratio
$k_\ell$ = liquid thermal conductivity
$L$ = submergenge depth
$\dot{m}$ = mass flow
$P$ = pressure
$Q$ = heat flow
$r$ = radius
$t$ = time
$u$ = water slug velocity
$V$ = velocity
$\mathcal{V}$ = volume of condensation region
$W$ = duration of vent underpressure
$X$ = submerged distance from pool surface
$Z$ = distance
$\alpha$ = thermal diffusivity
$\beta$ = apparent mass constant
$\rho$ = density
$\Gamma$ = specific heat ratio
$\mu$ = viscosity

Superscripts *non-dimensionalized quantities

Subscripts $\ell$ for liquid, $w$ for water
$con$ for condensation region

LIST OF FIGURES


| Figure | | Page |
|---|---|---|
| 1.1 | Schematic of BWR Containment(MARK I) | 3 |
| 1.2 | Thearetical Models for Steam Chugging | 6 |
| 2.1 | Photos of the Experomental Facility | 19 |
| 2.2 | Steam Injection System | 21 |
| 2.3 | Surge Tank | 22 |
| 2.4 | Test Chamber | 24 |
| 2.5 | Location of Instrumentation | 25 |
| 2.6 | Temperature Response of Thermocouple | 34 |
| 3.1 | The Condensation Regime Map | 43 |
| 3.2 | Condensation Regime 2 | 44 |
| 3.3 | Condensation Regime 3 | 45 |
| 3.4 | Condensation Regime 4 | 46 |
| 3.5 | Condensation Regime 5 | 47 |
| 3.6 | Photos of Interfacial Motion--Internal Chug | 51 |
| 3.7 | Photos of Interfacial Motion--Detached Bubble Chug | 55 |
| 3.8 | Photos of Interfacial Motion--Encapsulating Bubble Chug(plastic pipe) | 60 |
| 3.9 | Photos of Interfacial Motion--Encapsulatin Bubble Chug(steel pipe) | 62 |
| 3.10 | Photos of Interfacial Motion--Encapsulating Bubble Chug,High Pool Temperature(plastic pipe) | 64 |
| 3.11 | Pressure Spike of Detached Bubble Chug | 69 |
| 3.12 | Pressure Spike of Encapsulating Bubble Chug | 70 |
| 3.13 | Pressure Spike of Encapsulating Bubble Chug | 71 |
| 3.14 | Synchronized Data--Internal Chug | 74 |
| 3.15 | Synchronized Data--Detached Bubble Chug | 75 |
| 3.16 | Synchronized Data--Encapsulating Bubble Chug | 76 |
| 3.17 | Plot Maximum Chug Height vs. Pool Temperature | 80 |
| 3.18 | Vent Pressure Data | 87 |
| 3.19 | Steam Velocity Data | 88 |
| 3.20 | Mixed Vent Pressure and Steam Velocity Data | 89 |
| 3.21 | Surge Tank Pressure Data | 91 |
| 4.1 | The Vent Pipe Model During Water Slug Discharge and Chugging | 102 |
| 4.2 | The Vent Pipe Model During Bubble Growth and Collapse | 103 |
| 4.3 | Comparison of Theory Predictions with Experimental Data(Run No. ST1) | 135 |
| 4.4 | Comparison of Theory Predictions with Experimental Data(Run No. ST2) | 136 |
| 4.5 | Comparison of Theory Predictions with Experimental Data(Run No. ST3) | 137 |
| 4.6 | Comparison of Theory Predictions with Experimental Data(Run No. ST4) | 138 |

Figure Page

5.1 Pressure Measuring Points in Test Containment II (Japan Data) . . . . . 144
5.2 Water Level Measuring Points in Test Containment II (Japan Data) . . . . . 145
5.3 Japan Data Run 214 . . . . . 147
5.4 Japan Data Run 214 . . . . . 148
5.5 Japan Data Run 216 . . . . . 149
5.6 Japan Data Run 216 . . . . . 150
5.7 Comparison of Theory Predictions with Japan Data (Run 214) . . . . . 151
5.8 Comparison of Theory Predictions with Japan Data (Run 216) . . . . . 152

LIST OF TABLES


| Table | | Page |
|---|---|---|
| 1.1 | Summary of Existent Experimental Data | 9 |
| 2.1 | Test Matrix | 31 |
| 3.1 | Chugging Characteristics at Various Pool Temperatures | 81 |
| 3.2 | Summary of Movie Data Reduction in Bubble Growth and Collapse Times | 82 |
| 3.3 | Statistical Data on the Upstream Dynamics Experiments | 93 |
| 3.4 | The Characteristics of the Additional Pressure Spikes | 98 |
| 3.5 | Comparison of Chugging Frequencies in Steel Pipe Experiments and the Plastic Pipe Experiments | 98 |
| 4.1 | Summary of the Criteria Defined for Chugging | 114 |
| 4.2 | Physical Phenomena Not Included in the Present Model | 120 |
| 4.3 | Predicted Bubble Pressure Based on a Few Values of $UA_c$ vs Measured (Run. No. FM5) | 123 |
| 4.4 | Predicted Bubble Pressures vs Measured Pool Bottom Pressures | 129 |
| 4.5 | Predicted Maximum Pressure at the Pool Bottom vs Measured | 131 |
| 5.1 | Initial Conditions in Japan Data Run 214,216 | 146 |
| 5.2 | Comparison of Predicted Pool Bottom Pressures with Experimental Data | 153 |

# CHAPTER 1

# INTRODUCTION

## 1.0 Introduction

One of the major safety considerations in a Boiling Water Reactor (BWR) is the structural integrity of the containment system in the event of a Loss of Coolant Accident (LOCA). Present BWR containment designs (MARK I, II, III) invariably involve the venting of the steam discharged from the break during the accident into the suppression pool. The rapid condensation in the pool would prevent any severe pressurization in the containment. However, the condensation induced pressure oscillations in the suppression pool exert large loadings on the vent pipes, the pool walls, and other structures in the pool. In particular, towards the tail end of the LOCA when the vent flow is low, the pressure oscillations exhibit periodic occurrences of large magnitude but short-duration pressure spikes which imposes a direct threat to the structural integrity of the containment. The physical phenomenon associated with these pressure spikes is called "steam chugging."

This report, written for the U. S. Nuclear Regulatory Commission, describes the experimental and theoretical study at UCLA into this phenomenon. The prime objective of the study is to obtain a basic physical understanding of the nature and the origin of the chugging induced pressure oscillations; and, based on the physical observations, a theoretical base is formulated allowing the predictions of these loads.

## 1.1 Background

The Boiling Water Reactor (BWR) systems (Figure 1.1)have been designed with a pressure suppression containment (or wet well) to condense any steam released in the dry well during a LOCA, to act as a heat sink for Hot Standby and Relief Valve Operation, and to provide a source of water for the Emergency Core Cooling. Because of these critical functions, the integrity of the wet well is essential from the view point of public safety. Recent power plant experiences and experimental tests have revealed potential dynamic loadings on the wet well which could violate its integrity. The dynamic loads can result under the following conditions:

1. Loss of Coolant Accident (LOCA)
2. Relief Valve Discharge, and
3. Earthquake.

In the event of a LOCA, the steam discharged from the primary system quickly pressurizes the dry well causing a flow of air-steam mixture through the vents into the suppression pool. In the initial stage of the accident, the vent flow is primarily air and the flow rate is high. Towards the tail end of the accident, the vent flow is primarily steam and the flow rate is low. The low steam flow causes a phenomenon known as "steam chugging" to occur. This phenomenon is characterized by periodic rushes of water up the vent as well as large magnitude pressure spikes associated with the steam-water interfacial motion. These spikes can potentially damage the pressure suppression system and, therefore, are important to nuclear reactor safety.

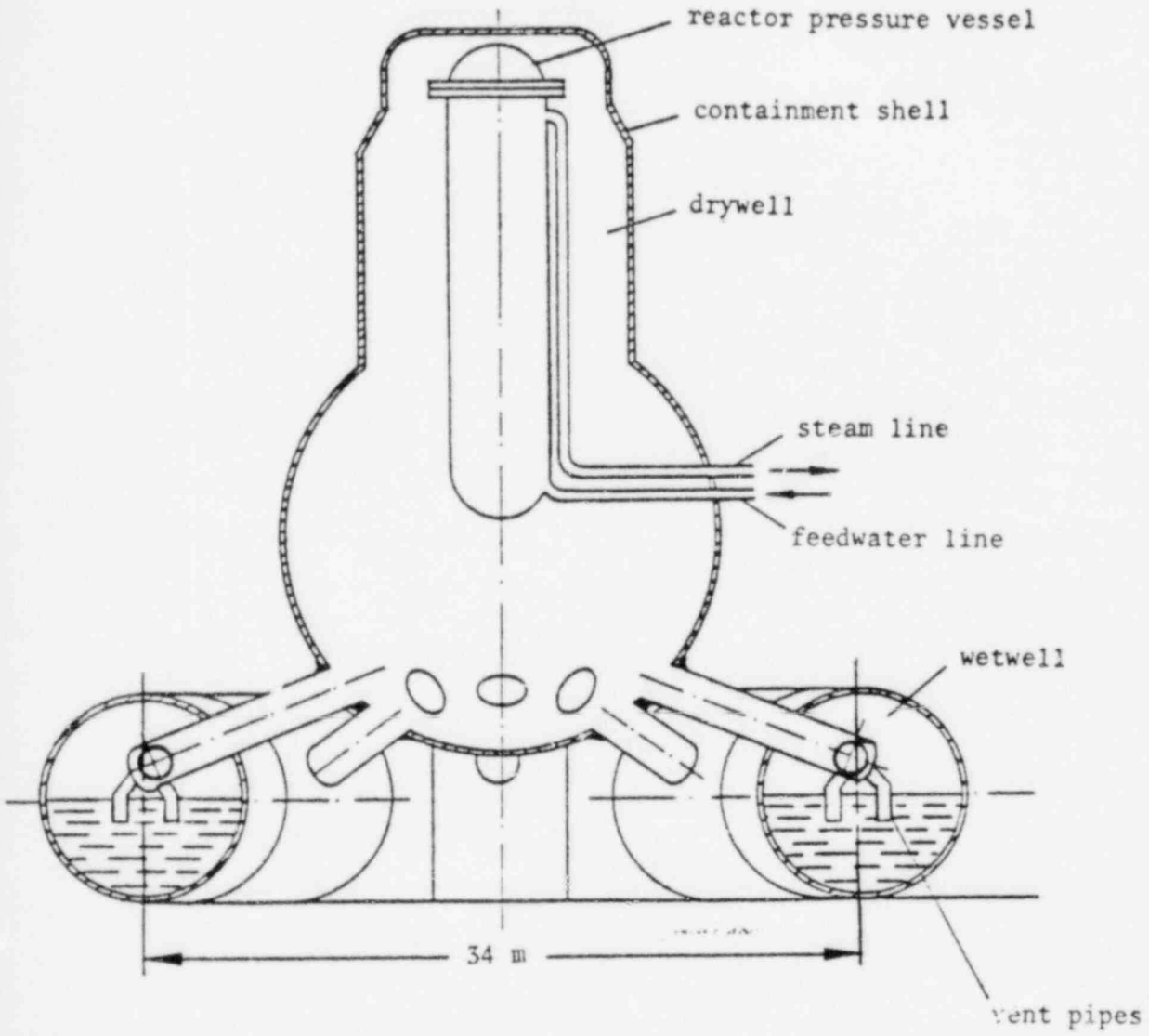


Fig. 1.1 Schematic of Boiling Water Reactor Containment(MARK I)

## 1.2 Past Work

When the question about the integrity of the suppression pool during a LOCA was raised, the hydrodynamical forces induced by the condensation process became a focal point of various research groups[1, 2, 3, 4, 5] around the world. In most of the theoretical studies, three areas are of most concern: (i) how the steam is injected into the pool, (ii) what is the heat transfer rate that causes the bubble to collapse, and (iii) what is the force imposed on the solid boundary. Sargis et al.[1] attempted to answer these questions. They used a one-volume model to approximate the steam in the vent pipe. Then, a hemispherical bubble is assumed to grow in the vent exit as the interface clears the vent (Figure 1.2(a)). The dynamics of the hemispherical steam-water interface was calculated using a mechanical energy balance where the rate of change of kinetic energy of the infinite liquid pool equal the rate of work done by the interface on the fluid. The computed interfacial motion was then used as a forcing function applied to the potential flow of a finite pool. The pressures on the pool wall were computed using the linearized transient Bernoulli equation. Their model predicted the general trends of the pressure oscillations observed in the chugging experiments. It is by far one of the more complete models which solves the entire problem relating the steam injection into the vent to the wall pressures at the pool boundary. A more simplified approach was taken by Kowalchuk & Sonin[3] who used just a single vent pipe model. The inertia of the liquid in the pool was modelled by using an equivalent mass of liquid attached at the end of the vent pipe. As the interface cleared the vent exit, a

cylindrical bubble with a radius equal to that of the vent pipe was assumed to form (see Figure 1.2(b)). Concerning the interfacial heat and mass transfer, they suggested that the condensation process could be vapor side limiting or liquid side limiting. In their model, the vapor side condensation was calculated by the kinetic theory with the accommodation coefficient as a parameter to be studied. The liquid heat transfer was modelled by a turbulent diffusion model. Their results indicated that the maximum peak-to-peak pressures in the calculated pressure oscillations was strongly affected as the accommodation coefficient varied from 0.1 to 1.0, but for values greater than 1.0 the maximum peak-to-peak pressures were unaffected. This indicated that the condensation was limited by the liquid side heat transfer. Class[2] developed a similar model except that a spherical bubble is assumed to form in an infinite pool. He also developed a method for the change in boundary conditions as the interface clears the vent exit. The one-dimensional pipe flow problem is coupled to the one-dimensional radial bubble expansion model. The turbulent mixing model was used to compute the heat transfer in the liquid which in turn determined the condensation rate. All three models were able to predict the trends in the pressure oscillations in the chugging process. However, none of these models were able to give a physical explanation for the sudden rapid condensation which initiated the bubble collapse. Furthermore, none of these models addressed to the pressures generated by the violent collapse of the steam bubble. These two aspects will be more thoroughly studied in the present investigation.

In addition to the theoretical modeling efforts there are

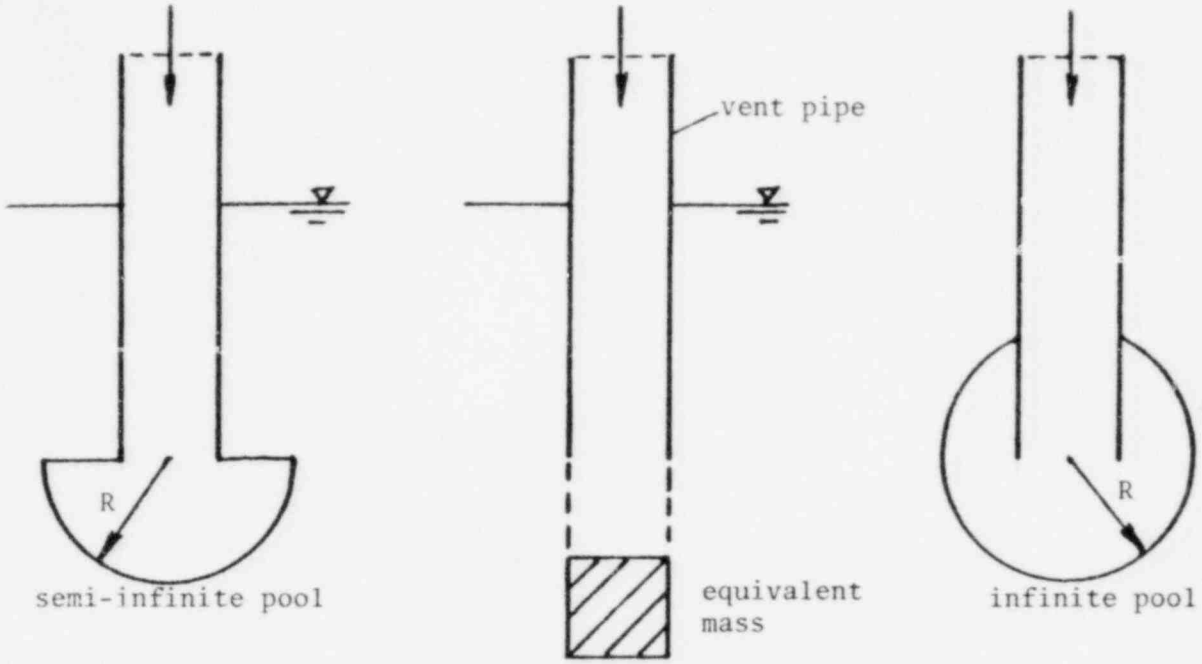


Sargis, et al.
JAYCOR CO.

(a)

Kowalchuk & Sonin
MIT

(b)

Class
GERMANY

(c)

Fig. 1.2 Theoretical Models for Steam Chugging

extensive experimental efforts for a better understanding of the chugging process. The first set of full scale containment experiments were performed in the Marviken power station located at Stockholm, Sweden. These experiments[6,7] included sixteen reactor vessel blowdown runs to study the containment responses and eight blowdown runs to study the pressure oscillations in the suppression pool. In each run, the steam generated by the primary system was discharged to the drywell vertically above the wetwell. Then the steam-air mixture in the drywell was vented through 58 downcomers into the suppression pool. The data from the pressure oscillation experiments showed that close to the end of the simulated LOCA, highly oscillatory pressures were developed in the suppression pool. The periodic pressure fluctuations were characterized by a sharp pressure undershoot which was immediately followed by a high-magnitude short-duration pressure spike and then a damped oscillation period which was called the "ring out". A Fourier analysis was performed in each case which showed that the oscillations were actually the superposition of oscillations at various frequencies. It also showed that the oscillations consisted of a fundamental frequency, e.g., in Run No. 19, it was 4.6 Hz.

A set of full scale single vent experiments were made by General Electric Company in the U.S. called the 4T (Temporary Tall Test Tank) tests[9,10]. Their results are proprietary but they claimed similar oscillations as in the Marviken Tests.

In order to establish some qualitative information about the scaling of the chugging phenomenon, Creare [11] performed a set of small

scale single vent experiments including the 1/10, the 1/6 and the 1/4 scale of the actual BWR. It was found that the magnitude of the pressure spike decreased as the scaling increases. The magnitude of the pressure spikes in the 1/10 scale test were considerably higher than that of the 1/6 and 1/4 scale tests. No physical justifications were given for the observed results. The validity of this is questionable.

To obtain some information about the steam-chugging behavior in a multi-vent system, General Electric Company performed another full scale experiment with 3 vents and 6 vents. These data indicated that the pressure oscillations in each vent was not in phase with other vents. Recently, two sets of data were completed, one of them was from a 1/6 scale test[13] performed in Japan and the other one is a 1/12 scale test[14] performed at Stanford Research Institute in the U.S. The former report included also multi-vent (3 vents) data. The latter one showed detailed motion pictures of the bubble formation process with no pressure data. However, an interesting question was raised in the latter report concerning the triggering mechanism for the observed bubble collapse.

Hence, it appears that although a large amount of data is available, the questions concerning the mechanism which initiates the bubble collapse and the cause of the large pressure spikes still remain. A compilation of the condition for all the above mentioned experiments is presented in Table 1.2.

In order to understand the chugging process one has to acquire a knowledge concerning vapor jets, bubble growth, bubble collapse,

TABLE 1.1

SUMMARY OF EXISTENT EXPERIMENTAL DATA

| | Mark II Containment | Marviken | GE (4T) | GE (Full Scale) | Creare | | | SRI | Japan |
|---|---|---|---|---|---|---|---|---|---|
| Scale | Full | Full | Full | Full | 1/4 | 1/6 | 1/10 | 1/12 | 1/6 |
| No. of Vents | 108 | 58 | 1 | 3,6 | 1 | 1 | 1 | 1 | 1,5 |
| Vent diameter,cm. | 61. | 30.5 | 61. | 30.5,61. | 6.4 | 10.1 | 15.2 | 2.5,5.1 | 10.1 |
| Drywell Vol.,$m^3$. | 5384. | 1927. | 53.6 | 76.5 | .65 | 1.7 | 3.8 | .026 | .25,1.25 |
| Wetwell Air Vol.,$m^3$. | 4250. | 1558. | 31.6 | 55.6 | .54 | 1.4 | 2.0 | .026 | .22,.71 |
| Wetwell Water Vol.,$m^3$. | 3400. | 538. | 20.8 | 28.9 | n/a | n/a | n/a | .028 | .12,.58 |

Note: (1) The test conditions vary in each experiment and most of them are not reported in the references.

(2) Wetwell airspace volume and water volume varies as submergence varies.

(3) Peak pressures, frequencies in each experiment are not available in references.

cavitation and cavitation damages on materials which is believed to have some relation to the chugging pressure spikes. The following paragraphs present discussions of the state-of-the-art in these areas.

Some experimental effort[15,16,17,18,19] has been made for high vapor injection rates. In this case, the vapor-liquid interface is very rough due to the interfacial instabilities caused by the high vapor velocity. The controlling transfer mechanism is therefore the vapor momentum. If the flow is high enough to cause sonic choking to occur at the injection pipe exit, the vapor flow in the liquid region takes the form of a stable cone. But when the vapor flow is not choked at the exit, an oscillatory vapor region exists in the liquid. The oscillations of the interface causes regular detachments of vapor bubbles from the vapor region. The possible explanation for this behavior is that in the case of sonic flow at the exit, the condensation phenomenon do not affect the vapor flow in the pipe. But when the exit flow is subsonic, the downstream condensation effects can be propagated upstream to cause pulsation in the vapor flow. The above phenomena were observed by Greef[15] (1973) and recently by Simpson.[19] Greef's work included also pressure measurements taken by a pressure transducer in the vicinity of the jet. These pressure traces indicated periodic pressure spikes occurring at high frequencies. Although his observations were not directly applicable to the low flow injection problem, they did show an unstable vapor region with large interfacial oscillations when the flow is unchoked at the nozzle exit. From these results it may be inferred that as the flow rate is lowered, a point may be reached that these interfacial oscillations are large enough

to cause the vapor region to exist only intermittently at the nozzle exit. This is the point where steam chugging occurs.

The growth of a steam bubble at the downcomer exit during the injection process is basically a bubble growth problem under the presence of a mass and energy source. Unfortunately, no previous analytical work or experimental work was found in this area. The literature search is then directed toward the subject of bubble collapse. Bubble collapse is an important part of the phenomena involved in the chugging process. The past work in this subject can be divided into two categories. The first one involves analyses and experiments relating to the mechanics of the collapse process. The second category involves the pressures developed during the late stages of the collapse process.

In the first category, Rayleigh[20] was the first to formulate the problem of a spherical bubble in an infinite pool of ideal fluid. The Rayleigh equation, which describes the radius-time history of the bubble wall is

$$R\frac{dv}{dt} + \frac{3}{2}v^2 = \frac{p - p_\infty}{\rho} \qquad (1)$$

where $p_\infty$ = pressure at infinite distance from the bubble
$p$ = pressure at the bubble wall
$\rho$ = density of the liquid
$v$ = velocity of the bubble wall
$R$ = bubble radius
$t$ = time

For a cavity $p = 0$ and $v = \frac{dR}{dt}$, the equation can be integrated to yield a relationship between the bubble radius and its velocity

$$v^2 = \frac{2P_\infty}{3\rho}\left(\frac{r_0^3}{R^3} - 1\right) \qquad (2)$$

From this he obtained the time to total collapse of the spherical cavity,

$$\tau = \sqrt{\frac{3\rho}{2P_\infty}} \int_{r_0}^{0} \frac{R^{3/2}\,dR}{(r_0^3 - R^3)^{1/2}}$$

$$= .91468\, r_0 \sqrt{\frac{\rho}{P_\infty}}$$

For the vapor bubble collapse, Florschuetz & Chao[21] were the first to formulate and solve analytically the case of a heat transfer controlled collapse when the collapse was initiated by a sudden decrease in the liquid temperature. Comparison of the analytical solution with their experimental data showed that their analysis was able to predict the trend of the measured radius-time history but the accuracy was not good. Recently, Lee & Chan[22] proposed a classification of the bubble collapse modes into two types based on how the collapse is initiated The first type is when the collapse is initiated by a sudden rise in the liquid pressure. The second type is when the collapse is initiated by a sudden decrease in the liquid temperature. The latter case is identical to the situation where a saturated vapor bubble is suddenly transferred to a subcooled pool of liquid, which resembles the case of low flow vapor injection. They also presented numerical solutions of the coupled problem of heat diffusion and liquid momentum. Their results showed distinctly different characteristics in the radius-time histories of the two types.

A fair amount of experimental effort had been devoted to study cavitation bubble collapse and cavitation damages on material surfaces. These studies were motivated by the large damages on turbine blades due to cavitation. Kling & Hammitt[23] made a photographic study of this phenomenon. They observed the formation of a high velocity microjet penetrating through the bubble as the bubble collapses. This phenomenon was also observed by Florschuetz & Chao in their experiments on vapor bubble collapse. Other investigators[24,25] also confirmed these observations in their experiments. Of particular interest is the work of Benjamin & Ellis[25] who were able to isolate the effect of gravity from the effect of a nearby wall. They concluded that in the presence of a gravitational field alone, the liquid jet would penetrate the bubble from below and advance vertically upwards. However, in the presence of a solid wall, the liquid jet would penetrate the bubble from the side towards the wall. Chapman[26] studied the problem numerically and confirmed the above observation for the wall effect.

The second category involves the pressures developed during the collapse of the vapor bubble. In the case of a cavity, the Rayleigh solution showed an infinite velocity at the bubble wall as $r \to 0$. To avoid this singularity, Hickling & Plesset[27] assumed the existence of a small amount of non-condensible gas in the bubble. Then they solved the compressible flow problem numerically for the pressures developed in the liquid for the cases of an isothermal compression or an adiabatic compression. The reason for solving the compressible flow equations was due to the fact that the liquid velocity at the bubble

wall approaches the velocity of sound in the liquid as the bubble reaches its minimum radius and starts to rebound. Their results indicated that the maximum pressures developed during a collapse decrease as the initial pressure of the non-condensible gas increased. However, in a real physical situation the amount of non-condensible gas in the bubble is difficult to estimate. No other analytical approaches were able to quantify the pressure developed at the end of a collapse. The attention was then focused on the previous experimental effort. Green & Mesler[28] studied the transient pressures during a bubble collapse. Their measurements showed a positive pressure pulse immediately after the collapse. Their measurements also showed that the magnitude of the pressure pulse is inversely proportional to the distance from the bubble which agrees with the analytical results of Hickling & Plesset.[27] However, no direct measurement was made at the point where the collapse was completed. No previous experiments were able to measure the exact pressure at that point. In a discussion by Plesset,[29] it was indicated that the pulse magnitude might easily exceed $10^3$ atm for cavitation bubbles. This magnitude was high enough to cause pitting on solid surfaces. It had been speculated that the cause of the pitting was from high velocity microjets which penetrated through the bubble and impinged onto the solid surface. However as was shown by Shutler & Mesler[22] the pits were caused by the pressure pulse created by the collapse process. Knapp et al.[30] suggested a simple model to relate the bubble size and the pit depth. The model was based on an energy argument, that the work done by the fluid during the collapse must equal the collapse energy, part of which was used in forming the pit. This model was only

able to give an order of magnitude type of estimate on pit depth.

Pressure force can be generated in the liquid by free surface motion. A good summary of the previous work up to 1966 is given in a report by Abramson.[31] Most of the work in this report involves analytical solutions to the hydrodynamic equations describing the fluid motion in a container of various simple geometries, but none of these offers a solution to the hexagonal test section used in the experimental part of this study.

Note : A theoretical model was recently developed by Pitts[39]; unfortunately his report arrived too late to be incorporated into this work.

## 1.3 Present Work

It is clear from the discussions in the previous section that the sporadic nature of the pressure spikes imposed considerable difficulty on any theoretical approach. Of the few theoretical modeling attempts made, none were able to offer a full explanation of the condensation phenomena. Although a considerable amount of experimental data, based on small scale experiments, are available, the question still remains: What is the origin of the pressure loading?

The objective of this study is to formulate a theoretical base from which the prediction of the chugging-induced hydrodynamic loads in a full size containment would be feasible. A physical understanding of the governing phenomena which is essential for the theoretical development is to be obtained by performing a small scale experiment. As a first step, the experimental study is started with a single-vent vapor injection system, although the actual system involves multi-vents.

The approach adopted in this study is divided into two stages : the first stage involves an experimental investigation of the process of steam injection into subcooled water and the second stage involves a first attempt to model the chugging phenomenon. The experimental investigation has two objectives. The first one is to obtain a qualitative understanding of the vapor injection process in general. The second objective is to investigate the nature of the interfacial motion in conjunction with the hydrodynamic loads. This will establish an understanding of the physical mechanisms which govern the pressure spike as well as other oscillations induced at the pool boundaries. These physical mechanisms could also be a result of the steam behavior

upstream of the vent exit. Thus the present work will include an experimental investigation of the upstream steam dynamics as well.

In the theoretical modeling of the steam-water system, based on the understanding gained in the experimental investigation, the bubble dynamics and the steam-water interfacial heat transfer are to be examined.

Following this introductory chapter, a description of the experimental apparatus is presented (Chapter 2). The physical observations from the experimental study are presented in Chapter 3; and the theoretical model is presented in Chapter 4. Chapter 5 shows the comparison between the theoretical model predictions and the Japan 1/6-scale data while the conclusion of the study is presented in Chapter 6.

# CHAPTER 2

# DESCRIPTION OF THE EXPERIMENT

## 2.0 General Description

This chapter describes the experimental apparatus, the techniques for various measurements. and the method of data acquisition.

Basically, the experimental apparatus is a small scale steam loop, the major components being the boiler, the superheater, the surge tank, and the test section. The steam, generated by a boiler, is delivered to the hexagonal test section where the injection phenomenon is being recorded by various instrumentation. The interfacial motion is recorded by a high-speed movie camera. The steam temperature is being measured by a thermocouple located at the vent exit. The induced pressure loads are being measured by the pressure transducers, one of which is located at the pool bottom right below the vent exit. The other one is mounted on the side wall of the hexagonal test section at the same elevation as the vent exit. The upstream steam conditions are measured by an anemometer and a few pressure transducers and thermocouples. The transient data are recorded by a PDP-11 computer. Figure 2.1 shows two photographs of the system. The upper photo shows the surge tank and the horizontal part of the injection line, and the lower one shows the test section, the control panel, and the PDP-11 computer.

The following sections describe in detail the experimental

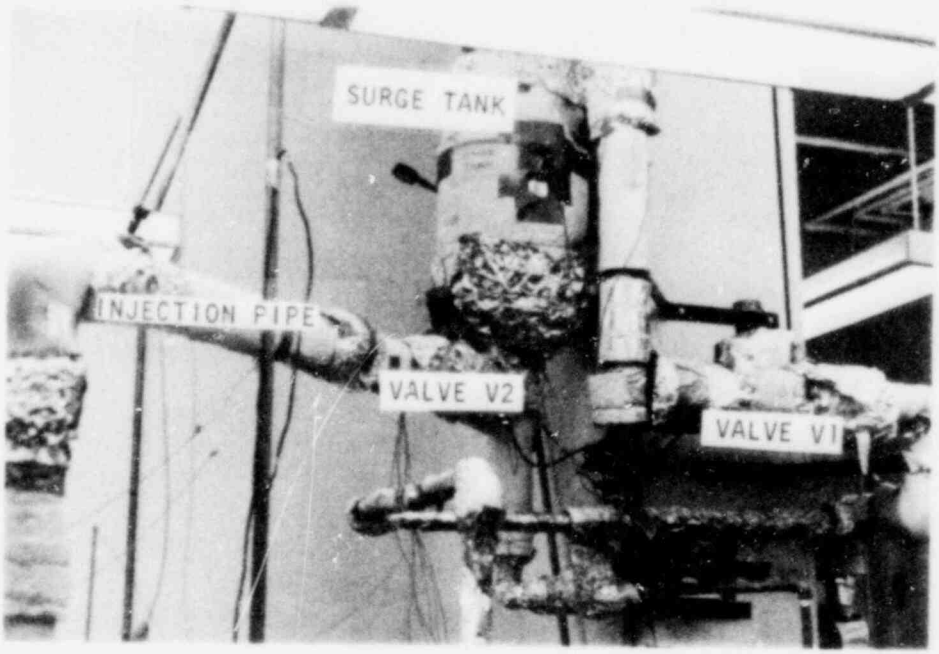


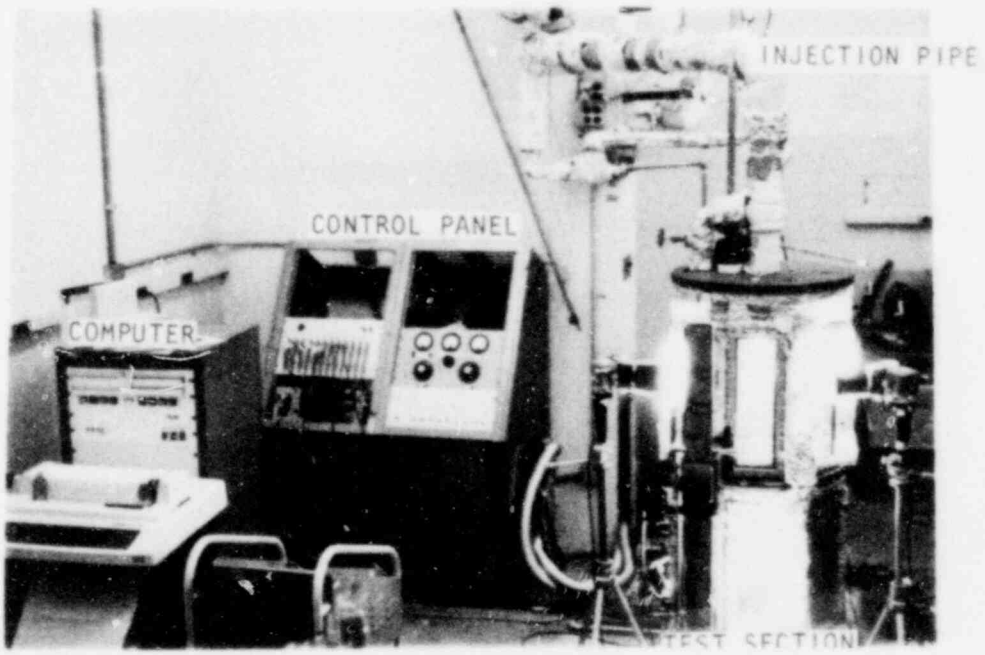


Fig. 2.1 Photos of the Experimental Facility

apparatus and test procedures; the instrumentation and the associated error bounds; and the data acquisition system.

## 2.1 Experimental Apparatus, Instrumentation, Data Acquisition System

The apparatus used for the steam tests consists of a boiler, a superheater, a surge tank, and a hexagonal test chamber. A schematic diagram of the experimental apparatus is shown in Figure 2.2. Demineralized water is pumped into the boiler by a high-pressure, low-capacity pump to provide a discharge pressure greater than 790 kPa and a water flow of 7.56 g/s. Saturated steam, up to 790 kPa, is generated in a Chromalox CES 18SS stainless-steel boiler. The boiler has a heat load of 17.0 kW with a maximum steady-steam generation rate of 7.56 g/s. The steam can be superheated up to 200°C by a stainless steel Chromalox superheater. The maximum heat output of the superheater is 1.5 kW. The superheated steam is then led to a surge tank (0.044 $m^3$ in volume), which is designed for up to 1185 kPa internal pressures. There are side openings on the surge tank for the insertion of a pressure transducer and thermocouples (Figure 2.3).

The steam is then led from the surge tank into the test chamber (Figure 2.2) through a 51 mm diameter quick-acting solenoid valve (V2). A Thermo-System Model 1269-W anemometer, a Statham PL131TC-50-350 pressure transducer and a fast response thermocouple are placed downstream of the valve at a location approximately 150 cm from the pipe exit (Figure 2.5). The exit end of the steel steam supply line is connected to either a plastic vent or a steel vent depending on the experiment.

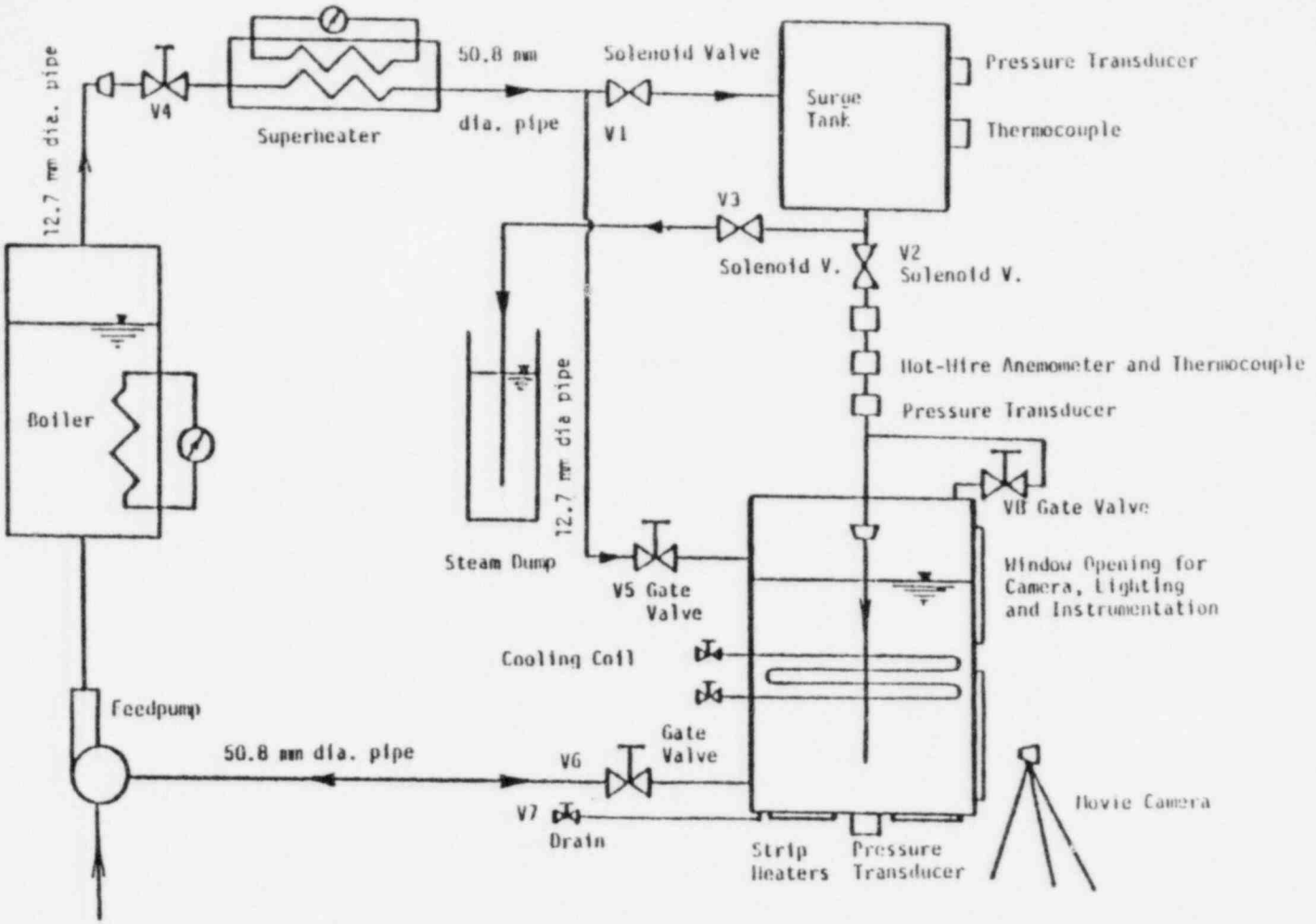


Fig. 2.2 Steam Injection System

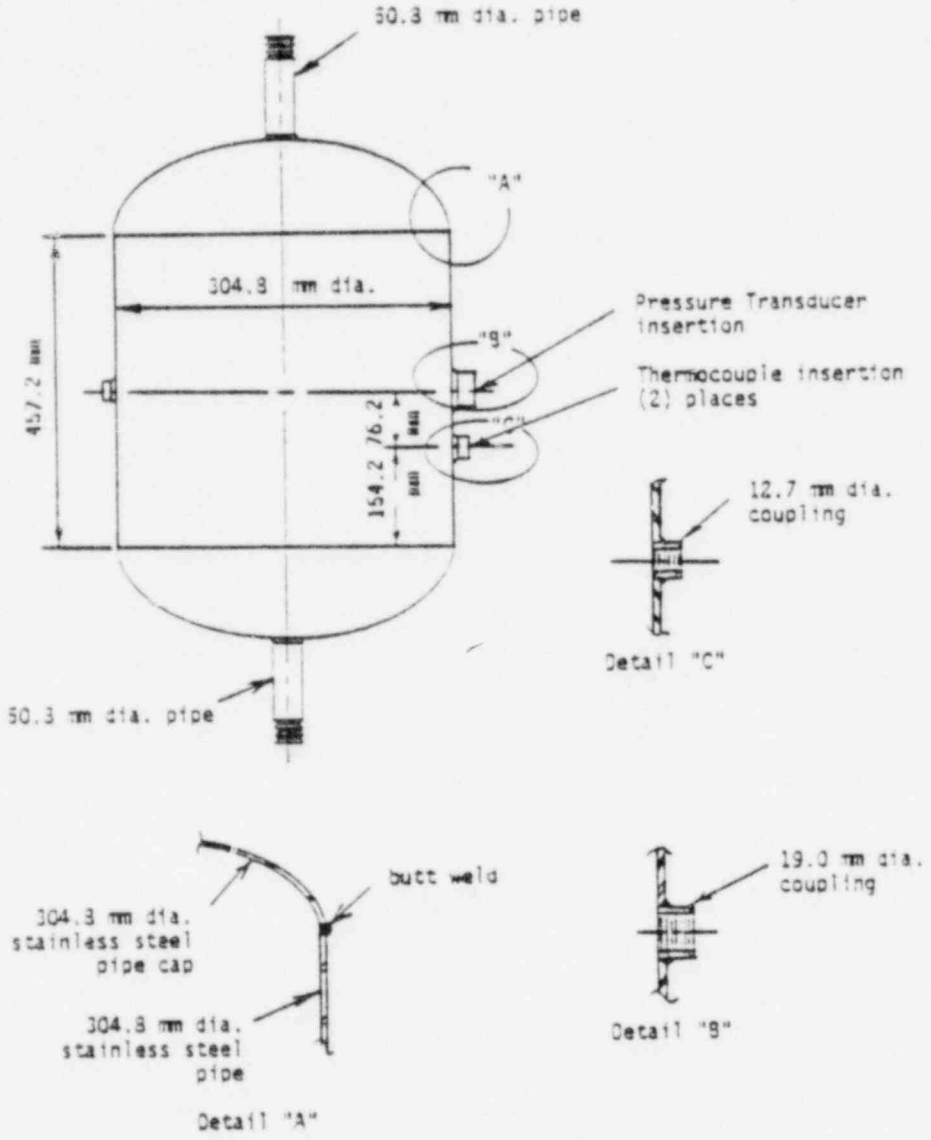


Fig. 2.3 Surge Tank

The test chamber (Figure 2.4) consists of two hexagonal sections, one stacked on top of the other. Each section has a cross sectional flat-to-flat dimension of 457 mm and a height of 602 mm. Each flat surface of the hexagon has a 101 mm x 229 mm window opening. These openings are for the glass or the stainless steel plate covers. The glass plate covers allow movie recording while the steel plate covers allow for insertion of various measuring devices. A 12.7 mm O.D., 50 mm pitch stainless steel cooling coil (inner diameter 9.7 mm) is attached to the inner surface of the hexagon at the middle of the test chamber. The bottom hexagon has two ports for connecting the test chamber to a fresh-water supply line and to a drain. As shown in Figure 2.1, there is a 12.7 mm line (V3) that leads the steam from the surge tank into the steam dump. There is also another 12.7 mm line, V5, for the degas process. The line V8 is for balancing the pressure between the downcomer and the test chamber. All the steam lines are wrapped with tape heaters and insulating materials to prevent condensation.

Two thermocouples are inserted near the pipe exit, one at a distance of 6 cm inside the pipe while the other at a distance of 4 cm below the pipe exit in the water (Figure 2.5). There is another thermocouple (No. 6) located in the water to measure the bulk pool temperature. A pressure transducer is located at the bottom of the pool right below the pipe exit. The thermocouples are made by 25.4 μm diameter chromel-alumel wire. The response time of these thermocouples is on the order of 4 - 5 milliseconds. The pressure transducers are regular, unbonded, strain gauge pressure transducers with

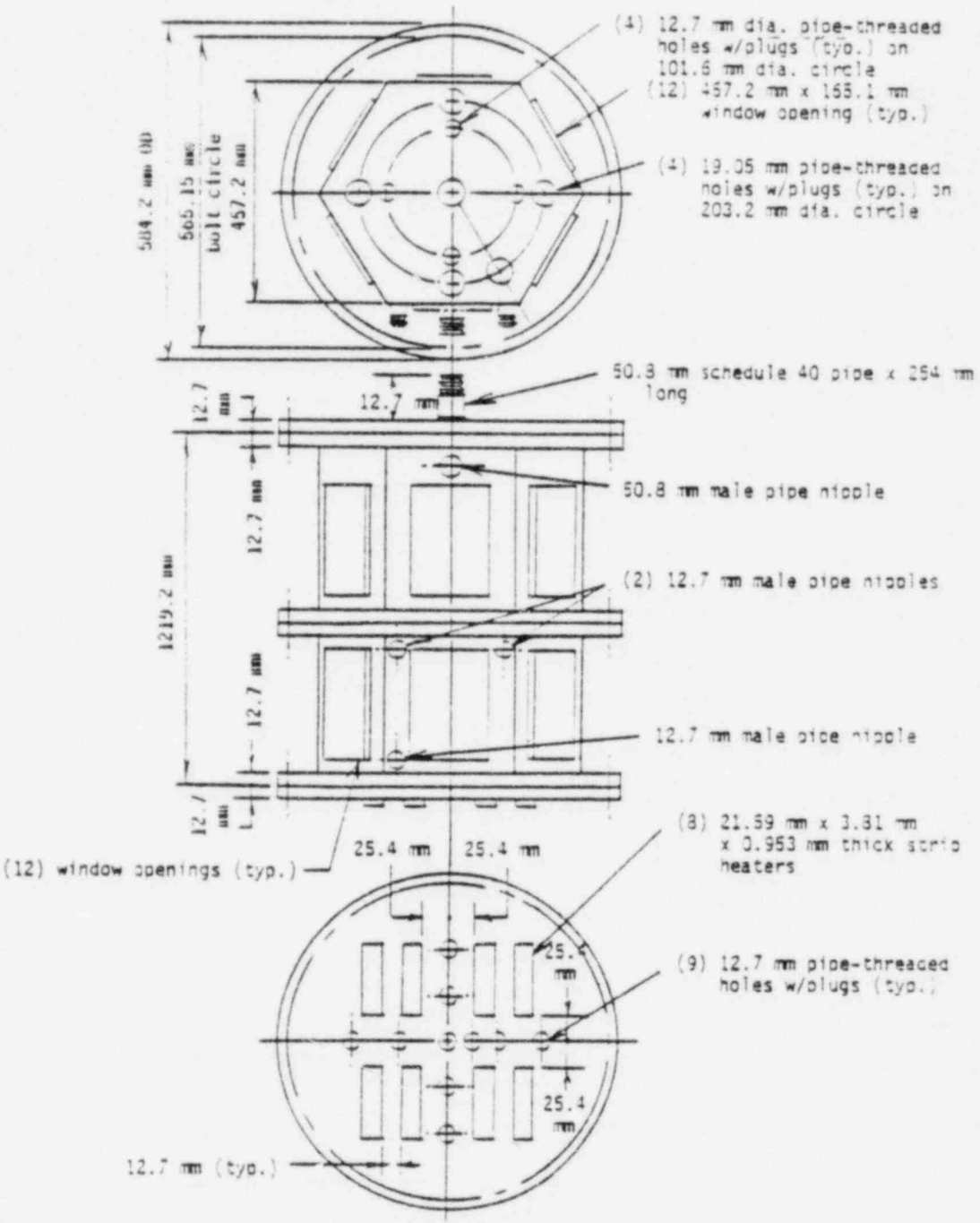


Fig. 2.4 Test Chamber

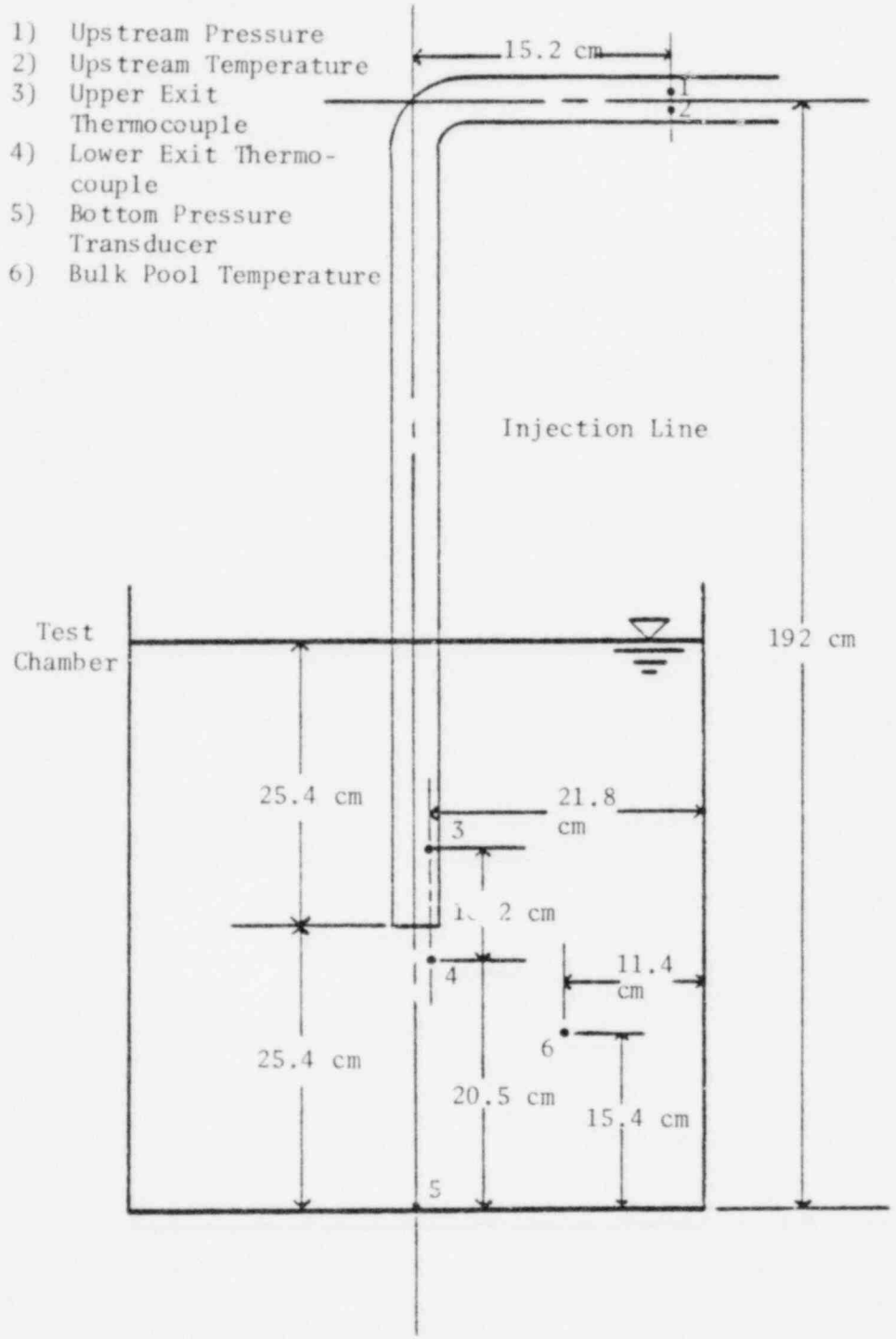


Fig. 2.5 Locations of Instrumentation

a response time of 0.6 ms. The thermal effects of the pressure transducer measurements were investigated and presented in Appendix A of Reference 33.

The electrical signals from all the instruments including thermocouples, pressure transducers, and flow meters are amplified by a set of amplifiers which has a gain of up to a thousand times and are able to respond to signals of frequency up to one mega-hertz. The amplified signals are then input into an analog-to-digital converter to be digitized and read into the computer core. Then the data in the core can be read onto disks for permanent storage and future data reduction. The computer core has a memory capacity of six thousand data points for each run, i.e., if there are six different measurements to be made, each measurement can only have a thousand data points. If the time interval between data points is chosen to be one millisecond then the total run time is one second. Since the phenomenon of steam chugging is characterized by large magnitude but short duration pressure pulses, the time interval between data points must be short in order to capture all these pressure oscillations. On the other hand, the system is limited by the maximum core memory capacity. If the time interval between data points is too small, e.g., 0.1 msec, then the total time available for a run is limited to 0.1 seconds. From visual observations, it is gathered that the time between chugs is on the order of 0.5 seconds. This means that the total run time must be on the order of two seconds in order to ensure that a couple of chugs are captured in each run. This is a limitation to the data acquisition system.

## 2.2 Experimental Procedures

Before any experimental test, the air present in the steam supply system was eliminated by steam purging while the air dissolved in the water was eliminated by heating the water with the bottom strip heater.

Step I: The air initially in the system was driven out by the steam generated in the boiler. This was achieved by turning on the boiler until the boiler pressure reaches the desired point. Then valves V4, V1, and V3 were opened with valve V2 closed (Figure 2.1). The air-steam mixture was discharged into the steam dump. Subsequently, valve V5 was opened so that the air initially in the pipe was driven into the test chamber atmosphere. Finally, the air initially in the vent pipe was driven into the pool by turning on valve V2 and turning off valves V3 and V5. To assure the total purging of the air in the system, this process is normally continued for an extended period of an hour

Step II: Actuation of the valve V6 allowed water to flow into the test chamber. By turning on the test chamber heater, the air initially dissolved in the water could be purged. Air was prevented from being reabsorbed into the water by maintaining a steady steam flow over the water surface through the line controlled by valve V5. This process was continued long enough to insure that all of the dissolved air was driven out of the water.

At the end of the degas process, valve V2 was closed so that no more steam was injected into the pool. Then, after the surge tank reached the desired pressure, valve V1 was closed and the

boiler was adjusted to a lower pool level to maintain a small steam-generation rate. The pool was allowed to set while the bottom heaters were turned off and cold water was allowed to run through the cooling coil to reduce the pool temperature to the desired subcooling. Steam generated in the boiler was continuously fed into the test section over the pool surface to keep the test section's pressure above atmospheric pressure for the prevention of a backflow of air into the test section.

After the steam loop and the test chamber conditions were set at the desired pressures and temperatures, the zero reference for all the instruments was taken, e.g., the zero for the steam flow was at zero velocity. The zero for pool bottom pressure transducer was atmospheric plus the static water head, etc. Then a calibration of the electrical signals were done such that the magnitude of the electrical signal could be related to the actual numbers recorded by the computer. A one milli-volt square wave was applied to all the input channels, then the computer output was printed. The difference between the output peak value and the bottom value represents one milli-volt of input signal. The calibration value for each channel was a little different but they all range from 164 to 174. These values were used in the data reduction process. After the calibration and the zero reference were taken, the experiments were performed.

If a steady flow test was made, the boiler power and flow rates were set to the desired values and the steam flow bypassed to the dump until steady flow was achieved. When transient tests were

made, the surge tank was pressurized to the desired pressure. Valve V2 was triggered to inject the steam from the surge tank into the pool.

The data acquisition procedure for steady state tests was slightly different from the transient tests. In steady state tests, data acquisition would be initiated after steady flow was reached. For transient tests, the data acquisition system was initiated before triggering valve V2 such that the initial conditions in all the instruments were recorded. The synchronization between the movie and the data acquisition was achieved by using a two-way switch which would simultaneously trigger the data acquisition system as well as a signal light. The signal light was placed at the side of the test section within the view of the camera. The data acquisition would automatically finish at the assigned termination point. The data set was then recorded on the floppy disks stored for the data reduction process.

After the test, the pool would be heated or cooled to the desired temperature for the next test.

## 2.3 The Test Matrix and the Data Reduction

Table 2.1 shows a tabulation of the conditions under which the experiments were performed. The range of pool temperatures covered was from 37°C to 95°C. The boiler steam generation rate was held constant in all these runs at 7.56 gm/sec. Two different types of injection pipes were used. The plastic pipe was used when detailed movie data on the interfacial motion inside the pipe was desired.

The stainless steel pipe was used when the vent pressure near the exit was desired since it allows the appropriate mounting of a pressure transducer. A set of runs (FM1 - 5) was performed to measure the side wall pressure in the pool. On the same set, the steam velocity was also measured. The vent pressure was measured in Runs VP1 - 4. The surge tank pressure was measured in Runs ST1 - 4.

A computer program was written to perform the data reduction. For the pressure transducer output, the input to the program was the calibration for the particular pressure transducer. For the thermocouple output, the standard voltage vs. temperature curve given for Chromel-Alumel thermocouples was incorporated into the program. For the steam velocity, the calibration equation is incorporated into the program; however, the three constants used in the equation vary from one flowmeter to another. Hence, these constants were left as inputs to the program(see Appendix B).

Photographic information was used to determine the displacement of the interface, the bubble growth and collapse rates, and the water slug height. The 16 mm movies were projected on a screen and a preliminary survey was made to determine the portions of interest. Starting from a frame in which the interface had just moved, the location of the interface was measured from the tube exit plane. The number of frames during which the interface moved a certain distance was then counted. The exact frame speed during this period was determined from the neon timing-light marks on the film. The movies have been coded according to the data and experimental conditions. The

TABLE 2.1 TEST MATRIX

| Run No. | Pool Temp. °C | Measurements | Pipe O.D./ I.D., cm. | Submergence Depth, cm. | Pipe Material | Steam Generation rate, gm/sec |
|---|---|---|---|---|---|---|
| 1 | 43.9 | A,B | 5.08/3.81 | 25.4 | Plastic | 7.56 |
| 2 | 50.0 | A,B | 5.08/3.81 | 25.4 | Plastic | 7.56 |
| 3 | 55.6 | A,B | 5.08/3.81 | 25.4 | Plastic | 7.56 |
| 4 | 61.7 | A,B | 5.08/3.81 | 25.4 | Plastic | 7.56 |
| 5 | 67.8 | A,B | 5.08/3.81 | 25.4 | Plastic | 7.56 |
| 6 | 73.9 | A,B | 5.08/3.81 | 25.4 | Plastic | 7.56 |
| 7 | 83.9 | A,B | 5.08/3.81 | 25.4 | Plastic | 7.56 |
| FM1 | 53.9 | A,B,C,D | 5.08/4.45 | 25.4 | Plastic | 7.56 |
| FM2 | 62.8 | A,B,C,D | 5.08/4.45 | 25.4 | Plastic | 7.56 |
| FM3 | 37.2 | A,B,C,D | 5.08/4.45 | 50.8 | Plastic | 7.56 |
| FM4 | 46.1 | A,B,C,D | 5.08/4.45 | 50.8 | Plastic | 7.56 |
| FM5 | 62.8 | A,B,C,D | 5.08/4.45 | 50.8 | Plastic | 7.56 |
| VP1 | 37.2 | A,B,E | 6.03/5.10 | 24.1 | Steel | 7.56 |
| VP2 | 46.7 | A,B,E | 6.03/5.10 | 24.1 | Steel | 7.56 |
| VP3 | 58.9 | A,B,E | 6.03/5.10 | 24.1 | Steel | 7.56 |
| VP4 | 64.4 | A,B,E | 6.03/5.10 | 24.1 | Steel | 7.56 |
| MIX1 | 57.2 | A,B,D,E | 6.03/5.10 | 25.4 | Steel | 7.56 |
| MIX2 | 61.7 | B,D,E | 6.03/5.10 | 25.4 | Steel | 7.56 |
| ST1 | 40.0 | B,E,F | 6.03/5.10 | 25.4 | Steel | 7.57 |
| ST2 | 46.7 | B,E,F | 6.03/5.10 | 25.4 | Steel | 7.57 |
| ST3 | 53.3 | B,E,F | 6.03/5.10 | 25.4 | Steel | 7.57 |
| ST4 | 61.7 | B,E,F | 6.03/5.10 | 25.4 | Steel | 7.57 |

A = Bottom Pressure, B = Exit Temp., C = Side Wall Pressure, D = Steam Velocity,

E = Vent Pressure, F = Surge Tank Pressure

movies are stored in the Nuclear Energy Laboratory of the Chemical, Nuclear, and Thermal Engineering Department of the School of Engineering and Applied Science at the University of California, Los Angeles. The movies and the raw data are available on request.

## 2.4 Experimental Error Bounds

This section gives a summary of the error bounds involved in the various instruments used in the experiments. In general, the error involved in these instruments was acceptable with the exception of the hot-wire anemometer.

(a) Error involved in temperature measurements:

The thermocouple output was connected to a galvanometer and the eye-ball accuracy of the scale of the instrument was $\pm$ 1.0°C. The error involved in the thermocouple itself is less than 1.0°C. The response time of the gage 36 chromel-alumel thermocouples was tested and was found to be on the order of 20 msec. A typical picture of the thermocouple response as seen on the screen of an oscilloscope is shown in Figure 2.6.

(b) Error involved in pressure measurements:

The reference pressure for the pool bottom pressure transducer could be off by approximately half an inch of water since the pool water level slightly changes throughout the experiment due to the steam injection. This corresponds to an error of .128 kPa. The error involved in the actual measurements was less than 0.75% of the rated value, e.g., for a 344.5 kPa transducer, the error will be less than 2.58 kPa. As for the time response, the manufacturer

provided a response time to a step pressure of less than one milli-second.

(c) Error involved in flow meter measurements:

Hot-wire anemometers were used to measure steam velocities. However, since most manufacturers were not equipped with a steam facility, a calibration test was performed. Due to the additional temperature effect on the electronics, large errors were expected in the velocity data up to a few hundred percent. Therefore, the magnitude of the velocity measured was not reliable. However, these probes have response times as fast as 0.1 ms. Hence, the measurements would give accurate times for which large velocity changes occur. Appendix B presents the details of the calibration test.

(d) The error in the synchronization:

A check was made on the synchronization by comparing the movie data and the exit temperature data. The time at which a step jump in temperature as the interface swept across the thermocouple junction was compared to the time from the movie data at which the interface clears the thermocouple. The comparison shows that the synchronization could be off by as much as 10 msec (the response time of the thermocouple was taken to be 20 msec in this comparison) in some runs. But for most of the runs, the comparison was within a few milli-seconds.

(e) Error in the neon timing lights on the film:

No exact value was given by the manufacturer, but the error between flashes was expected to be on the order of a micro-second.

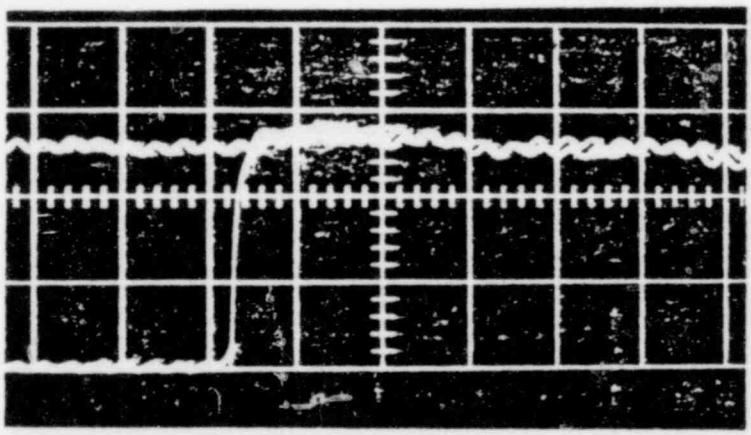

x = 50. ms/div.

y = 28.2$^{o}$C/div.

Fig. 2.6 Temperature Response of a Gage 36 Cr-Al Thermocouple When Dipped from Ambient to Boiling Water.

# CHAPTER 3

# RESULTS OF THE EXPERIMENTS AND OBSERVATIONS

## 3.0 Introduction

This chapter summarizes the results of the experimental study which represents the first stage of the approach taken to investigate the problem of low flow vapor injection. As mentioned in Chapter 1, two steps were taken in this stage. The first step began with a qualitative study of the problem of vapor injection in general. Then, the emphasis was focused on the low flow injection process or steam chugging. The results of this step provided a basic understanding of the vapor injection process, and also detailed information concerning the relationship between the interfacial motion and the hydrodynamic loads at the pool boundaries. In the second step, the emphasis was to obtain information concerning the dynamics of the steam upstream of the interface. The physical parameters concerning the thermal-hydraulics of the steam were measured in an attempt to relate the upstream phenomena to the interfacial motion observed in the first step. An overall physical picture was then formulated to facilitate the development of the theoretical model.

## 3.1 Visual Experiments--Qualitative

This section presents the results of the set of qualitative experiments made to obtain some general understanding of the vapor

injection problem in general.

It is well known in two-phase flow that numerous flow regimes exist and can be classified in terms of a flow regime map with the axes composed of the parameters signifying the physically competitive mechanisms: namely, the liquid phase flow rate and the gas phase flow rate . The vapor injection problem is similar in nature. It involves the competitive processes of vapor injection and condensation. Thus, a condensation regime map, which characterizes the numerous condensation modes, is expected to exist. The natural parameters for the classification are expected to be the pool subcooling, which characterizes the condensation rate and the vapor injection rate.

The following sections give the criteria used in separating the various condensation regimes, and the resulting condensation regime map. It is shown that the interfacial motion admits certain characteristic patterns for different ranges of the vapor injection rate and pool temperatures.

### 3.1.1 The Criteria for Separating the Condensation Regimes

As mentioned in Section 1.2, Greef, in his vapor injection experiments, had observed that the stable cone-shaped vapor jet which prevails at high vapor flow ceases to be stable as the flow becomes subsonic. Hence a natural dividing line between stable and unstable jets is the sonic transition. However, the main objective of the present study is focused on the low flow situation where the Mach number of the steam is on the order of 0.1. In this low flow

region, an additional complexity is introduced because of the peculiar dependence of the condensation processes on the pool temperature. Thus, in contrast to the high flow situation, with the steam flow being the only important parameter, in the low flow case, both the pool temperature and the steam flow are of equal importance.

Since vapor injection means the existence of a continuously fed vapor region in a subcooled liquid, the criteria established for differentiating the various condensation modes were hinged upon the dynamics of this vapor region. In the low pool temperature situation, the vapor region normally exists as a cone or a bubble with a diameter approximately the same as the injection pipe. Furthermore, this vapor region usually occupies the space below the pipe exit. However, in the high pool temperature situation, the vapor region usually has a diameter larger than that of the injection pipe. Furthermore, the vapor region tends to extend above the pipe exit and encapsulate part of the pipe. Hence a natural criteria to separate the condensation modes is whether the vapor region exists above or below the pipe exit. This leads to the horizontal separation line at around $75^{o}C$ on Figure 3.1.

The other criterion which leads to the vertical separation lines on Figure 3.1 is related to the release of steam bubbles from the oscillatory vapor region. In the low pool temperature situation, at high steam mass fluxes, the bubbles detach from the oscillatory cone at its tip, which is usually a couple of pipe diameters below the exit. As the mass flux reduces, the point at which bubble detachment occurs is moved up to within one pipe diameter below the

exit. This is where the bubble oscillation region begins. The distance between the point of detachment and the pipe exit is so close that the shape of the steam region resembles that of an oscillating spherical bubble. Further reduction in steam mass flux causes the detachment point to move closer to the vent exit and periodic rushes of water up the pipe occur. This is called the steam chugging region.

At high pool temperatures ($>80.^{o}C$), the bubble detachment process is similar but the point at which detachment occurs could be above the vent exit. In these cases, the detached bubble floats up towards the pool surface while condensing.

Using the above mentioned criteria, a condensation regime map was established. Owing to the crude methods used in estimating the steam mass flux, the boundaries of the various condensation regimes were only approximate. However, these estimates were accurate enough for illustrating the existence of the various characteristic interfacial motion patterns for different ranges of pool temperatures and steam mass fluxes.

### 3.1.2 The Condensation Regime Map

Figure 3.1 shows the results of this set of experiments based on the criteria established in the previous section. The range of mass flux covered was roughly from 175.0 $kg/m^2$-sec to 1.0 $kg/m^2$-sec. corresponding to Mach. Nos. of 0.1 to 0.5. The range of pool temperatures covered was from $30^{o}C$ to $90^{o}C$ while the pool pressure was atmospheric.

When the pool temperature is above $70^{o}C$, the steam region encapsulates the vent exit. At high mass fluxes, the steam region is ellipsoidal with a small diameter of approximately eight vent

diameters. The long axis of the ellipsoid is parallel to the vent pipe, and it has a length of about ten pipe diameters. It should be mentioned that although the initial pool level was only ten pipe diameters the steam injection caused a rise in pool level of about 10. - 12. cm. No obvious bubble detachment was observed. It is apparent that the wavy interface of the ellipsoid is responsible for all the condensation that is taking place.

At lower steam mass fluxes (Region 2), the steam region exists as a smaller ellipsoid as shown in Figure 3.2. The steam region still encapsulates the pipe exit due to the high pool temperature; however, an obvious detachment process is identified. Starting from the point when a detachment has just occurred, the steam region that encapsulates the pipe exit will start to grow again to attain an ellipsoidal shape. As the growth achieves a maximum, the ellipsoid begins to translate downwards due to the steam momentum, while a circumferential instability begins to develop around the steam region like a belt. Then, as the translation progresses, the "belt" develops into a penetrating layer of liquid which cuts off the lower portion of the ellipsoid. This portion once detached from the main region will collapse while another ellipsoid will develop at the exit and the process repeats. The detachment frequency of this type of bubble is about 11.0 Hz.

At still lower mass fluxes (Region 3) the steam region moves up to encapsulate more of the vent pipe as shown on Figure 3.3. The point at which detachment occurs is above the vent exit. The detachment process initially starts out as a liquid "belt" around the

cylindrical bubble which is translating upwards after it achieves its maximum size. As the liquid "belt" tightens, the steam region above the "belt" is separated from the steam region below. This separated volume of steam condenses as it floats up towards the pool surface. The lower steam region which is still encapsulating the pipe exit then begins to grow to another cylindrical column and then another "belt" forms and the process repeats. The detachment frequency is about 7. Hz for this type of bubble.

For pool temperatures below 70°C, at high mass fluxes (Region 4), the steam region exists as an oscillatory conical jet below the vent exit (Figure 3.4). The detachment point is about 1-1/2 pipe diameters below the vent exit. The bubble detachment process starts off as a liquid "belt" wrapped around the cone. As it begins to penetrate into the vapor cone, the vapor cone is translating downwards. Eventually when detachment occurs, the cone has already moved approximately half a pipe diameter's distance. This process may also be thought of as an instability which grows as the vapor region translates downwards away from the exit, and eventually the instability grows large enough to "cut off" a volume of vapor from the vapor cone. The frequency of detachment is around 40 Hz.

At lower steam mass fluxes, the initial position of the instability occurs at the pipe exit. Thus the actual point at which detachment occurs moves up to within one pipe diameter below the exit which causes a change in shape of the vapor region (Figure 3.5 ) from that of an oscillatory cone to that which resembles more of an

oscillatory bubble. The frequency of bubble detachment is about 26 Hz.

Further reduction in the steam mass flux causes the point of detachment to move toward the exit. Eventually, a point is reached where the point of detachment is right at the exit. This is taken as the boundary for the steam chugging regime because the vapor region could only exist periodically in the pool and the pool water periodically enters the pipe. The chugging regime can be separated into three different regions with distinct characteristics.

When the pool temperature is below $40^{\circ}C$(Region 6c),it is observed that all the condensation occurs basically inside the pipe. This type of chugging is therefore called internal chugging. Bubble formation at the pipe exit is a rare event, since the interface rarely moves below the vent exit. The frequency of this type of chug is about 2 - 3 Hz.

At higher pool temperatures($40^{\circ}C$-$60^{\circ}C$,Region 6b), the interface is able to progress beyond the pipe exit. A small cylindrical vapor region is formed below the pipe exit. However, immediately after the formation of the cylindrical bubble, a rush of the surrounding water toward the vapor region is observed. This rush of water simply separates the cylindrical vapor region from the pipe. Thus, a detached bubble is formed in the pool; and, therefore, this type of chugging is referred to as detached bubble chugs. After the detachment, a rush of water up the vent pipe follows. This type of chugging occurs at a frequency of about 2 - 3 Hz.

For pool temperatures around 60°C - 80°C, another type of

chugging process dominates. This type of chugging involves the formation of a bubble after the interface has progressed beyond the pipe exit. As the bubble grows, the vapor region begins to encapsulate the pipe exit. This type of chugging is therefore called the encapsulating bubble chug. The collapse of this type of bubble is also initiated by the formation of a circumferential instability around the bubble. It bears some similarities to the high pool temperature bubbles except for the fact that the collapse of this type of bubble generally leads to a rush of water into the exit. The frequency of occurrence for this type of chug is typically 1 - 2 Hz. The reduction in the frequency is due to the additional time taken for the bubble growth process.

The last condensation regime in this discussion (Region 7) involved no detachment process and the steam-water interface exists right at the pipe exit. The steam mass flux is very low in this regime; in fact, the flow is so low that it is impossible to determine the steam mass flux in the present experiments. This condensation regime is characterized by an oscillatory interface at the pipe exit. The oscillations are just sufficient to induce convective processes in the water to remove the heat from the condensation at the interface.

Finally, for pool temperatures above the dotted line at the top of Figure 3.1, steam is observed to escape from the pool surface.

Hence, the rather complicated phenomena involved in vapor injection could be systematically classified in terms of a simple condensation regime map. The coordinates of the map were the pool

Fig. 3.1 The Condensation Regime Map

Vent Dia. = 5.08 cm  Pool Equivalent Dia. = 4.8 cm
Pool Pressure = 1 Atm.  Submergence Depth = 25.4 cm
Exit to Bottom Clearance = 25.4 cm

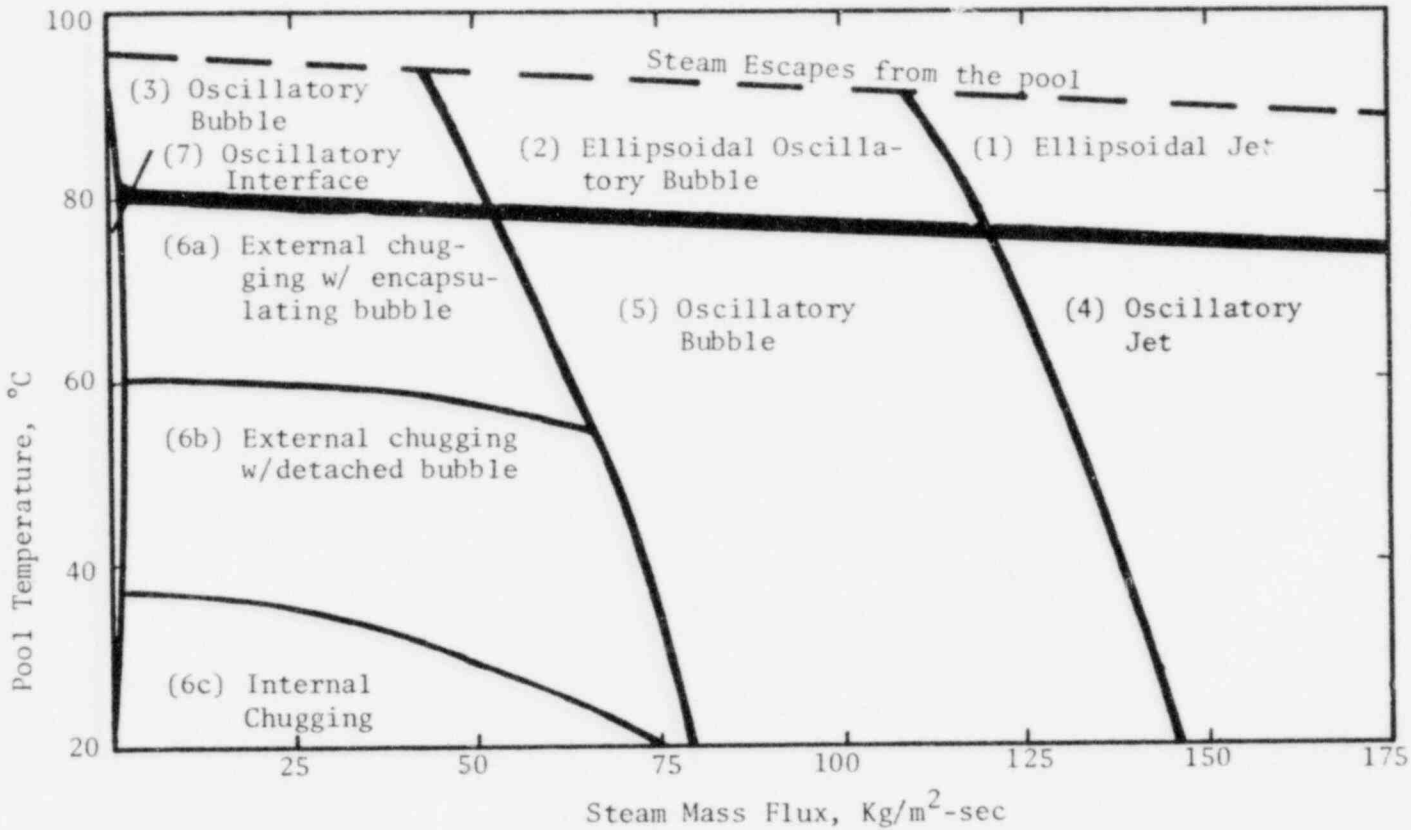

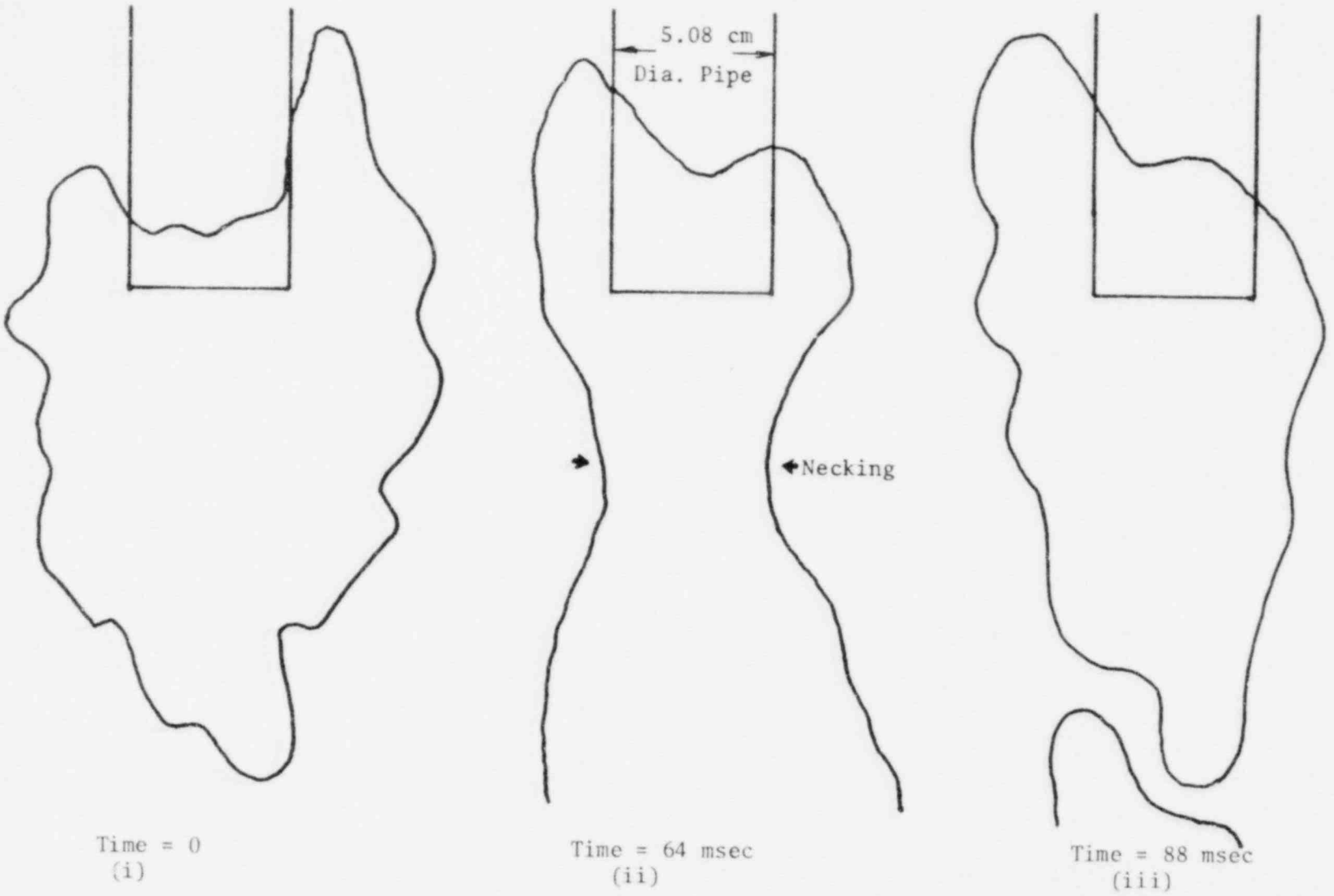


Fig. 3.2 Condensation Regime 2
High Pool Temperature, Intermediate Mass Flux
($>75.kg/m^2$-sec, $<150.kg/m^2$-sec)

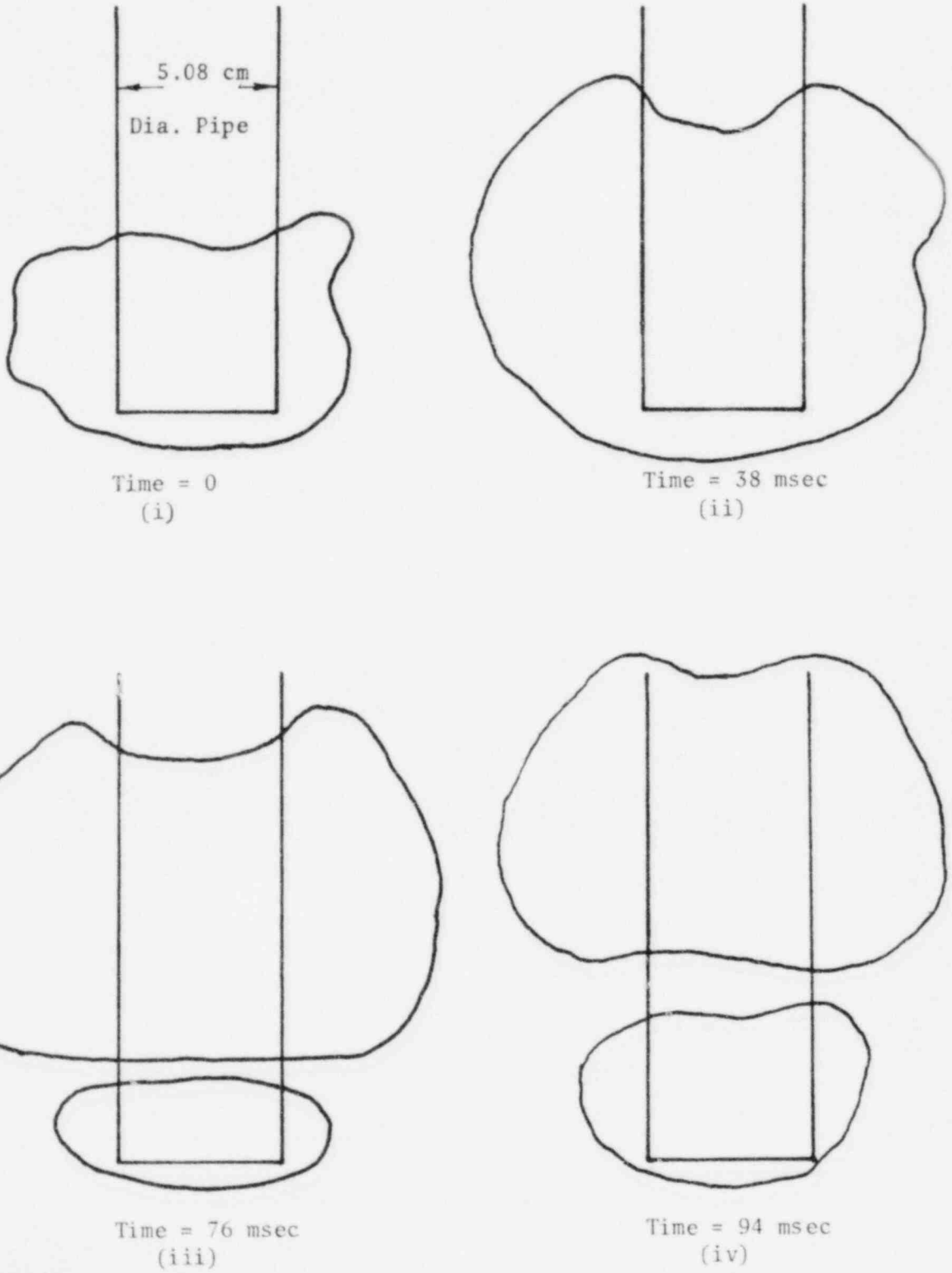


Fig. 3.3 Condensation Regime 3
High Pool Temperature, Low mass flux
($\lesssim 75. kg/m^2$-sec)

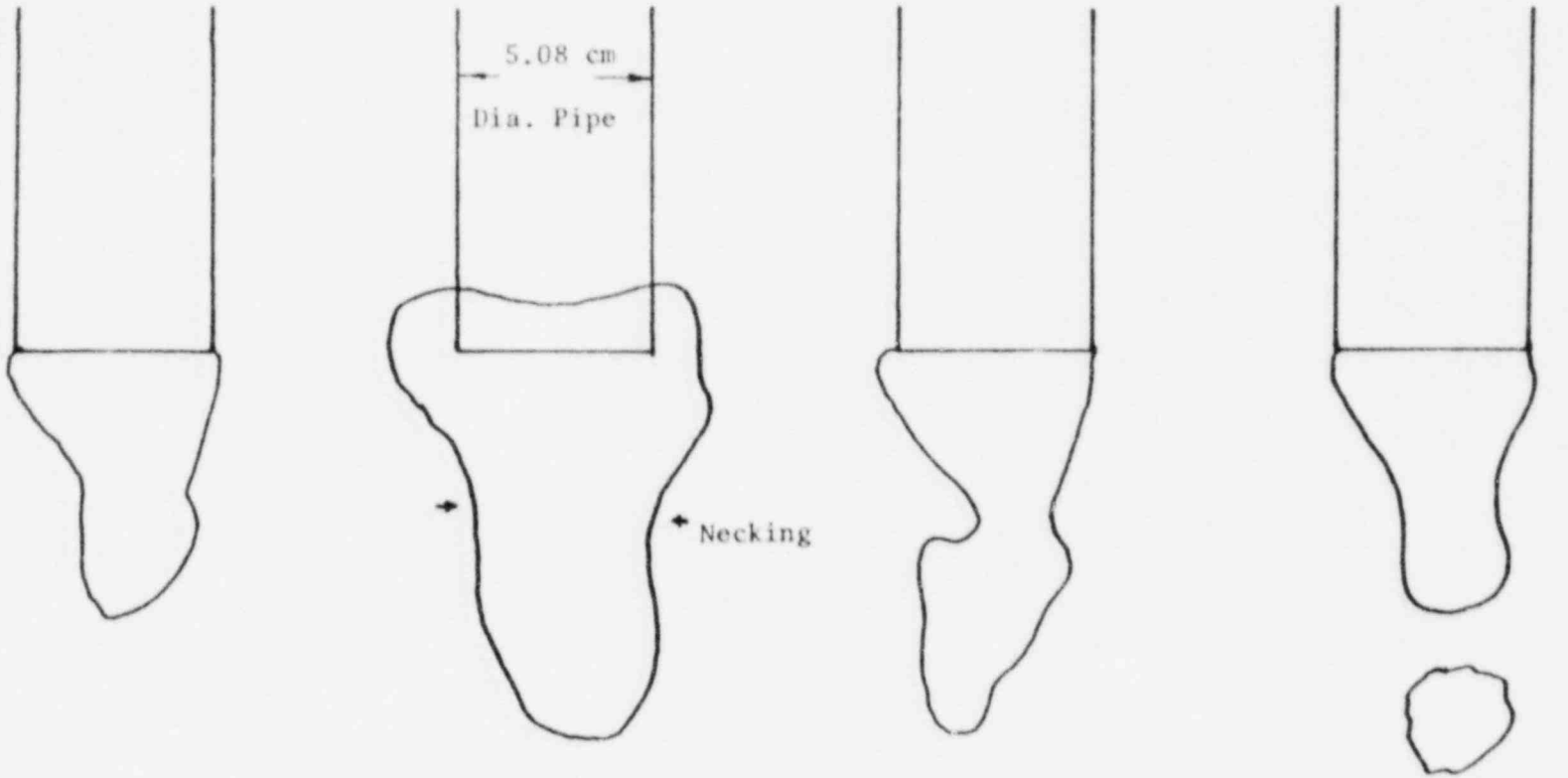


Time = 0
(i)

Time = 8 msec
(ii)

Time = 23 msec
(iii)

Time = 26 msec
(iv)

Fig. 3.4 Condensation Regime 4
Low Pool Temperature, High Mass Flux
(>150.kg/$m^2$-sec)

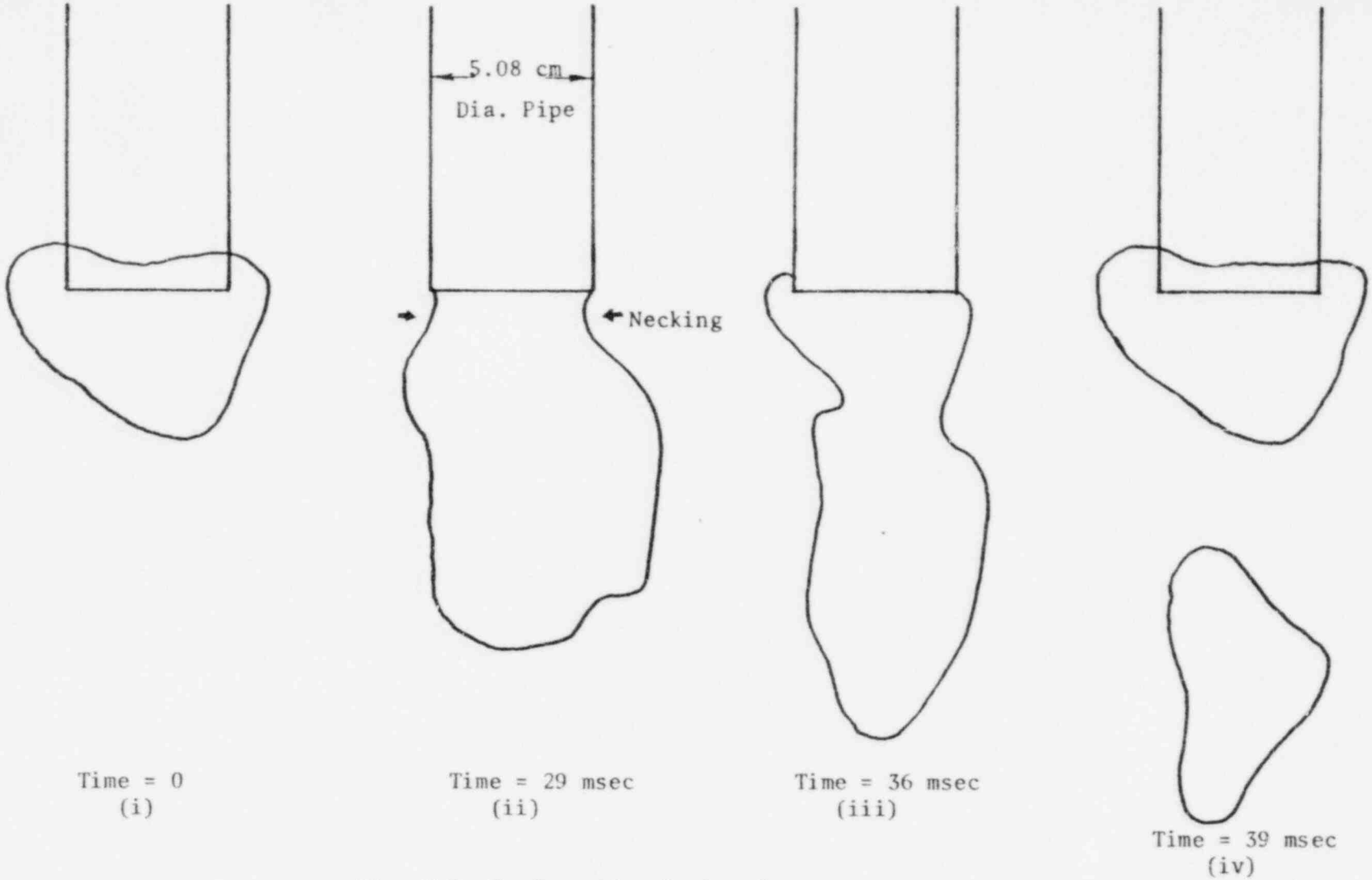


Fig. 3.5 Condensation Regime 5
Low Pool Temperature, Intermediate Mass Flux
($>75.kg/m^2$-sec, $<150.kg/m^2$-sec)

temperature which characterizes the condensation, and the steam mass flux which characterizes the driving mechanism. The classification was made based on two simple criteria involving the location of the vapor region relative to the injection pipe exit and the way at which bubble detachment occurs. Although this classification was obtained from a particular system geometry, it is apparent that all vapor injection systems behave in a similar way.

In the low steam mass flux situations, a phenomenon called steam chugging was observed. The corresponding pressure at the pool bottom indicated large negative and positive pressure spikes. The detailed study on these spikes are presented in the next section.

## 3.2 Detailed Experiments on the Interfacial Motion and the Hydrodynamic Loads on the Pool Structure

The qualitative results presented in the previous section indicated the existence of three different modes of condensation in the chugging process depending on the pool temperature. This section presents the results of the detailed experiments performed to study each of these modes. The first section (3.2.1) presents the detailed movie data as well as the physical observations, and the second section (3.2.2) shows the detailed pressure data measured at the pool solid boundaries.

### 3.2.1 Detailed Results on the Interfacial Motion

#### A. Internal Chug

At low pool temperatures ($\sim 40^{\circ}C$) the most frequent mode of chugging is the internal chug. The detailed interfacial motion

inside the vent pipe for an internal chug is shown on Figure 3.6. From the high speed movies it is observed that as the interface progresses down the pipe, an annular flow situation is developed such that the steam region is surrounded by a layer of liquid which is attached to the pipe wall. The development of this annular flow situation has to do with a flow separation phenomenon which occurs when the chug attains its maximum height in the vent. It is observed that as the water slug approaches its maximum height, the interface spreads from that of a horizontal flat interface to an inclined interface. A portion of the interface is retreating while the rest is still progressing upwards. Steam begins to flow towards the exit following the portion of the interface which is retreating. Thus a flow separation situation is created where the steam flows downwards towards the exit while the rest of the water slug is still moving upwards creating an annular flow situation inside the vent as depicted in pictures 1, 2, and 3. Notice the smooth and glassy nature of the interface during this period.

As the steam progresses further down towards the exit, a small interfacial instability begins to develop (picture 2). As this instability grows, it begins to penetrate into the steam region; and, eventually, it "bridges" the gap between the wall liquid layers isolating a small volume of steam from the main stream (picture 5). Following the "bridging," the isolated bubble starts to collapse. It reaches a minimum volume as shown in picture 6 and then rebounds in picture 7 while shattering to a mist of small bubbles at the same time. The steam in the bubble is being

compressed, due to the liquid inertia, to a high pressure; although in this case the compression is only moderate.

While the interesting bridging phenomenon is taking place at the end of the steam region, a more interesting phenomenon is occurring on the pipe wall. The stable glassy interface of the wall liquid layers in picture 2 are rapidly becoming wavy and rough as the water front stopped moving at picture 3. Notice that the water front stayed at approximately the same location from picture 3 to picture 8. This premature slow-down of the water slug motion indicates that the steam pressure in the vent is below that of the water in the pool. Moreover, it is apparent that as the water front stopped its motion, the liquid layers draining off of the upper part of the pipe began to accumulate at the vicinity of the water front. The phenomenon not only causes a rapid roughening of the interface, but also the formation of some water droplets due to the shearing force between the liquid layers. The rapid increase in the heat transfer surface causes a sudden rise in the local condensation rate. Thus, the initially low steam pressure suffered another rapid decrease which leads to the collapse of the entire steam region at that vicinity (picture 8). This is the physical mechanism which is responsible for the underpressure developed in the pipe which in turn provides the suction force to pull a slug of water up the pipe.

Hence, the "bridging" phenomenon, which causes the bubble to be isolated, is the initiating mechanism which leads to the hydrodynamic loads which are generated by the collapse and rebound of the isolated bubble. The accumulation of draining liquid layers at the

Run No. FM3, Pool Temperature = 37.2°C

Note : Arrows indicate direction of liquid jet penetrati· n

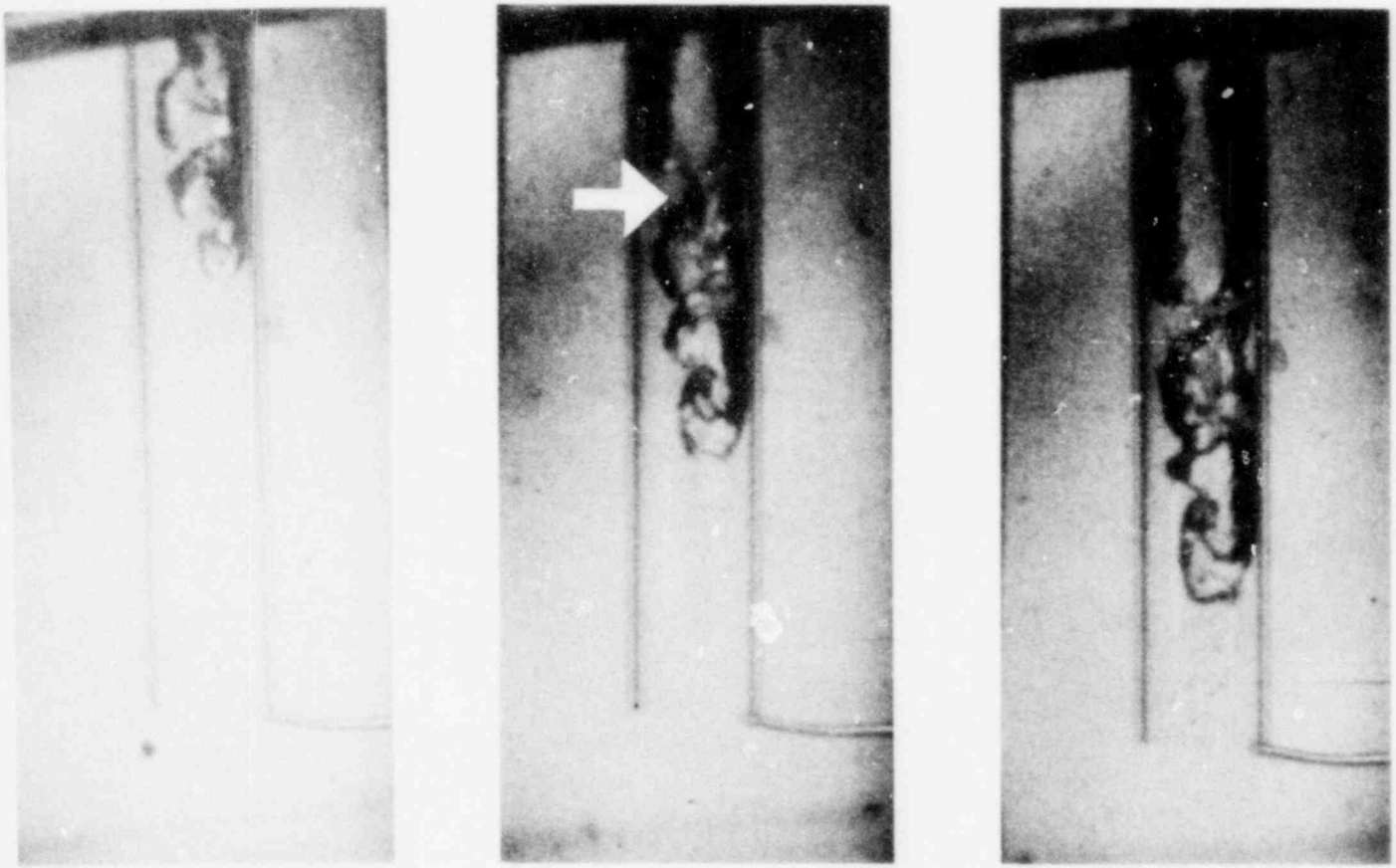

Picture (1) 0.0 ms

Picture (2) 15.6 ms
Liquid Bridging Begins

Picture (3) 24.8 ms
Bridging Continued

Fig. 3.6 Photos of Interfacial Motion:Internal Chug

Internal Chug

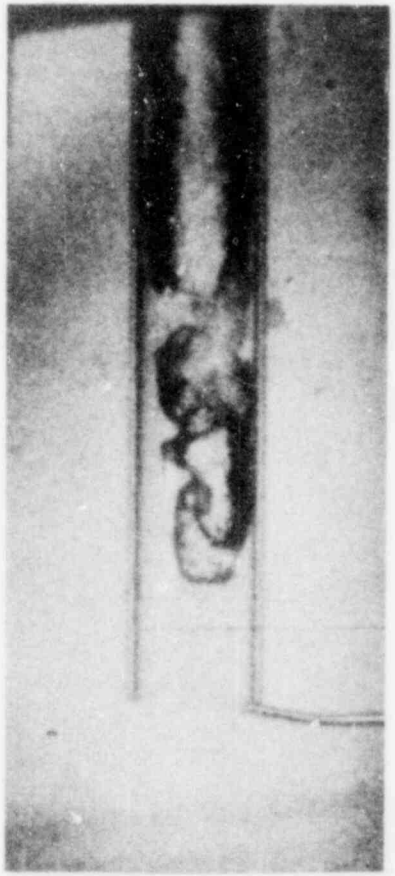

Picture (4) 27.2 ms
Bridging (cont'd)

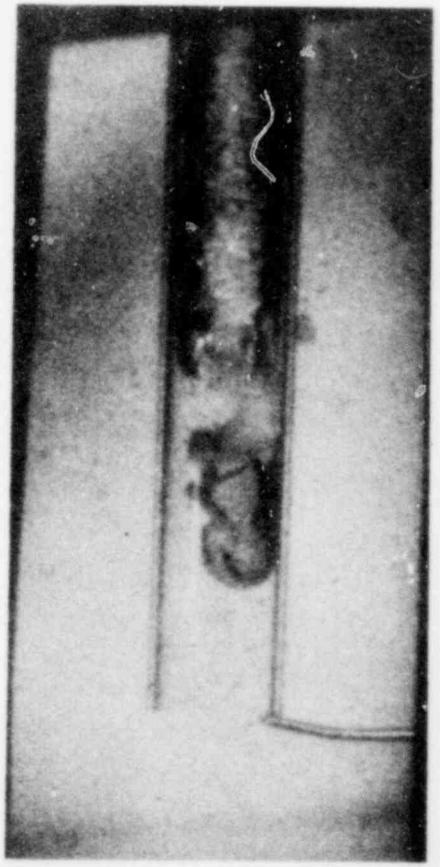

Picture (5) 29.6 ms
Bridging Complete

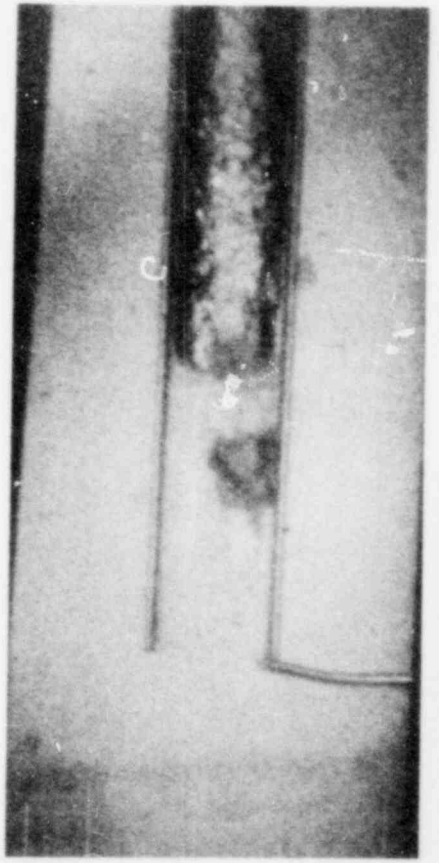

Picture (6) 30.8 ms
Collapse

Fig. 3.6 (Cont'd)

Internal Chug

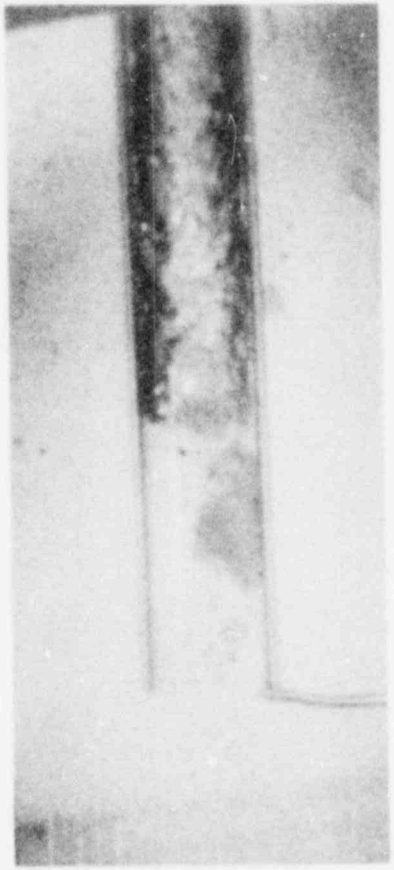

Picture (7) 32.8 ms

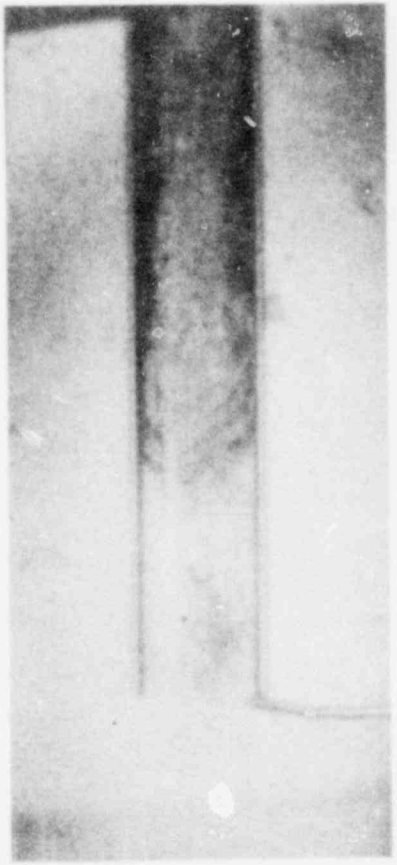

Picture (8) 42.8 ms

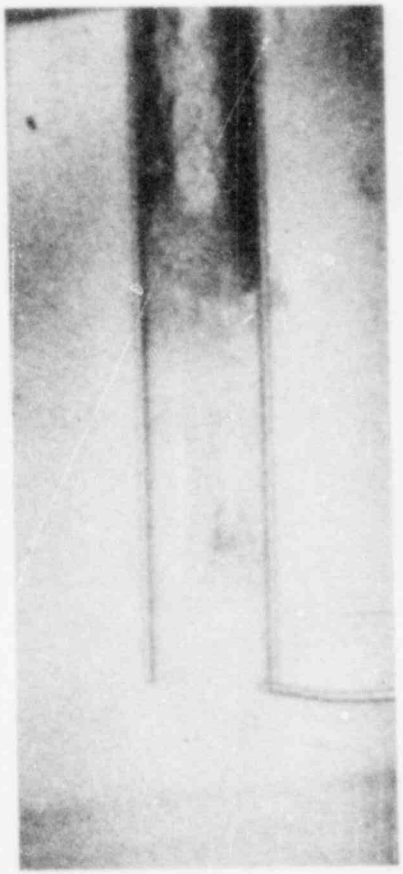

Picture (9) 60.8 ms

Fig. 3.6 (Cont'd)

exit is the main cause for the underpressure in the pipe that provided the suction force for the chug. Chug heights are usually very high (~10 pipe dia. above the exit) due to the large magnitude of the underpressure.

B. Detached Bubble Chug

Another frequently observed mode of chugging at low pool temperatures (~50°C) is the detached bubble chug. In this case the steam-water interface is able to progress beyond the pipe exit forming a cylindrical bubble in the pool (Figure 3.7, pictures 1 and 2). The interface velocity is seen to be high during the discharge. However, the resulting bubble in the pool immediately begins to collapse. This is apparent from the constrast depicted at the bubble surface. The glassy interface of picture 2, which is a characteristic of a stable growing steam region, turned into an unstable rough surface, a characteristic of a collapsing steam region. The immediate collapse indicates that the steam pressure at the interface as it clears the vent exit is below that of the surrounding pool water. However, the rapid collapse is a result of the penetration of a number of liquid jets into the bubble (picture 4). The upper ones which are closer to the exit cause the bubble to be detached from the pipe before the collapse is completed. The high interface velocities developed at the end of the collapse process indicate that the steam in the bubble suffered a large compression before it was finally shattered into a mist of small bubbles.

At the same time, the liquid layers draining off of the pipe wall start to accumulate at the exit; and, eventually, cause a

Run No. FM3, Pool Temperature = 37.2°C

Note : Arrows indicate direction of liquid jet penetration

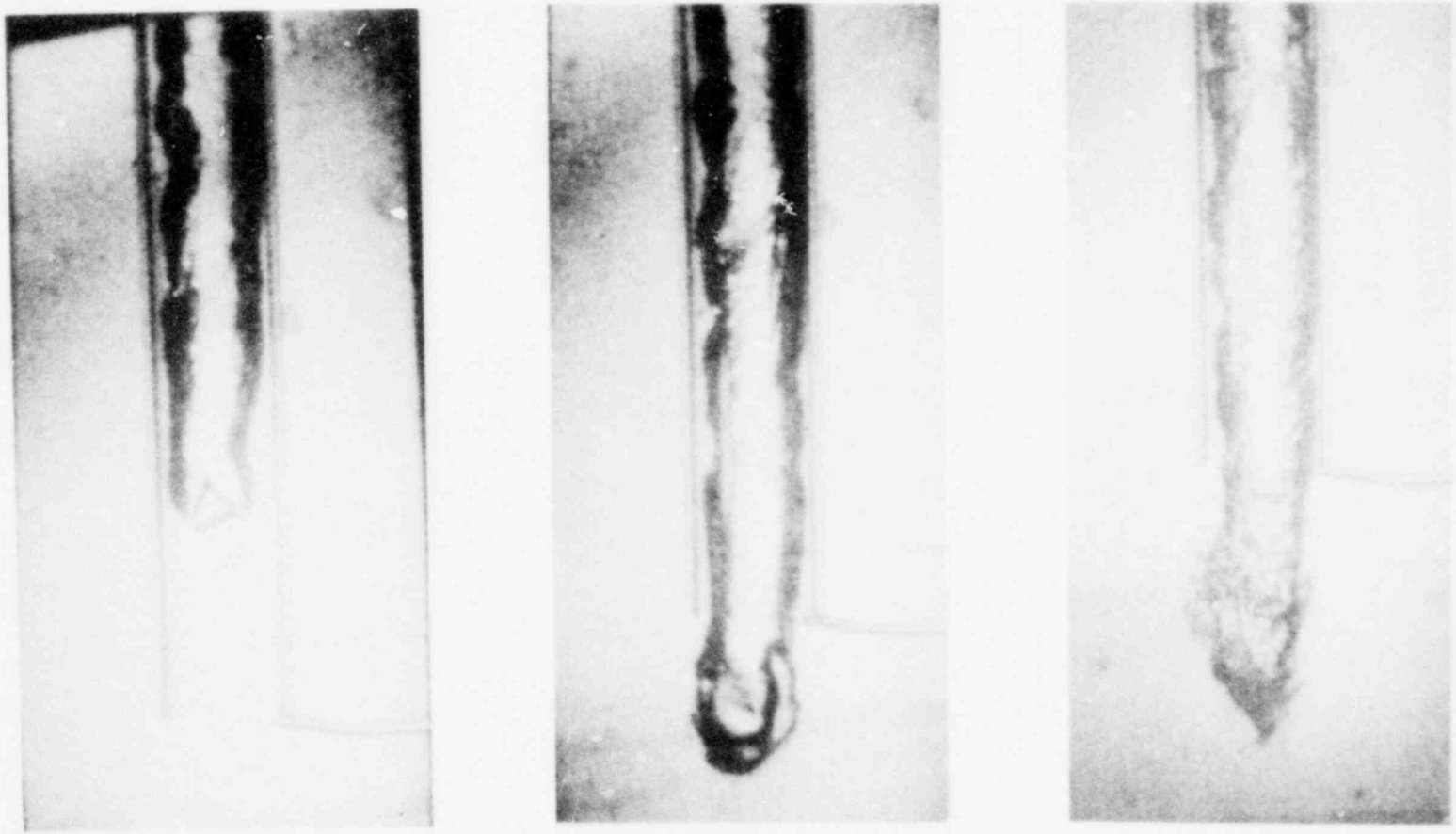

Picture (1) 0.0 ms

Picture (2) 26.8 ms

Picture (3) 40.0 ms

Fig. 3.7 Photos of Interfacial Motion:Detached Bubble Chug

Detached Bubble Chug

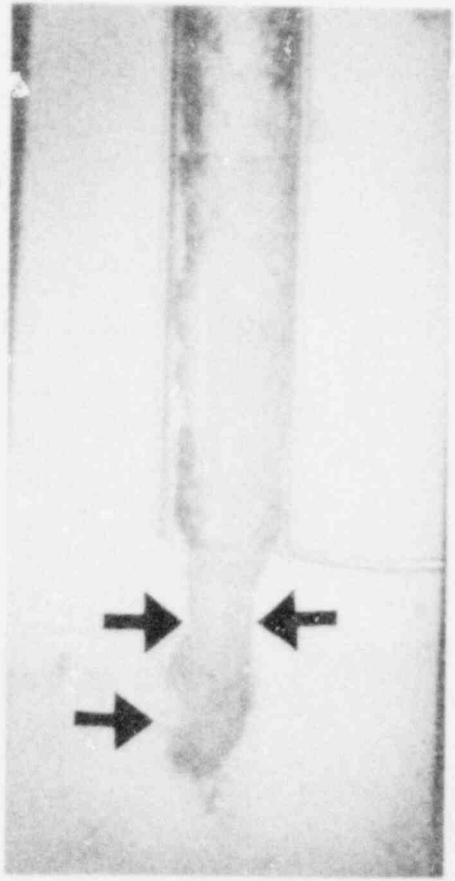

Picture (4) 42.2 ms

Picture (5) 43.6 ms

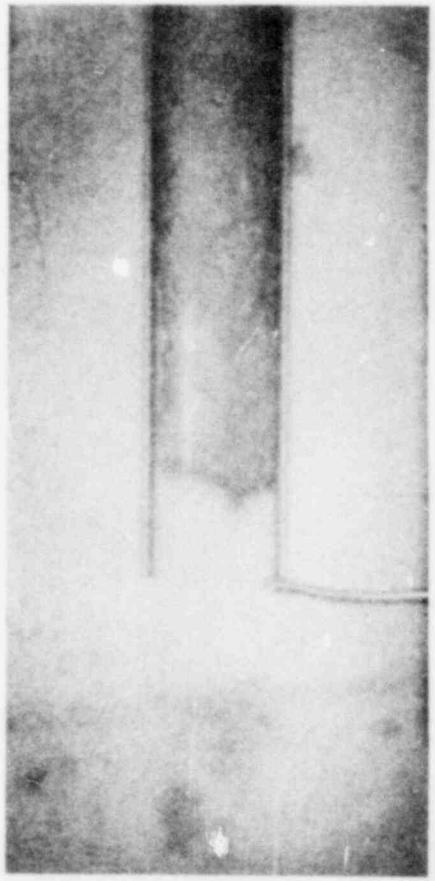

Picture (6) 48.8 ms

Fig. 3.7 (Cont'd)

collapse of the entire steam region at that vicinity, forming a two-phase mixture as depicted in picture 5.

This type of chugging is characterized by high chugging heights ($\sim$8 dia. above the exit), low steam pressure during interface clearing, and high discharge velocity. The hydrodynamic loads are again generated by the bubble collapse and shattering while the underpressure in the vent, caused by the liquid accumulating at the exit is responsibile for the suction force for the chug.

C. Encapsulating Bubble Chug

At higher pool temperatures ($\sim$50°C), the encapsulating bubble chugs are more frequent. The characteristics of this type of chug are: as the interface clears the vent exit the steam region immediately spreads out and grows upwards to encapsulate the vent. This indicates that the steam pressure is high as the interface clears the exit. The discharge velocity for this type of chug is generally low as compared to the detached bubble chug. Also the chugging heights are usually lower ($\sim$3 pipe dia. above the exit). As the growth reaches a maximum the bubble begins to translate upwards towards the pool surface while a liquid jet develops at the bottom of the bubble (Figure 3.8, pictures 6 and 7). The jet penetration from the bottom indicates that the bubble pressure, as well as the steam pressure near the vent exit at that moment, is below that of the surrounds. However, the collapse would have been quite mild if it were not for the penetration of the jet. In picture 8 the bottom of the bubble is flat as compared to the bubble in pictures 6 and 7. The liquid jet has already penetrated through the lower

part of the bubble into the vent pipe. It is clearly shown in pictures 9 and 10 that the lower half of the bubble is wavy and rough, indicating rapid condensation; while the upper half of the bubble is still smooth and shiny, indicating a stably growing interface. Picture 11 shows the shattered bubble after the collapse. In some cases, a rebound before shatter is observed, but generally the collapse is so rapid and irregular that the bubble shatters into a mist of smaller bubbles before the collapse is completed and no rebound is observed. However, the high interface velocity developed at the end of the collapse right before it shatters indicates that the steam is highly compressed and high pressures are generated.

The important feature of this type of chug is the liquid jet penetration from the bottom of the bubble. As the jet enters the vent exit from below, it not only cuts off the encapsulating bubble from the vent exit, but also becomes atomized and turns itself into a shower of droplets due to the liquid-solid impact. The sudden increase in heat transfer surface causes a rapid condensation of the steam in both the bubble and the vent exit vicinity. This leads to the rapid collapse of the bubble as well as an underpressure in the vent which provides the suction force for the chug. Another typical case for this type of chug is shown on Figure 3.9. The liquid jet penetration is even more obvious.

For this type of chug, the initiating mechanisms for both the bubble collapse and the vent underpressure is the penetration of the liquid jet. The bubble collapse in turn generates the hydrodynamic load while the vent underpressure causes the chug.

At still higher pool temperatures ($\sim$60°C), instead of having a liquid jet which penetrates vertically upwards, the liquid jet penetrates at an angle. Picture 5 in Figure 3.10 shows the initial penetration which resembles more of a circumferential penetration; however, the penetration occurs above the vent exit. The bubble is separated into two different bubbles, a lower one attached to the vent exit, and an upper one, surrounding the pipe. Both of them collapse at approximately the same time. In contrast to the previous case for lower pool temperatures, this type of chug does not lead to a large underpressure in the vent. The reason for this is due to the different way in which the liquid penetration occurs. The circumferential type liquid penetration does not cause an atomization in the vent because the penetration from the side is above the vent exit. The jet impinges onto the outside pipe wall, atomizes to a shower of droplets and causes the bubbles (upper and lower) to collapse rapidly. The underpressure which occurs in the vent caused by this type of chug is very mild as compared to the previous case. Thus, the chug heights are also reduced ($\sim$1 pipe dia. above exit). However, the hydrodynamic loads are expected to be comparable because the compression pressure caused by the collapse is expected to be about the same, the only difference being the smaller bubble size due to the separation. There may also be a "cushioning" effect, in the sense that one bubble acts as a cushion for the other during the collapse, which could reduce the collapse pressure. However, this is only valid when the bubbles collapse at different times.

Run No. FM3, Pool Temperature = 37.2°C

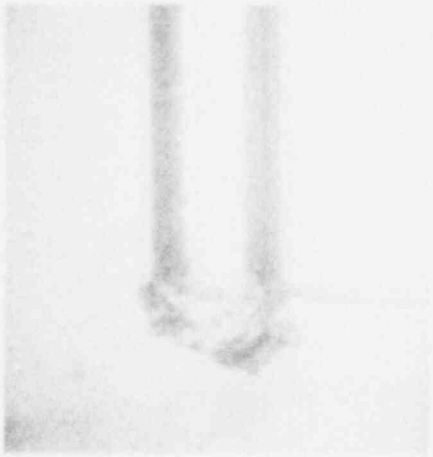

Picture (1) 0.0 ms

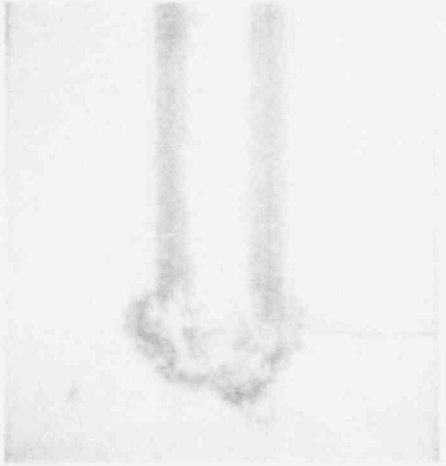

Picture (2) 8.8 ms

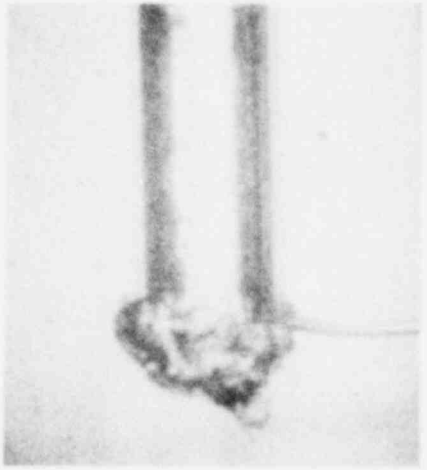

Picture (3) 13.2 ms

Note : Arrows indicate direction of liquid jet penetration

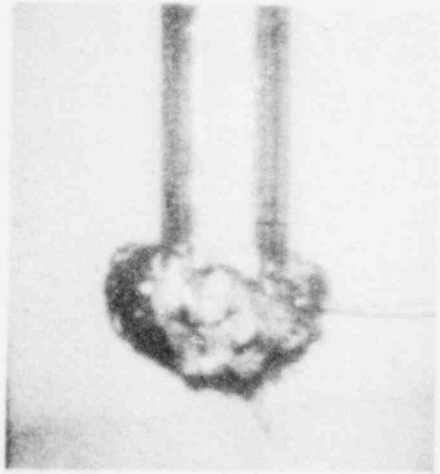

Picture (4) 18.4 ms

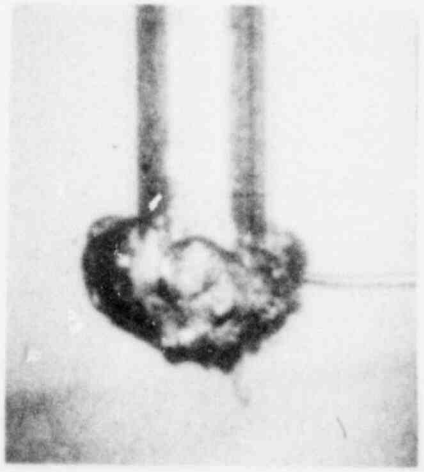

Picture (5) 22.4 ms

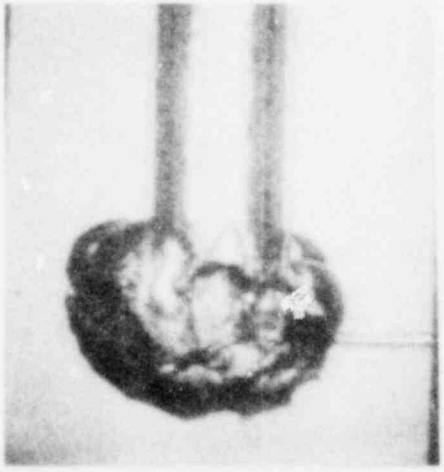

Picture (6) 37.2 ms

Fig. 3.8 Photos of Interfacial Motion:Encapsulating Bubble Chug

Encapsulating Bubble Chug

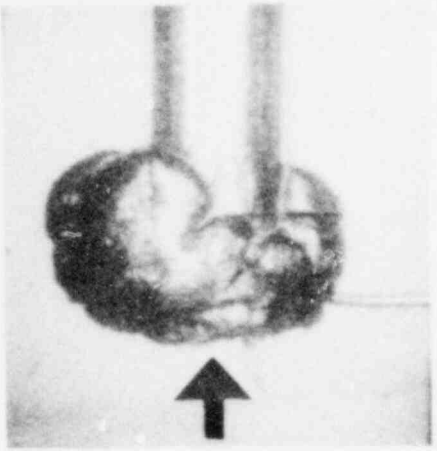

Picture (7) 51.2 ms

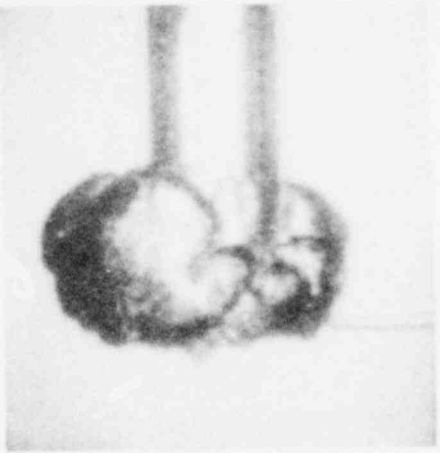

Picture (8) 62.8 ms

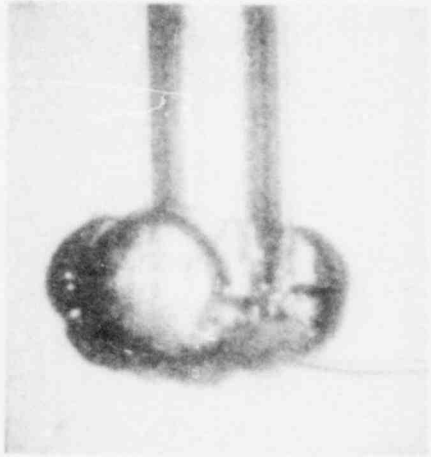

Picture (9) 63.2 ms

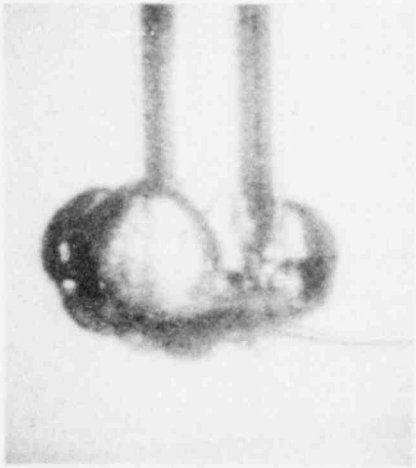

Picture (10) 64.0 ms

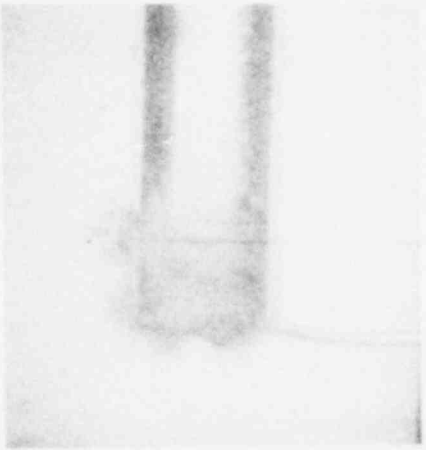

Picture (11) 66.0 ms
Fig. 3.8 (Cont'd)

Note : Arrows indicate direction of liquid jet penetration

Run No. VP3, Pool Temperature = 46.1°C

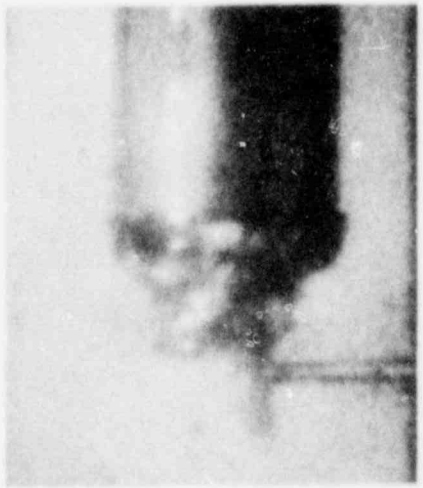

Picture (1) 0.0 ms

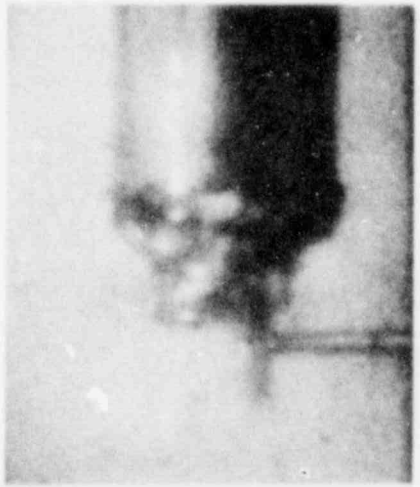

Picture (2) 2.0 ms

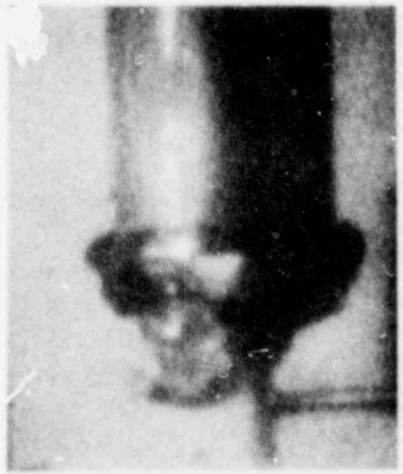

Picture (3) 6.4 ms

Note : Arrows indicate direction of liquid jet penetration

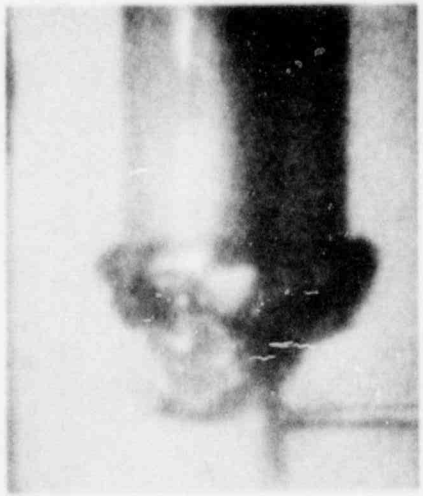

Picture (4) 8.4 ms

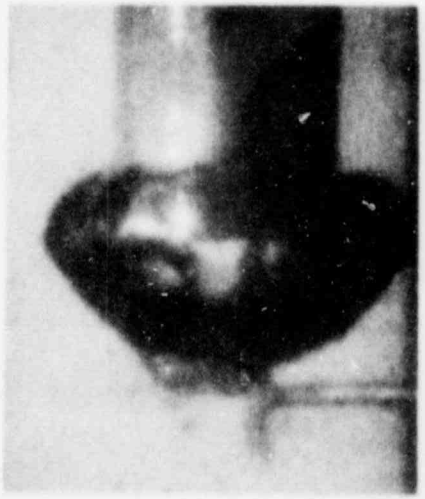

Picture (5) 20.4 ms

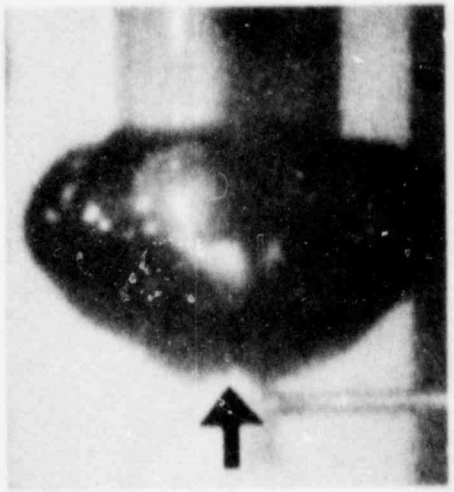

Picture (6) 36.8 ms

Fig. 3.9 Photos of Interfacial Motion:Encapsulating Bubble Chug (steel pipe)

Encapsulating Bubble Chug

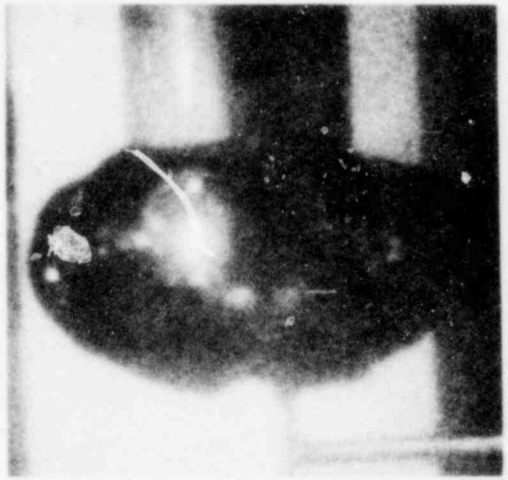

Picture (7) 48.4 ms

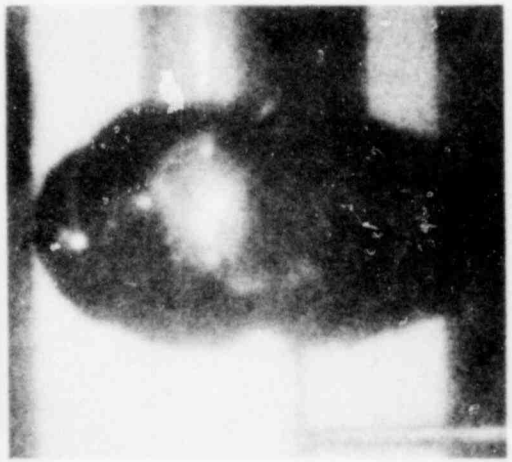

Picture (8) 56.0 ms

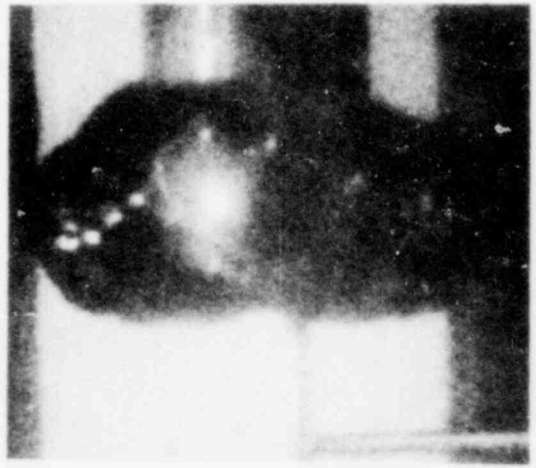

Picture (9) 64.8 ms

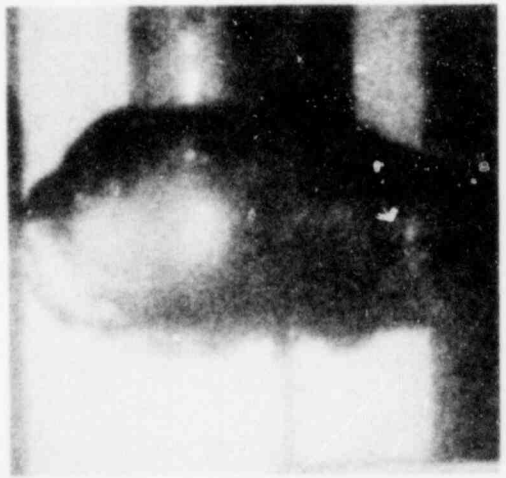

Picture (10) 70.8 ms

Picture (11) 72.4 ms

Picture (12) 73.6 ms

Fig. 3.9 (Cont'd)

Run No. FM5, Pool Temperature = 62.8°C

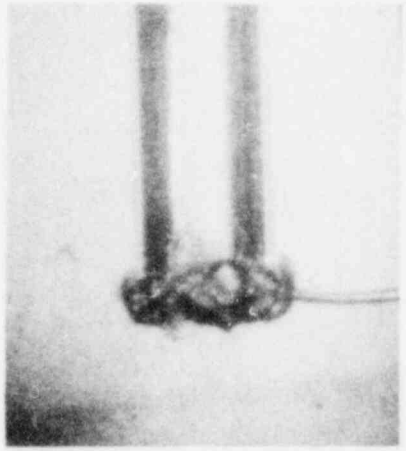

Picture (1) 0.0 ms

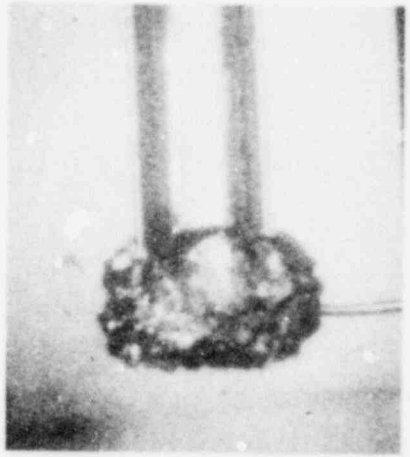

Picture (2) 15.6 ms

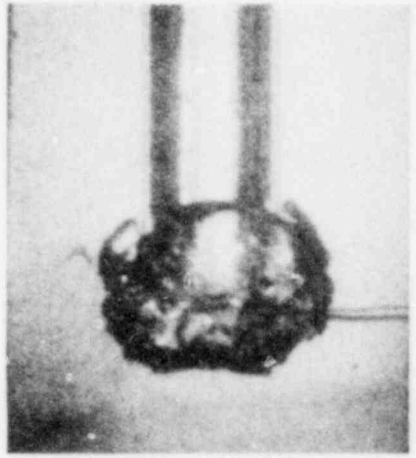

Picture (3) 25.6 ms

Note : Arrows indicate direction of liquid jet penetration

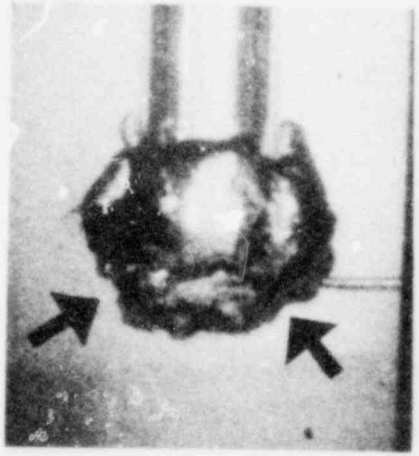

Picture (4) 35.2 ms

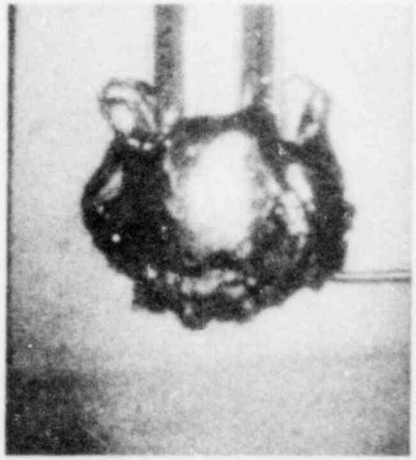

Picture (5) 42.4 ms

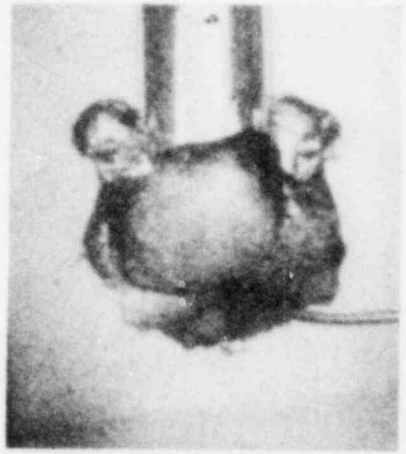

Picture (6) 50.4 ms

Fig.3.10 Photos of Interfacial Motion:Encapsulating Bubble Chug-High Pool Temp.

Encapsulating Bubble Chug - High Pool Temp.

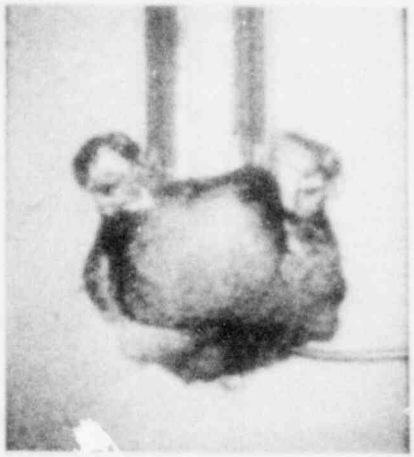

Picture (7) 51.6 ms

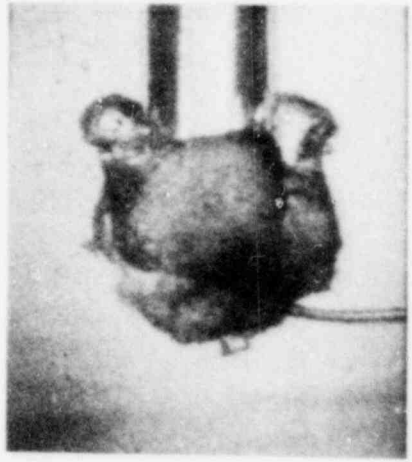

Picture (8) 52.8 ms

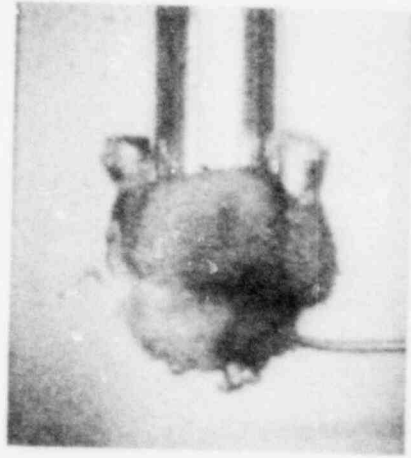

Picture (9) 54.0 ms

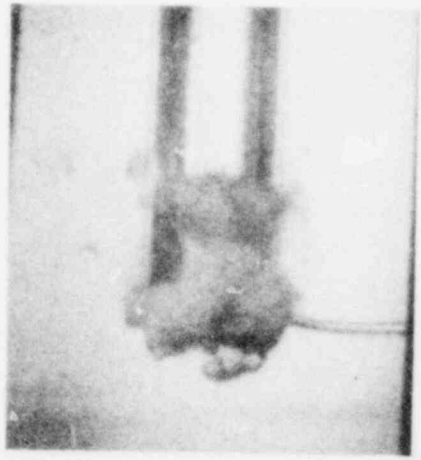

Picture (10) 56.0 ms

Note : Arrows indicate direction of liquid jet penetration

Fig. 3.10 (Cont'd)

### 3.2.2 Detailed Results on the Pressure Spikes at the Pool Solid Boundaries

#### A. Internal Chug

As described in the previous section, at low pool temperatures ($\sim$40°C), the most frequent type of chug is the internal chug. The measured pressure data at the pool boundaries indicate only mild pressure oscillations. This may be a consequence of two effects. First, the bubble collapses inside the pipe. Hence the pipe is acting as a shield preventing the pressure oscillations from propagating into the pool. Second, since the compression caused by the isolated bubble is observed to be quite mild (as shown in the motion pictures in the previous section), the pressures developed are expected to be small. Apparently, the initial size of the bubble has an effect on the compression. The collapse of larger bubbles normally leads to larger pressure overshoots. In this case, the initial bubble size is limited by the vent inner diameter, hence, the maximum pressures developed are only moderate.

#### B. Detached Bubble Chug

Pressure oscillations of considerable magnitude are observed for this type of chug. The measured pressure oscillations at the pool bottom show that a pressure undershoot is followed by a sharp overshoot. A typical pressure spike measured at the boundaries of the pool is shown on Figure 3.11. The magnitude of the spikes, both the negative and the positive, is approximately 10 kPa at the pool bottom and slightly less at the side wall. This type of chugging is most frequent for pool temperatures $\sim$50°C.

The pressure oscillations can be divided into two different

periods. The first one is from the point where the underpressure begins until the peak. The second period is referred to as the "ring out" by other workers in the field. It is believed that the "ring out" has to do with the fluid structure interaction following the initial pressure overshoot.

The physical picture obtained from the visual studies of the interfacial motion suggests that the initial pressure undershoot is due to the penetration of a liquid jet into the bubble. The increased heat transfer due to the jet causes an increase in the condensation rate which leads to a pressure undershoot. The reduced pressure in the bubble provides the driving force for the rapid collapse. However, towards the end of the collapse, the high velocities developed in the liquid tend to over-compress the steam which causes the pressure overshoot. The shattering of the bubble into a mist of minute bubbles terminates the event while the "ring out" continues.

From these observations, it can be deduced that the controlling parameters which affect the magnitude of the overshoot and the undershoot are the initial bubble radius and the heat transfer in the jet penetration period. The lower bound for the pressure undershoot in the bubble can be as low as the saturation pressure corresponding to the water temperature. This is true provided that the heat transfer caused by the liquid jet is high enough. Below that point the bubble pressure will cause boiling to occur at the bubble interface, which is not observed in the movies. The upper bound for the overpressure is more difficult to assign; it depends mainly on the initial size of the bubble, the initial underpressure caused by the jet, and

the particular way the bubble shatters. If the shatter occurs before the bubble reaches its first minimum during the collapse, the peak pressure would be reduced due to the "cushioning" effect of one bubble on the other. Furthermore, after the shatter, the sizes of the resulting bubbles are rather small, and, as discussed before, the collapse of small size bubbles does not generally lead to large pressure overshoots. On the other hand, if the shatter occurs after the bubble reaches its first minimum, the compression would be high. Therefore, an upperbound for the pressure overshoot in the bubble is the maximum compression pressure of a single bubble before its rebound.

C. Encapsulating Bubble Chug

At pool temperatures of about 60°C, the most frequent mode of chugging is the encapsulating bubble chug. A typical pressure trace at the pool bottom for this type of chug is shown on Figure 3.12. The corresponding pressure measurement at the side wall of the pool is shown on Figure 3.13.

For this type of chug, the pressure oscillations can be divided into three periods. The first period (designated as Region I on Figure 3.12) is from the time the pressure undershoot begins to the time the first spike begins. The second period (Region II) includes the entire period of the first spike, and the third period is the "ring out."

The interfacial motion studies suggest that the initial undershoot is caused by the jet penetration and the jet atomization upon impact with the vent. The pressure overshoot is due to the compression at the end of the collapse. The spike shown on Figure

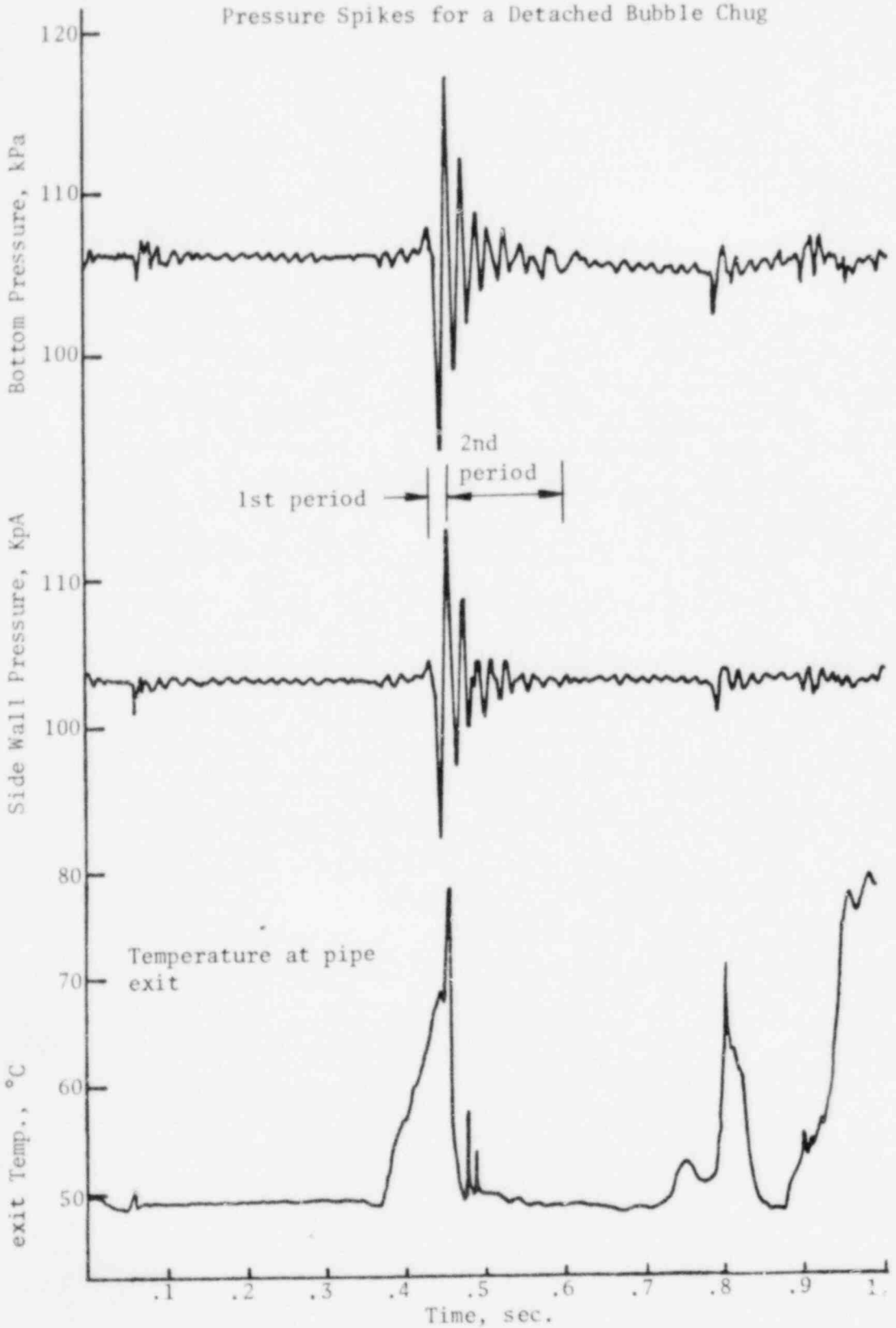


Fig. 3.11 Run No. FM4, Pool Temp = 46.1°C

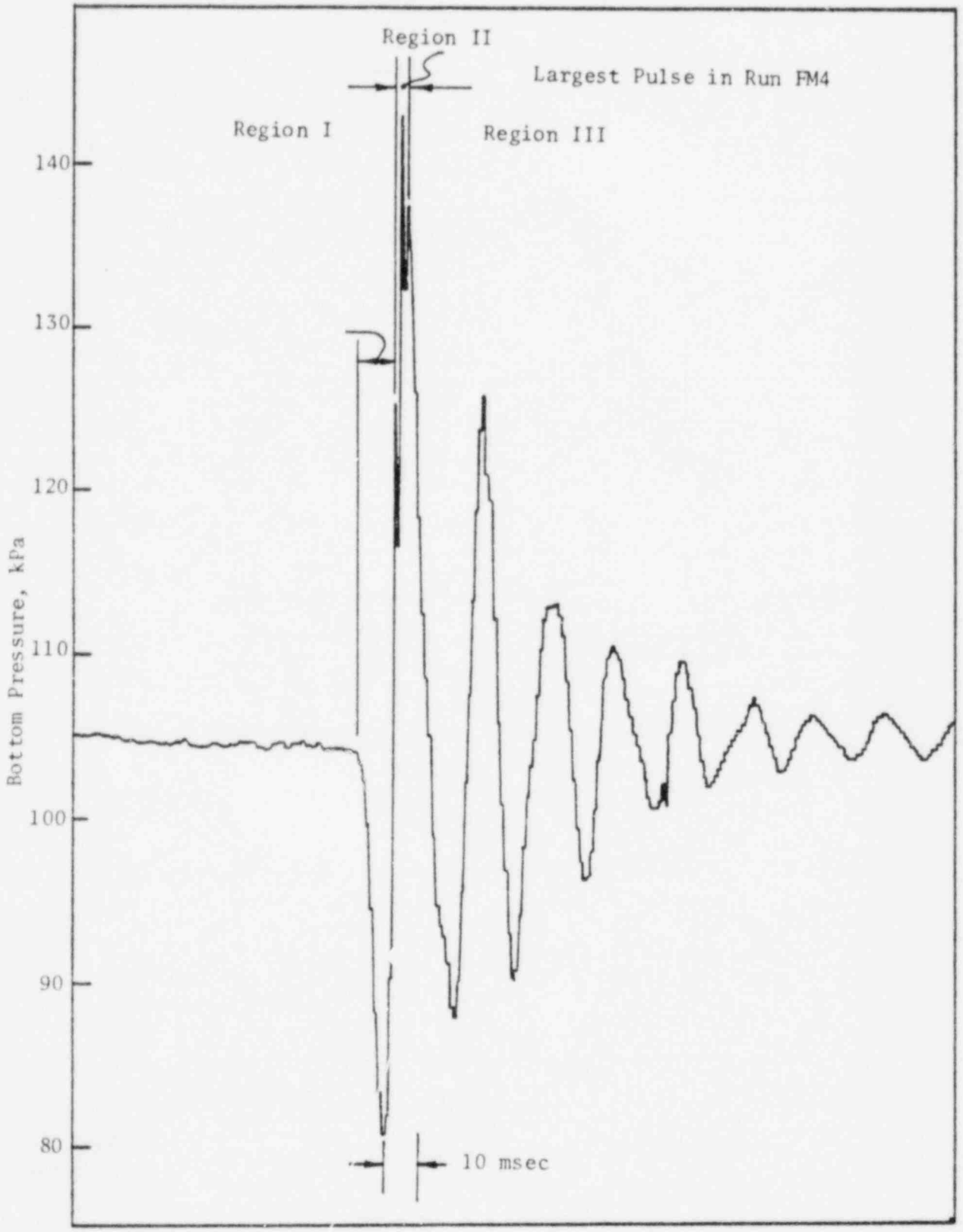
Region II
Largest Pulse in Run FM4
Region I
Region III
140
130
120
110
100
90
80
Bottom Pressure, kPa
10 msec

Fig. 3.12

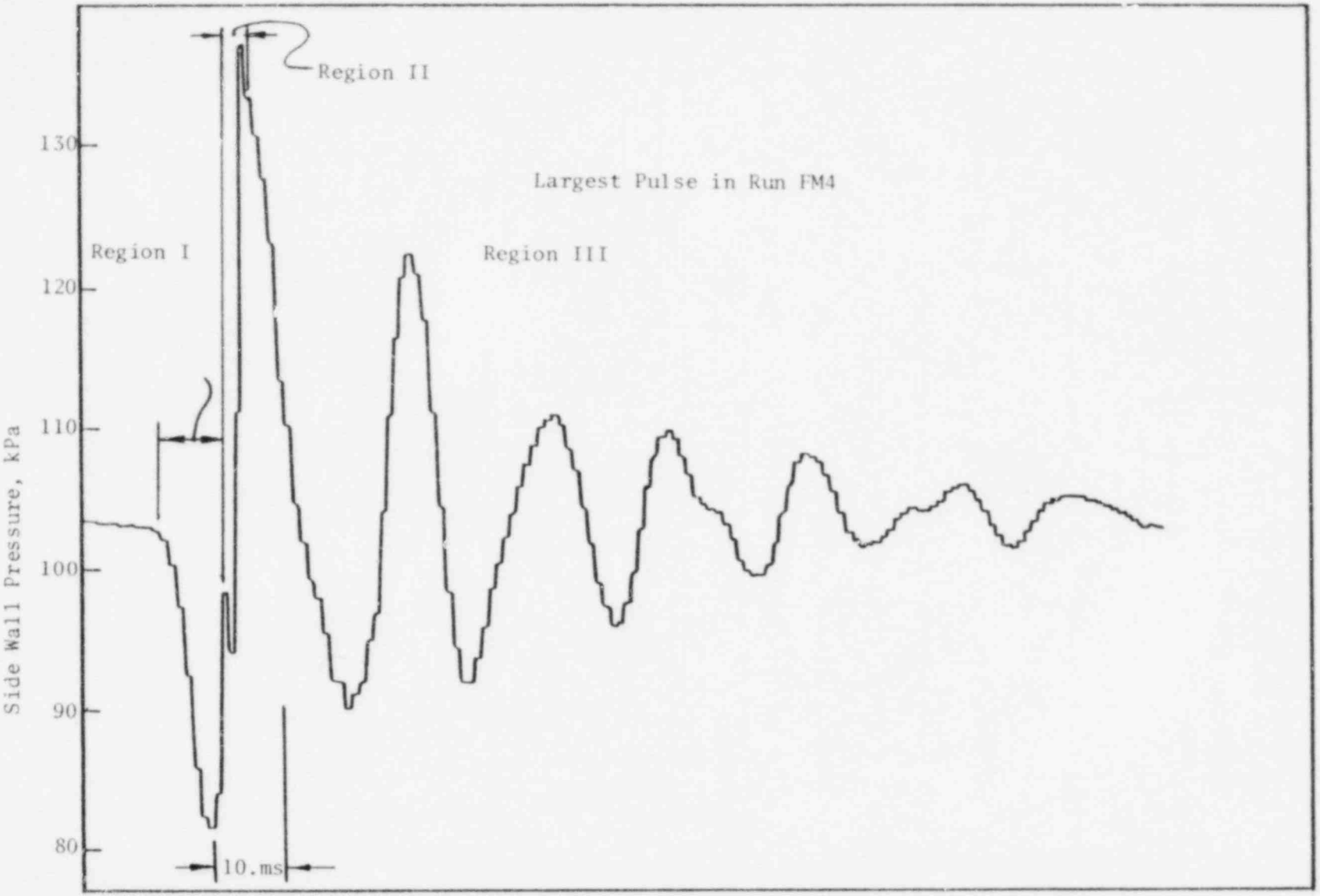
Region II
Largest Pulse in Run FM4
Region I
Region III
130
120
110
100
90
80
Side Wall Pressure, kPa
10.ms

Fig. 3.13

3.13 shows that a few peaks are present within one spike; the corresponding side wall pressure shows some of these peaks also. These fine peaks that occur at the end of the collapse are an indication that the bubble collapse is non-monotonic. The bubble shape may have been quite different from that of a sphere as the bubble volume reaches a minimum; thus, some oscillations in the bubble shape may have occurred before rebound and shatter occur. In other words, the bubble may have been compressed in different directions at slightly different times before a rebound and shatter occur. On the other hand, these oscillations may also have been the result of the rebound during which the shatter occurs.

The lowerbound for the pressure undershoot and the upperbound for the pressure overshoot for encapsulating bubbles are basically the same as the detached bubbles.

### 3.2.3 Synchronized Movie and Pressure Data

By synchronizing the interfacial motion data and the pool bottom pressure data, the following observations are made.

For the internal chug (Figure 13.14), the pool bottom pressure oscillations are small. The point at which liquid bridging occurs is when the first pressure undershoot is recorded.

In the detached bubble chug (Figure 13.15), pool bottom pressure oscillations are larger in magnitude. The point at which the liquid jet begins to "cut off" the bubble from the vent is when the first pressure undershoot occurs. The pressure undershoot reaches a minimum when the "cut off" is completed and the bubble has already become a misty region due to the very rough interface near

the end of a collapse. A rapid rise of the water slug up the vent follows (picture 3).

For the encapsulating bubble chug (Figure 13.16), some pool bottom pressure oscillations are recorded as the bubble grows to its maximum size (picture 1). The liquid jet penetration is at an angle to the vertical (high pool temperature case, see section 3.2.1.A) as shown by the arrows. The drop in bottom pressure immediately follows as the jet penetration begins. The bubble turns into a mist at approximately when the positive pressure spike occurs (picture 2), and a slug of water chugs up the vent after the collapse (picture 3).

Although the time correspondence between the bottom pressure data and the movie may be off by up to 10 milli-seconds, the sequence of events and the time-scales of each of the processes are clearly shown. The entire set of experiments is presented in Appendix A. Note that the sampling time interval used in these runs was 5 ms which is on the same order of magnitude of the pressure spikes; therefore these pool bottom pressure peaks may not represent the exact pressure peaks occurring at the pool bottom.

### 3.2.4 Statistical Data

Since the chugging phenomenon is statistical in nature, it is convenient to define a set of averaged quantities which are appropriate for illustrating the physical phenomena. The definitions of the various quantities are listed below:

1) Average Chugging Frequency - is the total number of chugs in the run divided by the total time of the run.

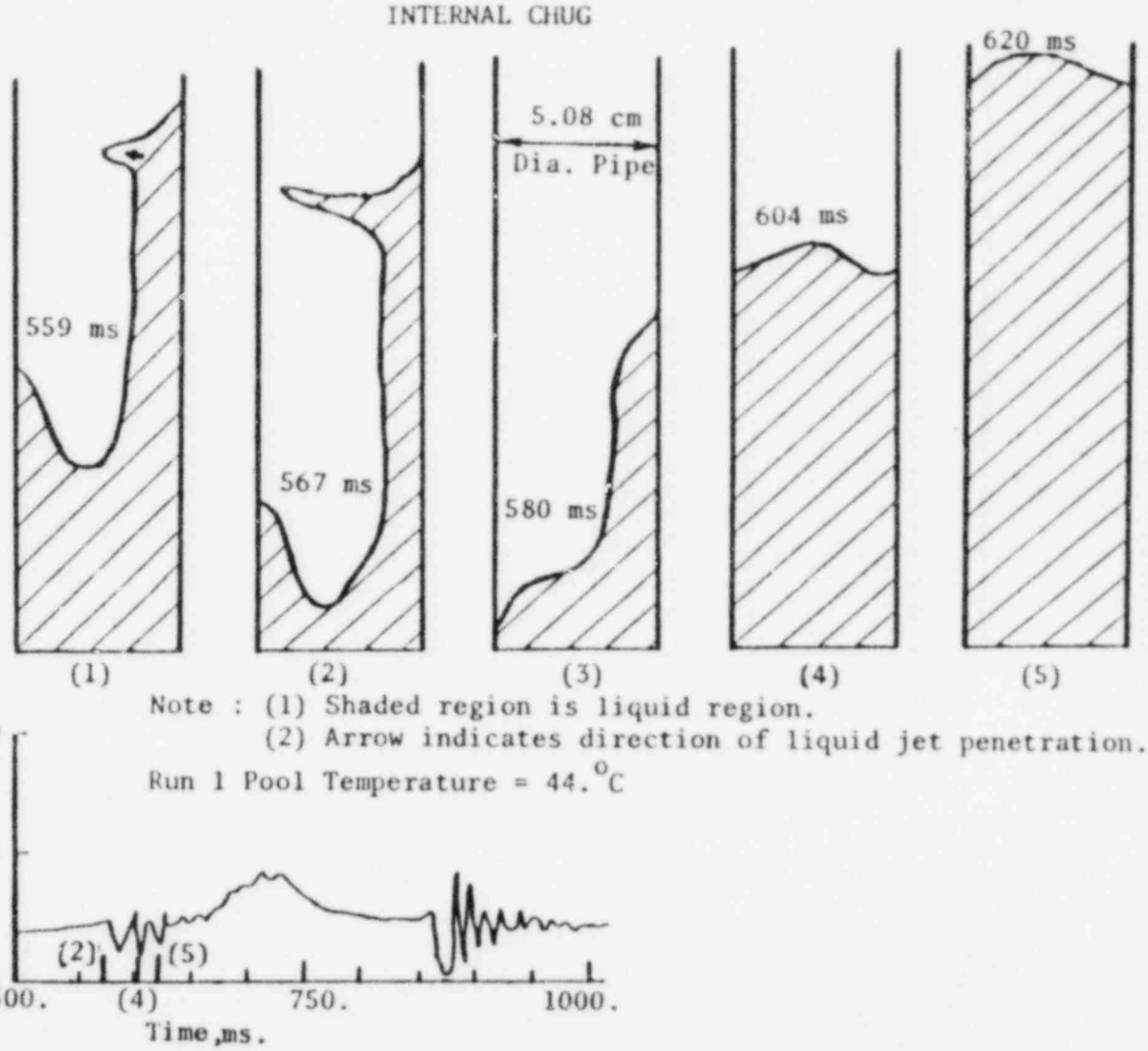


Fig. 3.14 Internal Chug

DETACHED BUBBLE CHUG

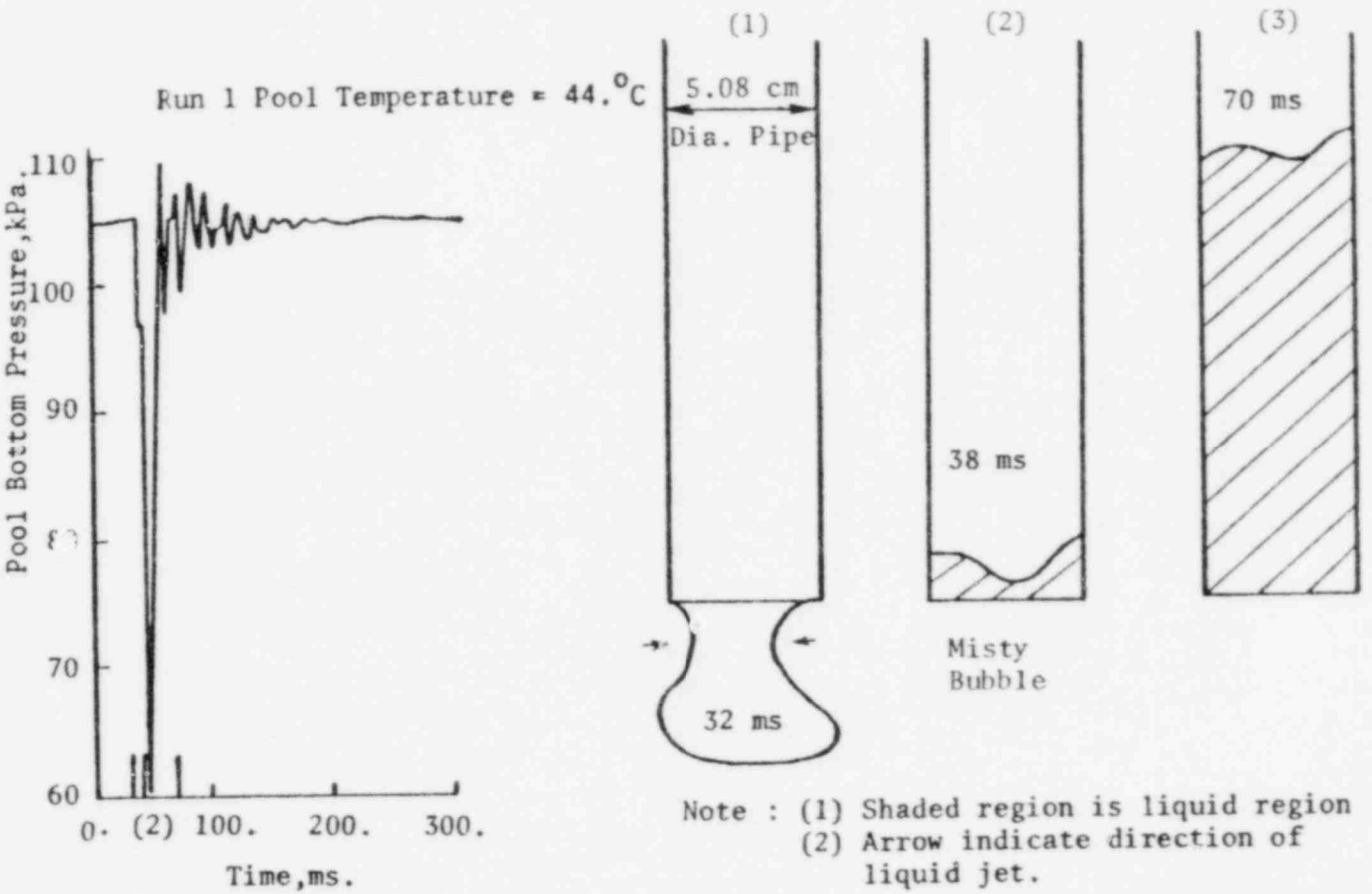


Fig. 3.15 Detached bubble chug

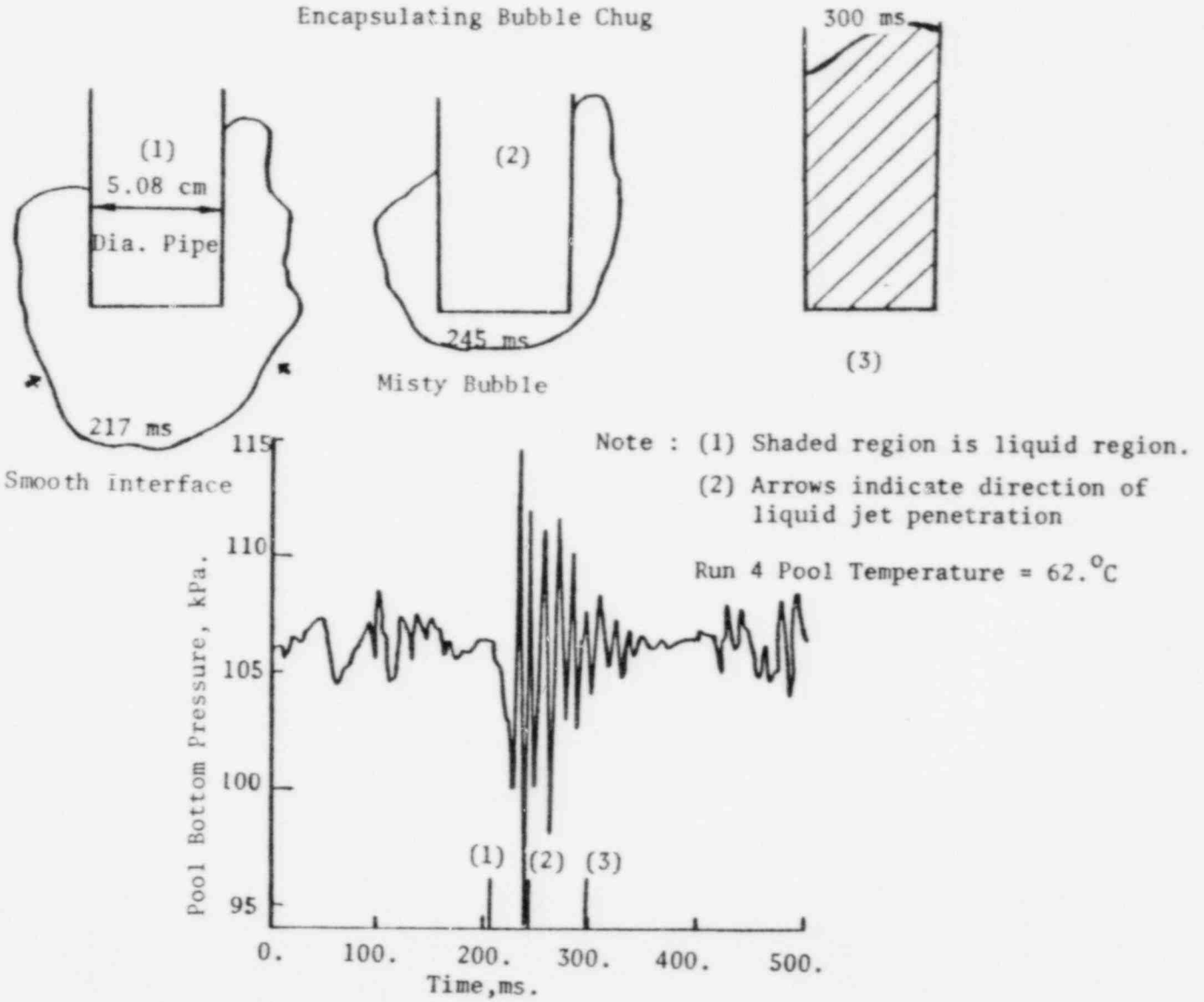


Fig. 3.16 Encapsulating bubble chug

2) Internal Chugging Frequency - is the total number of internal chugs in the run divided by the total time of the run.

3) Average Bubble Frequency - is the total number of bubbles in the run divided by the time available for the bubbling process.

4) Bubble Growth Time - is the time it takes for a typical large bubble to grow to its maximum volume. This includes the time period where the bubble stays at its maximum size for a while before it collapses.

5) Bubble Collapse Time - is measured from the time a typical bubble reaches its maximum volume to the time the collapse process is completed.

6) Average Duration of Chug - is the average time period that the water slug stays in the vent.

7) A Chug - is a rush of water into the vent.

By examining the movie data (presented in Appendix A), which are 5. seconds in duration, certain statistical data for steam chugging could be obtained (Table 3.1). Chugging frequencies ranging from zero to 3.2 chugs per second were observed at temperatures above 40°C. In this temperature range (40° - 60°C), what occurs inbetween two chugs has a strong influence on the chugging frequency. In general, after a chug, several bubbles will form and collapse at the vent exit and then another chug follows. These bubbles can be separated into two types. The first type, called the chugging bubble, usually occurring right before the chug, is large and the

collapse rate is high. The second type, called the intermediate bubble usually occurring after the chug and before the formation of the large bubble, is usually small ($\sim$ one half of the size of the chugging bubbles) and its collapse rate is low. The role of the small bubbles is to slowly warm up the water at the vicinity of the vent exit. The existence of these bubbles is believed to be related to the high heat transfer rate caused by the ring vortex or vortices generated during the slug discharge. As the water warms up the condensation rate reduces and eventually leads to the formation of the large bubble which causes the chug. After the chug, the pool water at the vicinity of the vent exit drops back to the bulk pool temperature due to the strong mixing and the process repeats.

The average chugging frequency is quite temperature dependent. This peculiar temperature dependence can be explained with the help of the flow regime map discussed previously. In the low temperature case ($\sim$40°C), chugging occurs mainly in the form of internal chugs. The internal chugging frequency is almost as high as the chugging frequency. Few bubbles form inbetween chugs in this range. In fact, bubble formation is a rare event. As the pool temperature increases, the number of bubbles formed inbetween two successive chugs increases which causes a reduction in the chugging frequency. The other cause of such a reduction in chugging frequency is the fact that at this temperature range, internal chugging becomes a very rare event. From Table 3.1, it is apparent that a threshold temperature exists around 50°C beyond which the internal chugging frequency drops off drastically. In fact, no internal chugging was observed in any

experiment where the pool temperatures were higher than 60°C. From this point of view, chugging regime (2b) can be considered as a region where two different modes of condensation exist. Above 50°C, internal chugging is a rare event while below 50°C bubble formation is a rare event. This means that from 40°C to 60°C is a transition region which exists inbetween the internal chugging regime (2a) and the bubble formation chugging regime (2c).

As the pool temperature increases, the chugging frequency begins to increase again due to a sharp decrease in the average duration of chug. This decrease is accompanied by a decrease in the maximum height of chug (Fig. 13.17). The chugging frequency reaches a high value of about 3 chugs per second at about 70°C and then starts to drop off since water does not enter the vent above a pool temperature of about 80°C.

For the bubble growth and collapse times, the movie data for the seven experimental runs were reduced and summarized in Table 3.2. Although the growth and collapse times show large ranges, it is apparent that the low pool temperature cases are quite different from the high pool temperature cases. In the low pool temeperature cases, growth times were long and collapse times were short. The opposite trend was observed for the high pool temperature cases.

## 3.3 Detailed Experiments on the Dynamics of the Steam Upstream of the Vent Exit

This section presents the results of the set of experiments performed to obtain more information concerning the dynamics of the steam in the injection pipe. They represent the second step of the

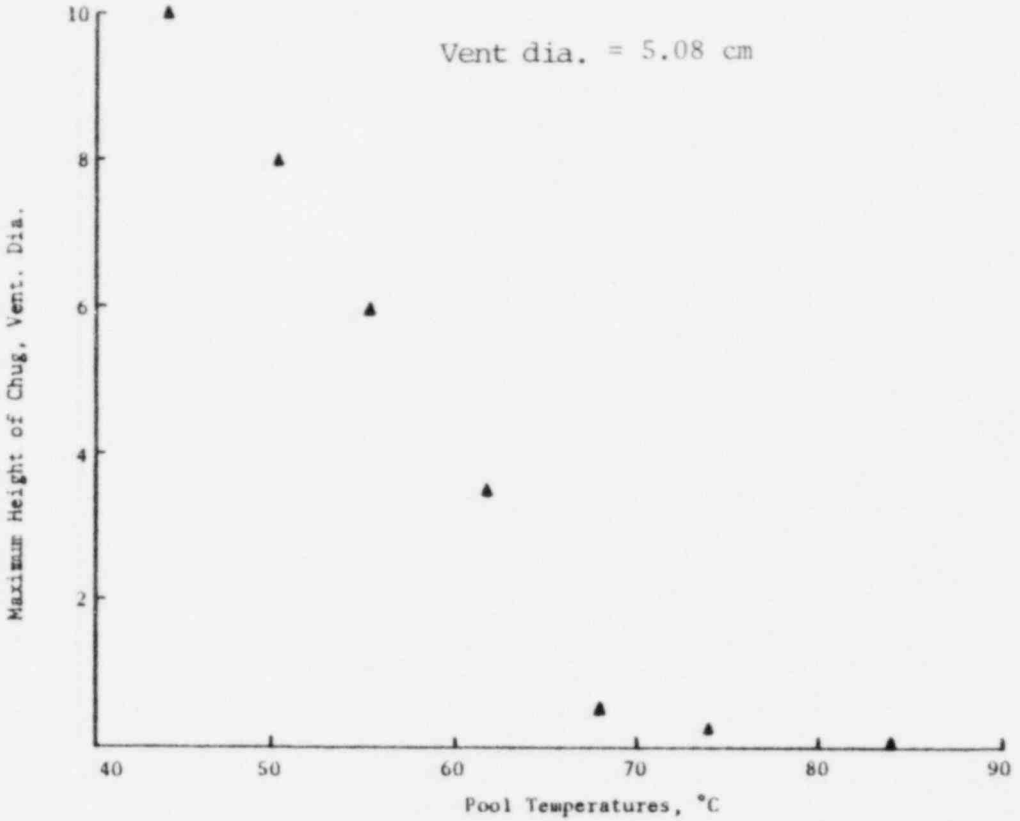


Fig. 3.17 Plot of Maximum Chugging Height vs. Pool Temperature

| Run No. | 1 | 2 | 3 | 4 | 5 | 6 | 7 |
|---|---|---|---|---|---|---|---|
| Bulk Pool Temperature (°C) | 43.9 | 50.0 | 55.5 | 61.7 | 67.8 | 73.9 | 83.9 |
| Average Chugging Frequency ($sec^{-1}$) | 3.2 | 2.7 | 1.8 | 2.5 | 3. | 1.9 | 0. |
| Internal Chugging Frequency ($sec^{-1}$) | 2.4 | .5 | .6 | .3 | 0. | 0. | 0. |
| Average Bubble Frequency ($sec^{-1}$) | 11.7 | 10.5 | 7.4 | 8.1 | 7.1 | 6.9 | 0. |
| Bubble Grwoth Time (msec) | 164. | 125. | 174. | 161. | 115. | 106. | 69. |
| Bubble Collapse Time (msec) | 12. | 19. | 24. | 19. | 22. | 39. | 50. |
| Average Duration of Chug (msec) | 274. | 212. | 229. | 175. | -0. | -0. | -0. |
| Maximum Height of Chug (Vent Dia.) | -10. | -8. | -6. | -3.5 | .5 | .25 | 0. |
| Average No. of Bubbles Between Chugs | -1.0 | -3.5 | -3.0 | -2.5 | -2.0 | -2.0 | -1. |

Table 3.1 Chugging Characteristics at Various Pool Temperatures (Steam Mass Flux = 5.0kg/$m^2$-sec)

TABLE 3.2

SUMMARY OF MOVIE DATA REDUCTION ON

BUBBLE GROWTH AND COLLAPSE TIMES

| Run No. | Pool Temp., $^{o}C.$ | Range of Bubble Growth Times, ms | Avg.* ms. | Range of Bubble Collapse Times, ms | Avg.* ms. |
|---|---|---|---|---|---|
| 1 | 43.9 | 117-157 | 137 | 13-29 | 21 |
| 2 | 50.0 | 56-167 | 81 | 8-39 | 28 |
| 3 | 55.5 | 63-174 | 130 | 11-35 | 20 |
| 4 | 61.7 | 77-177 | 117 | 10-43 | 23 |
| 5 | 67.8 | 48-137 | 87 | 25-53 | 35 |
| 6 | 73.9 | 55-120 | 86 | 22-49 | 34 |
| 7 | 83.9 | 35-85 | 62 | 33-76 | 48 |

* Arithmetic Average

experimental stage of this study. The importance of this step is two-fold. First, an understanding of the effect of the upstream conditions on steam chugging is crucial for obtaining a general physical picture. Second, these experiments also give the upstream boundary conditions as well as the initial conditions necessary for the theoretical analysis.

The experiments were performed in the following order. The first set concentrated on the study of the vent pressure about 50 cm from the vent exit. The second set measured the steam velocity at about 100 cm from the vent exit. The third set measured both the vent pressure and the steam velocity in order to establish the relationship between the two. The fourth set obtained the surge tank pressure which is useful as an upstream boundary condition for the steam flow in the vent.

### 3.3.1 Vent Pressure Experiments

The set of experiments and conditions for each run are presented in Appendix C. This set of experiments is intended to relate the interfacial phenomena, occurring at the pool exit, to the steam pressure variations in the pipe. They will be used, in a later chapter, to establish the initial conditions in the pipe for the theoretical comparison.

A typical case is chosen for this discussion. Figure 3.18 shows the simultaneous vent pressure data with the pool bottom pressure data and the vent exit temperature. The first chug in that run, an encapsulating bubble chug, occurred at 0.46 sec after data acquisition began. A drop in the pool temperature at that point from that of the steam to that of the pool water is shown. Comparing the pool bottom pressure data with the vent pressure data, it is apparent that at the time an underpressure begins in the pool bottom pressure, an

underpressure is also experienced in the vent. This indicates that the simultaneous undershoots in both the vent and the pool are initiated by the same phenomenon--the liquid jet penetration and atomization.

The second chug (at 1.1 sec.) is an internal chug; the interface was able to progress to approximately 2 cm. above the vent exit (where the exit thermocouple is located) and stopped there for a short period of time while the liquid layer draining off the pipe wall accumulating at the exit caused a rapid underpressure. The vent pressure data clearly shows a large underpressure. However, shortly after the interface chugged up the vent, another underpressure occurred. The cause of this second underpressure is unknown. However, it is apparent that the two underpressures are similar in nature in terms of magnitude and duration, although the second one is generally less than the first in magnitude. Therefore, it is suggested that the second underpressure may have been caused by a rapid increase in the heat transfer surface. As discussed in Section 3.2.1.A in regard to internal chugs, it is observed that as the slug coasts down to a stop, part of the interface begins to retreat while the rest continues to flow upward. This spread in the interface may have been the cause of the rapid condensation which leads to the second underpressure. Unfortunately, this set of runs was made using the steel pipe, which enables the mounting of the pressure transducer near the vent exit; but blocks the physical observation by the movies. However, the spread of the interface has been observed and a flow separation condition develops where the steam begins to penetrate into the water

slug through the part of the interface that is retreating and thus an annular flow situation is created as mentioned in the previous discussions on the internal chugs and the detached bubble chugs.

The third chug (at 2.3 sec.) is an encapsulating bubble chug again and the situation is similar to the first one.

The fourth chug is a detached bubble chug; the time at which the underpressure in the pool bottom occurs again corresponds to the liquid jet which caused the detachment and the underpressure inside the vent. However, the duration of the underpressure in the pool was short when compared to that of the vent. Apparently more condensation was continuing in the vent while the completion of the bubble collapse terminated the pressure undershoot in the pool. This is due to the fact that immediately after the bubble detachment, the liquid layers draining off the pipe begin to accumulate at the exit causing a rapid increase in the condensation rate at that vicinity. A second undershoot again occurred sometime after the chug rushed up the pipe. The time interval between the two undershoots is defined as $\Delta t$ , while the duration of the vent underpressure is defined as W as shown in Figure 3.18.

Although different types of chugs (i.e. internal, detached bubble, and encapsulating bubble) are identifiable from the bottom pressure characteristic, there is no particular characteristic in the vent pressure traces that could be related to the type of chug. This is because the nature of the rapid condensation at the exit is the same for all chugs: namely, a rapid increase in the heat transfer surface takes place.

### 3.3.2 Steam Velocity Experiments

Figure 3.19 shows the simultaneous velocity data with the pool bottom pressure data. It is clear that the rapid velocity increases correspond with the chugs. The first chug in that run is an encapsulating bubble chug. It is apparent that the velocity increase occurred after the initiation of the underpressure in the pool bottom pressure data. Thus it appears that the velocity increase was a consequence of the vent underpressure. Examination of the other runs in the set confirmed this observation. However, no particular characteristics are found between the three types of chugs in the velocity data. Although there are some inaccuracies involved in terms of the magnitude of the steam velocity, the responses of the flow meter to velocity variations are accurate. Figure 3.19 shows the steam flow transient inside the pipe.

### 3.3.3 Mixed Vent Pressure and Steam Velocity Experiments

This set of experiments was performed to confirm the observations made in the last two sets of runs. It is found that the velocity rise follows after the initiation of the vent underpressure in all the chugs. Figure 3.20 shows a typical set of simultaneous velocity data, vent pressure data, and the vent exit temperature data. Again, no direct relation between the velocity data and the three types of chugs were identified.

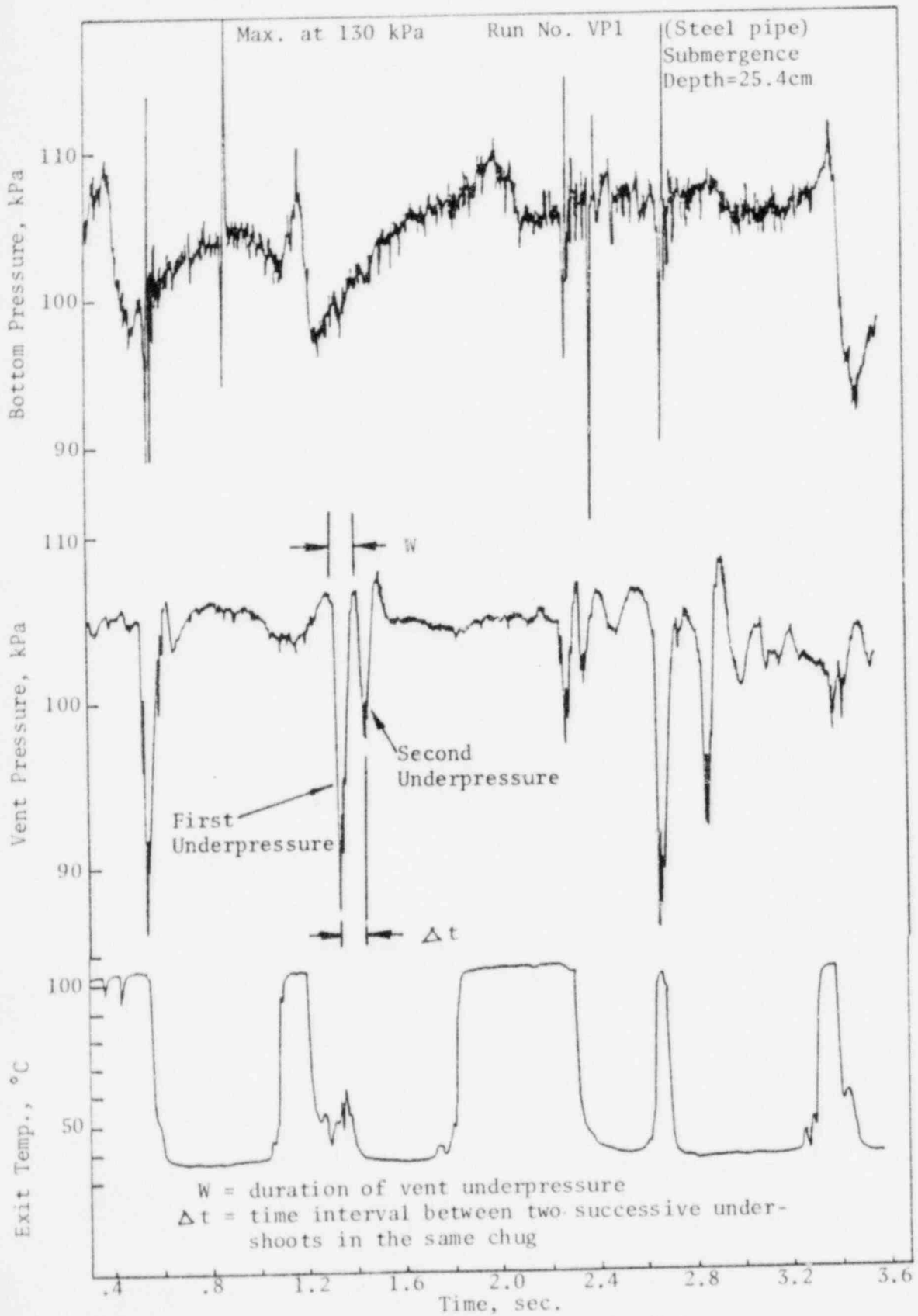


Fig. 3.18 Vent Pressure Data

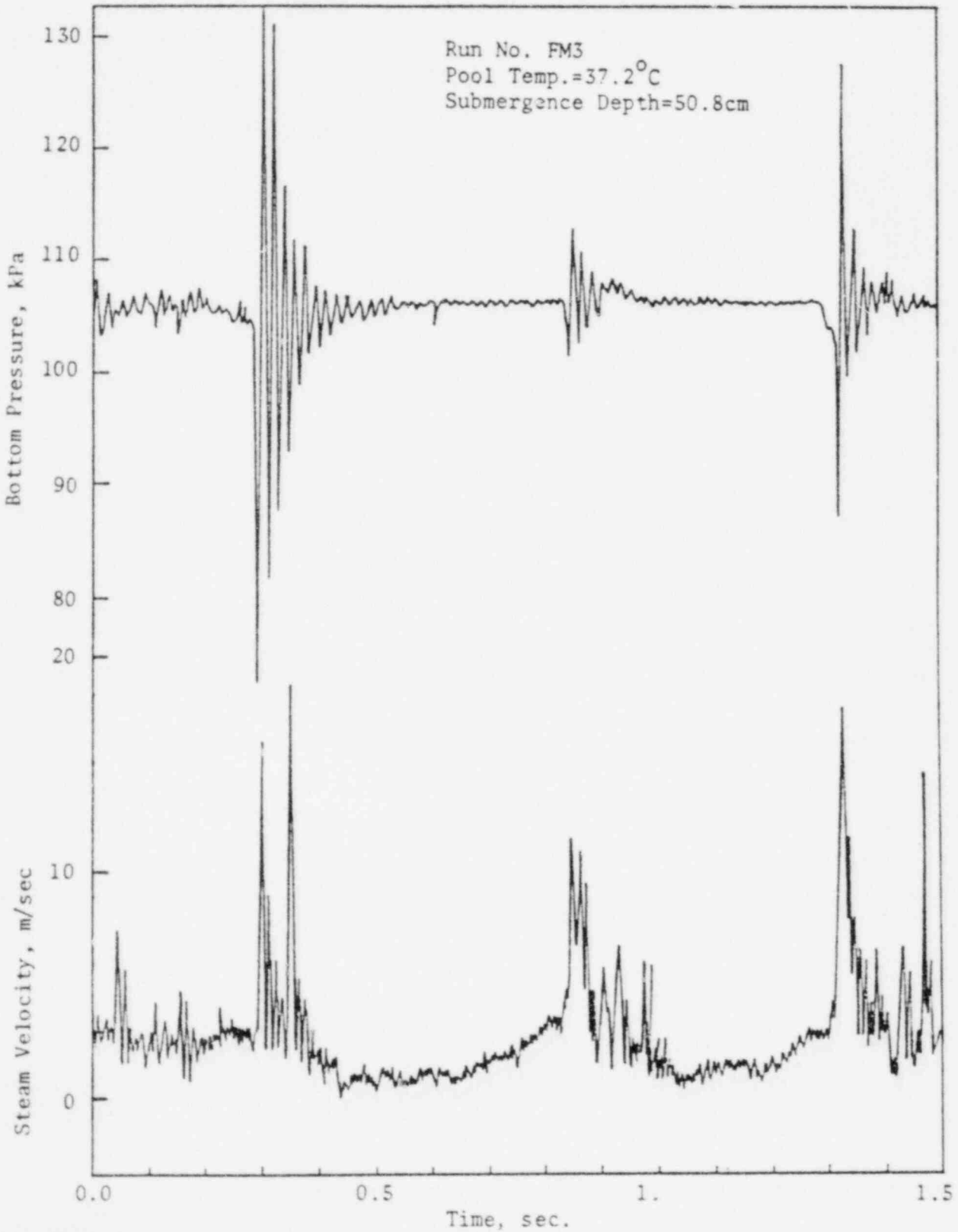


Fig. 3.19 Steam Velocity Data

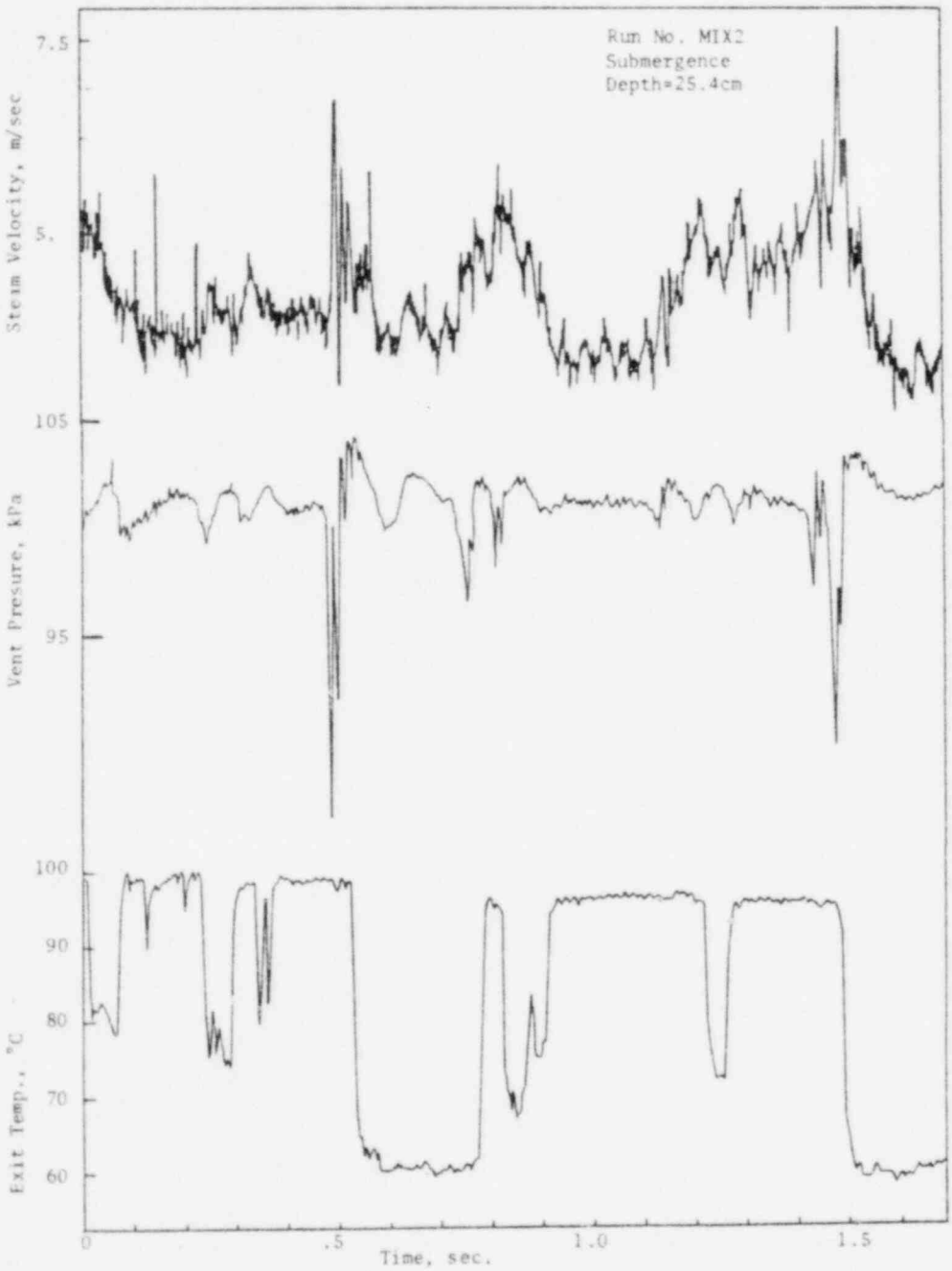


Fig. 5.20 Mixed Vent Pressure and Steam Velocity Data

### 3.3.4 Surge Tank Pressure Experiments

This set of experiments was performed to obtain the pressure fluctuations in the surge tank in relation to that in the vent. A typical set of simultaneous vent pressure and surge tank data is shown on Figure 3.20. It is found that a corresponding underpressure in the surge tank occurred slightly after the first underpressure in the vent pipe. The time difference between the initiation of the underpressure in the vent and that in the surge tank is approximately 12 msec in all cases. This period is approximately the time it takes for a rarefaction wave to propagate from the exit to the surge tank. This confirms the previous observation that the underprssure at the surge tank is a consequence of the rapid condensation at the vent exit.

### 3.3.5 Statistical Data

A set of statistical data obtained from this set of experiments is compiled and depicted on Table 3.3. The magnitude of the average vent underpressure decreases as the pool temperature is increased. This behavior of the vent underpressure agrees with the decline in chug height at high pool temperatures observed in the plastic pipe experiments. The average duration of the vent underpressure $\overline{w}$ is found to be quite insensitive to the pool temperature. Only a very mild increase in $\overline{w}$ is observed for the range of pool temperatures in these experiments. Of more interest is the time interval between two successive underpressures in a chug, $\overline{\Delta t}$. Although some statistical fluctuations are expected, it is seen that $\overline{\Delta t}$ is large at low pool temperatures and small at high pool

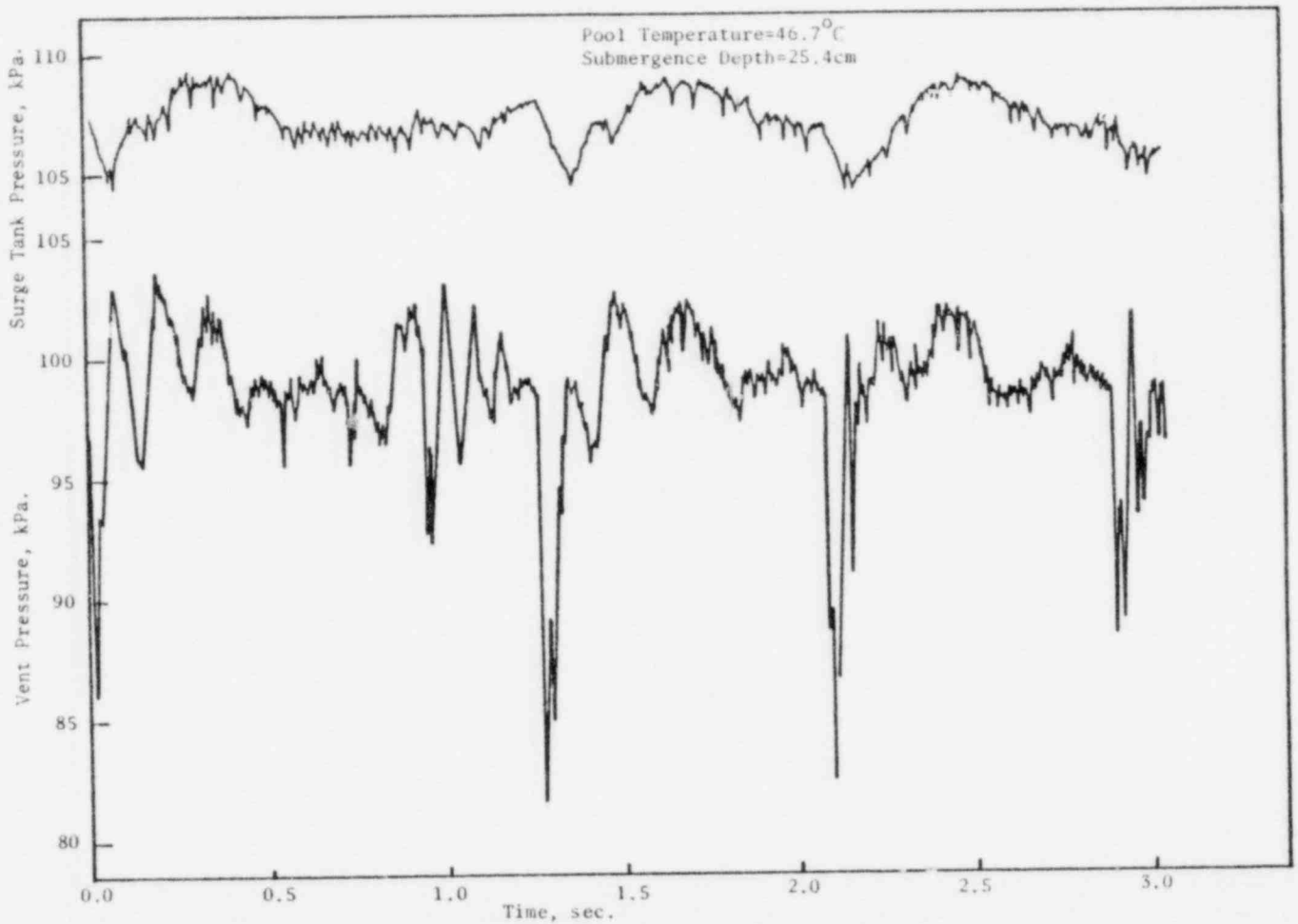


Fig. 3.21 Run No. ST2. Surge Tank Pressure Experiment

temperatures. This indicates that the second underpressure could be a result of a change in the water slug velocity or perhaps the direction of the acceleration. In the discussion of the vent pressure experiments (Section 3.3.1), it was pointed out that the second vent underpressure may have been caused by an interface spreading phenomenon occurring as the slug coasts down upon reaching its maximum chug height. This temperature dependence of $\overline{\Delta t}$ seems to reinforce that explanation because the chug heights are usually higher at low pool temperatures and the time taken to reach its maximum is also longer.

## 3.4 Summary of the Physical Observations and Discussion

The results of the qualitative visual experiments show that the interfacial motion admits certain characteristic patterns for various ranges of the vapor injection rate and pool temperatures. Hence, the rather complicated phenomena involved in vapor injection are systematically classified based on the observed differences in the interfacial motion patterns. A simple condensation regime map is formulated based on two criteria that defined the separation lines between various condensation regimes. The first one is concerned with whether the steam region exists above or below the vent exit. The second one involves the location where the bubble detachment occurs. When the point of detachment is at the pipe exit, the existence

TABLE 3.3 STATISTICAL DATA ON THE UPSTREAM DYNAMICS EXPERIMENTS

| Run No. | Pool Temp., °C | Submergence Depth, cm. | Vent Underpressure, kPa. Average | Vent Underpressure, kPa. Minimum | Vent Underpressure, sec. $\bar{W}$* | Vent Underpressure, sec. $\Delta t$** |
|---|---|---|---|---|---|---|
| VP1 | 37.2 | 24.1 | 86.1 | 85.4 | .059 | .054 |
| VP2 | 46.7 | 24.1 | 92.3 | 87.5 | .059 | .066 |
| VP3 | 58.9 | 24.1 | 93.0 | 83.4 | .061 | .044 |
| VP4 | 64.4 | 24.1 | 97.3 | 95.1 | .065 | .042 |
| ST1 | 40.0 | 25.4 | 85.4 | 76.5 | .051 | .057 |
| ST2 | 46.7 | 25.4 | 86.1 | 81.3 | .057 | .047 |
| ST3 | 53.3 | 25.4 | 91.4 | 90.3 | .059 | .060 |
| ST4 | 61.7 | 25.4 | 95.1 | 91.6 | .081 | .038 |

*$\bar{W}$ = average duration of an underpressure event in the vent.

**$\Delta \bar{t}$ = average time interval between two successive vent underpressure events in the same chug.

of the steam region in the water becomes intermittent. This is the point where steam chugging is considered to occur.

Detailed interfacial motion pictures indicate the existence of three different modes of chugging. The first type is the internal chug where all condensations occur inside the vent pipe. The characteristics of this type of chug are the high chugging heights, and the low vent pressure during water discharge. The detached bubble chug is the second type, where the bubble is "cut off" from the pipe upon interface clearing. They are characterized by the high chugging heights, the high velocity and the low steam pressure during interface clearing. The third type is the encapsulating bubble chug, where the steam region grows to encapsulate the vent exit after interface clearing. This type of chug is characterized by lower chugging heights, low discharge velocity but high steam pressure during interface clearing.

For the first two types of chugs, the mechanism that causes the chug is the rapid condensation of the vapor by the layers of liquid draining off of the pipe wall at the pipe exit. For the encapsulating bubble chugs, the liquid jet penetration and atomization at the pipe exit is the mechanism responsible for causing the chugs.

The pressure measurements at the pool solid boundaries indicate that only mild fluctuations are experienced for internal chugs. However, both the detached bubble chugs and the encapsulating bubble chugs cause large pressure undershoots and overshoots. The magnitude of these fluctuations is higher for the encapsulating bubbles. By the nature of the pressure fluctuations, three different periods can

identified. The first period begins with the undershoot until the overshoot occurs. This is caused by the rapid condensation occurring in the bubble as the liquid jet penetrates into the bubble. The second period includes the entire pressure overshoot which is found to be non-monotonic. This is a consequence of the over-compression at the end of the rapid bubble collapse following the liquid jet penetration. The third period is called the "ring out" which includes the oscillations subsequent to the initial pressure peak. These observations are confirmed by a set of synchronized movie and pool bottom pressure experiments.

The lower bound for the underpressure is the saturation pressure corresponding to the water temperature. The upper bound for the overpressure is the collapse of a bubble, under the influence of the rapid condensation introduced by the liquid jet; with no bubble shatter until a full compression is achieved. Early bubble shatter leads to smaller pressures due to the "cushioning" effect.

Statistical data give the general trends of the chugging phenomena at various pool temperatures. The existence of these trends is a direct consequence of the characteristics of the three chugging modes. The chugging frequency is high in the internal chug region, where pool temperature is low, and also in the encapsulating bubble chug region, where pool temperature is high; however, for intermediate pool temperatures, the chugging frequency is low. The explanation for this peculiar pool temperature effect is that the low temperature internal chugs involve short bubble formation time while the high pool temperature encapsulating bubble chugs involve short chugging

time since the chugging heights are low. However, for the intermediate pool temperatures, both chugging time and bubble growth time are long; and, in addition, there are the intermediate bubbles which grow and collapse before the formation of the large bubble which causes the chug. These effects tend to reduce the chugging frequency. Besides the chugging frequency, the chug heights also show a dependence on the pool temperature. As the pool temperature increases, the chug height rapidly decreases because of the change in the direction of the liquid jet penetration at higher pool temperatures from vertically upward. The jet penetration is then pointed more to the outside wall of the vent rather than directly into the vent.

The experiments concerning the upstream steam behavior indicate that an underpressure condition in the vent occurs prior to all the chugs. The data also show that the vent underpressure as well as the pressure undershoot in the pool are initiated by the same mechanism: the rapid condensation caused by the liquid jet penetration into the bubble. A rise in steam velocity follows immediately after the vent underpressure; and after a time of 10 ms the travelling time of a rarefaction wave, the surge tank pressure suffers a decrease.

The statistical data obtained from this set of experiments show that the magnitudes of the average vent underpressure and the average steam velocity both decrease as the pool temperature is increased. The decreased vent underpressure at high temperatures agrees with the observed decline in the chugging height. However, the average duration of the vent underpressure $\overline{W}$ is found to be quite insensitive to the pool temperature. On the other hand,

the average time interval between two successive underpressures in the same chug ( $\overline{\Delta t}$ ) is found to decrease as pool temperature is increased.

In comparing the steel pipe experiments with those of the plastic pipe, some important differences are worth mentioning. First, the steel pipe experiments indicate that pressure spikes other than those generated by the bubble collapse are present. They generally occur at interface clearing or during a chug. These spikes are characterized by short durations ($\sim$2.ms) and large magnitudes. In addition, in contrast to the spikes generated by the bubble collapse, these spikes are generally not followed by a "ring out." Table 3.4 depicts the magnitude of these spikes as a function of pool temperature. A definite decrease in the magnitude of the underpressure is observed as pool temperature is increased. However, the magnitude of the overpressure does not show any pool temperature dependence. Second, a difference in the chugging frequency is observed between the plastic pipe experiments and the steel pipe experiments. Table 3.5 shows a comparison. Lower chugging frequencies are observed for the steel pipe experiments which may be a result of the additional condensation on the pipe wall due to the high heat capacity of the steel pipe.

TABLE 3.4

THE CHARACTERISTICS OF THE ADDITIONAL PRESSURE SPIKES
(in steel pipe)

| Run No. | Pool Temp., °C | Min. Pressure in a spike, kPa | Max. Pressure in a spike, kPa |
|---|---|---|---|
| VP1 | 37.2 | 48.2 | 130.9 |
| VP2 | 46.7 | 37.9 | 109.6 |
| VP3 | 58.9 | 49.6 | 130.2 |
| VP4 | 64.4 | 91.6 | 114.4 |

NOTE: The occurrence of these spikes is usually during interface clearing or during the chugging of a slug up the vent. They do not correspond to the pressures generated by the bubble collapse.

TABLE 3.5

COMPARISON OF CHUGGING FREQUENCIES IN STEEL PIPE EXPERIMENTS AND IN PLASTIC PIPE EXPERIMENTS

| Run No. | Pool Temp., °C | Chugging Frequency, chug/sec. |
|---|---|---|
| VP3 | 58.9 | 1.6 |
| VP4 | 64.4 | 1.9 |
| FM1 | 53.9 | 2.6 |
| FM2 | 62.8 | 2.6 |

# CHAPTER 4

# THEORETICAL ANALYSIS

## 4.0 Introduction

The analysis presented in this chapter represents the second stage of the investigation of steam chugging. The basis to establish the present theoretical model is the physical picture established in the previous chapter. However, it is clear from the discussions there that a fair amount of the physical phenomena concerning the interfacial motion are not well understood; and, a considerable amount of research is still needed before a satisfactory physical understanding can be established. The present theoretical model, despite its complexity, is only a first step in the modelling of the complicated phenomena. The basic objective is to see whether the steam chugging process could be described by some simple physical laws. The model also serves as a basis for future improvements when more information concerning the numerous unknown phenomena previously discussed become available. In the following sections the physical processes are being modelled by (i) the vent pipe model which computes the water slug motion and the bubble formation during chugging and (ii) the bubble collapse model which computes the bubble collapse pressures.

## 4.1 General Description of the Theoretical Models

The vent pipe model for steam chugging computes the dynamics of the steam when the water slug is in the pipe, and after vent clearing during bubble growth. The theoretical model is shown in Figure 4.1. The injection pipe is divided into two regions. Region I represents the part of the pipe where no condensation occurs. The one-dimensional transient pipe flow equations are used to describe the steam flow in this region. When the pressure at the vent inlet is known as a function of time, the steam velocity boundary condition of the pipe is defined. Region II is the part of the pipe where large amounts of condensation occur. It represents the part of the pipe where a liquid layer is attached to the wall during slug discharge; but only the submerged, cooled section of the pipe during slug upflow. Since rapid heat transfer takes place in this region, the behavior of the steam is assumed to be isothermal. By requiring that the steam pressure is continuous across the boundary, the two regions are coupled.

A one-dimensional momentum equation is used to describe the motion of the water slug, the driving force being the pressure difference between the condensation region and the pool.

Upon vent clearing, the slug is allowed to progress down a distance $\frac{4r_0}{3}$ where $r_0$ is the pipe radius. The volume of this additional length is equal to a bubble with radius $r_0$ . This is the assumed initial bubble volume at the pipe exit. The bubble dynamics calculation will not start until the interface has moved this distance. This additional length is shown on Figure 4.1.

After the slug is discharged, the calculation is switched to the bubble dynamic model as shown in Figure 4.2; the condensation region is eliminated while Region I is extended to include the entire pipe. The transient pipe flow equations are used to describe the steam flow in the pipe. The infinite pool, one-dimensional bubble dynamics model (given in Appendix G) is used to describe the bubble dynamics. By requiring the pressure of the steam at the exit to be equal to that in the bubble, the bubble region and the steam region are coupled. The flow of steam into the bubble is then determined from the pipe flow equations. To account for the condensation at the pipe wall, the calculated amount of condensation is subtracted from the exit steam flow. This defines the net amount of steam injected into the bubble.

The time at which a bubble collapse occurs defines the time for the slug to flow up the pipe. The calculation then switches back to the first model on Figure 4.1 with the slug position at the pipe exit.

During the bubble collapse, since the penetration of the liquid jet acts to separate the bubble from the pipe exit, the chug is assumed to be decoupled from the collapsing bubble. Thus, while the vent pipe model continues to compute the slug motion, another calculation is made to compute the collapse history of the isolated bubble in the pool.

To compute the bubble collapse pressures, an infinite pool, spherical vapor bubble model is used to determine the dynamics of the collapsing bubble as well as the final maximum pressures generated

Fig. 4.1 The Vent Pipe Model During Water Slug Discharge and Chugging

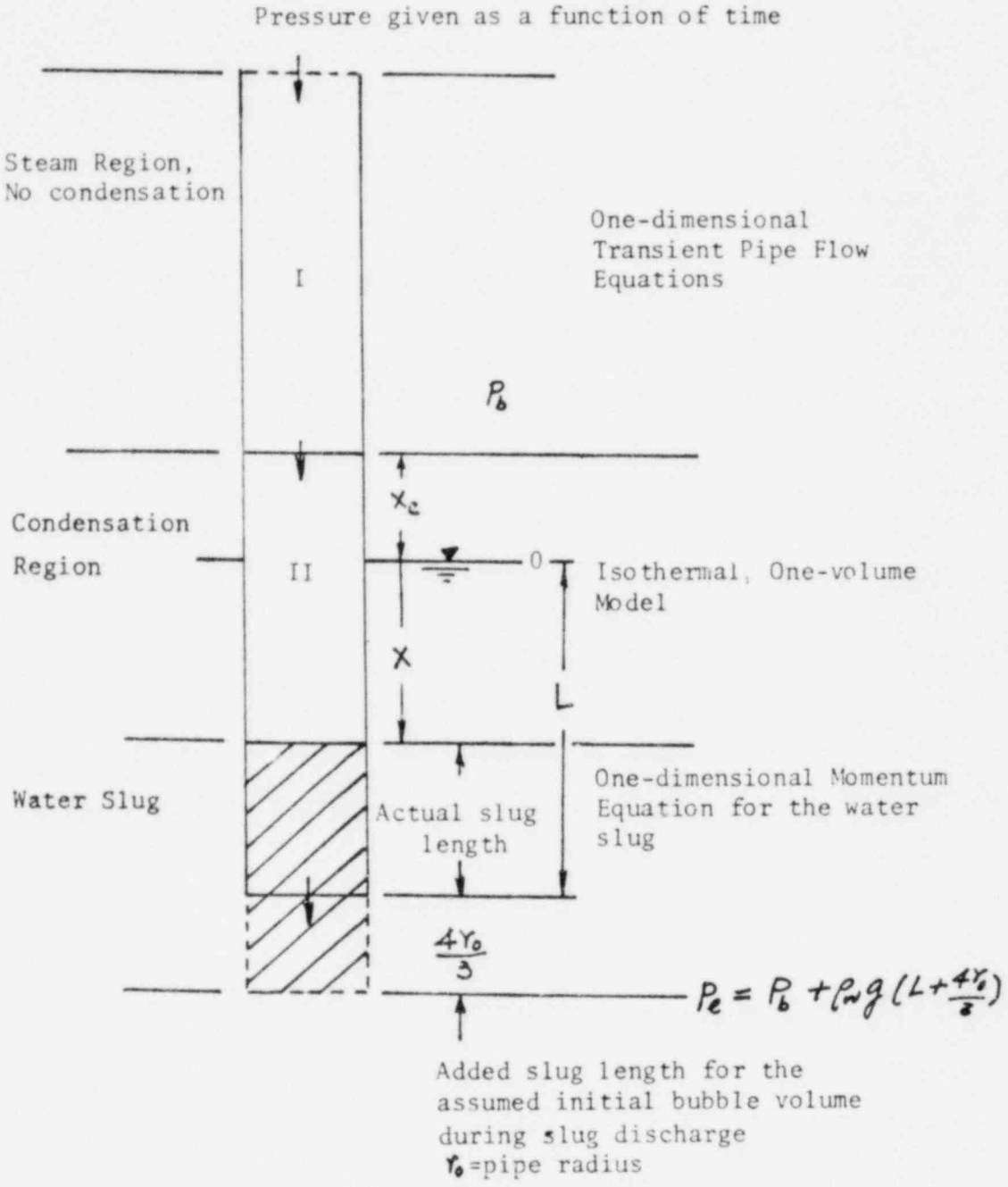

Fig. 4.2 The Vent Pipe Model During Bubble Growth and Collapse

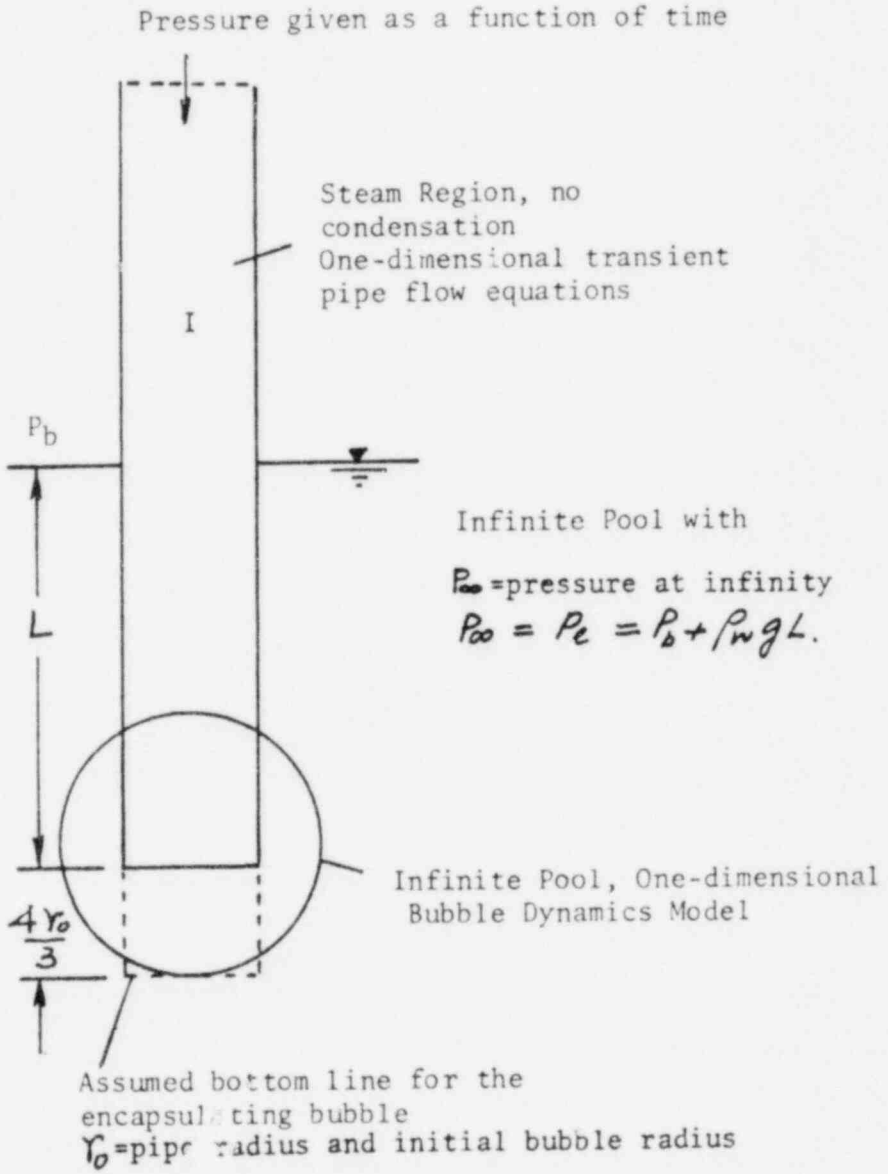

at the end of the collapse. The heat transfer to the liquid jet as well as the droplets produced during the jet atomization process is accounted for by an overall heat transfer parameter to be determined from the experimental data. The initial conditions for this calculation are obtained from the bubble growth claculation while the bubble is still attached to the pipe exit. The conditions in the bubble at the point the bubble reaches its maximum size define the initial conditions for the collapse calculation. The calculation is terminated after the bubble reaches its first minimum radius and a peak pressure generated due to the compression. The bubble is considered to have shattered during its first rebound. The subsequent pressures generated by the shattered bubble, as well as the ensuing "ring out," are neglected in the model.

### 4.1.1 Transient Pipe Flow Analysis (Region I)

The transient one-dimensional conservation equations for steam flow are:

Mass Conservation

$$\frac{\partial \rho}{\partial t} + \frac{\partial}{\partial z}(\rho v) = 0. \tag{4.1}$$

Momentum Conservation

$$\frac{\partial v}{\partial t} + v\frac{\partial v}{\partial z} + \frac{1}{\rho}\frac{\partial p}{\partial z} + \frac{f}{D}\cdot\frac{v|v|}{2} = 0 \tag{4.2}$$

Energy Conservation

$$\frac{\partial h}{\partial t} + v\frac{\partial h}{\partial z} - \frac{1}{\rho}\left(\frac{\partial p}{\partial t} + v\frac{\partial p}{\partial z}\right) - \frac{f}{D}\frac{v^2|v|}{2} = 0. \tag{4.3}$$

Assuming the steam behaves as an ideal gas

$$h = \frac{k}{k-1}\frac{p}{\rho} \tag{4.4}$$

$$c^2 = k\frac{p}{\rho} \tag{4.5}$$

where $\rho$ = steam density

p = pressure

v = velocity

h = enthalpy

c = speed of sound for steam

k = specific heat ratio

f = friction factor

D = pipe diameter

t = time

$\zeta$ = distance

This set of equations are solved by the method of characteristics (Shapiro, reference 37), the resulting equations for the forward or backward characteristics are:

$$dP \mp \rho c\, dv = \frac{f}{D}\frac{\rho}{2} v|v|[(k-1)v \mp c]dt \tag{4.6}$$

along $$\frac{d\zeta}{dt} = v \pm c \tag{4.7}$$

and the path characteristic is:

$$d\rho - \frac{1}{c^2}dP = -\frac{1}{2}\frac{f}{D}(k-1)\frac{\rho}{c^2} v^2|v|\, dt \tag{4.8}$$

along $$\frac{d\zeta}{dt} = v \tag{4.9}$$

These equations are non-dimensionalized by the following

parameters:

$$V^* = k\frac{V}{C_i} \qquad z^* = \frac{z}{L}$$

$$P^* = \frac{P}{P_i} \qquad \rho^* = \frac{\rho}{\rho_i} \tag{4.10}$$

$$t^* = t\frac{C_i}{L}$$

where subscript $i$ denotes the initial conditions in the pipe. The resulting non-dimensionalized equations are:

$$dP^* \pm \rho^* C^* dV^* = \frac{fL}{D}\frac{\rho^*}{k}\frac{V^*|V^*|}{2}\left[\frac{k-1}{k}V^* \mp C^*\right]dt^* \tag{4.11}$$

$$\frac{dz^*}{dt^*} = \frac{V^*}{k} \pm C^* \tag{4.12}$$

$$dp^* - \frac{dP^*}{kC^{*2}} = -\frac{fL}{D}\left(\frac{k-1}{k^2}\right)\frac{\rho^*}{C^{*2}}\frac{V^{*2}}{2}|V^*|dt^* \tag{4.13}$$

$$\frac{dz^*}{dt^*} = \frac{V^*}{k} \tag{4.14}$$

For the upstream boundary condition, when the pressure is prescribed at the pipe inlet, the steam velocity and density are obtained from the backward travelling characteristic and the path. In the downstream boundary, the pressure matching condition is imposed such that the pressure in Region II equals the pressure at the last spacial node of Region I. This condition coupled with the equation for the pressure in Region II allows the determination of the steam velocity and density at the boundary from the forward travelling characteristic and the path.

4.1.2 Condensation Region in the Pipe (Region II)

A one-volume, isothermal model is used to describe the behavior of this region. The mass balance in this region is

$$\frac{d\rho_{CON}}{dt} = \frac{1}{V}\left(\dot{m}_{in} - \dot{m}_c - \rho_{CON}\frac{dx}{dt}A\right) \tag{4.15}$$

where $\rho_{CON}$ = steam density

$\dot{m}_{in}$ = Rate of steam flowing into Region I

$\dot{m}_c$ = Condensation rate in Region II

$\frac{dx}{dt}$ = Slug velocity

$V = (x + x_c)A$

and $x$ = Distance from pool surface to the interface.

The volume of the condensation region $V$, is a function of the location of the interface (Figure 4.1); and, $x_c$ is chosen to be 30. cm such that the height of the condensation region is higher than the chugging height for all chugs observed in the experiment. This way the singularity at $V=0$ is circumvented. The choice of $x_c$ and its effects on the final solution have been studied. They are reported in Appendix H. It is found that the solution is rather insensitive to the choice of this parameter.

The mass flux flowing into this region at any instant is given by

$$\dot{m}_{in} = \rho_N V_N A \tag{4.18}$$

where $\rho_N$ and $V_N$ are the steam density and velocity at the boundary between Regions I and II.

The condensation rate $\dot{m}_c$ at any instant is

$$\dot{m}_c = h A_p (T_{sat} - T_\ell) \tag{4.19}$$

where $A_p = 2\pi r_o X_1$

$h$ = heat transfer coefficient

$T_{sat}$ = Saturated steam temperature

$T_\ell$ = Pool water temperature

The length of $X_1$ therefore defines the heat transfer surface in this region. During slug upflow, the value of $X_1$ is equal to the length between the pool free surface to the interface position representing the part of the pipe which is cooled by the outside pool water. During slug discharge $X_1$ is the length of the water film left on the wall which is assumed to be the distance from the maximum chug height to the interface position.

The pressure in this region is related to the density by the isothermal relation for steam,

$$\frac{P_{CON}}{\rho_{CON}} = k_1 \tag{4.20}$$

where $k_1 = P_i / \rho_i$

i.e., $k_1$ is given by the initial conditions in the pipe which is assumed to be saturated.

### 4.1.3 Water Slug Motion

The motion of the water slug into and out of the vent pipe is based on the slug model developed by Chan and Liu.[32] The model is a one-dimensional momentum balance of the water slug in the pipe. The complicated processes of the interface spreading, and the flow separation are not accounted for by this simple model.

The momentum balance for the water in the vent (see Figure 4.1) is given by

$$\frac{d(mu)}{dt} = -\rho_w u^2 A + A(P_{CON} + \rho_w g(L-x) - P_e) \quad (4.21)$$

where $u$ = Slug velocity

$L$ = Submergence depth

and $P_e$ = Pressure of the water at the pipe exit.

$P_{CON}$ is the pressure in the condensation region, and $m$ is the total mass of the slug which consists of the actual mass of the water column and an apparent mass which is assumed to be proportional to the length of the steam column in the pipe below the pool surface. Thus,

$$m = \rho_w (L-x) A + \beta \rho_w A x,$$

where $\beta$ is the proportionality constant. In the case of no interfacial mass transfer, $\beta$ was found to be between 0.2 and 0.4 for slug discharge.[32] For the slug upflow, no apparent mass is expected, and $\beta$ is set to zero.

The coupling between the slug and the condensation region is more complicated. The slug position governs the volume of the condensation region, its velocity affects the density changes in the region, while steam pressure in turn affects the slug acceleration.

### 4.1.4 Bubble Dynamics Model at the Pipe Exit

The bubble at the pipe exit is modelled by a one-dimensional, spherical vapor bubble with a vapor source in an infinite pool. The equations that describe the dynamics of this bubble are the conservation equations for the vapor, the liquid and the interface. The equations are presented in Appendix G.

From physical observation during the growth phase, the bubble shape resembles that of a pear, the interface is smooth and glassy

but irregular (see Figure 3.4.5 or 6). During the bubble collapse phase, the surface becomes rough with liquid jets penetrating into the bubble at certain preferential locations, for example, the circumferential "belt" which forms near the bottom of the encapsulating bubble. Thus, the spherical bubble model is only a crude description of the actual bubble. Furthermore, if the pool boundaries and the free surface are close to the bubble (e.g., within a few bubble radii), they would also affect the bubble dynamics for both the growth and the collapse processes. These boundary effects are not accounted for in the present model.

The coupling between the bubble dynamics and the steam in the vent pipe is given by the requirement that the pressure at the exit equal that in the bubble. In addition, the steam flow at the pipe exit acts as a vapor source for the bubble. To account for the condensation in the pipe during this period while the bubble is growing at the pipe exit, the calculated condensation in the pipe is subtracted from the steam flow at the pipe exit, and the net flow is injected into the bubble.

The pressure matching condition is again used as the boundary condition at the pipe exit (see Section 4.1.1). The mass and energy balances in the bubble with the vapor injection are:

$$\frac{d\rho_B}{dt} = \frac{3}{r_B}\left(-m_c - \rho_B \frac{dr_B}{dt} + \frac{m_v A}{4\pi r_B^2}\right) \qquad (4.21)$$

$$\rho_B C_v \frac{dT_B}{dt} = \frac{3}{r_B}\left(-m_c \frac{P_B}{\rho_B} - P_B \frac{dr_B}{dt} + \frac{m_v A C_v (\Gamma T_v - T_B)}{4\pi r_B^2}\right) \qquad (4.22)$$

where $P_B$ = steam density in the bubble

$r_B$ = Bubble radius

$\Gamma$ = Specific heat ratio

$C_v$ = Specific heat

The vapor injection rate is $\dot{m}_i A$ which is given by

$$\dot{m}_i A = \rho_e V_e A - \dot{m}_{cp} \tag{4.23}$$

$P_e$ and $V_e$ are the density and the velocity of the steam at the pipe exit respectively. $\dot{m}_{cp}$ is the condensation on the inner and the outer wall of the pipe. The heat transfer area on the outer wall is equal to the area encapsulated by the bubble. Since experiments show that the growth of encapsulating bubbles is toward the pool surface, the bottom of the bubble is assumed to be at a distance $\frac{4 r_B}{3}$ below the exit. Hence the outside pipe area which is encapsulated by the bubble is

$$A_{op} = 2\pi R_o \left(2 r_B - \frac{4}{3} r_o\right)$$

where $R_o$ = Outer pipe radius

$r_B$ = Bubble radius

$r_o$ = Inner pipe

and the total condensation rate is given by

$$\dot{m}_{cp} = h(A_p + A_{op})(T_{sat} - T_\ell) \tag{4.24}$$

where h = Heat transfer coefficient

$T_{sat}$ = Saturated steam temperature

$T_\ell$ = Pool water temperature

$A_p = 2\pi r_o L$

and L = Submergence depth

The heat transfer coefficient appearing on this equation does not

have the same physical meaning as the h given for the condensation in the pipe during slug discharge. However, they are expected to be on the same order of magnitude and in the present model the same value of h is assumed flor slug upflow, discharge, and during bubble growth.

The criteria concerning the initiation of the bubble collapse which leads to the chug is based in the physical observation described in the previous chapter. These criteria, called the chugging criteria, are depicted on Table 4.1. As the interface progresses toward the exit during the slug discharge calculation, if the slug flow reverses before the interface reaches the pipe exit, an internal chug is assumed. If the interface crosses the pipe exit and enters the pool, the pressure at interface clearing is recorded. If this pressure exceeds that of the ambient water, $P_{\ell}$, an encapsulating bubble at the pipe exit is assumed to form. If this pressure is less than $P_{\ell}$, a detached bubble is assumed to form at the vent exit.

For the detached bubble, two conditions have to be simultaneously met before the water slug is allowed to re-enter the vent. First, the bubble must have collapsed to $0.9\,\gamma_o$. Second, the average vent pressure at that time must be less than $P_{\ell}$.

For the encpasulating bubble, three conditions have to be simultaneously met before the water slug is allowed to re-enter the vent. First, the bubble must have attained a radius greater than $1.5\,\gamma_o$. Second, the large bubble must be collapsing and the collapse has led to a decrease in bubble volume by 5.% from its maximum. Third, the average vent pressure must be below the ambient water pressure $P_{\ell}$.

The above criteria for the initiation of chugging are based on either experimental observations or physical arguments. One of the major differences between the encapsulating bubble chugs and the detached bubble chugs is whether the steam pressure at the interface as it clears the vent exit is greater or less than the ambient pressure $P_\ell$. When this pressure is greater than $P_\ell$ an encapsulating bubble is formed; otherwise, a detached bubble is formed. For detached bubbles, since it collapses immediately after formation, its radius never exceeds that of the pipe ( $r_0$ ). A reasonable assumption is that the chug occurs when the bubble radius is reduced to 0.9 $r_0$ . For encapsulating bubbles, the bubble starts to grow immediately after its formation. However, a few intermediate bubbles may grow and collapse before a large chugging bubble is formed. The requirement that the bubble radius must exceed 1.5 $r_0$ is to ensure that a large chugging bubble is formed before the water slug is allowed to reenter the vent. Experimental observations indicate that the radius of the large chugging bubble is generally larger than 1.5 $r_0$ . As the bubble collapses, a jet of liquid is observed to penetrate into the bubble from the bottom. The experimental data show that the bubble volume is decreased by approximately 5.0% from the maximum bubble volume when the rapid collapse of the lower part of the bubble is observed. Finally, on physical grounds, the vent pressure must be low during the liquid jet penetration since some driving force is required for the water slug to flow up the vent. Therefore, the last criterion requires the average vent pressure to be below $P_\ell$.

In sum, other than the internal chug where the calculation

TABLE 4.1

SUMMARY OF THE CRITERIA DEFINED FOR CHUGGING

| Type of Chug | Chugging Criteria |
|---|---|
| Internal Chugs: | (1) Water slug reverses flow direction during discharge. |
| Detached Bubble Chugs: (Steam pressure at Vent Clearing $< P_e$) | (1) Bubble radius reduces to 0.9 $r_o$<br>(2) Average vent pipe pressure $< P_e$ |
| Encapsulating Bubble Chugs: (Steam Pressure at Vent Clearing $> P_e$) | (1) Bubble radius exceeds 1.5 $r_o$<br>(2) Bubble volume reduced by 5.0% for maximum<br>(3) Average vent pipe pressure $< P_e$ |

Note : $P_e$ = water pressure at the pipe exit

automatically predicts the slug flow reversal during the discharge, both the detached bubble chug and the encapsulating bubble chug requires that the chugging criteria described above be met before the calculation is switched back to the first model (Figure 4.1) where the motion of the water slug re-entering the vent is calculated.

The vent pipe model is basically completed at this point, except for the unknown heat transfer coefficient to be determined. The set of equations governing the condensation region and the slug motion is solved by the Euler method. After slug discharge, the condensation region is eliminated and the pipe flow model is directly coupled to the bubble dynamics model at the pipe exit. The detailed solution procedure is described in Appendix H.

### 4.1.5 Bubble Collapse Model and the Peak Pressure Developed

The model used to compute the bubble collapse and the resulting peak pressure is the infinite pool, spherical vapor bubble model described in Appendix G. However, instead of having a vapor source, a vapor sink is introduced to model the condensation caused by the liquid jet. The magnitude of the sink is to be determined from the experimental data.

As has been stated, the penetration of the liquid jet is the main cause for the rapid bubble collapse. Not only is the jet responsible for the introduction of a vapor sink into the bubble, it is also responsible for separating the bubble from its vapor source, i.e.,

the vent exit. The situation is similar to an isolated bubble collapsing under the influence of a sudden pressure reduction, which represents the rapid condensation initiated by the jet penetration and atomization. Since the actual bubble is not spherical, and the pipe solid boundary is neglected, the model is not expected to give exact values for the overpressure developed near the vent exit due to the rapid collapse. Accordingly, only an order of magnitude type of accuracy is expected from this model.

Inside the bubble, the heat transfer to the liquid, either to the liquid jet or the droplets from the atomization, is calculated by an overall heat transfer coefficient, $UA_c$ . The heat transfer to the liquid is then given by

$$Q = UA_c (T_{sat} - T_\ell) \tag{4.25}$$

Since both $U$ and the surface area for condensation $A_c$ are unknown, they are lumped together as a single parameter to be determined from the experimental data. From the pool bottom pressure data, the most accurate information concerning the bubble collapse is the time period $\Delta t_c$ from the minimum pressure when the collapse starts to the maximum pressure when the collapse is completed. If $UA_c$ is assumed to be a constant, then by varying this constant in a number of theoretical computations, the correct value can be identified by matching the predicted time periods ( $\Delta t_c$ ) to those experimentally measured. The motivation for using this method in estimating $UA_c$ is mased on two observations. First, it

should be recalled from section 1.2 that the collapse time for a spherical cavity with radius $r_c$ is given by

$$\tau = 0.91468\, r_c \sqrt{\frac{\rho_w}{p_\infty}} \qquad (4.27)$$

For a bubble of 4 cm. radius, which is about the observed sizes in the experiment, the collapse time is approximately 3.5 msec for the conditions in the experiments. If $\forall A_c$ is infinite the collapse time would be equal to this value, which is a lowerbound for the collapse time. If $\forall A_c$ is small, then the maximum pressure based on theory would be delayed to a much longer time. Thus an $\forall A_c$ exists where the time scale could be made the same as those observed in the experiments (which is about 9.0 msec). The second observation is that at the beginning of the collapse, the pool motion is slow and the flow is incompressible. Thus, any pressure change in the bubble is transmitted instantaneously; this means that the underpressure in the bubble is immediately transmitted to the pool bottom. At the end of the collapse, the velocity of the interface is high and the flow may be incompressible; however, the distance of the pool bottom to the bubble is only 25. cm; thus, considering the high velocity of sound in water, the transmission of this pressure pulse is on the order of a fraction of a milli-second. As far as the experimental data are concerned, this is instantaneous. Consequently, this method is chosen for the determination of $\forall A_c$.

The most important observation in the bubble collapse movies is that the bubble is usually shattered right before the collapse reaches a minimum or during the first rebound; and, as mentioned previously, a premature shatter of the bubble leads to smaller

peak pressures. Thus, by assuming that the shatter occurs during the first rebound, an upperbound estimate of the peak pressures is obtained. Accordingly, the theoretical calculation is terminated after the bubble reaches its first pressure peak at which time the collapse should be almost completed.

### 4.1.6 Physical Phenomena Neglected in the Model

There are a number of physical mechanisms that are observed in the experiments but are not included in the theoretical model. This section examines the effects of these phenomena on the theoretical results.

During the water slug discharge, the interface is assumed to remain flat. The interface spreading, and the flow separation phenomena during the slug downflow, are neglected in the model. Since some water is left in the pipe during the discharge, the actual moving mass in the water column is reduced. Therefore, the resulting pressure in the vent as computed by the model would be higher than the measured since it requires more pressure to discharge the slug.

During the water slug discharge period, the flow of the slug into the pool induces the formation of a ring vortex or vortices around the exit, such that upon vent clearing and bubble formation, the heat transfer rate is very high at the vicinity of the exit. The growth and collapse of the smaller bubbles, mentioned in the statistical data, may have a lot to do with these vortices. In any event, this is not included in the present model. The effect on the theoretical results is that the bubble formation process is faster than

the experimentally measured for the case of encapsulating bubbles. In the case of detached bubbles the effect is small since bubble detachment occurs.

The second vent pressure drop is believed to be caused by the interface spread upon slug coast down at its maximum height. The additional rapid heat transfer due to this phenomenon is not modelled. This would cause an underestimate of the maximum chug height since the further drop in vent pressure is expected to cause the slug to rise up further into the pipe.

The effects of the pool free surface, pool solid boundaries on the bubble growth and collapse process have been totally neglected. It is expected that for the geometric conditions in the present experiments, they play only a minor role; but, for other geometries, they may have a large effect on the bubble dynamics. The infinite pool assumption needs to be examined.

Finally, the vent pipe solid boundary plays an important part in both the bubble growth and collapse. Exactly how the vent pipe affects the bubble motion is unknown. This is a major inadequacy in the present model.

TABLE 4.2

PHYSICAL PHENOMENA NOT INCLUDED

IN THE PRESENT MODEL

| | Phenomenon | Effect on Theoretical Results |
|---|---|---|
| (1) | Interface spread | Higher vent pressures |
| (2) | Vortices in the pool | Faster bubble growth |
| (3) | Heat transfer during interface spread | Lower chug heights |
| (4) | Pool boundary effects | Unknown (Not important in the present experimental geometries) |
| (5) | Vent pipe boundary effect | Unknown (Expected to be important during bubble collapse) |

## 4.2 Determination of the Heat Transfer Coefficients for the Theoretical Model

There are basically two heat transfer mechanisms during the entire steam chugging process: one is related to the steam condensation caused by the liquid jet penetration during the collapse stage; the other is related to the steam condensation caused by the liquid inside the vent pipe during the bubble growth stage, and during the upward and the downward motion of the water slug inside the pipe.

### 4.2.1 Determination of the Condensation Heat Transfer Coefficient During Bubble Collapse

As was mentioned previously, the time period from the bubble minimum pressure to the bubble maximum pressure, $\Delta t_c$, during a bubble collapse can be accurately identified from the experimental data. At the end of this period the bubble collapse is generally completed. Based on the physical reasoning given in Section 4.1.5, this time period can be used to determine the heat transfer during the jet penetration and atomization. The basic procedure is to vary the overall heat transfer parameter $UA_c$ in the theoretical computations until the predicted matches the measured values of $\Delta t_c$ In the computations, $UA_c$ is assumed to be a constant until the bubble radius has reduced to one-half of its original radius. Then $UA_c$ is assumed to be proportional to the volume of the bubble. This assumption is introduced because, physically, a bubble with zero volume cannot contain a liquid jet.

Based on the above criteria a set of computer runs was made

to determine the value of $UA_c$ which matches the experimentally measured time period $\Delta t_c$. In these calculations the initial bubble radius is determined from the movie data for experimental Run FM5. the initial bubble pressure is chosen to be atmospheric (the vent pressure data supports this choice). Table 4.3 shows the comparison between measured pool bottom pressure and the predicted bubble pressures for three different values of $UA_c$. For $UA_c$ = 0.437 kw/°C, the predicted $\Delta t_c$ is found to be 20 msec. For $UA_c$ = 4.37 kw/°C, the predicted $\Delta t_c$ matches the measured. For $UA_c$ greater than 4.37 kw/°C, the predicted $\Delta t_c$ remains constant. Thus, the present method does not seem to give a unique value of $UA_c$. In this study, the minimum value of $UA_c$ ( = 4.37 kw/°C) is chosen. It should be cautioned that this value only gives the minimum order of magnitude of the heat transfer rate. The actual overall heat transfer rate may be higher.

### 4.2.2 Determination of Condensation Heat Transfer Coefficient in the Pipe

This section is concerned with the determination of the heat transfer coefficients associated with the slug upflow, slug discharge, and during bubble growth. For simplicity they are assumed to have the same value. Thus, only one heat transfer coefficient is determined in this study.

#### A. Initial Conditions in the Pipe

Before the theoretical calculations are made, the initial conditions in the pipe need to be identified. This is done with the physical picture obtained in the vent pressure experiments. Recall,

TABLE 4.3

PREDICTED BUBBLE PRESSURES BASED ON A FEW VALUES OF $UA_c$ VS. MEASURED (RUN NO. FM5)

| Time, ms. | Measured Pool Bottom Pressure, kPa | Predicted Bubble Pressure, kPa $UA_c = 0.437$ | $UA_c = 4.37$ | $UA_c = 43.7 \frac{kw}{^oC}$ |
|---|---|---|---|---|
| 0 | 94.4 | 101.3 | 101.3 | 101.3 |
| 1 | 92.6 | 88.6 | 76.3 | 67.9 min. |
| 2 | 92.0 min. | 86.1 | 72.2 min. | 68.7 |
| 3 | 95.4 | 87.5 | 74.5 | 70.7 |
| 4 | 98.9 | 82.9 min. | 79.5 | 74.2 |
| 5 | 103.6 | 89.8 | 86.7 | 70.4 |
| 6 | 104.0 | 111.2 | 95.4 | 85.4 |
| 7 | 119.8 | 122.1 | 107.3 | 110.5 |
| 8 | 112.3 | 129.4 | 126.4 | 690.6 max. |
| 9 | 132.8 max. | 129.4 | 711.8 max. | $r_{min} = .2r_{max}$ |
| 10 | | 120.5 | $r_{min} = .2r_{max}$ | |
| 11 | | 109.3 | | |
| 12 | | 98.5 | | |
| 13 | | 92.1 | | |
| 14 | | 89.5 | | |
| 15 | | 92.0 | | |
| 16 | | 98.1 | | |
| 17 | | 106.5 | | |
| 18 | | 112.5 | | |
| 19 | | 123.8 | | |
| 20 | | 163.0 $r_{min} = .3r_{max}$ | | |
| $\Delta t_c$ | 7.0 ms | 16.0 ms | 7.0 ms | 7.0 ms |

Note: $r_{max}$ = Initial bubble radius determined from the movies,

$T_p$ = Pool water temperature,

$r_{min}$ = Bubble radius at peak pressure.

Run No. FM5

$r_{max} = 4.98$ cm

$T_p = 62.8^oC$

from section 3.3, that the vent underpressure, induced by either the draining of the liquid layer off the pipe wall and their accumulation at the exit (for internal chugs and detached bubble chugs), or the liquid jet penetration and atomization phenomenon (for encapsulating bubble chugs), always occurs before a rapid rise in the steam velocity takes place. At this point, where the first vent underpressure just reached its minimum, the steam velocity is still low; and the water is right at the exit ready to chug up the vent. This is the point where all the conditions are known. Taking advantage of this observation, the initial conditions for the calculation are then approximately determined.

For the steam velocity, the exact value is unknown, a low velocity 7.6 m/sec is assumed. Other values such as 15.2 m/sec, and 3.8 m/sec, for the velocity, have been used; it is found that the effect on the vent clearing time is small. For the vent pressure, since the underpressure occurs at the exit of the pipe, it is reasonable to assume that the average pressure in the vent is one-half of the magnitude of the underpressure. Thus, the initial conditions already included the first vent underpressure. Finally, since the slug position is right at the exit, no approximation is required.

The conditions in the surge tank are determined from the surge tank experiments where the pressure there is measured. A typical encapsulating bubble chug is selected from Run ST4. Then the measured surge tank pressure for that chug is used as input into the theoretical model defining the upstream boundary condition. The calculation may then proceed when the total heat transfer coefficient is assumed.

B. Determination of h

Since steam condensation in the pipe, albeit the complicated interfacial conditions, resembles the free falling laminar film condensation, it is assumed that the total heat transfer coefficient h is related to the Nusselt film condensation coefficient [40] However, due to the wavy steam-water interface it is expected that the heat transfer coefficient is greater than the Nusselt coefficient. A multiplier C is used to account for these effects:

$$h = C\, h_{Nu} \tag{4.28}$$

where $h_{Nu}$ for a flat plate of length $x$ is

$$h_{Nu} = 1.13 \left( \frac{g \rho_w^2 h_{fg} x^3}{\mu_\ell k_\ell \Delta T} \right)^{1/4} \tag{4.29}$$

and $\Delta T = T_{sat} - T_{pool}$

The maximum heat transfer coefficient from a vapor to a cooled surface of its own liquid as reported by Maa[38] is approximately a hundred times the Nusselt film coefficient. Thus C is bounded between one and a hundred. In the present study C is determined by matching the calculated vent clearing time and bubble growth time to the experimental results. The best value, based on comparison with Run ST4, is C=14.0. In general, a larger value of C would cause the chugging height to increase and a delay in the vent clearing time. However, the large value of C clearly indicate that the assumed laminar film condensation coefficient failed to describe the actual condensation process.

## 4.3 Comparison with Experimental Data and Discussion

This section presents the comparisons of the model predictions against the experimental data. But, before the comparisons are

presented, a critique on the present models is put forth here to examine the compatibility of the model with the physical phenomena involved in steam chugging.

In the vent pipe model, in addition to the numerous neglected phenomena discussed in Section 4.1.6, a number of other effects which play various roles in the chugging process need to be mentioned. First, irregular bubble surface during the bubble growth phase is observed in the movies. The cause of these surface irregularities is unknown. They may be a result of the non-uniform heat transfer rate at different parts of the surface. More rapid condensation may occur at a few spots at the bubble surface. They may also be a result of the non-uniform temperature distribution in the pipe. In any event, the end result of these irregularities is that they affect the growth of the bubble, and, thus, the maximum size of the bubble which controls the final pressures developed in the collapse. They also serve as preferential spots for the collapse to take place. Second, the effect of the vent pipe solid boundary, as well as the free surface, may also affect the growth and the collapse of the bubble. Exactly how each of these affects the final pressures developed in a collapse is not known.

In the bubble collapse model, the collapse pressure is affected by the vent pipe solid boundary and the translational motion of the bubble. It is observed in the movies that as the bubble reaches its maximum size it begins to translate towards the free surface. The effect of this translational motion on the collapse pressures is unknown and not modelled. Moreover, the heat transfer

at the bubble surface is observed to be non-uniform; during initiation of the collapse, the bubble bottom is seen to be rough and wavy, indicating rapid condensation, while the top part is still glassy and smooth. All these effects may seriously affect the bubble collapse pressures.

The simple one-dimensional spherical bubble model during bubble growth and bubble collapse is simply inadequate. Considering the numerous assumptions, approximations, and crudely determined heat transfer parameters (i.e., the h for the condensation in the pipe, and $UA_c$ for the liquid jet penetration and atomization), it is expected that the present simple model is incapable of predicting the complicated phenomena. As mentioned before, the present modelling effort is only a first step. It gives an account of the numerous modelling difficulties encountered, highlights the areas of deficiencies in the physical understanding, and provides a basis for future improvements. Hence, in the following comparisons, exact magnitudes of the measured and the predicted are not important; however, it would be interested to see if certain experimentally observed trends are reflected by the model.

There are two different sets of comparisons: one compares the measured pool bottom pressure with the predicted; and, the other compares the vent clearing time and the bubble growth time. The former is based on the bubble collapse model and the latter is based on the vent pipe model.

### 4.3.1 Comparison of Experimental Pool Bottom Pressures with Bubble Collapse Model Predictions

Based on the determined overall heat transfer rate, $UA_c$ = 4.37 kw/°C, a comparison against four other encpasulating bubbles at various pool temperatures is made. The comparisons are shown in Table 4.4. The predicted time period in each case, $\Delta t_c$ , agrees well with the experimental data. Moreover, the predicted peak pressures are higher in the low pool temperature cases. This agrees with the observed trends in the measured pool bottom pressures.

Next, based on the peak pressures determined for these cases, and, by assuming that the magnitude of the pressure spike decreases inversely with the distance from the bubble collapse center [28], the pool bottom pressures can be computed and compared against the measured pressure spikes. Table 4.5 depicts the resulting comparison. In the theoretical calculations, the bubble collapse center is assumed to be at the pipe exit. The initial bubble radius in each case is determined from the movies, and the initial conditions in the bubble are assumed to be saturated at atmospheric pressure. The vent pressure data supports this choice for the initial bubble pressure.

The resulting comparisons are shown on Table 4.5. Runs FM1 and FM2 have the same submergence depth and, therefore, in the theoretical calculation the only differences between the two cases are the initial bubble radii and the pool temperatures. The theory predicted a decrease in pool bottom pressure as the pool temperature is increased. This agree in trend with the measured. Similar agreement is found for the other set of runs (FM3, 4, 5) with a different

TABLE 4.4

Comparison of Predicted and Measured $\Delta\tau_c$ and

Predicted Bubble Pressure vs Measured Bubble Pressure

$UA_c = 4.37$ kw/°C

| Run No. | Predicted $\Delta t_c$, ms. | Measured $\Delta t_c$, ms. |
|---|---|---|
| FM1 | 5 | 6 |
| FM2 | 6 | 7 |
| FM3 | 5 | 5 |
| FM4 | 5 | 5 |
| FM5 | 7 | 7 |

| | Time, ms. | Measured Pool Bottom Pressure kPa | Predicted Bubble Pressure kPa |
|---|---|---|---|
| Run No. FM1 | 0 | 98.4 | 101.3 |
| $r_{max}$=4.66cm | 1 | 95.9 | 70.2 |
| $T_p$=53.9°C | 2 | 93.6 | 65.1 * |
| L=25.4cm | 3 | 92.0 * | 68.0 |
| | 4 | 92.1 | 74.3 |
| | 5 | 95.1 | 83.5 |
| | 6 | 100.4 | 97.4 |
| | 7 | 113.9 | 121.4 |
| | 8 | 152.7 * | 791.7 * |
| Run No. FM2 | 0 | 98.5 | 101.3 |
| $r_{max}$=4.8cm | 1 | 96.3 | 75.1 |
| $T_p$=62.8°C | 2 | 94.4 | 71.5 * |
| L=25.4cm | 3 | 93.8 * | 73.9 |
| | 4 | 94.3 | 78.8 |
| | 5 | 96.7 | 85.7 |
| | 6 | 100.7 | 94.2 |
| | 7 | 106.7 | 102.8 |
| | 8 | 115.9 | 134.7 |
| | 9 | 152.9 * | 601.7 * |
| Run No. FM3 | 0 | 79.2 | 101.3 |
| $r_{max}$=4.52cm | 1 | 74.2 | 62.5 |
| $T_p$=37.2°C | 2 | 72.4 * | 54.9 * |
| L=50.8cm | 3 | 83.9 | 57.6 |
| | 4 | 109.6 | 65.6 |
| | 5 | 120.6 | 80.0 |
| | 6 | 129.9 | 114.3 |
| | 7 | 148.8 * | 1466.2 * |

(continued)

TABLE 4.4 (continued)

| | Time, sec. | Measured Pool Bottom Pressure kPa | Predicted Bubble Pressure, kPa |
|---|---|---|---|
| Run No. FM4 | 0 | 88.0 | 101.3 |
| $r_{max}$=4.28cm | 1 | 83.2 | 71.6 |
| $T_p$=46.1°C | 2 | 80.8 * | 59.6 * |
| L=50.8cm | 3 | 81.9 | 62.8 |
| | 4 | 90.3 | 70.5 |
| | 5 | 125.5 | 85.1 |
| | 6 | 116.6 | 112.8 |
| | 7 | 143.1 * | 1234.1 * |
| Run No. FM5 | 0 | 94.4 | 101.3 |
| $r_{max}$=4.98cm | 1 | 92.6 | 76.3 |
| $T_p$=62.8°C | 2 | 92.0 * | 72.2 * |
| | 3 | 95.4 | 74.5 |
| | 4 | 98.9 | 79.5 |
| | 5 | 103.6 | 86.7 |
| | 6 | 104.0 | 95.4 |
| | 7 | 119.8 | 107.3 |
| | 8 | 112.3 | 126.4 |
| | 9 | 132.8 * | 711.8 * |

Note: $r_{max}$ = maximum bubble radius determined from the movie data.

TABLE 4.5 PREDICTED MAXIMUM PRESSURES AT THE POOL BOTTOM VS. MEASURED (for encapsulating bubbles)

| Run No. | Pool Temp., °C | Predicted Minimum Bubble Radius, cm. | Predicted Pool Bottom Pressure, kPa | Measured Pool Bottom Pressure, kPa |
|---|---|---|---|---|
| FM1 | 53.9 | 1.305 | 35.3 | 51.4 |
| FM2 | 62.8 | 1.387 | 27.2 | 50.3 |
| FM3 | 37.2 | 1.118 | 59.8 | 47.3 |
| FM4 | 46.1 | 1.084 | 47.9 | 41.8 |
| FM5 | 62.8 | 1.379 | 32.7 | 31.6 |

| Run No. | Submergence Depth, cm. | Initial Bubble Radius,* cm |
|---|---|---|
| FM1 | 25.4 | 4.66 |
| FM2 | 25.4 | 4.80 |
| FM3 | 50.8 | 4.52 |
| FM4 | 50.8 | 4.28 |
| FM5 | 50.8 | 4.98 |

* Measured from movies

submergence depth. In general, the same trend is observed in all other experiments. Therefore, the model predicted the correct dependence of pool bottom pressure on the pool temperature.

Runs FM2 and FM5 have the same pool temperature and approximately the same initial bubble radius. The only difference is the submergence depth. The model predicts a decrease in pool bottom pressure with submergence but the data shows the opposite trend. It was reported in reference 11 that generally the measured pool bottom pressure decreases with submergence which conforms with the trend predicted by the model. Some other effect is responsible for the higher measured pool bottom pressure in FM2. Apparently some of the neglected effects such as those given in Section 4.3 are not negligible. Moreover, the crude value of $UA_c$ used to represent the condensation caused by the liquid jet penetration and atomization may be inadequate. The crudeness of the present model cannot give the exact cause of the higher measured pool bottom pressure in FM2.

In sum, the comparisons have shown the inadequacy of the present model; however, the general trends observed in the experiments are predicted.

### 4.3.2 Comparison of Experimental Data with Vent Pipe Model Predictions

This section presents the comparison between predictions from the vent pipe model and the experimental data. The four experiments (Runs ST1 - ST4) with the surge tank pressure data, are used for the present comparison. The results are shown on Figures 4.3 through 4.6.

A typical encapsulating bubble chug is chosen from each experiment for the comparison. In the calculations, the initial conditions in the vent and the upstream pressure at the surge tank are obtained from the experiments. The starting point in the calculation is at the initiation of the bubble collapse where the slug position is at the vent exit. The initial conditions in the vent are obtained based on the method described in Section 4.3.1.A.

Figure 4.3 shows the comparison with Run ST1. The vent clearing time for the water slug is predicted correctly; however, the model failed to predict the bubble collapse which leads to the next chug. This is due to the fact that the chugging criteria given for encapsulating bubbles requires the bubble radius to exceed 1.5 $Y_0$ before a collapse which causes the water slug to re-enter the vent is allowed. In the present case, the bubble radius never exceeded 1.5 $Y_0$. The chugging criteria are not met. Therefore, the collapse which leads to the next chug is not predicted.

In Runs ST2 and ST3, early vent clearing is predicted in both cases. Examining the experimental data, it is found that for both cases, a large second vent underpressure occurred. As discussed in Section 4.1.6, the second vent underpressure tends to increase the chug height which means an increase in the vent clearing time. In the case of Run ST1, the second vent underpressure is mild and, therefore, neglecting it does not cause an early vent clearing. But, for ST2 and ST3, the magnitude of the second vent underpressure is large; and since the model neglects the second vent underpressure it predicted an early vent clearing for both cases.

For the last case (Run ST4), the vent clearing time is again predicted since the second vent underpressure is small; however, the bubble growth time is underpredicted. This is an expected result because the high heat transfer rate at the bubble surface caused by the ring vortices generated during the slug discharged is not modelled.

Based on the comparisons with runs ST1 and ST4, some general trends of the theory predictions can be observed. First, the predicted chug heights are found to decrease as the pool temperature increases. This agrees with the trends observed in the plastic pipe experiments. Second, the predicted maximum bubble sizes are found to increase with the pool temperature. This, again, agrees with the experimentally observed trends.

In sum, these results indicated the inadequacies of the present model. But, again, the general trends observed in the experiments are predicted which is encouraging. This also indicates that further improvements in the theoretical model may eventually lead to success.

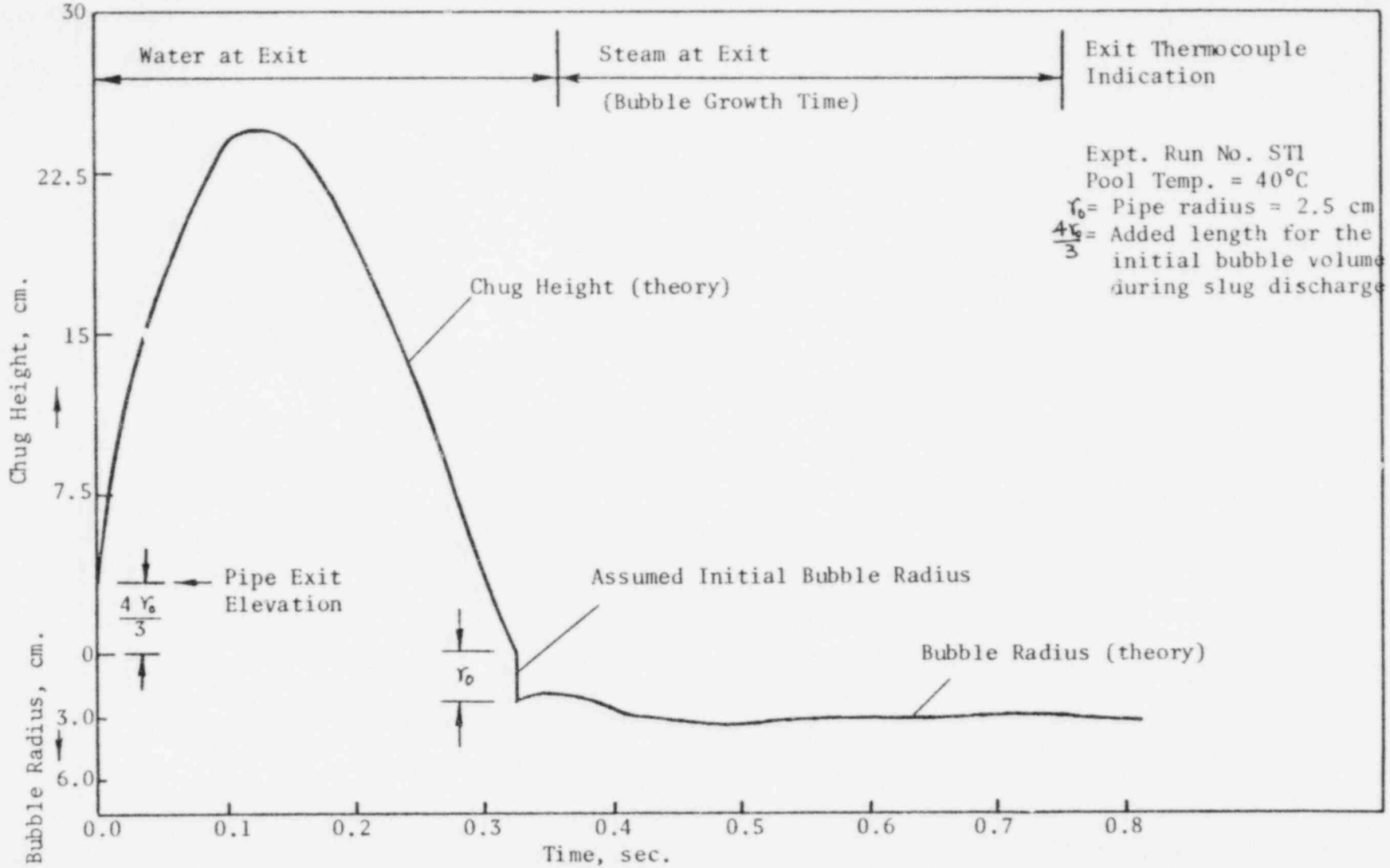


Fig. 4.3 Comparison of Theory Predictions with Experimental Data

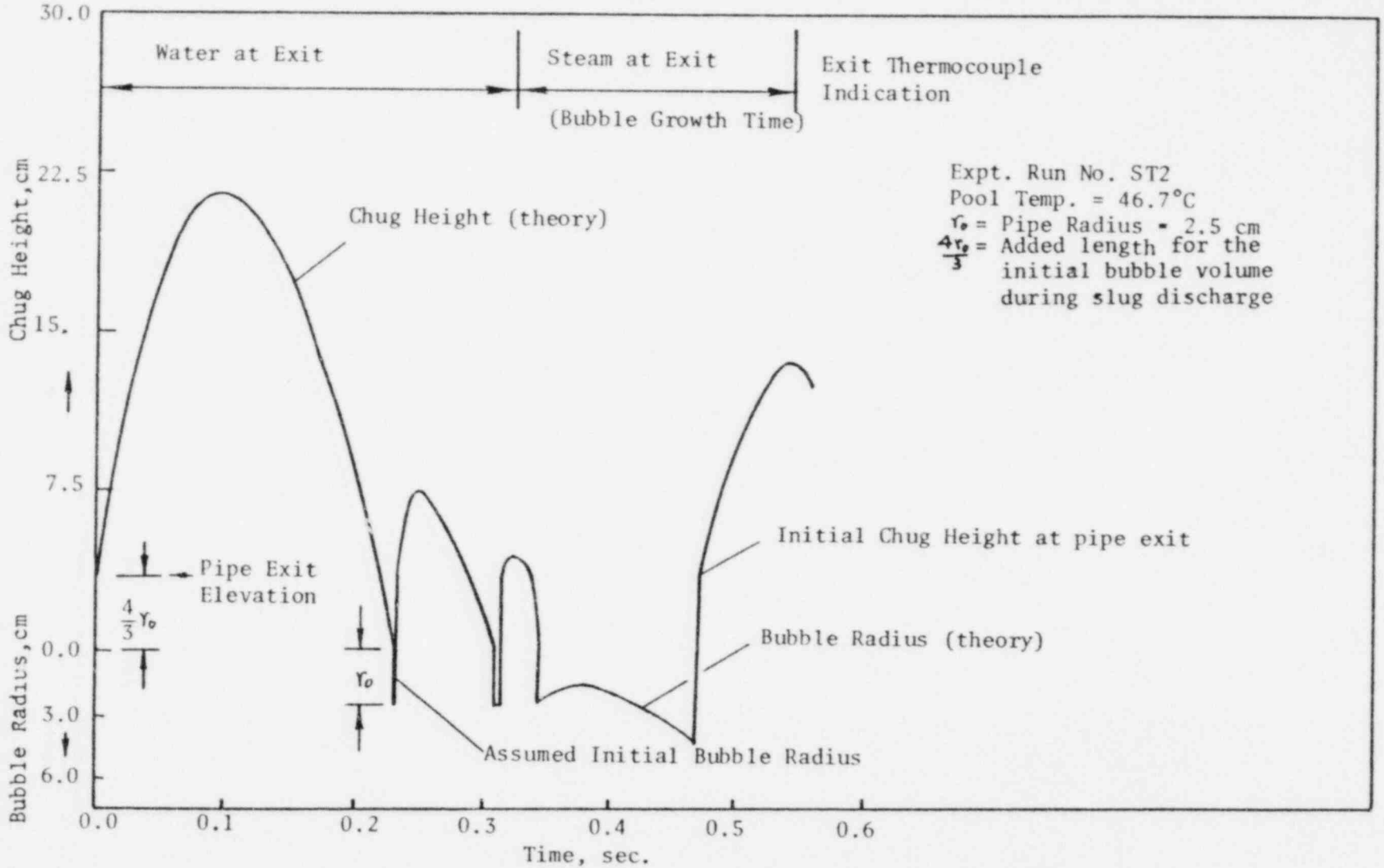


Fig. 4.4 Comparison of Theory Predictions with Experimental Data

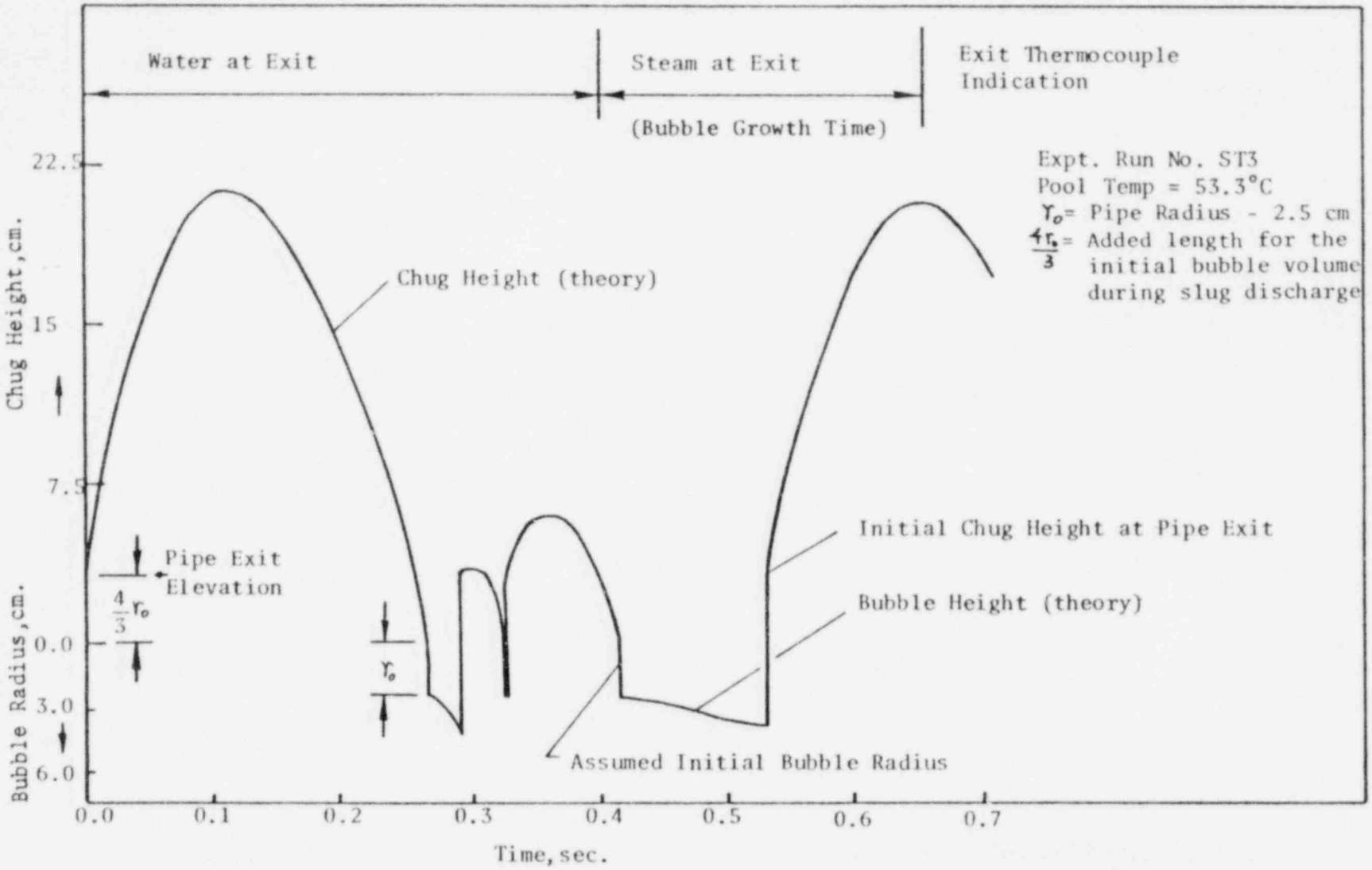


Fig. 4.5 Comparison of Theory Predictions with Experimental Data

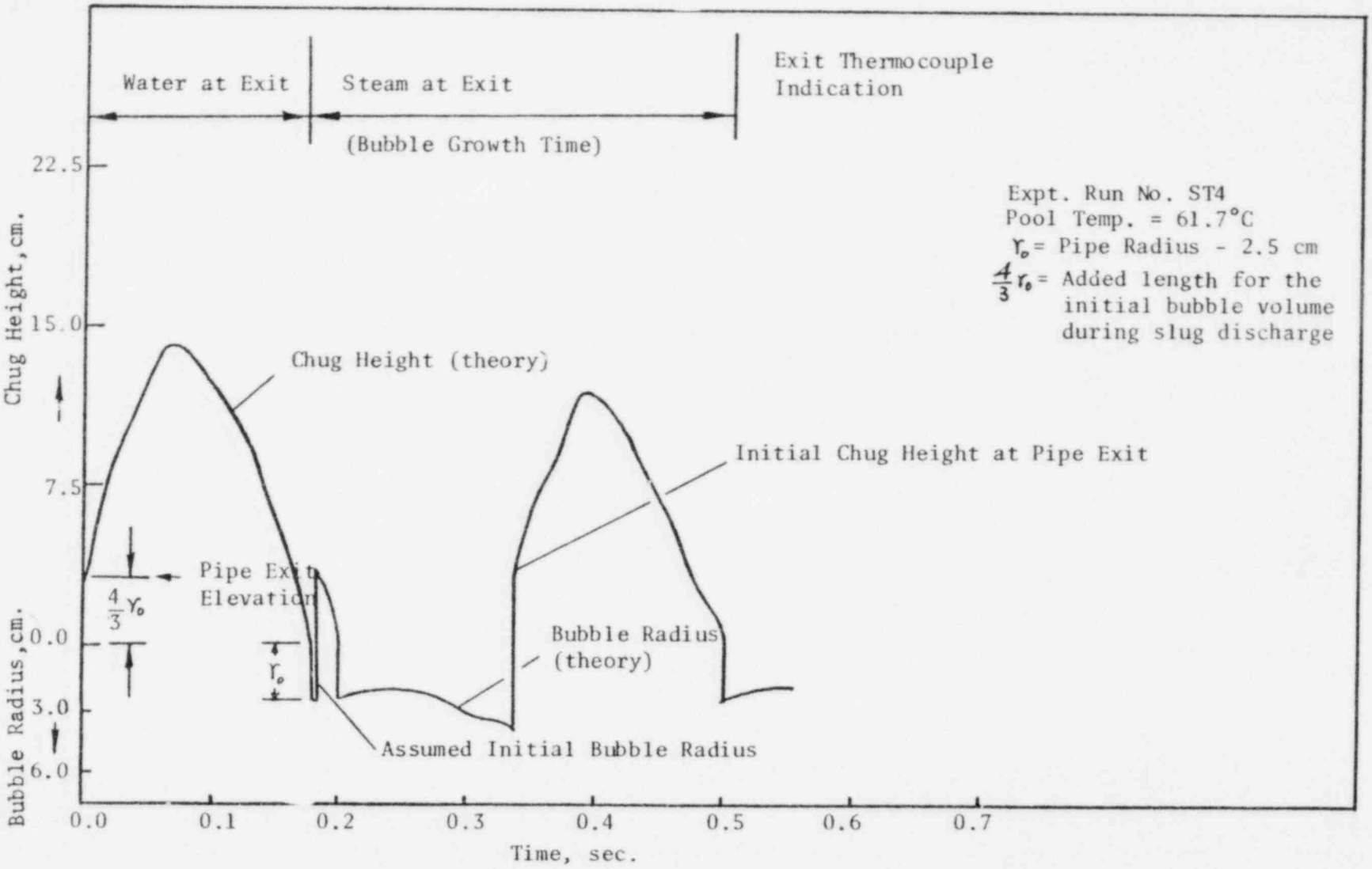


Fig. 4.6 Comparison of Theory Predictions with Experimental Data

# CHAPTER 5

# COMPARISONS OF THEORY PREDICTIONS WITH JAPAN 1/6-SCALE DATA

## 5.0 Introduction

Although the present theoretical models are far from perfect, it would be interesting to see how the models perform when applied to a larger scale system.

In this chapter, a comparison of the model prediction against the Japan 1/6-scale data is made. Of the numerous blowdown experiments presented in their report, only three of the single vent blowdowns are in the steam chugging condensation regime. However, two of these have the same pool temperature. Hence, only two cases with different pool temperatures are chosen for the present comparison.

## 5.1 System Geometry and Thermal-Hydraulic Conditions for the Comparison

Figure 5.1 shows the geometry of the Japan facility. The steam from a storage tank is discharged into the drywell, and then into the cylindrical wetwell through a 10.2 cm diameter vent pipe. A set of water level gages is placed at the exit end of the vent to measure the water level in the pipe during a chug (Figure 5.2). The two runs chosen for the present comparison are Run 214 and

Run 216. The conditions for these runs are depicted on Table 5.1. Steam at 558 kPa and 156°C is discharged from the storage tank into the drywell through an orifice which controls the discharge rate. The submergence depth in the two cases are the same (55 cm). The measured data for these two runs are reproduced and shown on Figures 5.3 through 5.6. The particular chug chosen for the comparison is marked on the figures. In Run 216, the variations of the pressure in the pool are small and an average pressure as shown on Figure 5.5 is used. In Run 214 the pool surface pressure variation is large; and, because the variations resemble a step change they are approximated by the step change as shown on Figure 5.3.

The calculation starts at the point where the bubble collapse is initiated by the liquid jet. At this point, the slug position is at the vent exit ready to chug into the vent. The assumed initial pressure in the vent for the calculation is uniform and equal to one-half of the measured vent underpressure at that point (same assumption as used in the comparisons in the last chapter). The initial vent pressure for the calculation is shown on Figures 5.3 to 5.5 for Runs 214 and 216 respectively. The initial steam velocity is uniform and is equal to 7.6 m/sec (same value as given in Section 4.1.3.A).

## 5.2 Results of the Comparison and Discussion

The comparisons are shown on Figures 5.7 and 5.8. In both cases, the predicted vent clearing time compares well with the measured. This indicates that the heat transfer coefficient determined in the present analysis

$$h = 14\, h_{Nu} \qquad (5.1)$$

is applicable to the Japan system. However, the measured rise in the water level is more rapid than the predicted. This indicates that the initial pressure in the vent may be lower than the value assumed in the calculation or an underestimate of the heat transfer coefficient during slug upflow.

On the bubble growth times, the comparisons are remarkably good. This is rather surprising because in all of the comparisons made in the last chapter, the theory invariably underpredicts the bubble growth time because the additional heat transfer caused by the vortices induced during the water slug discharge is not modelled. It is speculated that the good comparison may have been related to a counter effect at the pipe exit: the bubble which was formed in the experiment did not fully encapsulate the vent exit. A smaller bubble which only partially encapsulated the exit was formed. However, in the analytical model, a fully encapsulating bubble was assumed to exist and the heat transfer was computed based on the surface of a full-size bubble. Thus, the additional heat transfer surface acts to compensate for the neglected heat transfer caused by the vortices.

Regarding the pool bottom pressures, the predicted values and the measured values are tabulated in Table 5.2 Again, it is assumed that the magnitude of the pressure spike decreases inversely with distance from the bubble collapse center which is assumed to be at the pipe exit. The initial conditions for the bubble collapse calculation are found from the vent pipe calculation when the bubble radius reaches its maximum. The heat transfer parameter $VA_c$ during

collapse is scaled by assuming that

$$UA_c \propto \text{pipe radius} \qquad (5.2)$$

The results show that the bubble collapse model tends to overpredict the pool bottom pressure, particularly in Run 214, where the predicted is four times the measured. This overprediction is probably due to the differences between the calculated conditions for the bubble collapse and the actual conditions in the bubble in the experiment.

A major observation from the bubble collapse calculations in these comparisons is: the vent radius plays an important role in the bubble growth and collapse and hence it governs the bubble collapse pressure.

The comparisons between the predicted chug heights and the measured show good agreement. A definite steam mass flux effect on the chug height is also observed. In Run 214, although the pool water temperature is lower than that in Run 216, the maximum chug height is lower. Examining the Japan data, it is found that the steam injection rate from the storage tank into the drywell is controlled by an orifice. The larger the orifice diameter the higher the injection rate. In the case of Run 214 the orifice diameter was 25 mm, while in Run 216 the orifice diameter was 17 mm.

The comparisons have shown that the theoretical model is able to predict the vent clearing time, the bubble growth time, and the chug height in a large scale system. Peak pressures at the pool bottom are generally overpredicted; although the predictions are still within the same order of magnitude as those measured.

It should be cautioned that the agreement obtained in these comparisons cannot be taken as a proof of the validity of the present models. From the physical understanding of the phenomenon, the simple model is not adequate for the complicated phenomena involved. For the comparisons made in the present study, the data base is too small to give a legitimate assessment of the validity of the models. However, as a first step, these comparisons do seem to be encouraging, and it is believed that further effort in improving the analytical models would lead to more fruitful results.

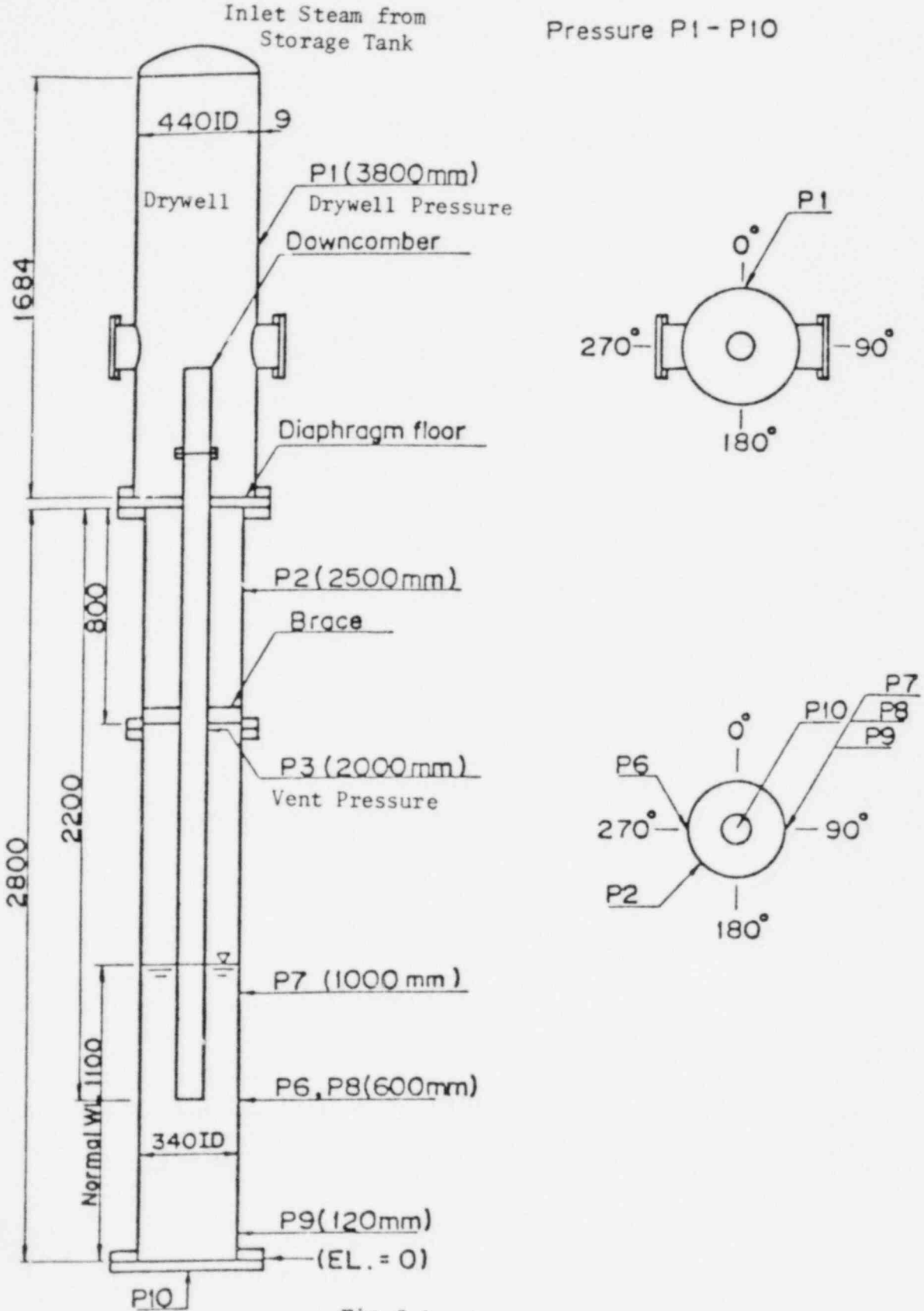


Fig 5.1 Pressure measuring points in test containment II

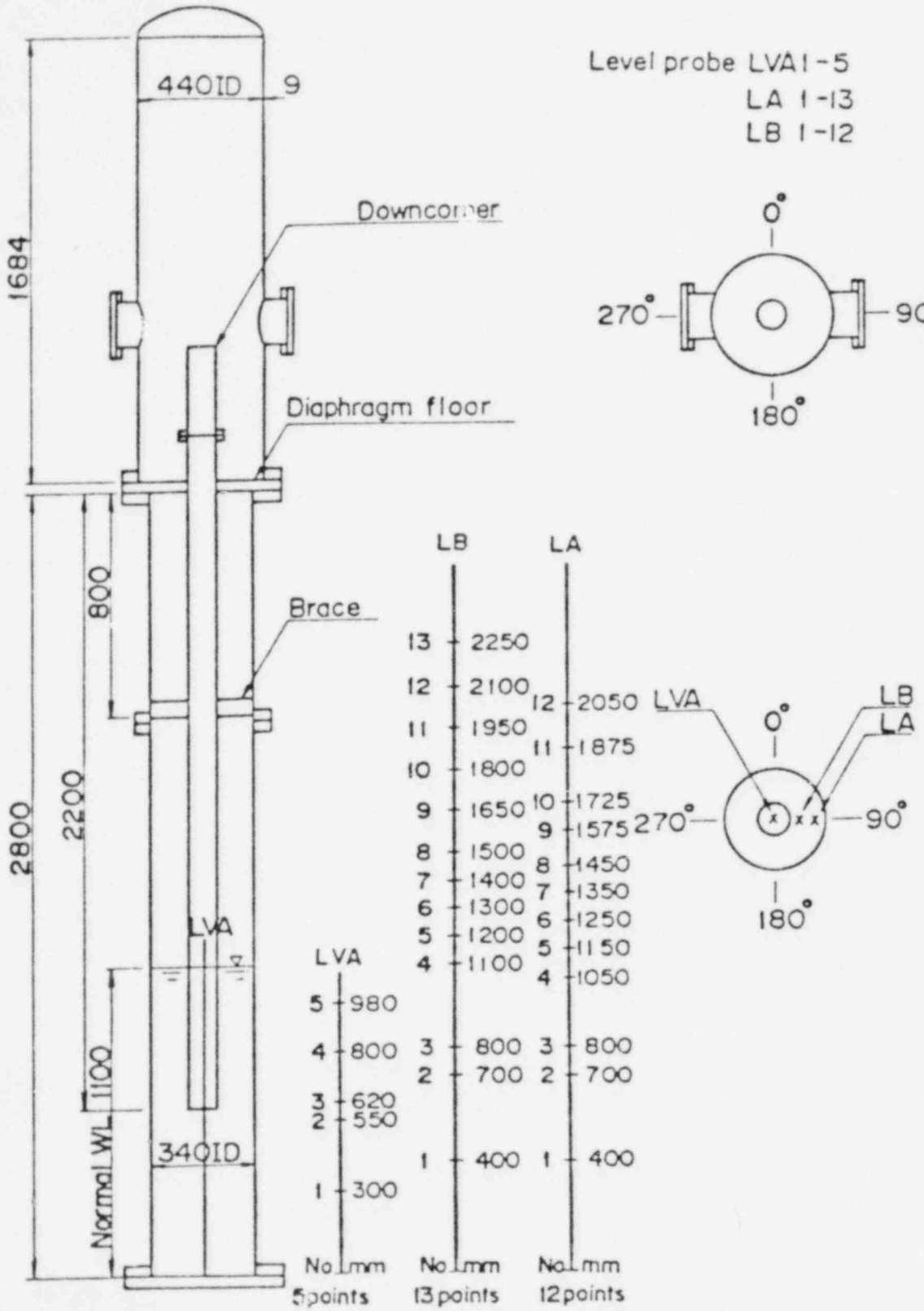


Fig 5.2 Water level measuring points in test containment II

MARK II 1/6-SCALE PRESSURE SUPPRESSION TEST

| | | | | |
|---|---|---|---|---|
| Run No. | 216 | | 214 | |
| Date of Performance | Mar. 26, 1977 | | Mar. 26, 1977 | |
| Test Mode / Case No. | 2 | - 1 | 2 | - 2 |
| Test Containment No. | II | | II | |
| DISCHARGE CONDITIONS | | | | |
| Tank Pressure ($kg/cm^2$ abs) | 5.7 | | 5.7 | |
| Tank Temperature (deg. C) | 156 | | 156 | |
| Orifice Diameter (mm) | 17.5 | | 25.0 | |
| Prepurging | YES | | YES | |
| CONTAINMENT INITIAL CONDITIONS | | | | |
| Pressure D.W1/W.W1 ($kg/cm^2$ abs) | | 1.62 | | 1.73 |
| Temperature D.W1/W.W1 (deg. C) | | 59 | | 30 |
| Pool Level (mm) | 1150 | | 1150 | |
| Pool Temperature (deg. C) | 35* | | 16* | |
| DOWNCOMER CONDITIONS | | | | |
| Number of Downcomers (-) | 1 | | 1 | |
| Initial Submergence (mm) | 550* | | 550* | |
| Orifice Diameter (mm) | None | | None | |

* Used as input in theoretical model.

Table 5.1 Initial conditions for performed tests.
(Steam condensation tests)

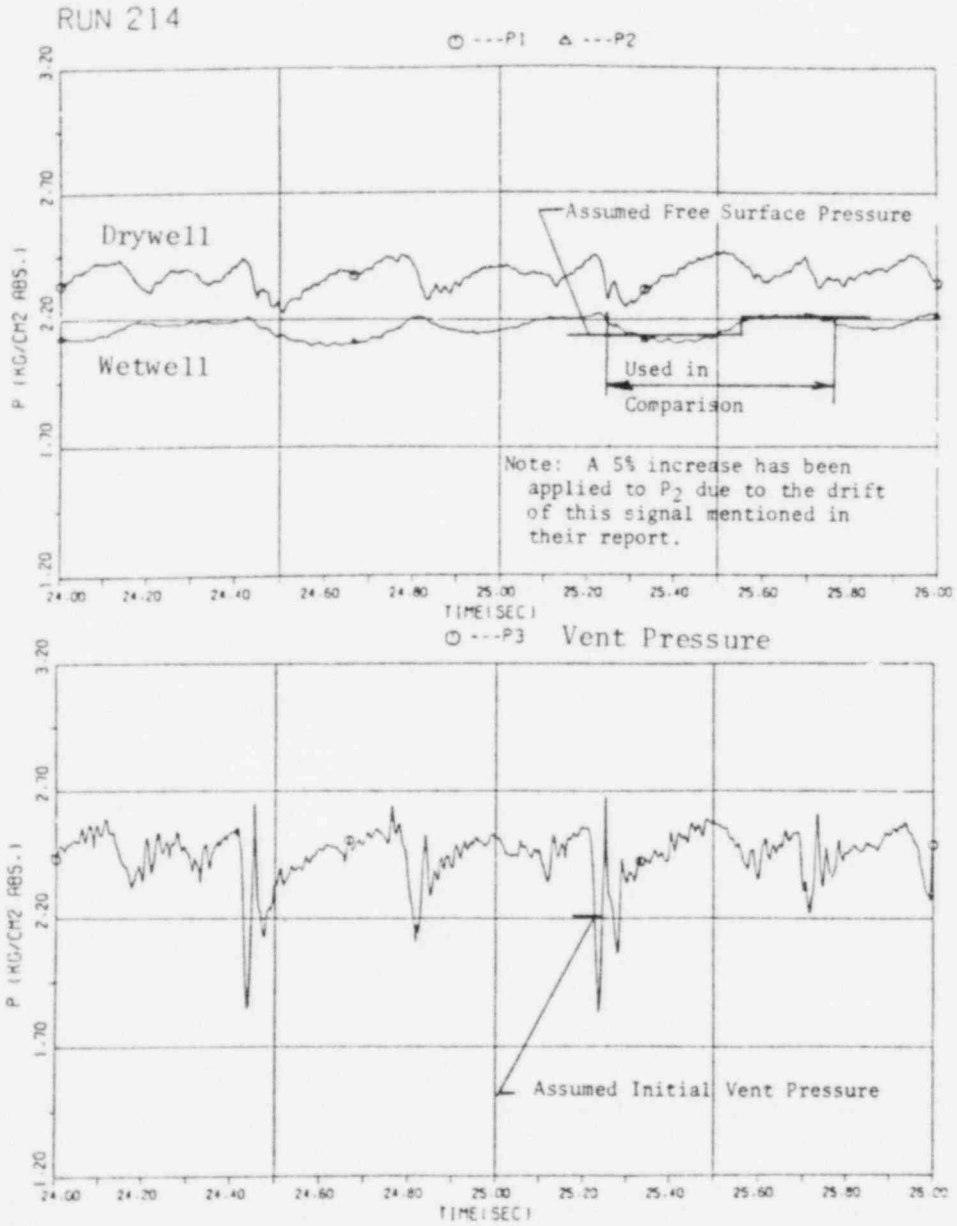


Fig 5.3 Pressure oscillations of steam condensation test #2

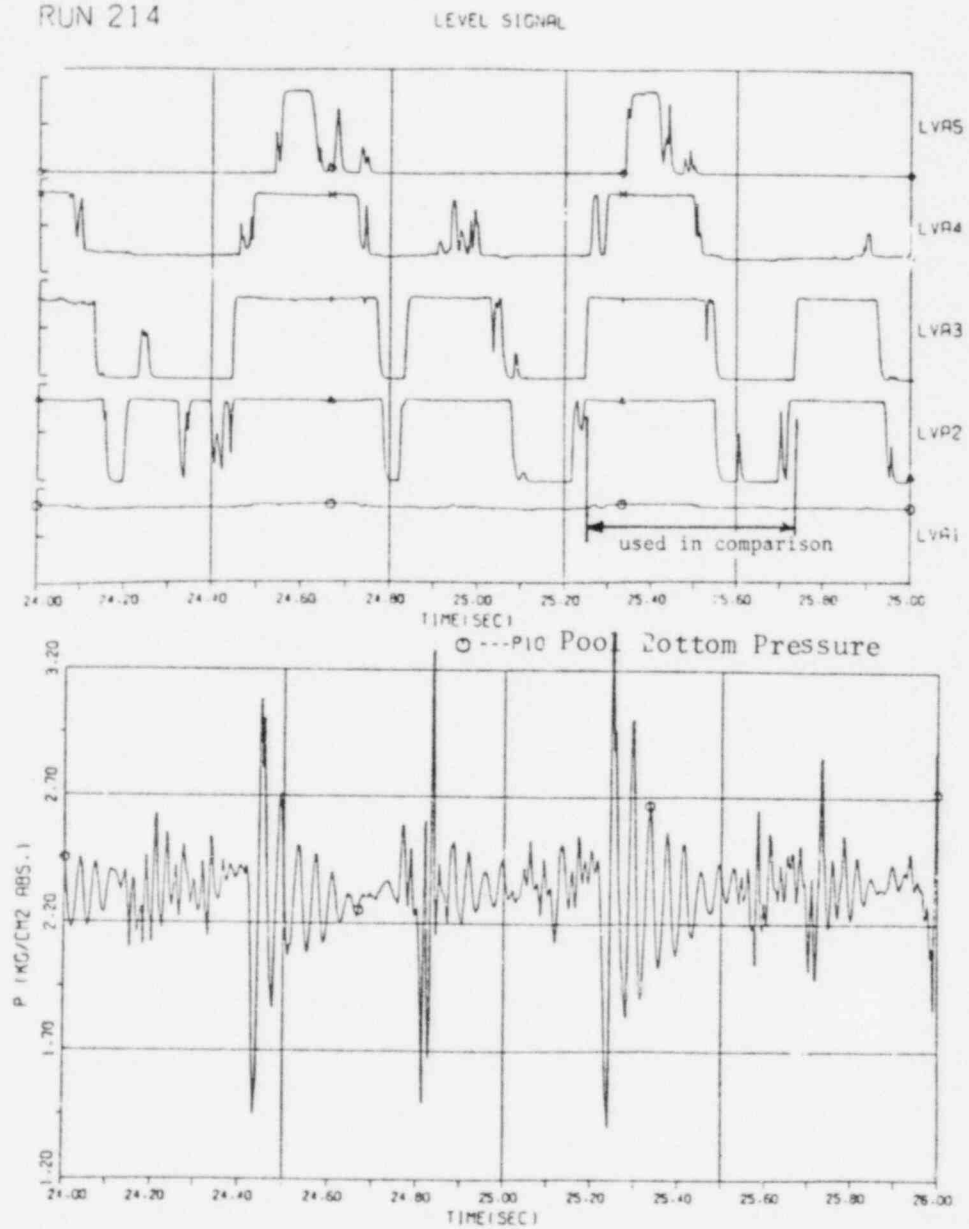


Fig 5.4 Pressure oscillations of steam condensation test #2

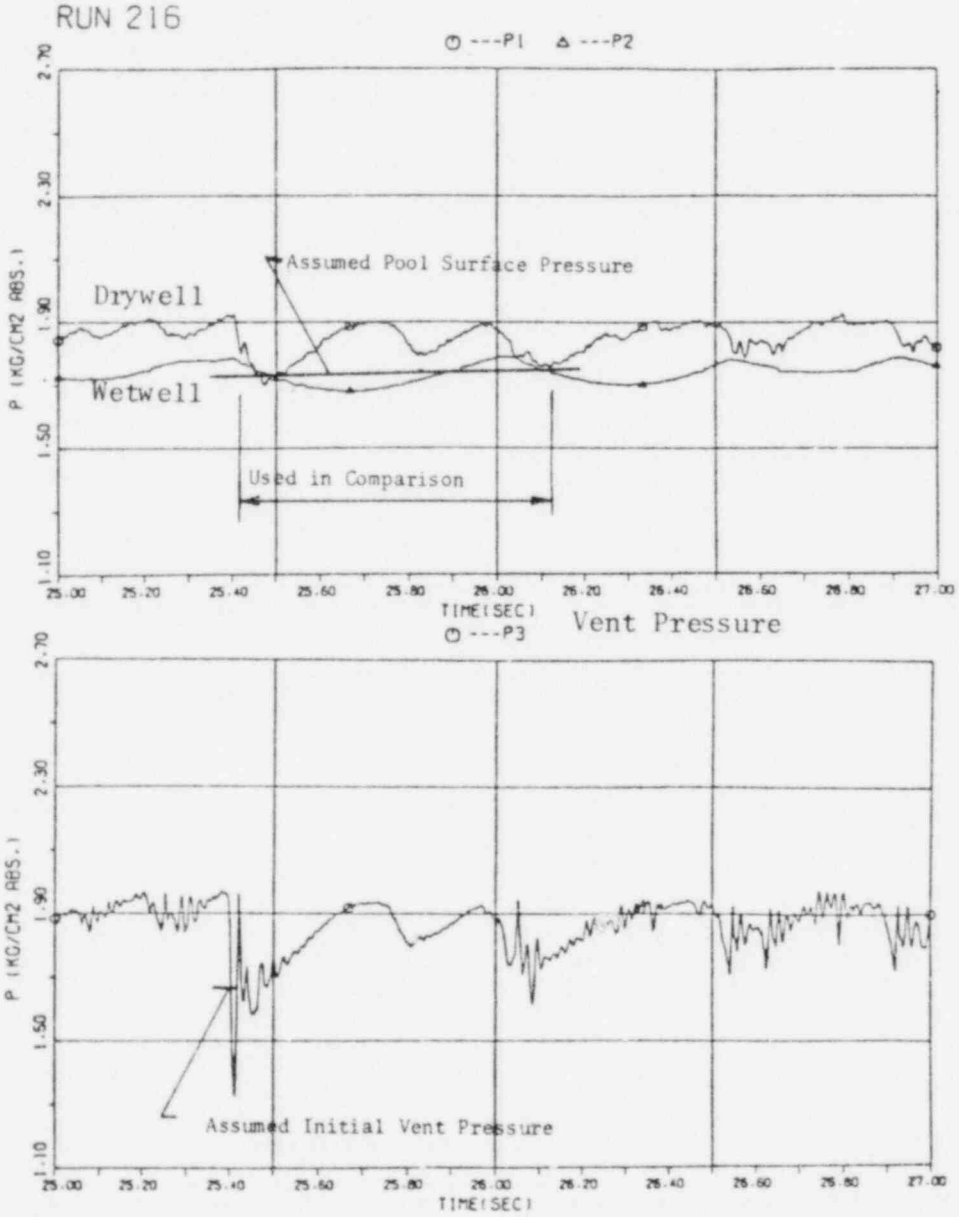


Fig 5.5 Pressure oscillations of steam condensation test #1

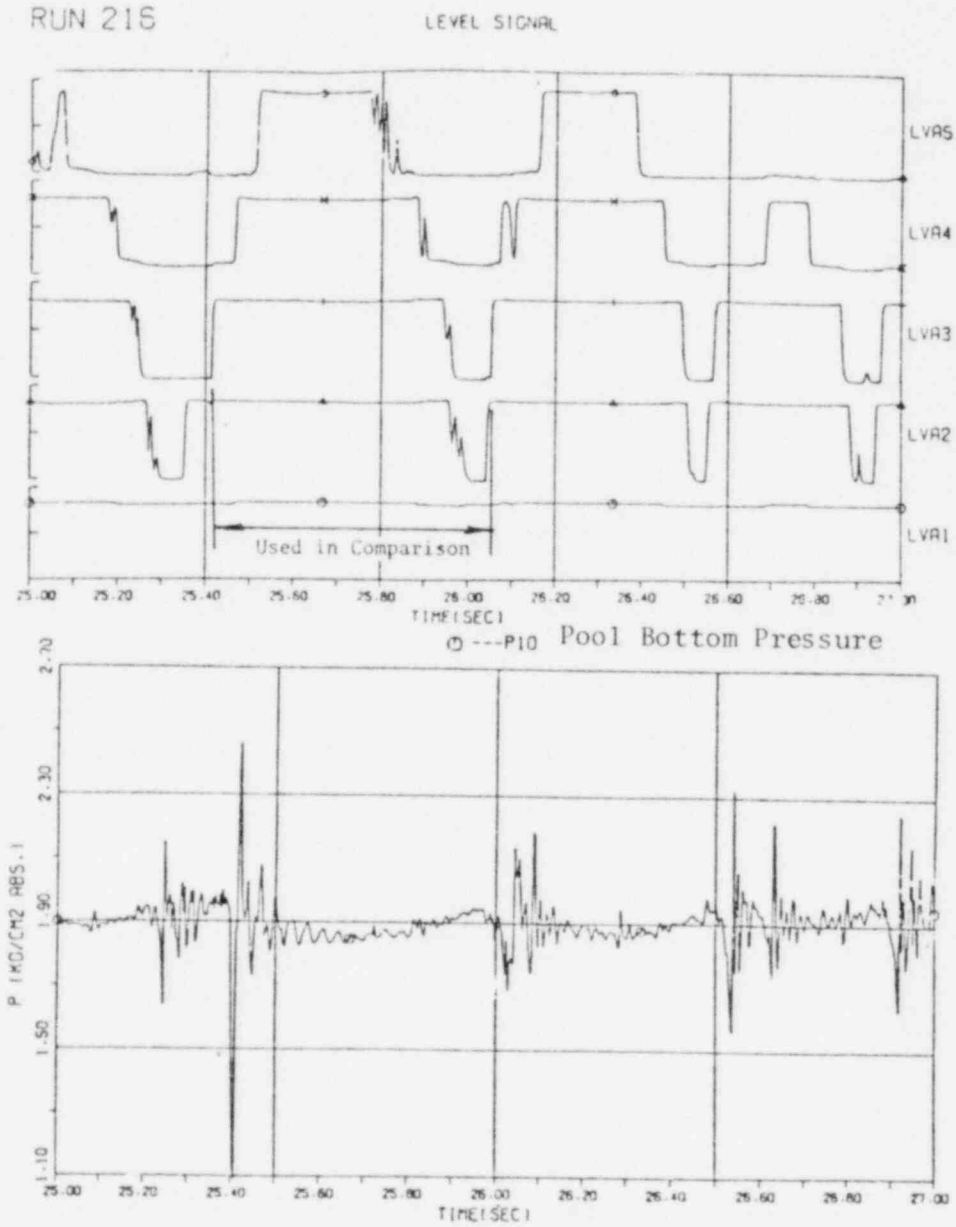


Fig 5.6 Pressure oscillations of steam condensation test #1

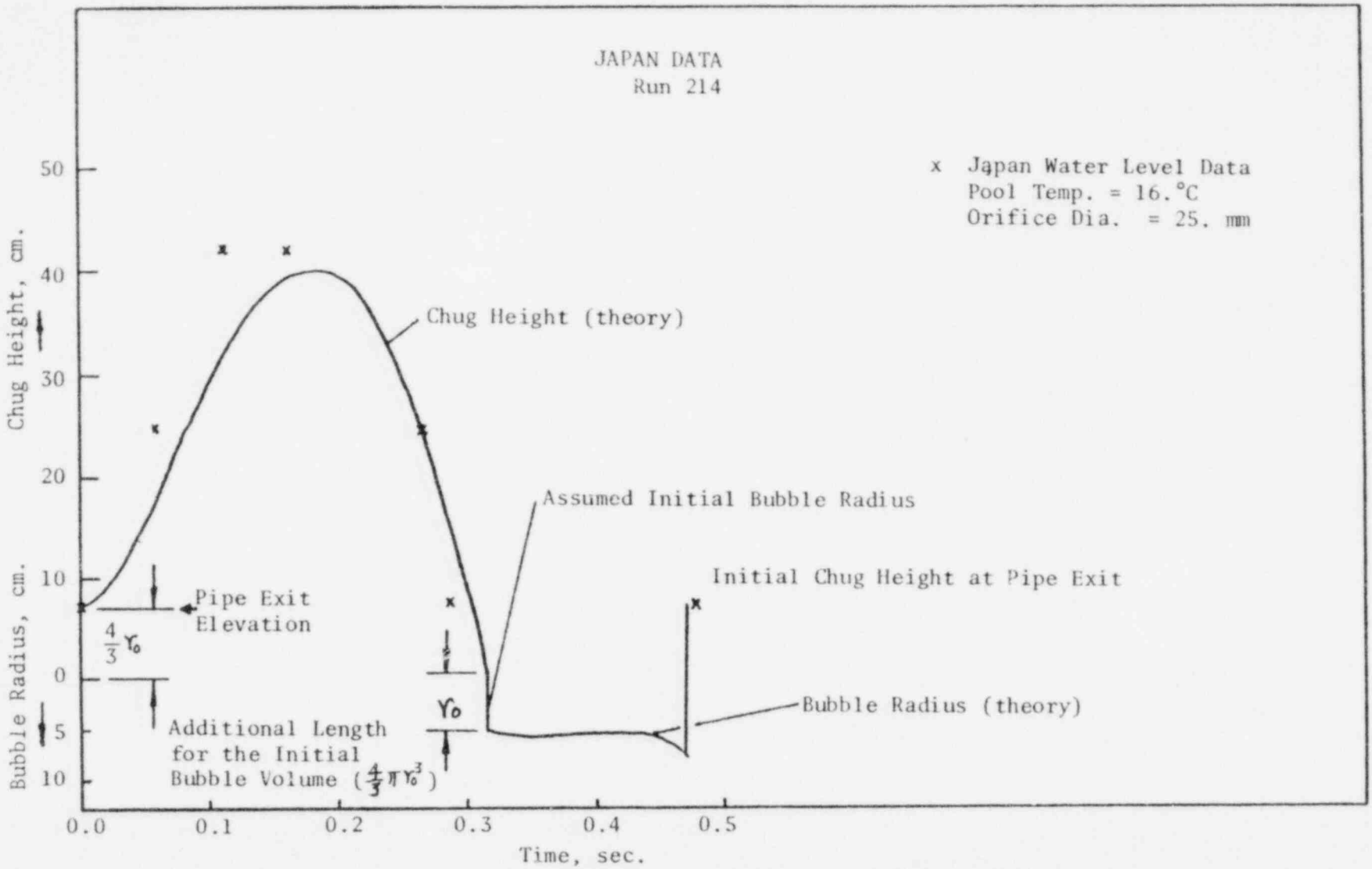


Fig. 5.7 Comparison of Theory Prediction with Japan Data

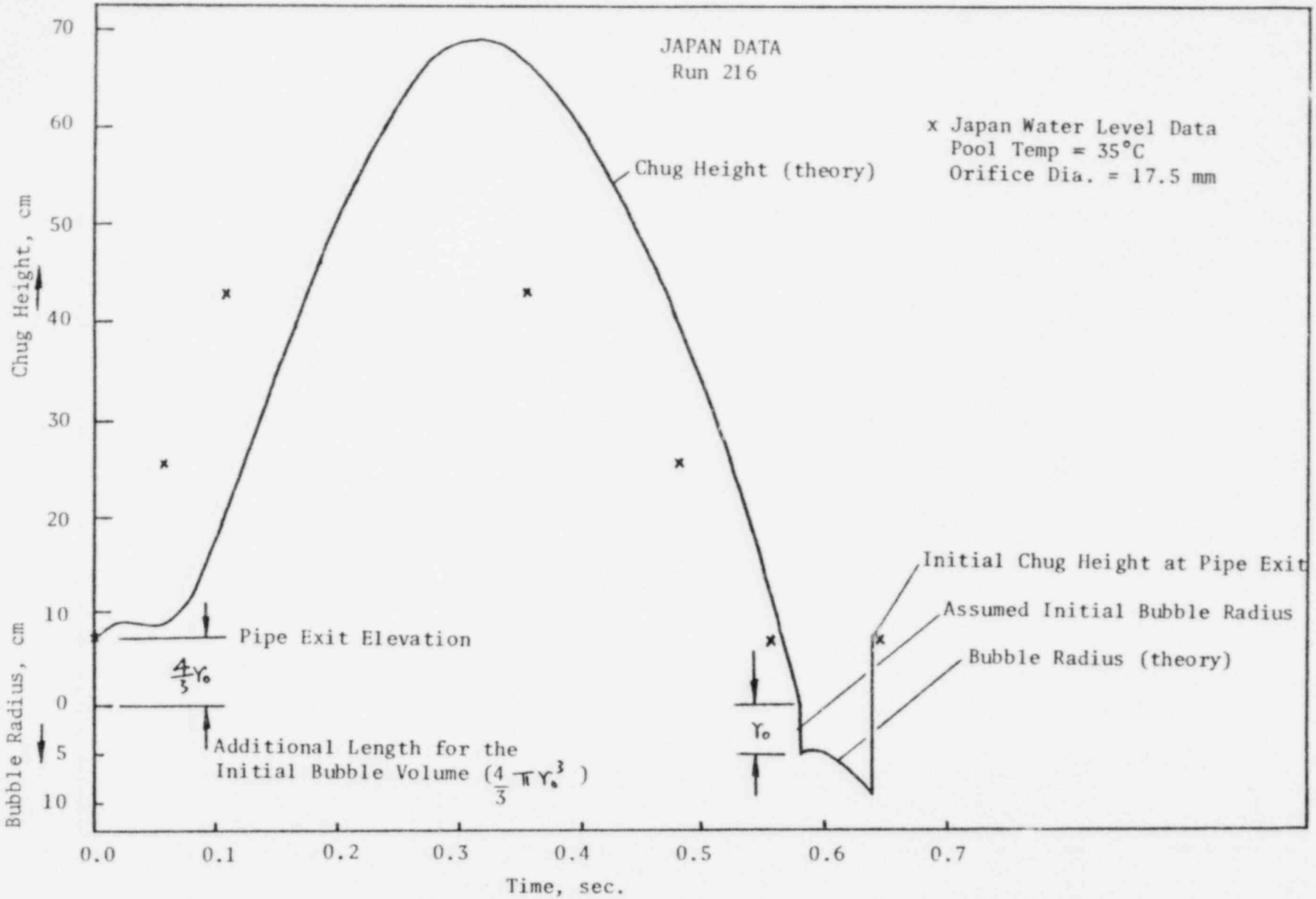


Fig. 5.8 Comparison of Theory Prediction with Japan Data

TABLE 5.2

COMPARISON OF PREDICTED POOL BOTTOM PRESSURE WITH EXPERIMENTAL DATA

Assumed scaling : $UA_c \propto$ Pipe Radius

| Japan Data Run No. | Initial Bubble Pressure, kPa | Final Bubble Pressure, kPa | Minimum Bubble Radius, cm |
|---|---|---|---|
| 214 | 165.6 | 4188.7 | 2.524 |
| 216 | 134.8 | 1344.1 | 2.207 |

| Japan Data Run No. | Initial Bubble* Radius, cm | Predicted Pool Bottom Pressure, kPa (gage) | Measured Pool Bottom Pressure, kPa (gage) |
|---|---|---|---|
| 214 | 7.815 | 161.0 | 41.7 |
| 216 | 8.821 | 47.8 | 47.0 |

* Calculated maximum bubble radius from vent pipe model.

# CHAPTER 6

# SUMMARY AND CONCLUSION AND RECOMMENDATIONS

## 6.0 Summary and Conclusion

The hydrodynamic loads, induced by the steam chugging phenomenon, in a Boiling Water Reactor suppression pool, are studied by a small scale experiment. The experimental effort established an overall physical picture of the phenomenon which enabled the development of a theoretical model intended for the prediction of these loads in the full size containment. The experimental study is limited to single vent injection.

From the qualitative steam injection experiments it is observed that the motion of the steam water interface in the pool admits certain characteristic patterns for various ranges of the pool temperature and the mass flux of steam injection. A systematic classification of these characteristic patterns is made, based on these two parameters, resulting in a condensation regime map. Although the boundaries between various regimes are system dependent, the corresponding characteristic patterns would remain the same. In general, the classification can be divided into three types: the jet at high mass fluxes ($> 150$ kg/m$^2$-sec), the bubble oscillation at intermediate mass fluxes, and the steam chugging at low mass fluxes ($< 75$ kg/m$^2$-sec).

Steam chugging occurs below a steam mass flux of about 75.

$kg/m^2$-sec , and below a pool temperature of about 80. °C. Within this condensation regime, three different types of chugs are observed: the internal chug where all condensation occurs within the pipe; the detached bubble chug where the bubble is "cut off" from the vent during bubble formation; and the encapsulating bubble chug where the bubble encapsulates the vent during bubble formation. The first two types of chugs are characterized by high chug heights, high interface velocity upon vent clearing, but low steam pressures at the interface. The last type, on the other hand, is characterized by low chug heights, low interface velocity upon vent clearing, but high steam pressures at the interface.

The magnitudes of the pressure overshoot at the pool bottom associated with internal chugs, detached bubble chugs, and encapsulating bubble chugs are: mild ($\sim$ .1 atm.), moderate ($\sim$ .3 atm.), and large ($\sim$ .5 atm.) respectively. For internal chugs, the loads are generated by the collapse and rebound of a bubble within the vent. For the other two types, the loads are generated by the collapse of the bubbles in the pool. Pool bottom pressure data indicate that the pressure oscillations associated with detached bubbles are characterized by two different periods. The first period includes the pressure undershoot and the spike; the second period is the "ring out." For encapsulating bubbles, the pressure oscillations are characterized by three different periods. The first period includes only the pressure undershoot. The second period includes the duration of the pressure spike which consists of a few fine peaks. The third period is the "ring out." Generally, the violent bubble collapse is initiated

by the penetration of a liquid jet into the bubble. For detached bubbles the liquid jet penetrates from the side, while for encapsulating bubbles, the liquid jet penetrates from the bottom.

Synchronized movie data and pool bottom pressure measurements show that the rapid pressure undershoot occurs during jet penetration while the sharp pressure overshoot occurs near the completion of a violent collapse. The rapid condensation introduced by the liquid jet causes the rapid decrease in the bubble pressure which initiates the violent collapse. The liquid inertia developed during the violent collapse over-compresses the steam causing the sharp pressure overshoot. If bubble shatter occurs before the compression, the magnitude of the overshoot is decreased. Consequently, an upperbound for the magnitude of the overshoot is the full compression of the bubble without shatter until the first bubble minimum size is reached and the bubble begins to rebound. A lowerbound for the pressure undershoot is the saturation pressure corresponding to the pool temperature.

The chug of water up the vent is caused by a pressure undershoot in the vent which is resulted from the rapid condensation occurring at the pipe exit. For internal chugs and detached bubble chugs, the rapid condensation is caused by the liquid layers draining off the pipe wall and accumulating locally at the exit. For the encapsulating bubble chugs, the liquid jet penetration and atomization phenomenon is responsible for the rapid condensation at the vent exit.

The dynamics of the steam in the vent and the surge tank are governed by the condensation at the exit. The rapid condensation causes a drop in the vent pressure followed by a sharp increase in steam velocity and a mild pressure undershoot in the surge tank.

The vent pipe model is developed to predict the chug height in the vent and the bubble behavior at the pipe exit. A one-dimensional pipe flow model for the vent is coupled to a one-volume model for the condensation region at the pipe exit to predict the slug motion in the vent; and, upon vent clearing, the pipe flow equations are coupled to an infinite pool spherical vapor bubble model, to predict the bubble growth in the pool. The condensation heat transfer coefficient in the pipe is determined by comparing the experimental data with the vent pipe model predictions for various values of h. The best value is

$$h = 14. \times h_{Nu} \qquad (6.1)$$

At the end of the bubble growth, the bubble will start to collapse. A set of physically based chugging criteria is assigned giving the required conditions in the vent as well as the collapsing bubble which would allow the re-entry of the water slug into the vent. These criteria differ from one type of chug to another. They are summarized in Table 4.1.

Comparisons of the vent pipe model predictions with experimental data show that the model is inadequate in predicting the chugging phenomenon; however, the general trends observed in the experiments are predicted. These trends are listed as follows:

(i) The predicted chug height increases as the pool temperature is decreased.

(ii) The predicted maximum bubble size increases with pool temperature.

The condensation caused by the liquid jet penetration and atomization is modelled by an overall heat transfer parameter $UA_c$ determined from the experiments to be 4.37 kw/°C. The bubble collapse model is an infinite pool spherical vapor bubble model with rapid condensation induced by the liquid jet. By assuming that the peak pressure decreases inversely with distance from the vent exit, the pool bottom pressures are predicted.

Comparisons of the predicted pool bottom pressures with the measured indicate that this model is unable to predict the bubble collapse phenomenon in steam chugging; however, the predicted trends do agree with the general trends observed in the experiments. These trends are listed as follows:

(i) The predicted pool bottom pressure decreases as pool temperature is increased.

(ii) The predicted pool bottom pressure decreases with submergence.

Comparisons of the model predictions with the Japan 1/6-scale data show good agreements in the vent clearing time as well as the bubble growth time. These comparisons are interesting but non-definitive concerning the validity of the present models. However, an observation made from these results is that the vent diameter is a controlling parameter affecting the peak pressures

developed at the pool bottom.

In general, the simple theoretical models are incapable of predicting the complicated steam chugging phenomenon. However, the present modelling effort has generated an account of the numerous analytical difficulties encountered in the process of modelling. Moreover, the models are able to predict the experimentally observed trends. As a first step in the modelling of such a complicated process, the performance of the model is considered satisfactory. It is believed that further improvements on the theoretical models will lead to more fruitful results.

## 6.1 Recommendations

The following research areas are recommended for future efforts to improve the understanding of the steam chugging phenomenon:

(1) The heat transfer to the liquid jet during the bubble collapse is still not well predicted. Further research needs to be done to study this problem because the bubble collapse loads are directly related to the amount of condensation induced by the liquid jet penetration and atomization phenomena.

(2) In the present model, the pool boundary effects have been totally neglected. In the actual BWR suppression pool, numerous structures, e.g. baffles, pipe supports, walls, etc., exist around the vent pipe; the bubble growth would be seriously affected by these solid boundaries. This may also lead to a preferential spot for bubble formation and also the bubble collapse. This will generate a preferential direction for the forces on the vent pipe. More

studies in this regard are important for the integrity of the vent in the event of a loss of coolant accident.

(3) The present theory can be extended to the multi-vent calculations. However, before that is done, more physical understanding concerning the second vent underpressure, and the high heat transfer rates during initial bubble growth caused by the vortices induced during the slug discharge process, is required.

(4) Photographi information concerning the bubble growth in a large system is crucial for predicting the hydrodynamic loads. As mentioned in the previous section, the two-dimensional effect which causes the formation of partially encapsulating bubbles rather than fully encapsulating bubbles may exist. Incorporating this effect into the present theory will improve the theory predictions.

(5) Further experimental study is needed to investigate the additional pressure spikes discussed in Section 3.4. These spikes do not correspond to those generated by the bubble collapse. The magnitudes of these spikes may be higher than those generated by the bubble collapse.

REFERENCES


(1) Sargis, D. A., et al., "A Fundamental Thermal Hydraulic Model to Predict Steam Chugging Phenomena," Paper presented at ASME winter meeting, December, 1978.

(2) Class, von G., "Theoretical Investigation of Pressure Pulse Development During Steam Condensation in Pressure Reducing System of BWR," Nuclear Research Center Karlsruhe, Report KFK 2487, 1978.

(3) Kowalchuk and Sonin, "A Model for Condensation Oscillations in a Vertical Pipe Discharging Steam into a Subcooled Water Pool," NUREG/CR-0221, 1978.

(4) Sarsock, J. P. and Duffey, R. B., "Condensation of Steam Bubbles in a Subcooled Pool," paper presented at ASME winter meeting, December, 1978.

(5) Healzer, T. M., et al., "Single Vent Chugging Model," NEDE-23703-P, General Electric Company, September 1977.

(6) The Marviken Full Scale Containment Experiments, MXA-1-221, 222, 223, 301. Joint Committee on the Marviken Experiments.

(7) Slaughterbeck, D. C. and Ericson, Leif, "Nuclear Safety Experiments in the Marviken Power Station," Nuclear Safety, Vol 18, No. 4, p. 481, July, 1977.

(8) The Marviken Full Scale Containment Experiments, "Marviken Test Conclusion and Recommendations," MXA-0-402. Joint Committee on the Marviken Experiments.

(9) McIntyre, T. R., et al., "Mark II Pressure Supression Test Program," NEDE-13442-P-01, General Electric Company, May, 1976.

(10) Grafton, W. A., et al., "Mark II Pressure Suppression Test Program Phase II and III Tests," NEDE-13468-P, General Electric Company, October, 1976.

(11) Bein, M., et al., "Chugging Load Mitigation Testing (small scale)," NEDE-21747-P, General Electric Company, November, 1977.

(12) Bilanin, W. J., et al., "Mark II Level Plant Topical Report," NEDE-23617-P, General Electric Company, July, 1977.

(13) Kukita, T., et al., "Research Study Report Regarding the Soundness of a One-sixth Scale BWR Housing Container," USNRC Translation #274, NUREG/TR-0036, JAERI-memo 7167, Japan Atomic Energy Research Institute, June, 1977.

(14) Andeen, G. B. and Masko, J. S., "Analysis and Testing of Steam Chugging in Pressure Systems," EPRI-NP-908, The Electric Power Research Institute, October, 1978.

(15) Greef- C. P., "A Study of the Condensation of Vapor Jets Injected into Subcooled Liquid Pools," Central Electricity Generating Board, Research Department, Berkeley Nuclear Laboratories, RD/B/N3262.

(16) Cumo, M., et al., "Direct Heat Transfer in Pressure-Suppression Systems," paper presented at 6th International Heat Transfer Conference, Toronto, August, 1978.

(17) Young, R. J., et al., "Vapor-Liquid Interaction in a High Velocity Vapor Jet Condensing in a Coaxial Water Flow," Heat Transfer 1974, 3, 225 (1974).

(18) Stanford, L. E. and Webster, C. C., "Energy Suppression and Fusion Product Transport in Pressure Suppression Pool," ORNL-TM-3448, Oak Ridge National Laboratory, 1972.

(19) "Hydrodynamics of a Vapor Jet in Subcooled Liquid", UCLA Masters Thesis, University of California at Los Angeles, June 1979.

(20) Rayleigh, Lord, "On the Pressure Developed in a Liquid During the Collapse of a Spherical Cavity," Phil. Mag., 34, 94-98, August, 1977.

(21) Florschuetz, L. W., and Chao, B. T., "On the Mechanics of Vapor Bubble Collapse," Trans. ASME, 87, Ser. C, Jr., Heat Transfer, 209-220, 1965.

(22) Lee, C. K. B., and Chan, C. K., "The Effects of Initial Conditions on Vapor Bubble Collapse," paper presented at ASME Winter meeting, December, 1978.

(23) Kling, C. L. and Hammitt, F. G., "A Photographic Study of Spark-Induced Cavitation Bubble Collapse," Jr. Basic Engineering, p. 825-833, December, 1972.

(24) Shutler, N. D. and Mesler, R. B., "A Photographic Study of the Dynamics and Damage Capabilities of Bubbles Collapsing Near Solid Boundaries," Jr. Basic Engineering, p. 511-517, June, 1965.

(25) Benjamin, T. B. and Ellis, A. T., "Cavitation," Phil. Trans. Royal Soc. (London), A, 260, 221-240, 1966.

(26) Chapman, R. B., "Nonspherical Vapor Bubble Collapse," Ph.D. Thesis, California Institute of Technology, 1970.

(27) Hickling, R., and Plesset, M. S., "Collapse and Rebound of a Spherical Cavity in Water," Physics of Fluids, 7, 7-14, 1964.

(28) Green, N. W., and Mesler, R. B., "An Experimental Study of Transient Pressures Accompanying Vapor Bubble Collapse in Water," Paper presented at ASME conference, May, 1970, Detroit, Michigan.

(29) Plesset, M. S., "Shockwaves from Cavity Collapse," Phil. Trans. Royal Soc. (London), A, 260, 241-244, 1966.

(30) Knapp, R. T., et al., "Cavitation," McGraw Hill Book Co., Engineering Societies Monographs, 1970.

(31) Abramson, H. N., "The Dynamic Behavior of Liquids in Moving Containers," NASA SP-106, National Aeronautics and Space Administration, 1966.

(32) Chan, C. K., et al., "Suppression Pool Dynamics," UCLA, NUREG-0264-3, 1977.

(33) Chan, C. K., et al., "Steam Chugging in Pressure Suppression Containment," UCLA, 1977/78 Annual Report.

(34) Wallis, G. B., "One Dimensional Two-Phase Flow," McGraw Hill Book Co., 1969.

(35) Crane Co., "Flow of Liquids through Valves, Fittings, and Pipe," Tech. paper, No. 410, Crane Co., 1969

(36) Shapiro, A. H., "The Dynamics and Thermodynamics of Compressible Fluid Flow," Vol. 1, Ronald, N.Y., 1953.

(37) Maa, J. R., "Condensation of Vapor on a Very Cold Liquid Stream," I-EC Fundamentals, Vol. 8, No. 3, Aug. 1969.

(38) Pitts, J. H., "Analysis of Boiling Water Reactor Steam Chugging," GRS-A-259, Lawrence Livermore Laboratory, 1979.

(39) Kreith, F., "Principles of Heat Transfer," Int. Textbook Company, 1969.

## GLOSSARY

| | |
|---|---|
| Annular Flow | A situation in two-phase flow where the vapor is surrounded by an annulus of liquid. |
| Atomization | The physical process of generating a shower of droplets by shooting a liquid jet into a sharp edge. |
| Bubble | A vapor region, of arbitrary shape, which is surrounded by a liquid. |
| Bubble Shatter | The process of an instantaneous fragmentation of a bubble. |
| BWR | Boiling Water Reactor |
| Chug | A rush of water into the injection pipe. |
| Chug Height | The maximum height the water level reached during a chug. |
| Chugging | The entire process of low flow vapor injection where periodic rushes of water into the injection pipe occur. |
| Chugging Bubble | The bubble, at the injection pipe exit, which upon collapsing causes a rush of water into the injection pipe. |
| Condensation Regime | A region, in a two-dimensional map, defined by the pool water temperature and the vapor injection rate, where a repetitive interfacial motion pattern exists. |
| Condensation Region | The part of the injection pipe at the exit where large amounts of condensation occur. |
| Containment | A sealed structure which encloses the reactor vessel and portions of the primary coolant system in a nuclear power plant. |
| Detached Bubble Chug | A type of chugging where the steam bubble is immediately detached from the injection pipe upon bubble formation at the pipe exit. |

| | |
|---|---|
| Encapsulating Bubble Chug | A type of chugging where the steam bubble grows to encapsulate the exit end of the injection pipe during bubble formation. |
| Hydrodynamic Load | The force exerted on the injection pipe, or the pool container, due to rapid motion of the water in the pool. |
| Interface | A surface separating the steam region from the water region. |
| Interface Clearing | The process where the interface is clearing out of the injection pipe. |
| Interface Spread | The process during a chug where the interface changes from a horizontal flat surface to an inclined surface, consequently increasing the surface area of the interface. |
| Intermediate Bubble | The bubble, inbetween two chugs, which slowly grows and collapses at the pipe exit without causing a chug. |
| Internal Chug | The type of chugging where all the condensation occurs inside the pipe and no bubble is formed in the pool. |
| Liquid Jet Penetration | The initiating process for a rapid bubble collapse where a water jet penetrates into the steam region causing rapid condensation. |
| LOCA | Loss of Coolant Accident |
| Separated Flow | The flow situation where a portion of the flow is retreating while the rest of the flow is progressing. |
| Vent (or Vent Pipe) | The injection pipe. |
| Vent Clearing | The process at which the water is being cleared out of the vent. |
| Vent Clearing Time | The time period from when the chug enters the vent to the time when the water slug is cleared out of the vent. |

# APPENDIX A

## POOL BOTTOM PRESSURE EXPERIMENTS

## (SYNCHRONIZED WITH MOVIE)

Pool Bottom Pressure Experiments(plastic pipe)

| Run No. | Pool Temp., °C |
|---|---|
| 1 | 43.9 |
| 2 | 50.0 |
| 3 | 55.5 |
| 4 | 61.7 |
| 5 | 67.8 |
| 6* | 73.9 |
| 7* | 8[illegible].9 |

(1) Pool Bottom Pressure measured by Statham PL-131-tc-50 pressure transducer(error 2.6kPa,Response Time=.56 ms)

(2) Exit Temperature measured by gage 36 Chromel-Alumel thermocouple.

(3) Boiler steam generation rate = .00756kg/sec.

(4) Submergence Depth = 25.4 cm.

(5) Data sampling time = 5. ms.

* Data not shown since pressure load is very small.

1) Upstream Pressure (Not Used)
2) Upstream Temperature
3) Upper Exit Thermocouple
4) Lower Exit Thermocouple
5) Bottom Pressure Transducer
6) Bulk Pool Temperature

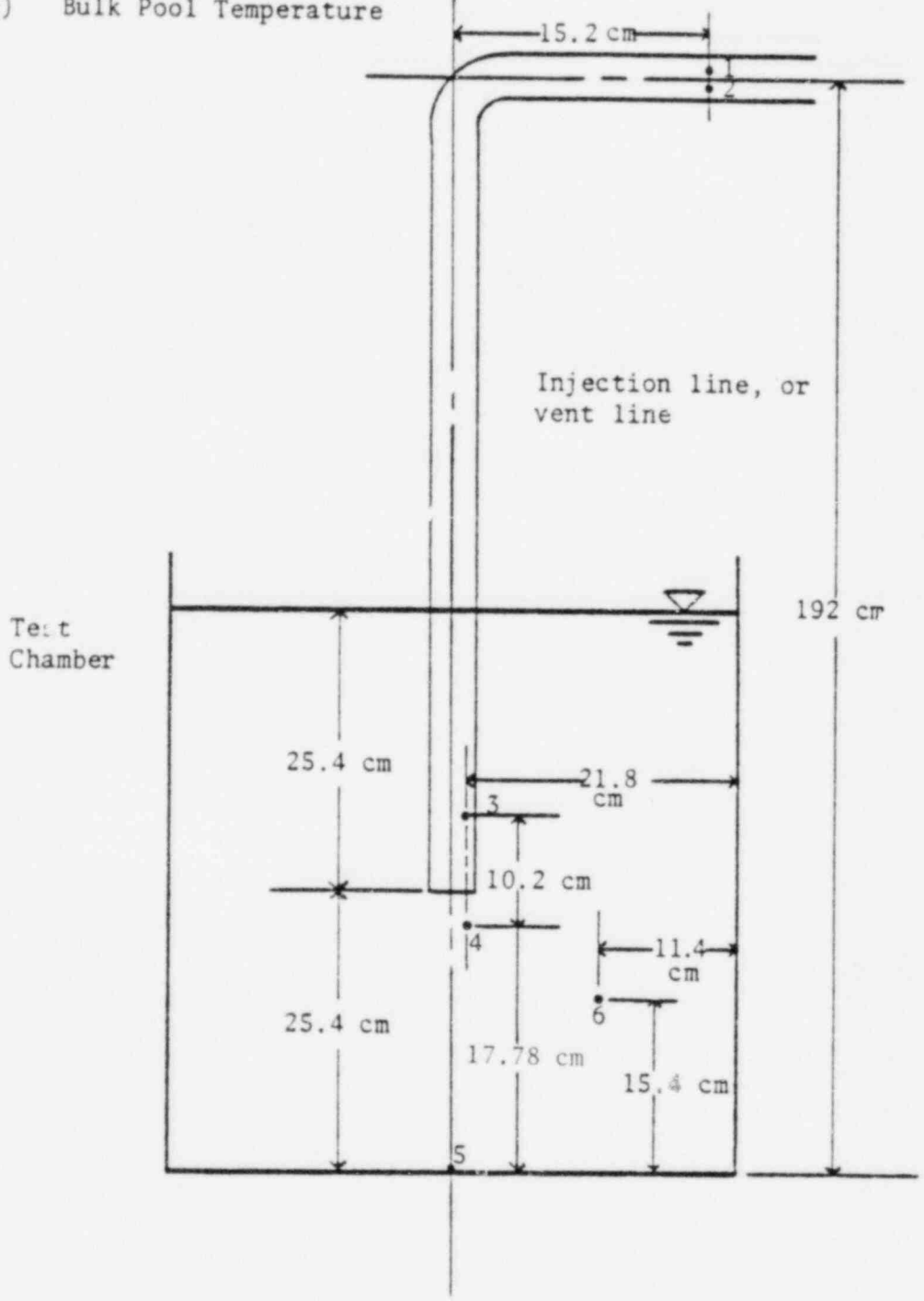


Fig. 2.1.4. Locations of Instrumentation

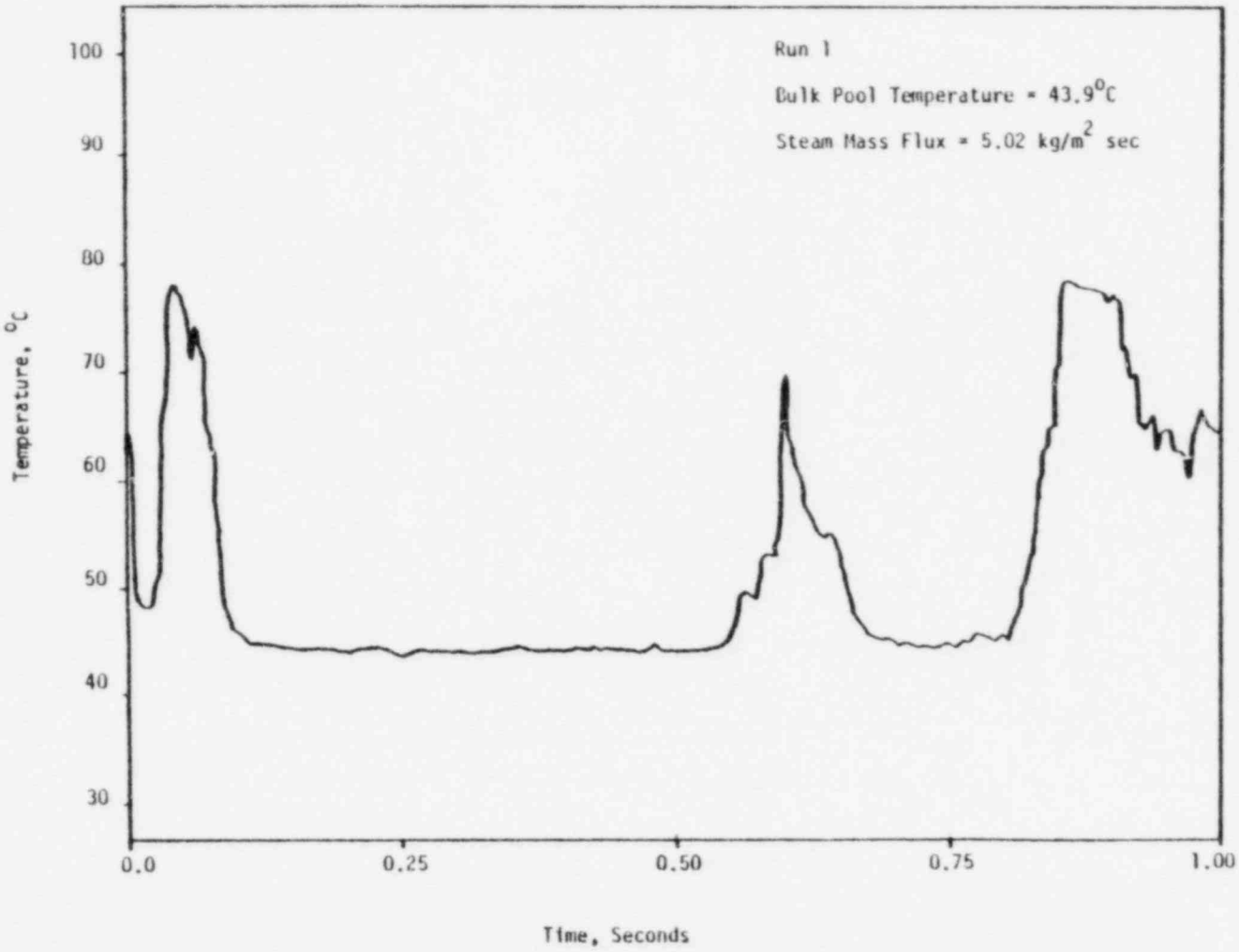


Fig. A.1 Lower Vent Exit Thermocouple Reading for Run 1

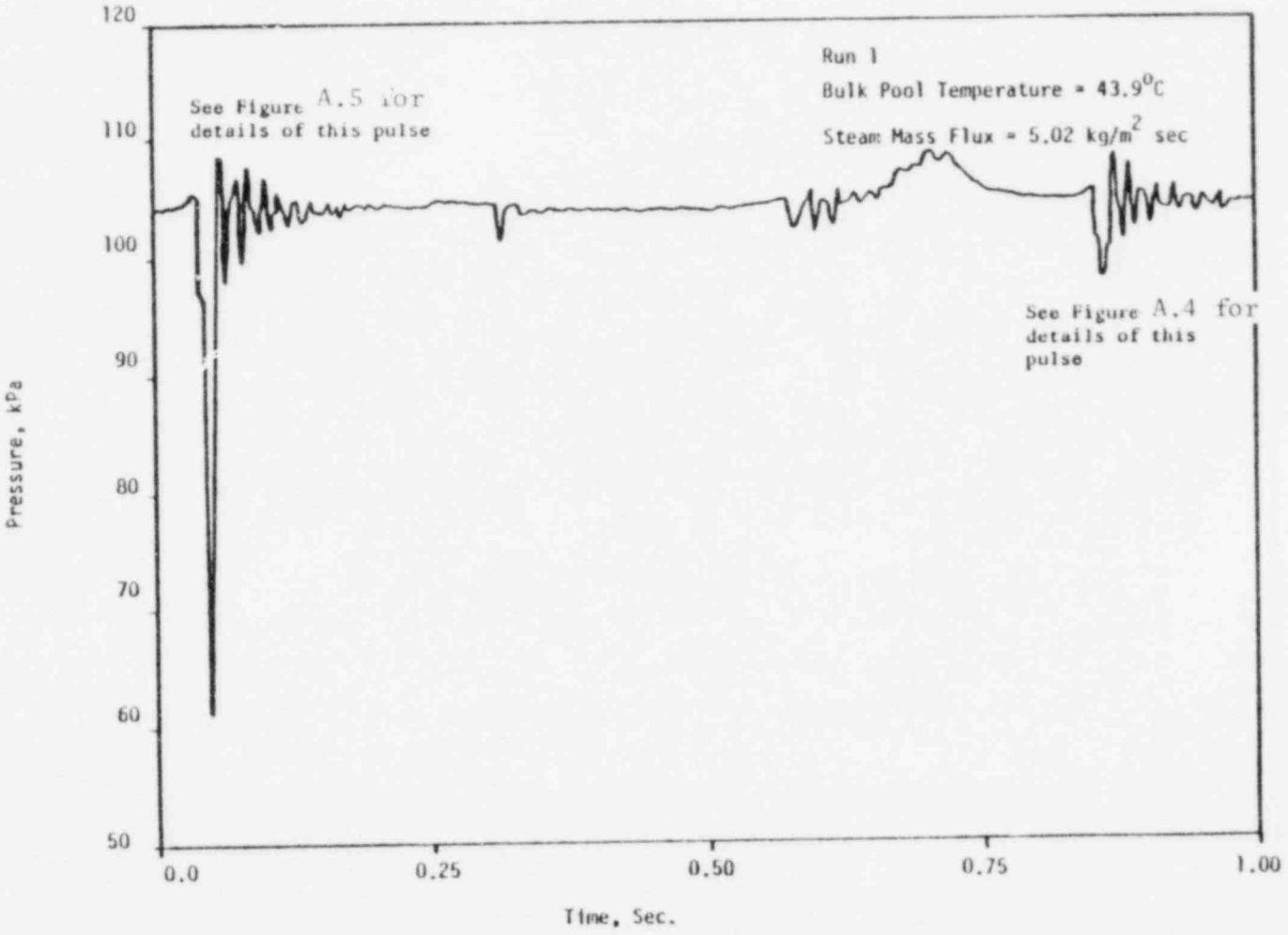


Fig. A.2 Bottom Pressure Transducer Reading for Run 1

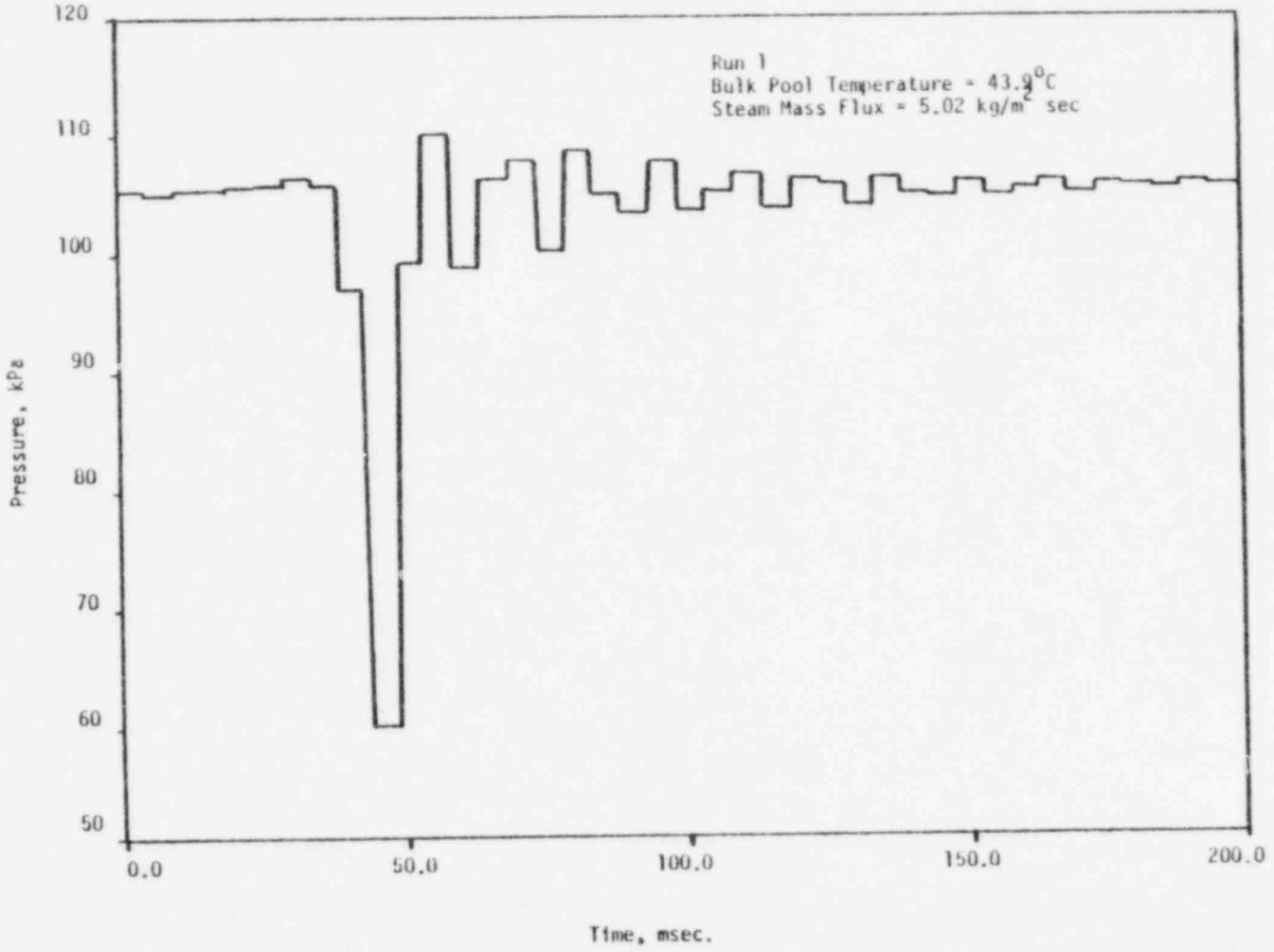


Fig. A.3 Detailed Bottom Pressure Transducer Reading for Run 1

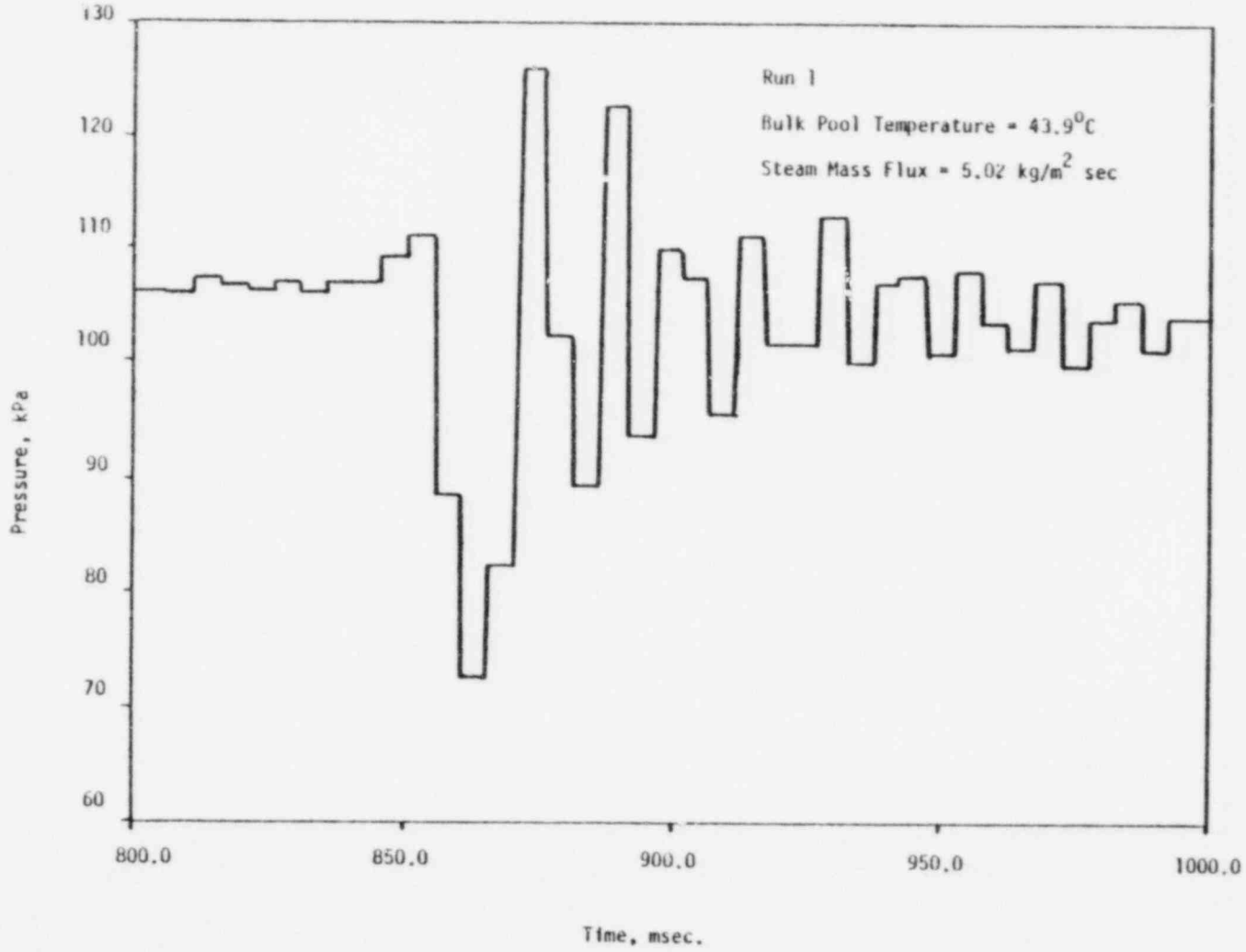


Fig. A.4 Detailed Bottom Pressure Transducer Reading for Run 1

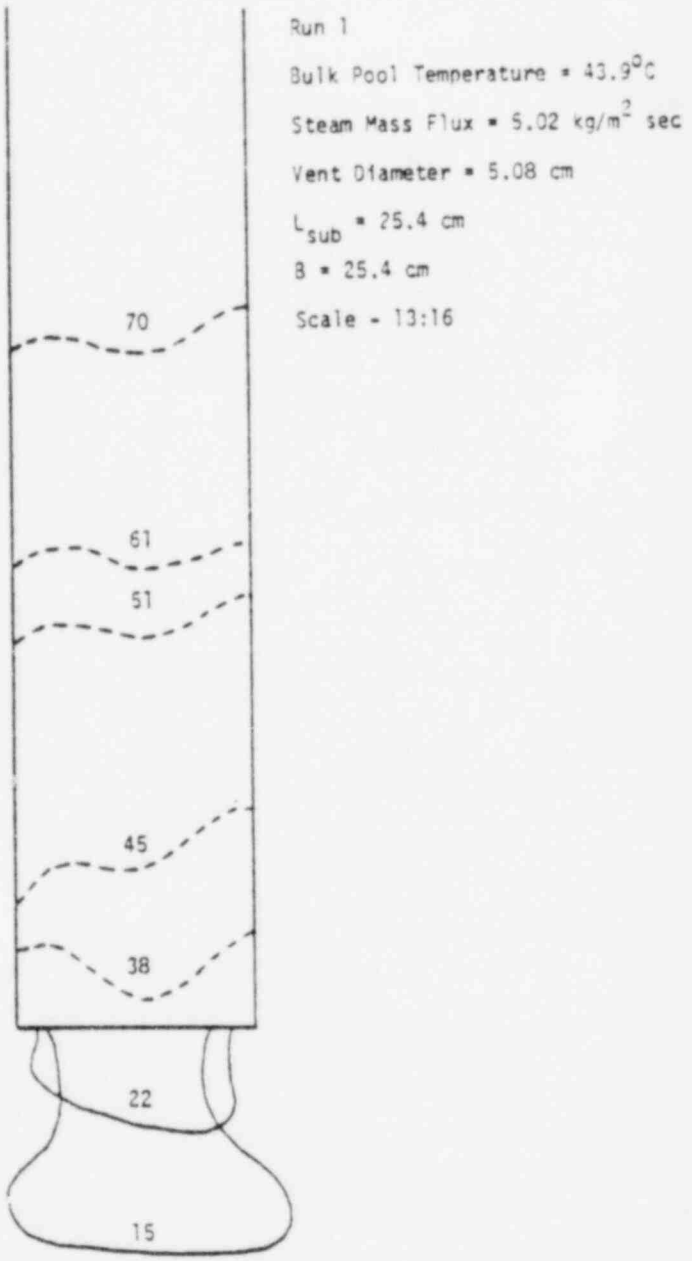


Fig. A.5 Interfacial History for Run 1

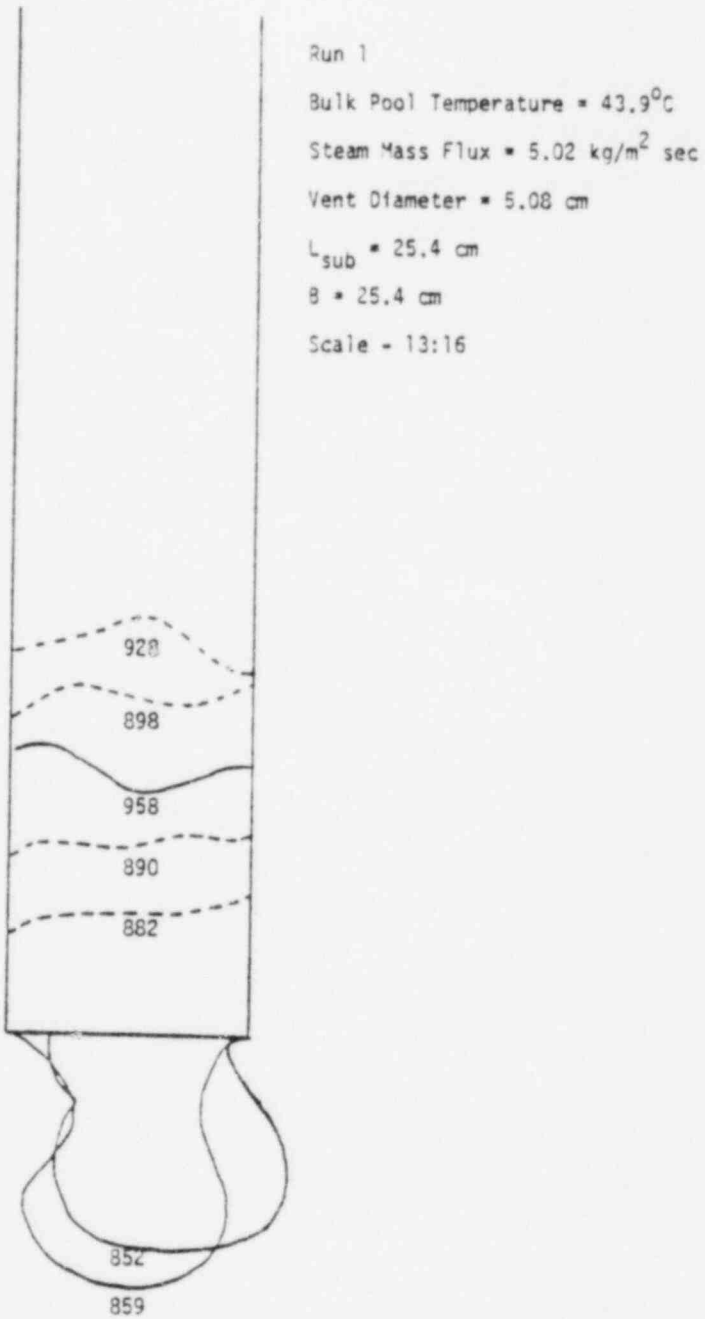


Fig. A.6 Interfacial History for Run 1

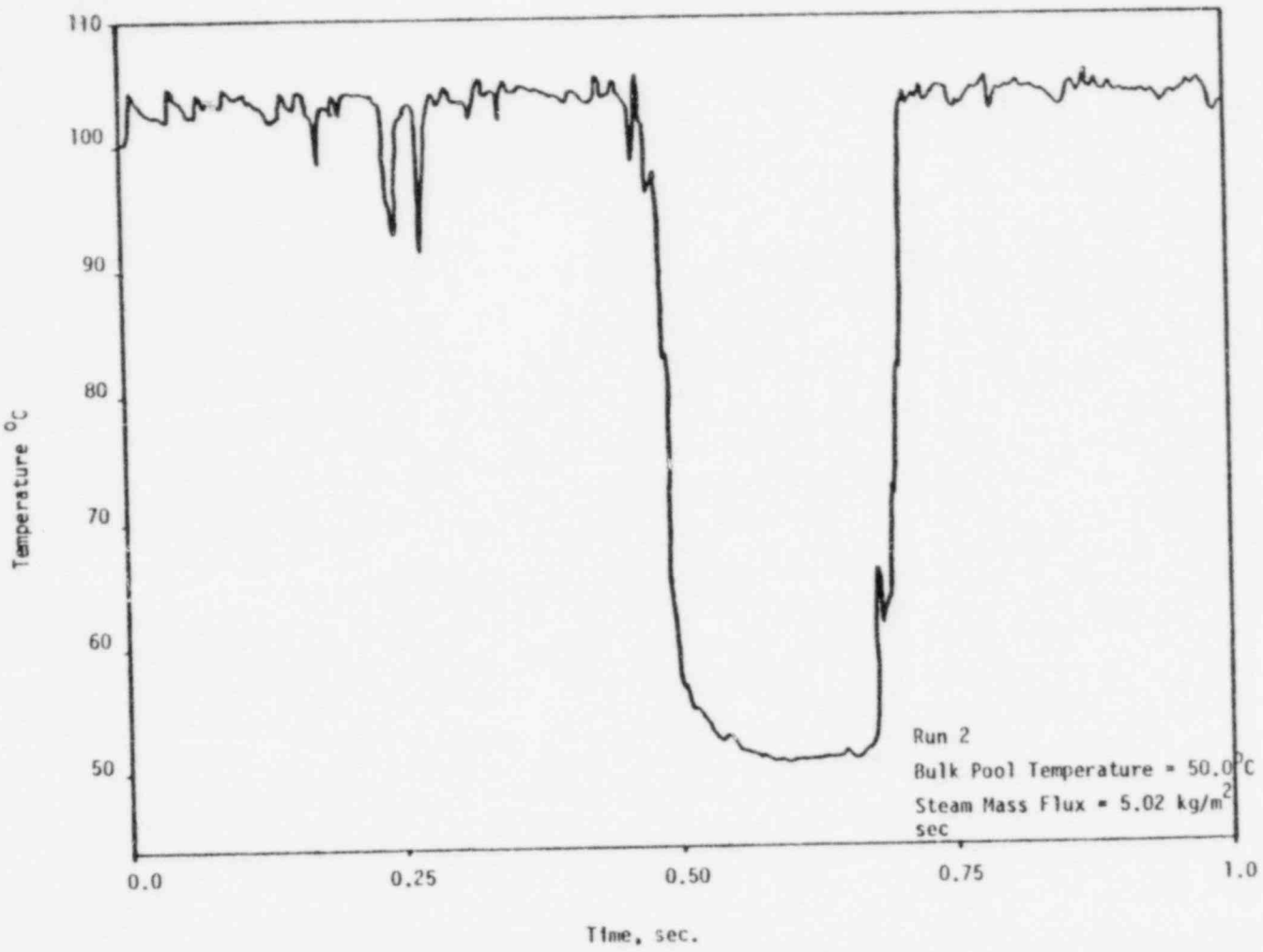


Fig. A.7 Upper Vent Exit Thermocouple Reading for Run 2

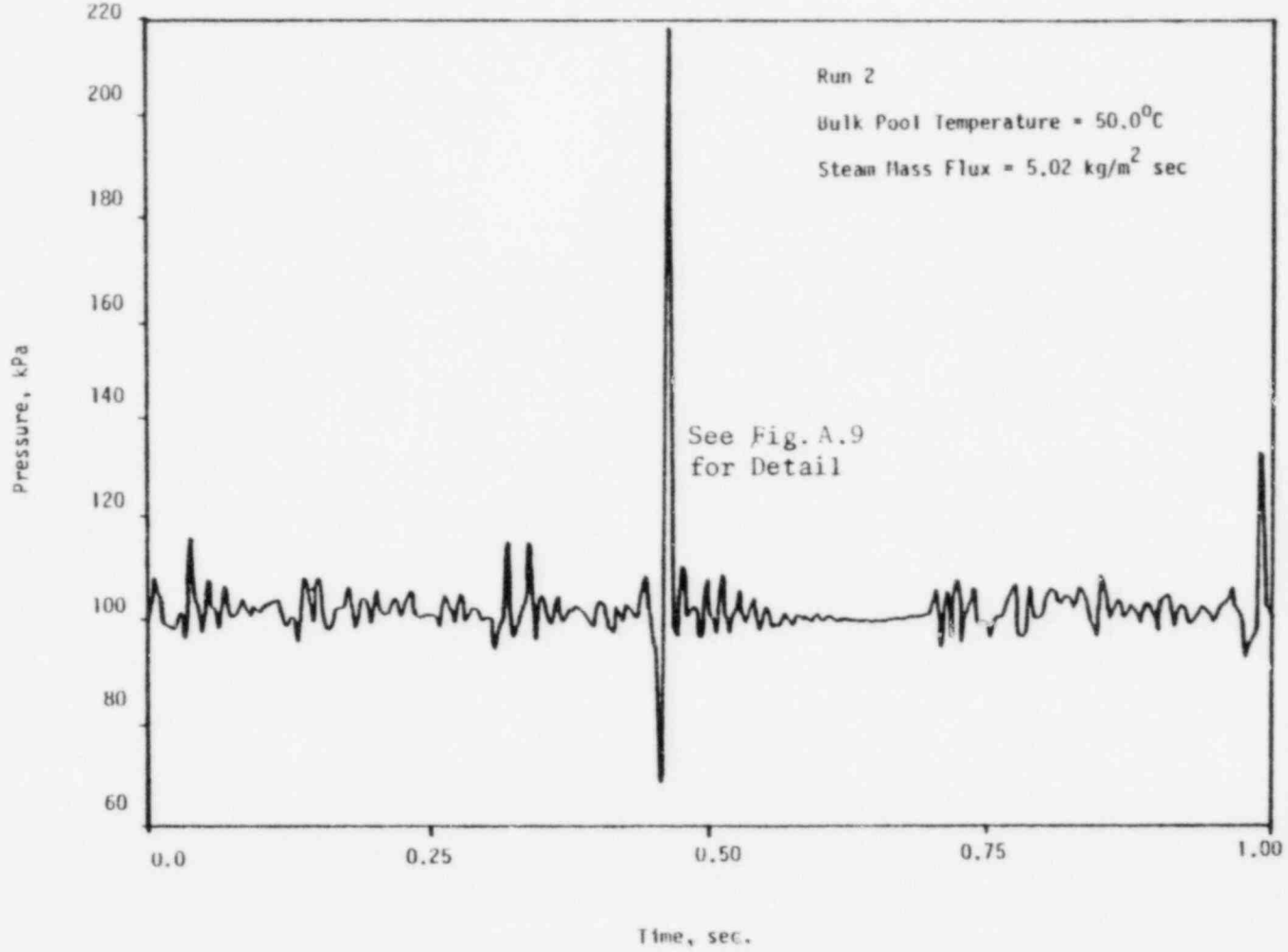


Fig. A.8 Bottom Pressure Transducer Reading for Run 2 (Tp=50°C)

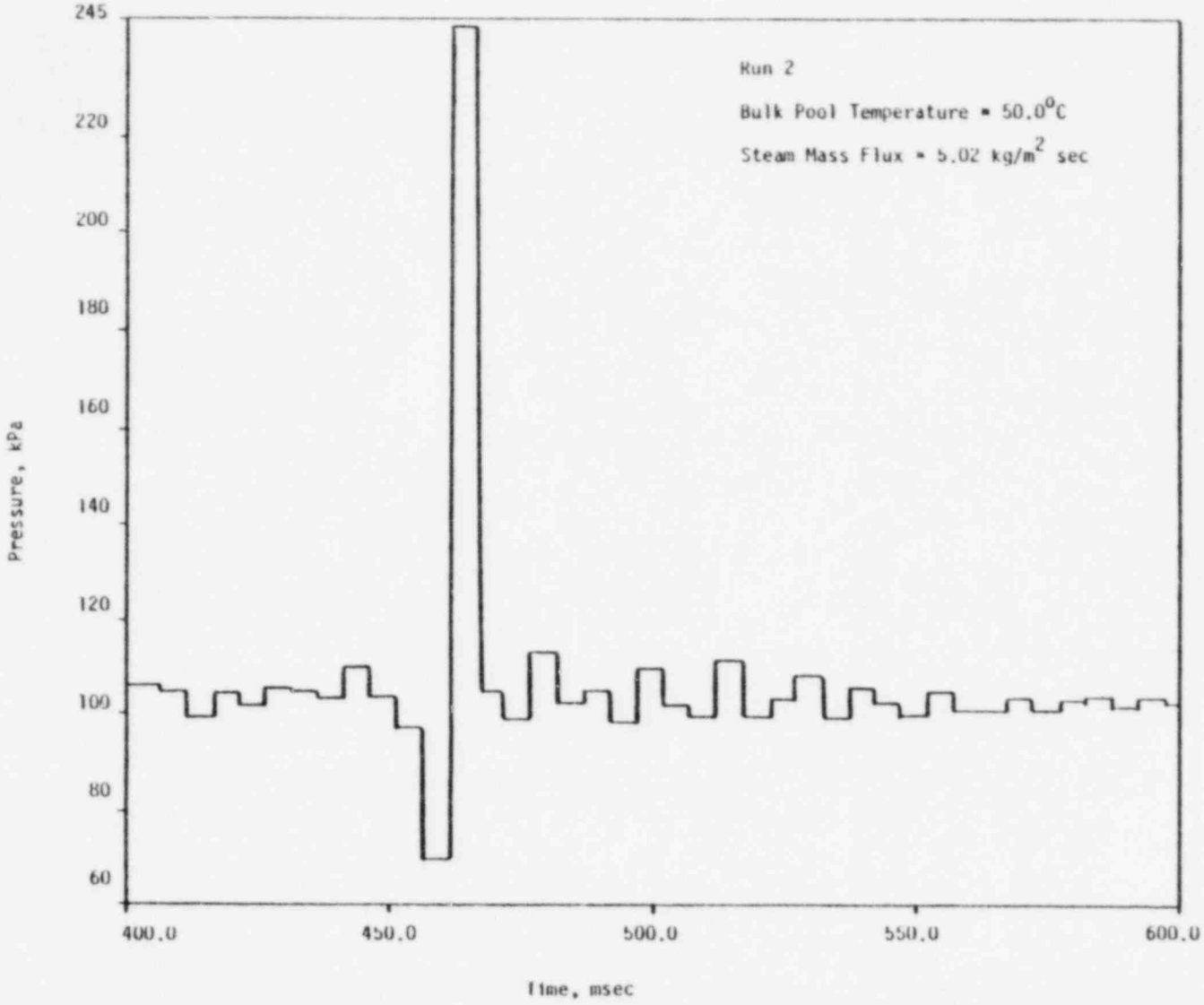


Fig. A.9 Detailed Bottom Pressure Transducer Reading for Run 2

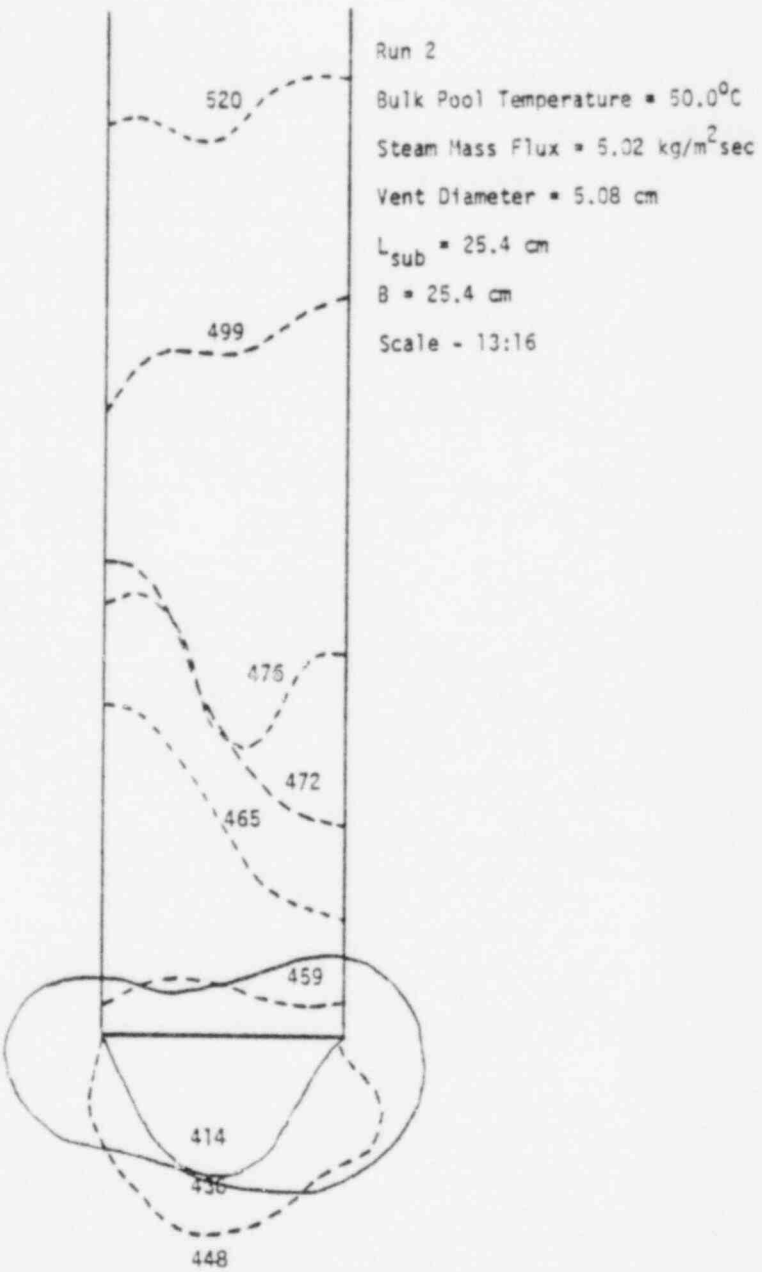


Fig. A.10 Interfacial History for Run 2

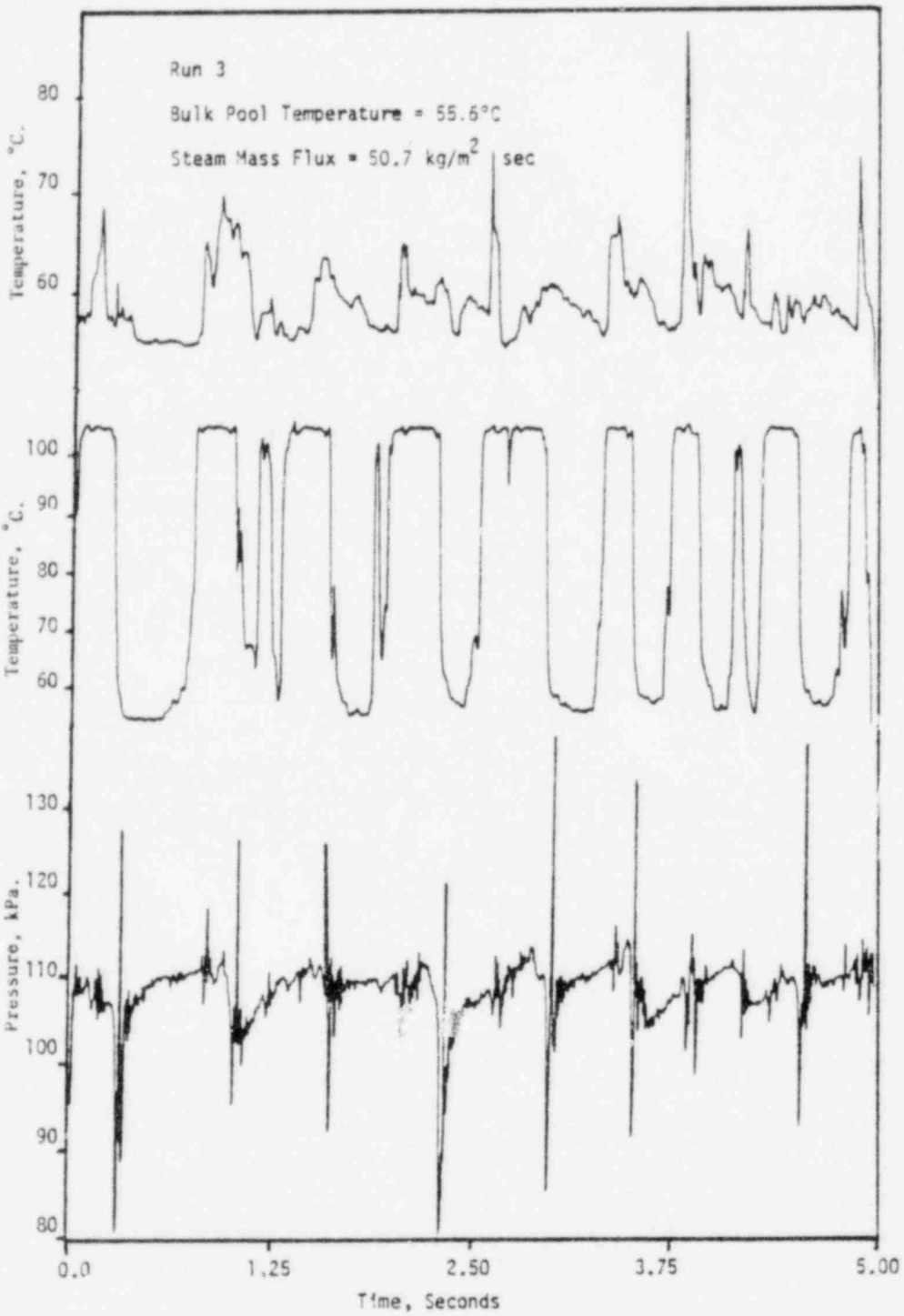


Fig. A.11 Synchronized Temperature and Pressure Data for Run 3

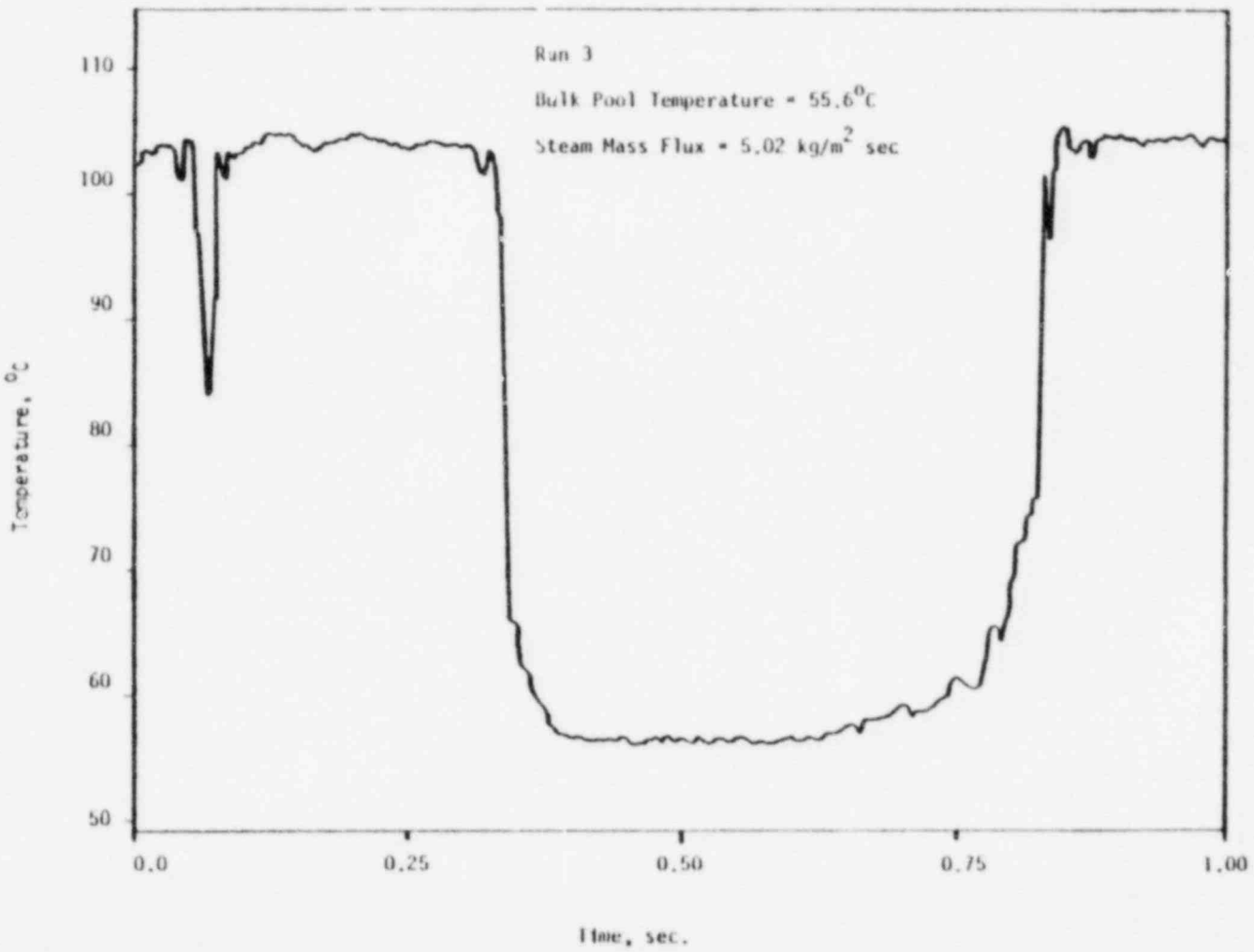


Fig. A.12 Upper Vent Exit Thermocouple Reading for Run 3

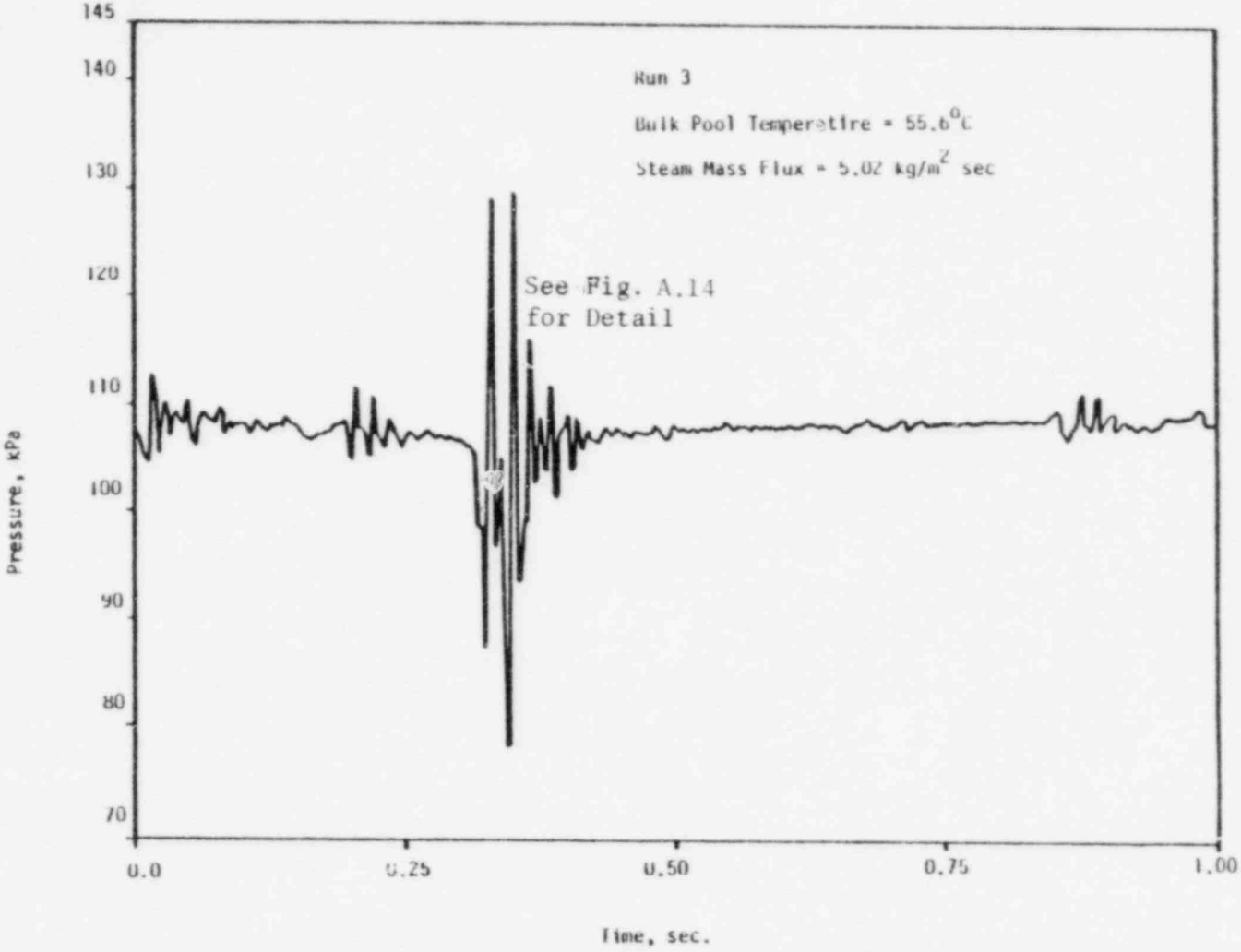


Fig. A.13 Bottom Pressure Transducer Reading for Run 3

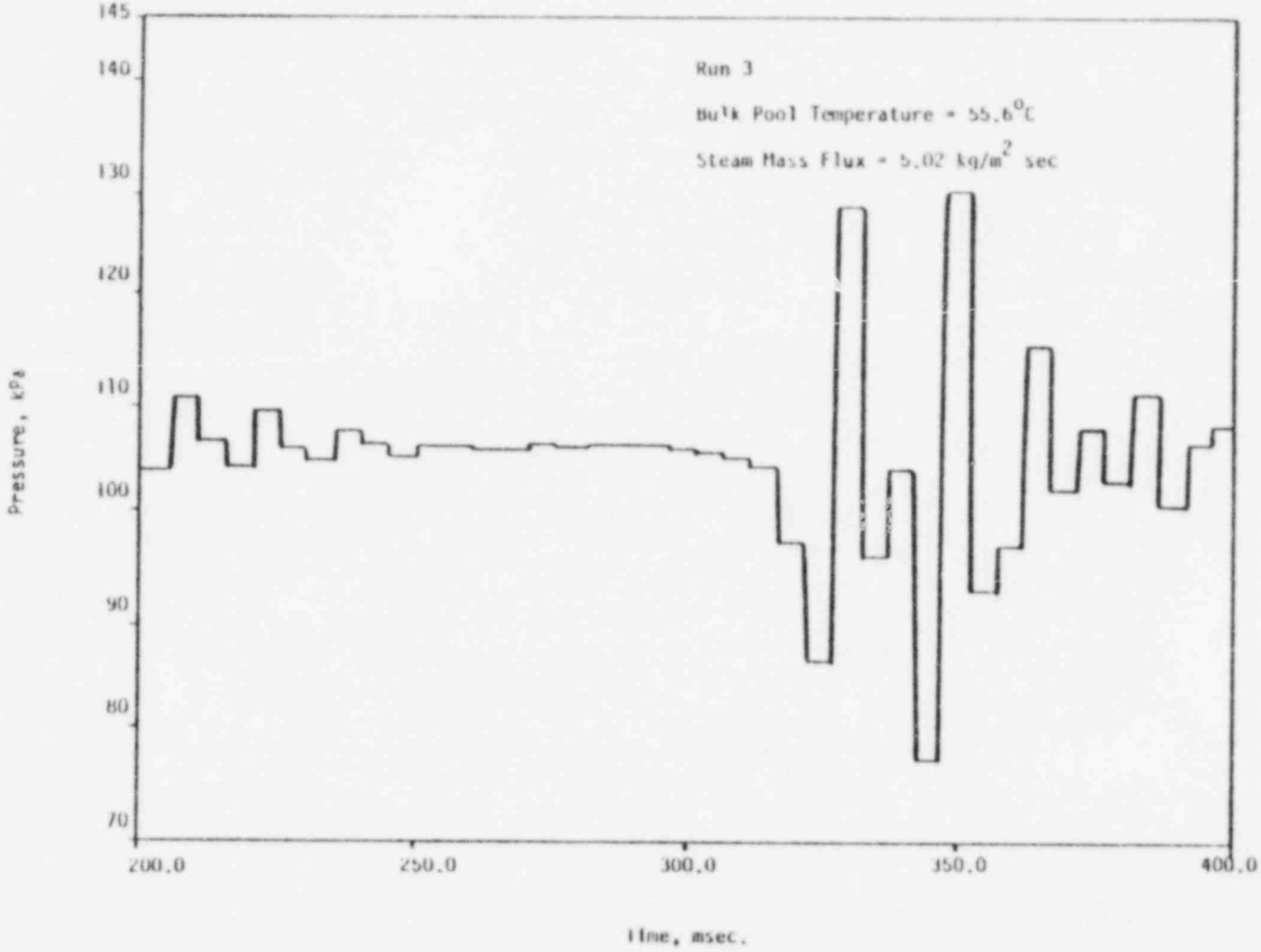


Fig. A.14 Detailed Bottom Pressure Transducer Reading for Run 3

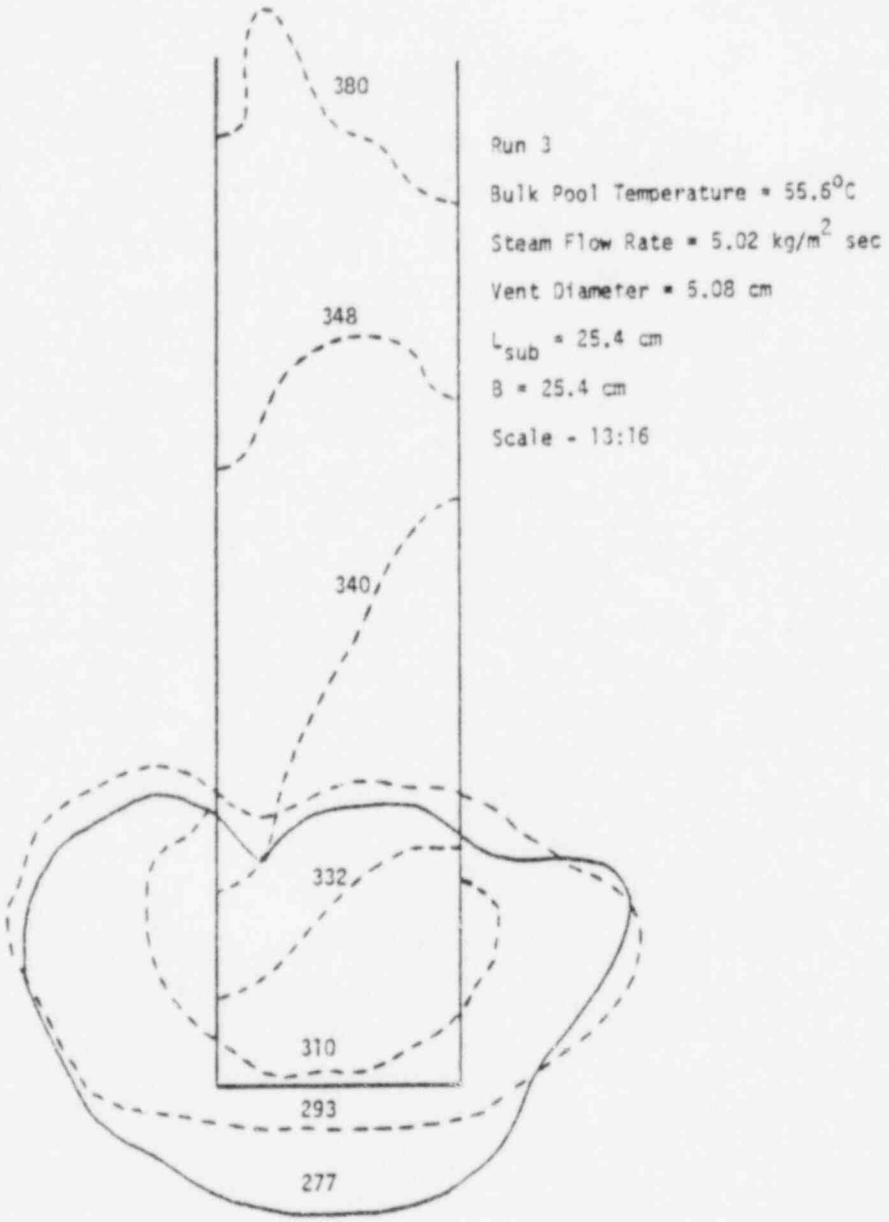


Fig. A.15 Interfacial Movement for Run 3

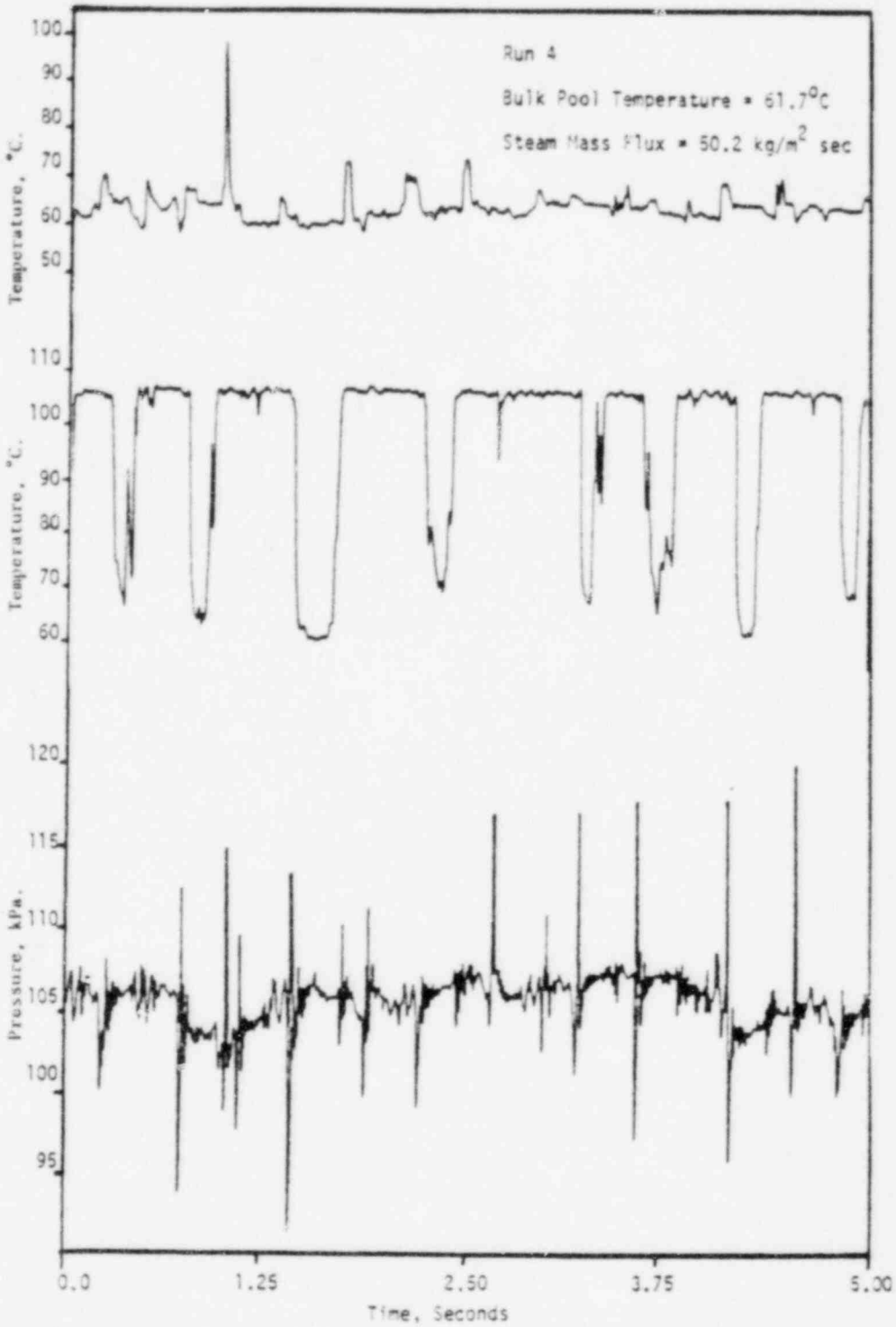


Fig. A.16 Synchronized Temperature and Pressure Data for Run 4

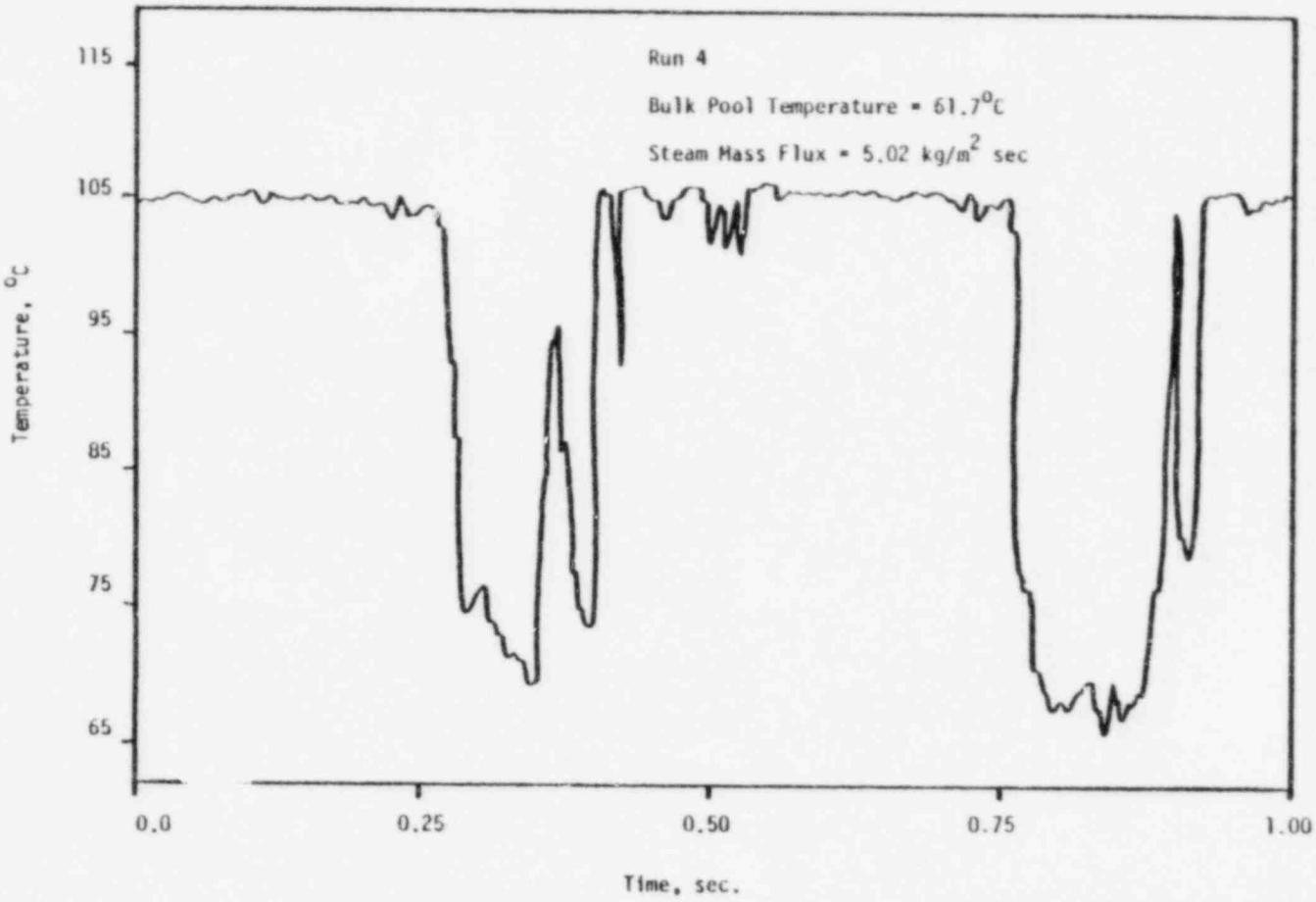


Fig. A.17 Upper Vent Exit Thermocouple Reading for Run 4

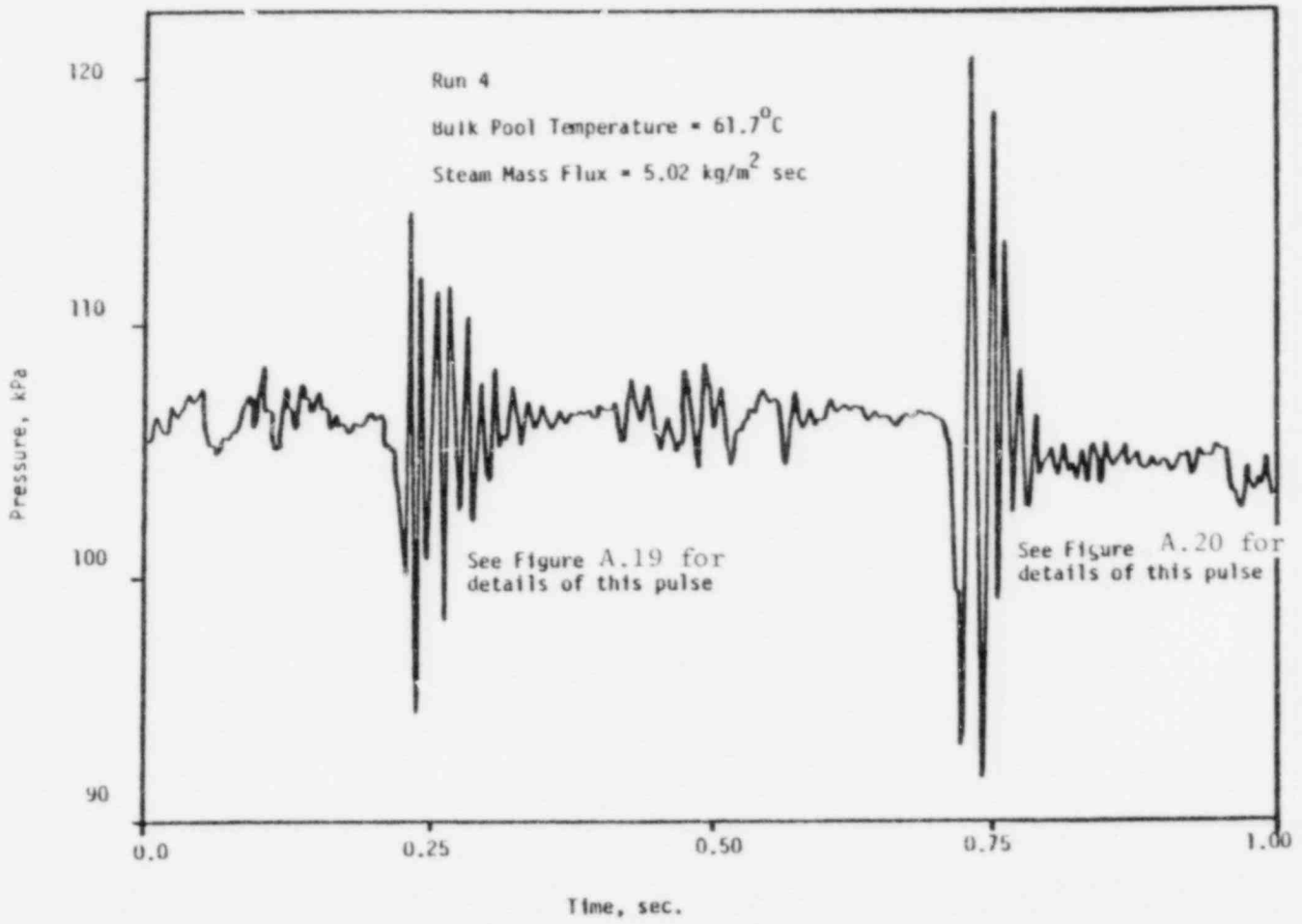


Fig. A.18 Bottom Pressure Transducer Reading for Run 4

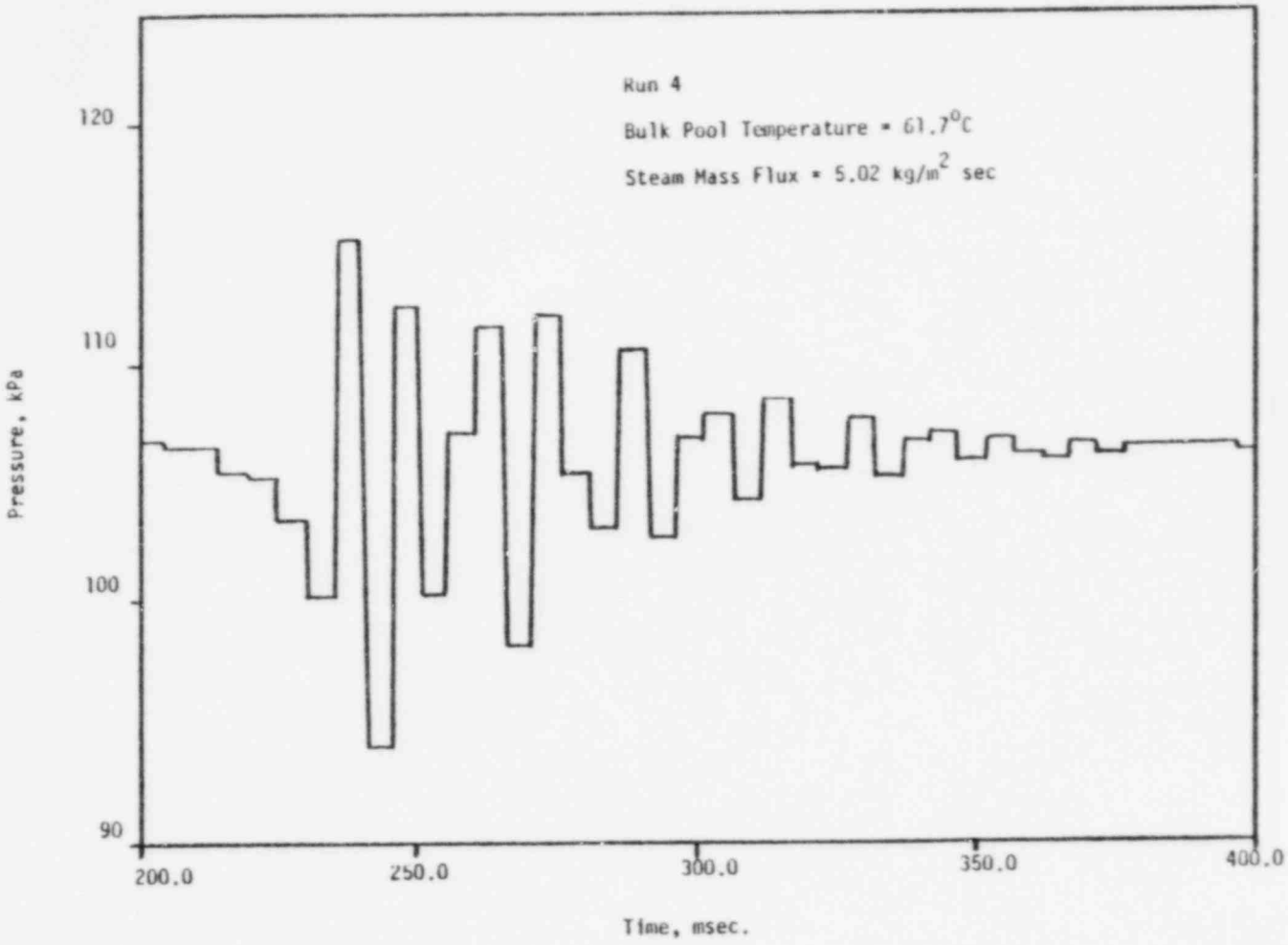


Fig. A.19 Detailed Bottom Pressure Transducer Reading for Run 4

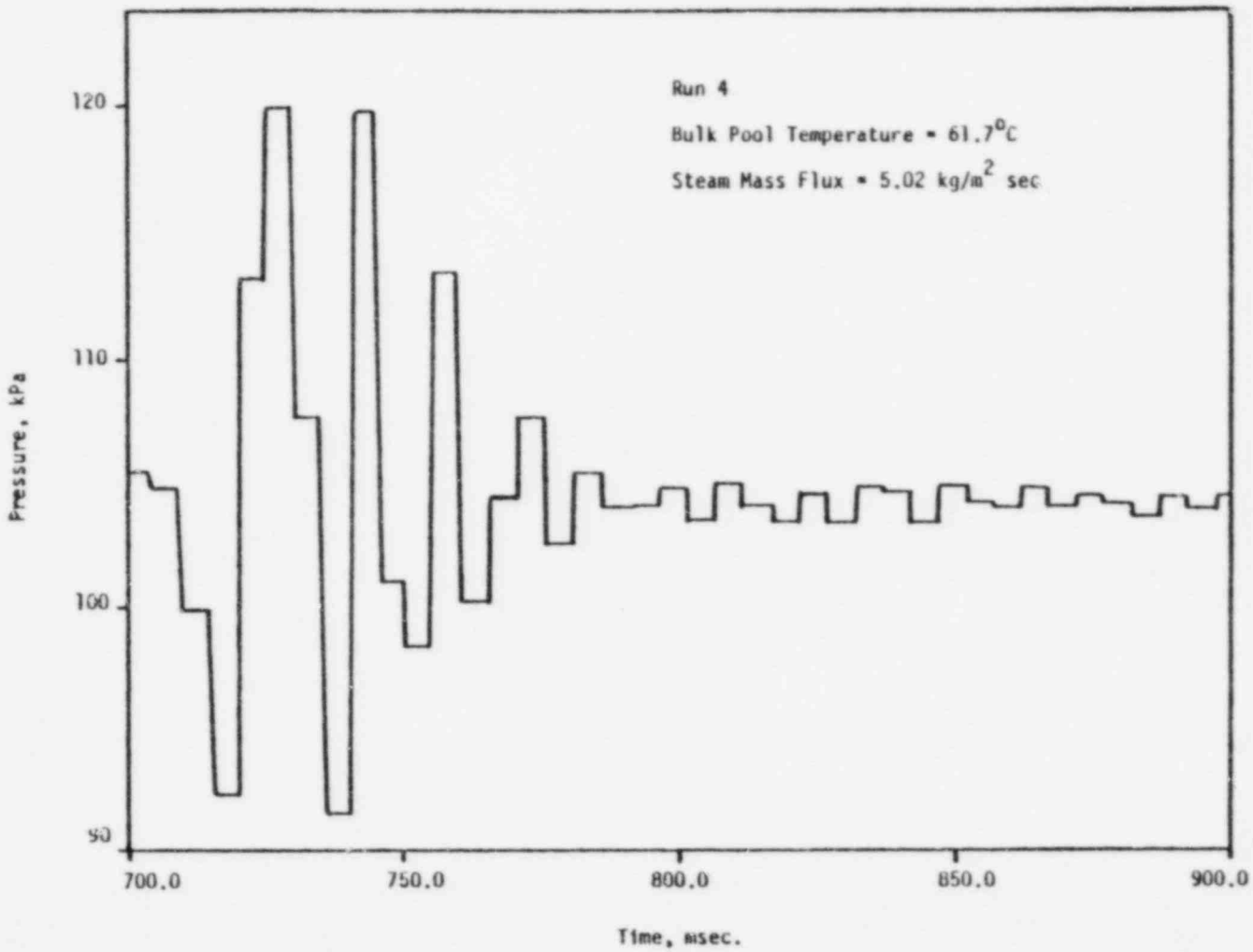


Fig. A.20 Detailed Bottom Pressure Transducer Reading for Run 4

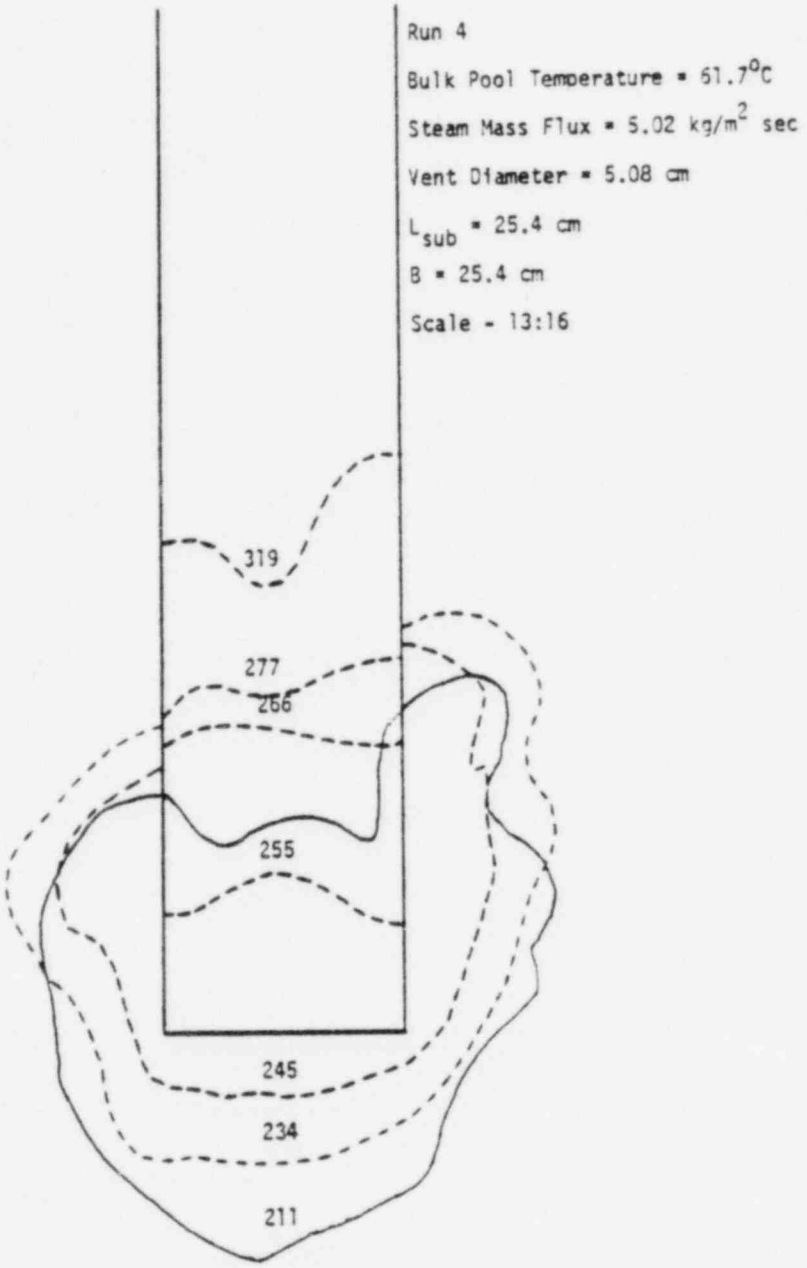


Fig. A.21 Interfacial Movement for Run 4

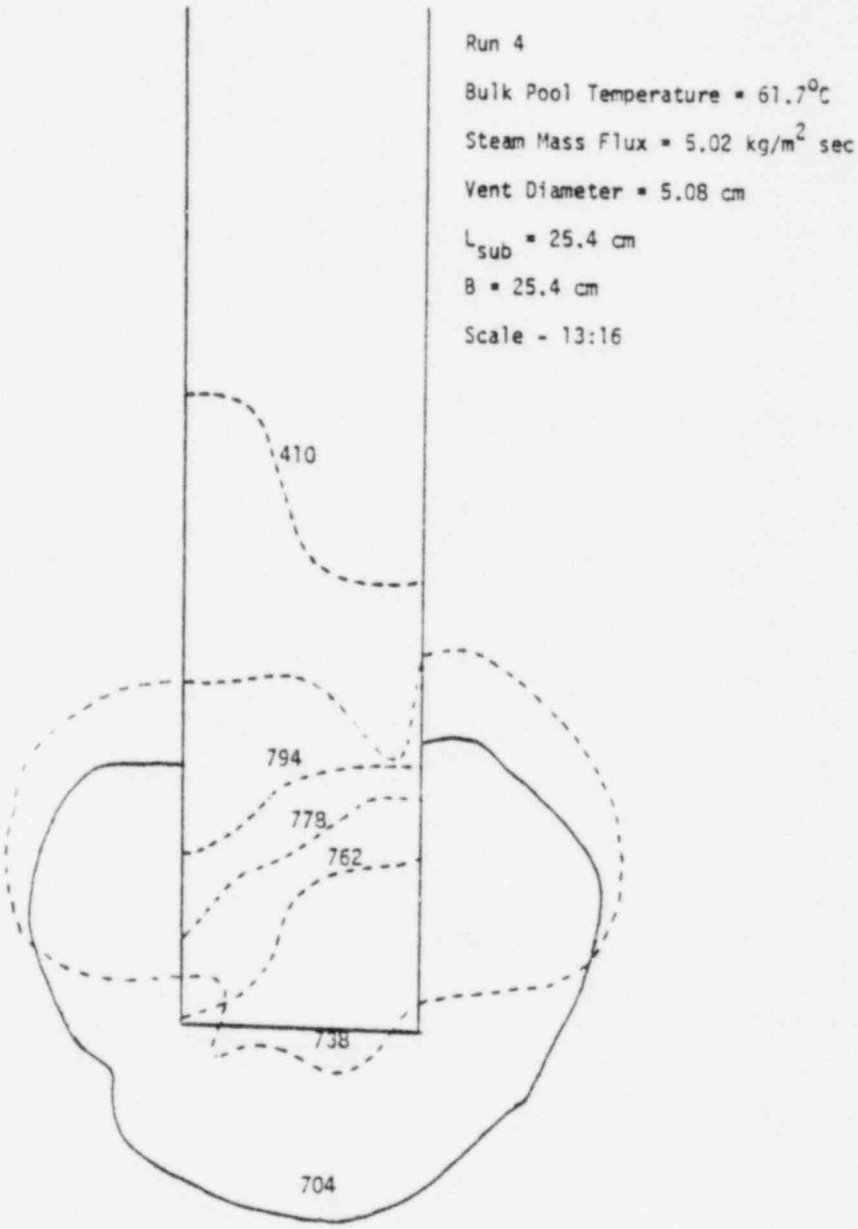


Fig. A.22 Interfacial Movement for Run 4

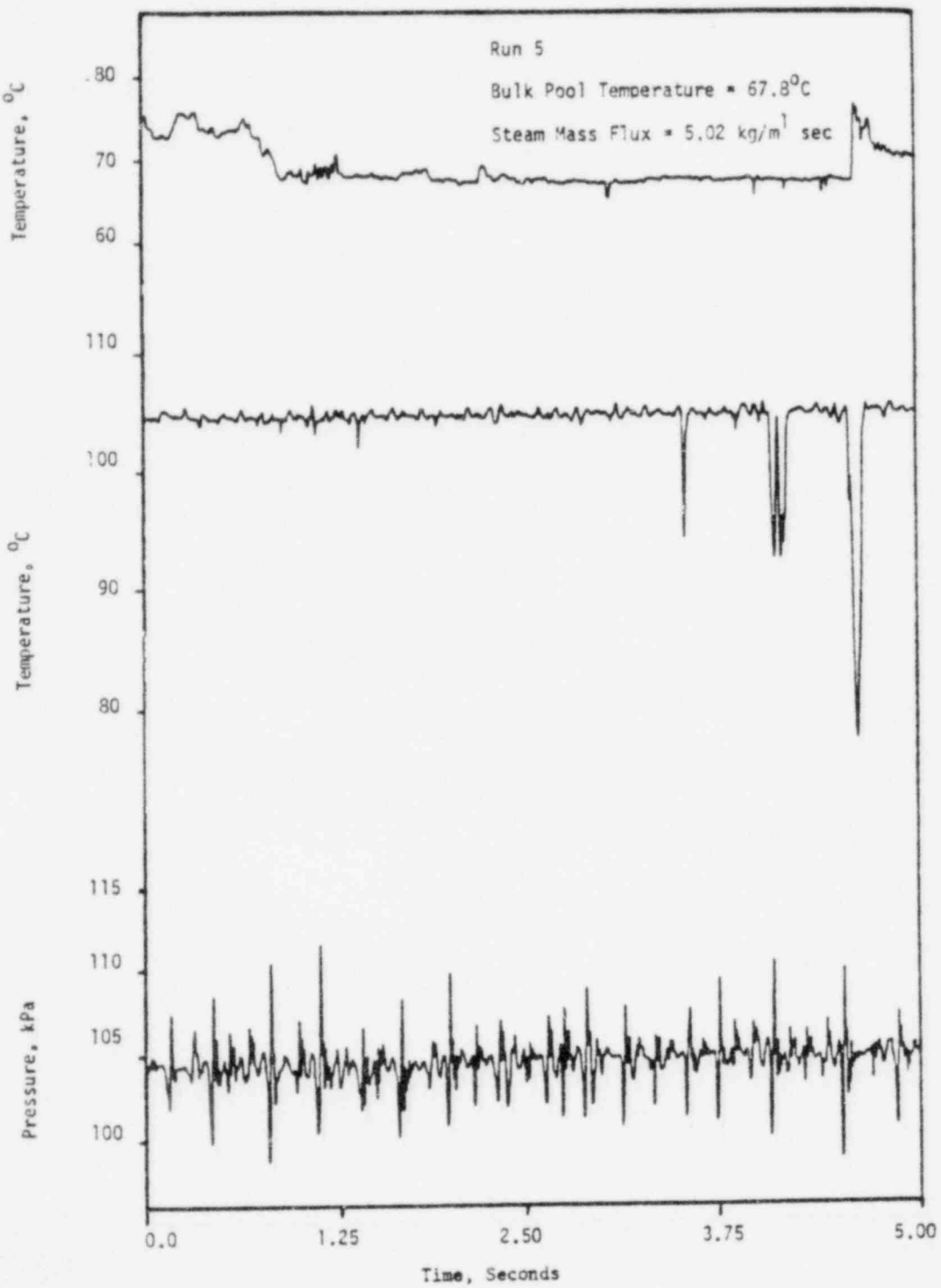


Fig. A.23 Synchronized Temperature and Pressure Data for Run 5

# APPENDIX B

# FLOW METER CALIBRATION

Flow Meter Calibration

In the steam chugging experiments, one of the important measurements was the steam velocity. The method adopted to make these measurements was to use hot wire anemometers. The advantage of using this method was the fast time responses associated with these hot wire probes. Typically for the wires with diameters on the order of .001 in., the response times are on the order of a milli-second. Since the steam velocity in the chugging experiments was expected to change quite rapidly, the use of this type of flow measurement technique seemed to be appropriate.

Two different types of anemometers were used in the steam chugging experiments. The first type was a hot wire probe. The second type was a ruggedized probe where a hot wire was embedded in a metal support. The metal support strengthens the wire such that the occasional droplets entrained in the steam flow would not cause damage to the wire. Therefore the latter type of probe would normally last longer than the former. Since the probe manufacturers were not equipped with steam facilities for flow calibrations, in order to use these probes to measure steam velocity, two methods for calibrating these probes were adopted. The first one simply used the air calibration data given by the manufacturer, and converted it to a correlation which would apply to the steam conditions. The second one was to do a calibration experiment using the steam facility in the chugging experiments. Both methods are described in the following sections.

Method I: Conversion of Air Calibration Data to Steam Conditions

A set of data was furnished by the manufacturer which gave a calibration of the probe (No. TSI-F654) in air at 75°F. This set of data could be fitted by the least-square method using a correlation having the form as King's law for long cylinders:

$$Q = (A + B\,U^n)\,(T_p - T_e) \qquad (1)$$

where A, B, n are constants

Q = heat loss

U = velocity

$T_p$ = probe operating temperature

$T_e$ = temperature of fluid

The constant A is proportioned to the thermal conductivity R while the constant B is proportioned to the ratio $R/V^n$ where V is the kinematic viscosity. In order for the probe to maintain a constant operating temperature, the amount of heat lost to the steam must be balanced by an increase in the heat generated by the electrical resistance, i.e., $Q = \frac{V^2}{R}$ where V is the voltage across the probe and R is the resistance of the wire. Equation (1) could be rewritten as:

$$V^2 = (A + B\,U^n)\,(T_p - T_e) \qquad (2)$$

where the resistance R was lumped into the constants A and B. From the least-square fit, the constants A, B, and n were determined and the equation for the calibration was

$$V^2 = (.0773 + .01967\,U^{.61})\,(T_p - T_e) \qquad (3)$$

This equation could then be converted to the steam flow situation by changing the constants A and B according to the difference in heat transfer properties between air at 75°F (manufacturer

calibration was made at this temperature) and steam at 212°F which was the expected steam temperature in the chugging experiments. This introduced a 2 per cent decrease in the constant A and a 20 per cent decrease in the constant B, so for steam in the chugging condition

$$V^2 = (.0758 + .0157\ U^{.61})\ (T_p - T_e)$$

where for this probe $T_p = 482°F$, and the range of air velocities in the calibration was from 0. to 500 ft/sec. However, due to the change in the electrical resistances of the wires connecting to the hot wire probe due to the temperature effect, the constant A in the experiments at zero flow was found to be 0.027. The final equation used in the data reduction is:

$$V^2 = (0.027 + 0.157\ U^{.61})\ (T_p - T_e) \qquad (4)$$

Method II: Calibration Method Using Steam Facility

The method chosen to calibrate the probe was the method of calorimetry. This method involved the discharge of a steam jet into a pool of water where the pool temperatures were recorded as a function of time. By the energy balance,

$$\dot{m}\ h_{fg} = MC_p \frac{dT}{dt}\ , \qquad (5)$$

where T = pool temperature

$h_{fg}$ = latent heat

$C_p$ = specific heat

M = pool water mass

$\dot{m}$ = steam injection rate

t = time

the steam flow could be determined when the pool temperature was

given as a function of time. The steam velocity could be computed from $\dot{m}$ as determined from equation (5) by knowing the steam density. An experiment to determine the steam flow rate was designed based on this method.

Steam Flow Experiments

The apparatus used to perform the steam flow calibration experiments was the same as that used for the chugging experiments except that a reducer nozzle was mounted at the exit of the pipe. The diameter of the nozzle was .3175 cm. The location of all the instrumentation was presented in Figure B.1. Three measurements were made at the upstream port. Aside from the flow meter reading, the steam temperature and steam pressure were also taken at that point such that the steam density could be derived. The pool water temperature was measured at three different locations in the pool. One of them was located at the corner of the pool such that any non-uniform pool temperature could be detected.

In the experiments, the upstream was pressurized to approximately 50 psia before the solenoid valve was triggered to allow the steam to be discharged into the pool. Since the nozzle diameter was small, choked flow was maintained at the exit for approximately half a minute. The data were recorded by a PDP-11 computer

Data Reduction and Analysis

The data reduction process was divided into two steps. The first step was a time averaging process which attempted to smooth out the irregularities in the pool temperature data. Temperature

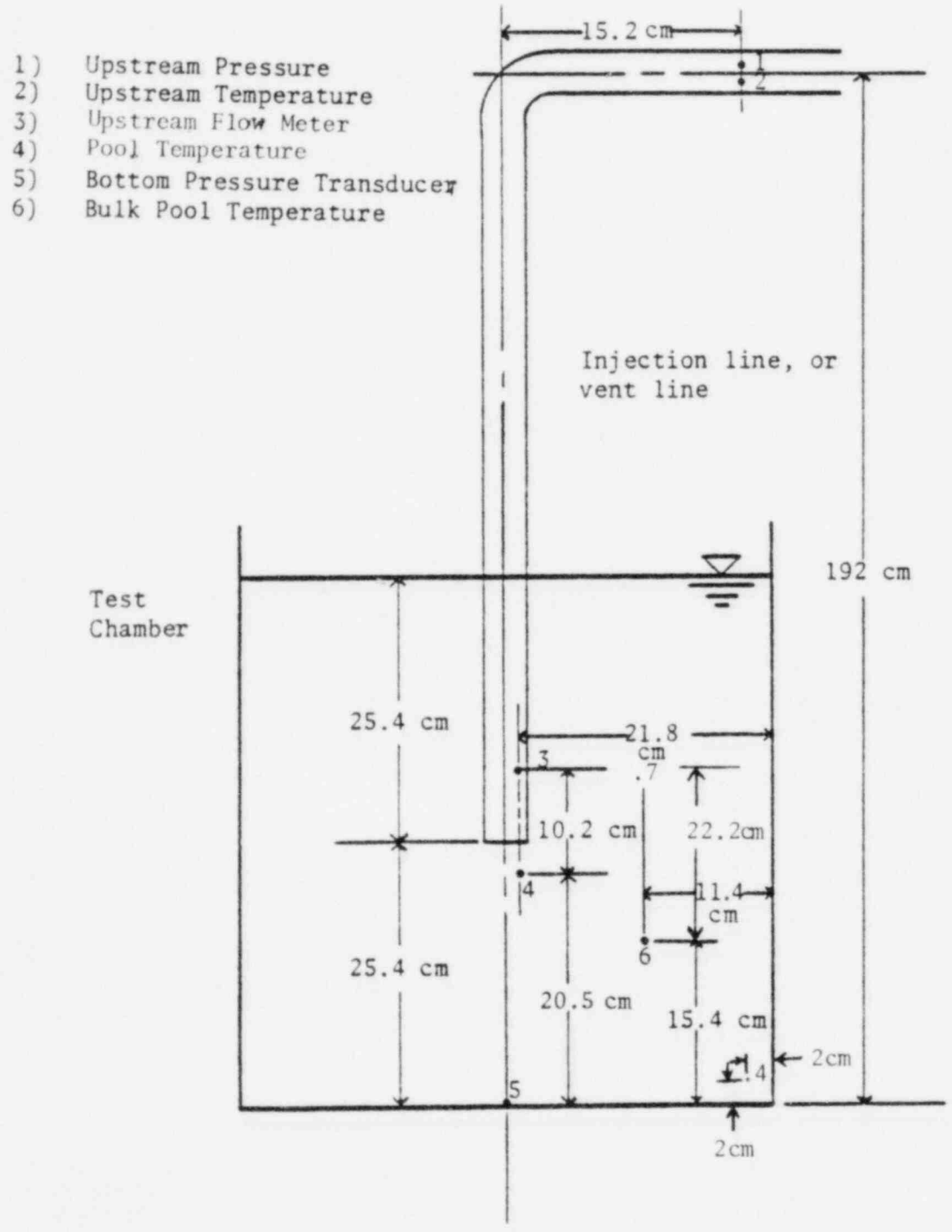


Fig. B.1 Locations of Instrumentation

fluctuations were observed in the pool which caused the pool temperature rise to be non-monotonic. These irregularities were caused by the pool circulation which was induced by the jet. The time averaging process involved taking the set of data and dividing it into N time intervals, then the time average of the data in each interval was computed. As long as the interval was large compared to the period of the fluctuations, the resulting pool temperature rise would be monotonic. The time averaging process was also applied to the other measurements for consistency. Then the time derivative of the pool temperature was computed using a forward differencing scheme and the steam injection rate was computed from equation (1). Since the experiment was quasi-steady, it could be assumed that the steam flow rate at the exit would be equal to the steam flow rate at the upstream port. Then the velocity at the upstream port would be given by

$$U = \frac{\dot{m}}{\rho A_p} \tag{6}$$

where $A_p$ = pipe area

$\rho$ = steam density

The steam density could be deduced from the temperature and pressure measurements. In the calibration experiments, the temperature of the steam was slightly superheated, but they were so small that the density of the steam could be assumed to be saturated. The velocity could then be computed based on equation (2).

The second step in the data reduction and analysis process was to correlate the flow meter output against the computed velocity data. This process was aided by the use of King's law, as in equation (2). Here, it should be recalled that the constant A

was to be found from the experiments at zero flow while the constant B was proportional to the ratio $k/V^n$ where V was the kinematic viscosity. For n = 1 this ratio changed by approximately 1. per cent over the range of temperatures in the experiment while k changed by 2 per cent. So in the correlation A and B could be considered constants. From equation (4) the correlating parameters were found to be $\xi$ and U. The relationship was

$$\xi = \frac{V^2}{Tp - Ts} = A + B\,U^n$$

$\xi$ was found directly from the experiment. U was deduced from the experiment by using equation (1). The unknowns were A, B, and n. Amongst these, A could be determined from the zero flow reading of the anemometer output. It could also be determined from the experimental data, both zeros should check. After A was determined, then B and n could be determined by a linear fit of the experimental data as follows. The first step was to take the natural log of equation (5). The resulting equation was

$$\ln (\xi - A) = \ln B + n \ln U$$

then by letting $y = \ln (\xi - A)$

$$C = \ln B$$

$$x = \ln U$$

equation (5) finally became

$$y = n\,x + c \qquad (6)$$

The least square method for a linear fit was then used to determine the constants n and C. Using this method, a correlation was obtained for the ruggedized probe.

For this probe (TSI - 1269W), the correlation was based on

time-averaged data from one experimental run. When sixteen time-averaged intervals were used the resulting correlation was

$$V^2 = ( .1044 + .00233\ U^{1.05})\ (T_p - T_s) \qquad (9)$$

If ten time-averaged intervals were used, the resulting correlation was

$$V^2 = (.1044 + .00226\ U^{1.11})\ (T_p - T_s) \qquad (10)$$

The two correlations were approximately the same which acted as a consistency check on the choice of the interval sizes.

Here, it should be mentioned that the constants B and n were obtained based on minimizing the least-square error when ln ($\xi$ - A) was plotted against ln U. The error involves the log of the data rather than the data points themselves. In other words, if the actual data were used rather than the log of the data, the curve that minimizes the least-square error may not be the same, B and n could be different. To check the consistency of the previous method, the correlations presented in equations (7) and (9) were checked by letting $y = U^n$,

then $\xi = A + B\ y$

$\xi$ and y were given by the data, while A and B would be determined by a least square fit which minimizes the least square error based on $\xi$ and y. If the set of data $\xi$ and U could be approximated by $\xi = A + B\ U^n$, then B and n could be determined by the previous method, and therefore the constants A and B as determined by equation (11) should be approximately the same as those given in equations (7) and (9). Since n was approximately equal to one, a least-square fit was made for just $\xi = A + B\ U$. The resulting

equation was

$$V^2 = (.10425 + .0026318\ U)\ (T_p - T_s)$$

which compared very well with equations (9) and (10).

Finally, due to doubts about the large value of n, another check then was made for lower steam flow rates. In this case the velocity of the steam derived from equation (5) was averaged. Then the output voltage from the anemometer, and the steam temperatures were averaged over the entire run to obtain an averaged $\overline{\zeta}$. The same procedure was applied to the previous set of data used to derive equation (9) and another averaged $\overline{U}$ and $\overline{\zeta}$ were obtained. The results were as follows:

Run #1 $\quad \overline{\zeta} = .11395 \qquad \overline{U}_1 = 3.6587$

Run #2 $\quad \overline{\zeta} = .10736 \qquad \overline{U}_2 = 1.0447$

Based on these two points the value of B and n were obtained and the resulting equation was

$$V^2 = (.1044 + .00284\ U^{.93})\ (T_p - T_s) \qquad (11)$$

which compared well with equations (9) and (10). From isentropic compressible flow steady state hand calculations, it was found that for the steam pressure range in the calibration experiments, the steam velocity was approximately constant throughout the experiment. In the same conditions as Run #1, the steam velocity was found to be 3.6 ft/sec which compared well with $\overline{U}_1$ given above. Therefore it was believed that the averaged data were more reliable and equation (11) was chosen to be the correlation used to obtain steam chugging data. Due to the small changes in the transport properties since the steam temperature range in the calibration experiments

were $\sim$ 300°F compared to the conditions in the chugging experiments $\sim$212°F, a correction was made to the constant B. The correct equation appropriate for the steam chugging condition was

$$V^2 = (0.1044 + .00293\ U^{.93})\ (T_p - T_s) \qquad (12)$$

Error Analysis

To assess the error involved in these two equations, namely equation (3) and equation (11), it should be mentioned that for equation (3) since the equation was derived from the air flow calibration data given by the manufacturer, the error could be assessed by checking the predictability of the correlation on the original data set in the velocity range of interest. Table B.1 shows the results of this calculation. The maximum deviation was 33 per cent.

For equation (11), the error involved could be found by taking the derivative of the equation which gives

$$\Delta \dot{\xi} = B\ \Delta U \cdot U^{-.07}$$

could be determined from the experimental data. The maximum error was +57 per cent and -68 per cent.

Conclusion

Owing to the crude methods used in obtaining the calibration for these probes, it is expected that large error would be incurred. The error in either probes could easily be of the order of a few hundred per cents. However, the probes were very sensitive to velocity variations. The response time for these probes is on the order of 100. micro-seconds.* Therefore, the velocity data in the

chugging experiments would be useful in considering velocity variations over a chug.

---

*Letter from J. Burgos, Chief Engineer at Thermo-Systems, Inc., to myself.

TABLE B.1

| $\zeta$ | $U_m$, measured velocity, ft/sec | $U_p$, predicted velocity, ft/sec | Deviation $\frac{U_p - U_m}{U_m} \times 100\%$ |
|---|---|---|---|
| .0973 | 1. | 1.028 | 2.8 |
| .1003 | 1.2 | 1.292 | 7.6 |
| .1048 | 1.5 | 1.732 | 15.5 |
| .1113 | 2.0 | 2.453 | 22.6 |
| .1171 | 2.5 | 3.175 | 27.0 |
| .1207 | 3.0 | 3.659 | 22.0 |
| .1311 | 4.0 | 5.204 | 30.1 |
| .1398 | 5.0 | 6.654 | 33.0 |
| .1695 | 9.75 | 12.58 | 29.0 |
| .1889 | 14.62 | 17.21 | 17.7 |
| .2074 | 19.49 | 22.13 | 13.5 |
| .2233 | 24.36 | 26.74 | 9.7 |
| .2384 | 29.24 | 31.42 | 7.5 |
| .2521 | 34.11 | 35.92 | 5.3 |
| .2732 | 38.94 | 43.29 | 11.2 |
| .2887 | 43.85 | 49.05 | 11.8 |
| .3023 | 48.73 | 54.33 | 11.5 |
| .3241 | 58.47 | 63.22 | 8.1 |

# APPENDIX C

# VENT PRESSURE EXPERIMENTS

Vent Pressure Experiments (Steel Pipe)

| Run No. | Pool Temp., °C |
|---|---|
| VP1 | 37.2 |
| VP2 | 46.7 |
| VP3 | 58.9 |
| VP4 | 64.4 |

(1) Vent Pressure measured by Statham PL-131-TC-15 pressure transducer (error $\leq$ 0.78KPa, Response Time = 0.83 ms).

(2) Bottom Pressure measured by Statham PL-131-TC-100 pressure transducer (error $\leq$ 5.17 KPa, response time = 0.45 ms).

(3) Exit Temperature measured by gage 36 Chromel-Alumel thermocouple.

(4) Boiler Steam Generation Rate = .00756 Kg/sec.

(5) Pipe Exit to Pool Bottom Clearance = 25.4 cm.

(6) Submergence Depth = 25.4 cm.

(7) Data sampling time = 2. ms.

1) Upstream Pressure (Not Used)
2) Upstream Temperature
3) Upper Exit Thermocouple
4) Lower Exit Thermocouple (Not Used)
5) Bottom Pressure Transducer
6) Bulk Pool Temperature
7) Vent Pressure Transducer

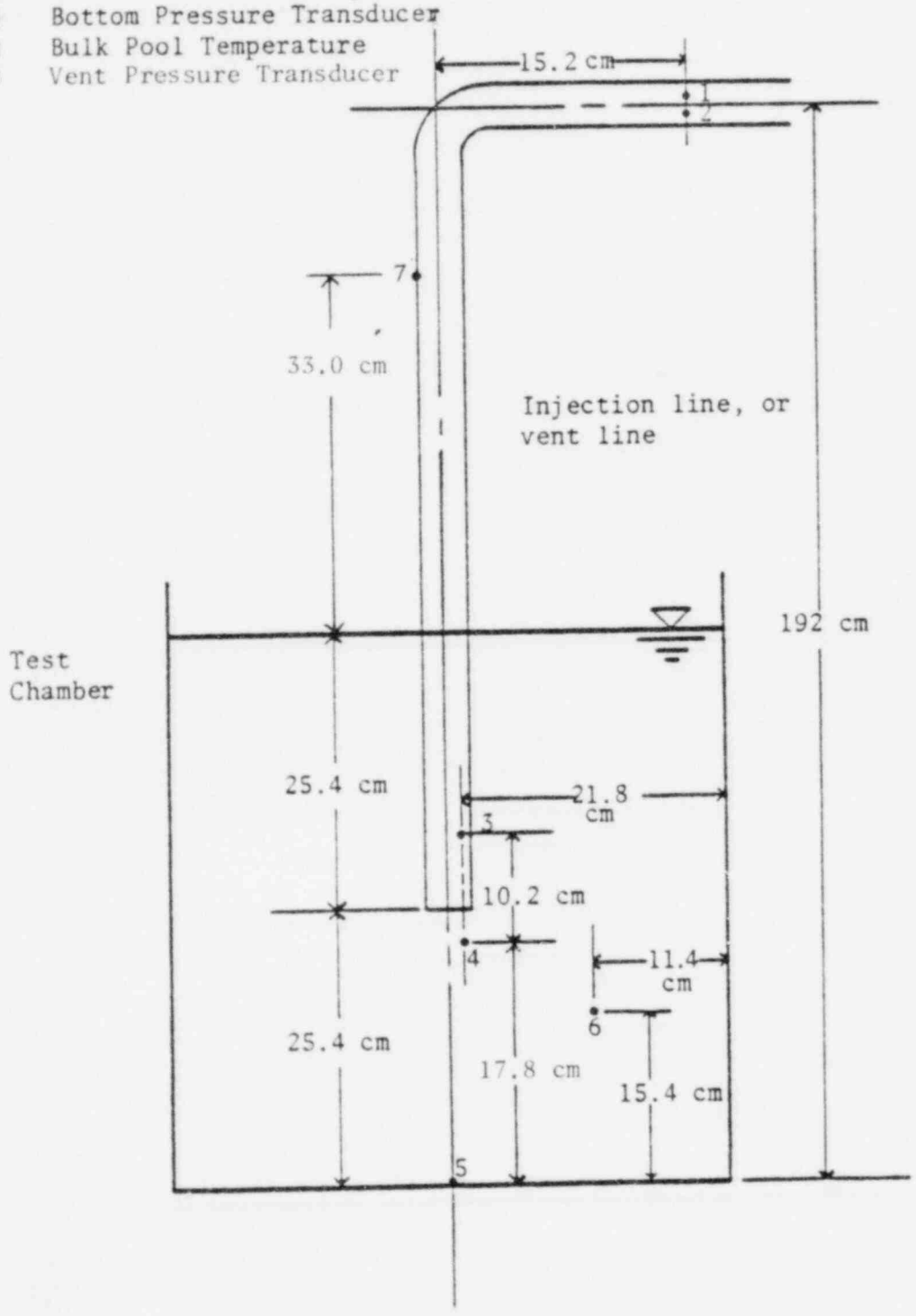


Fig. C.1 Locations of Instrumentation

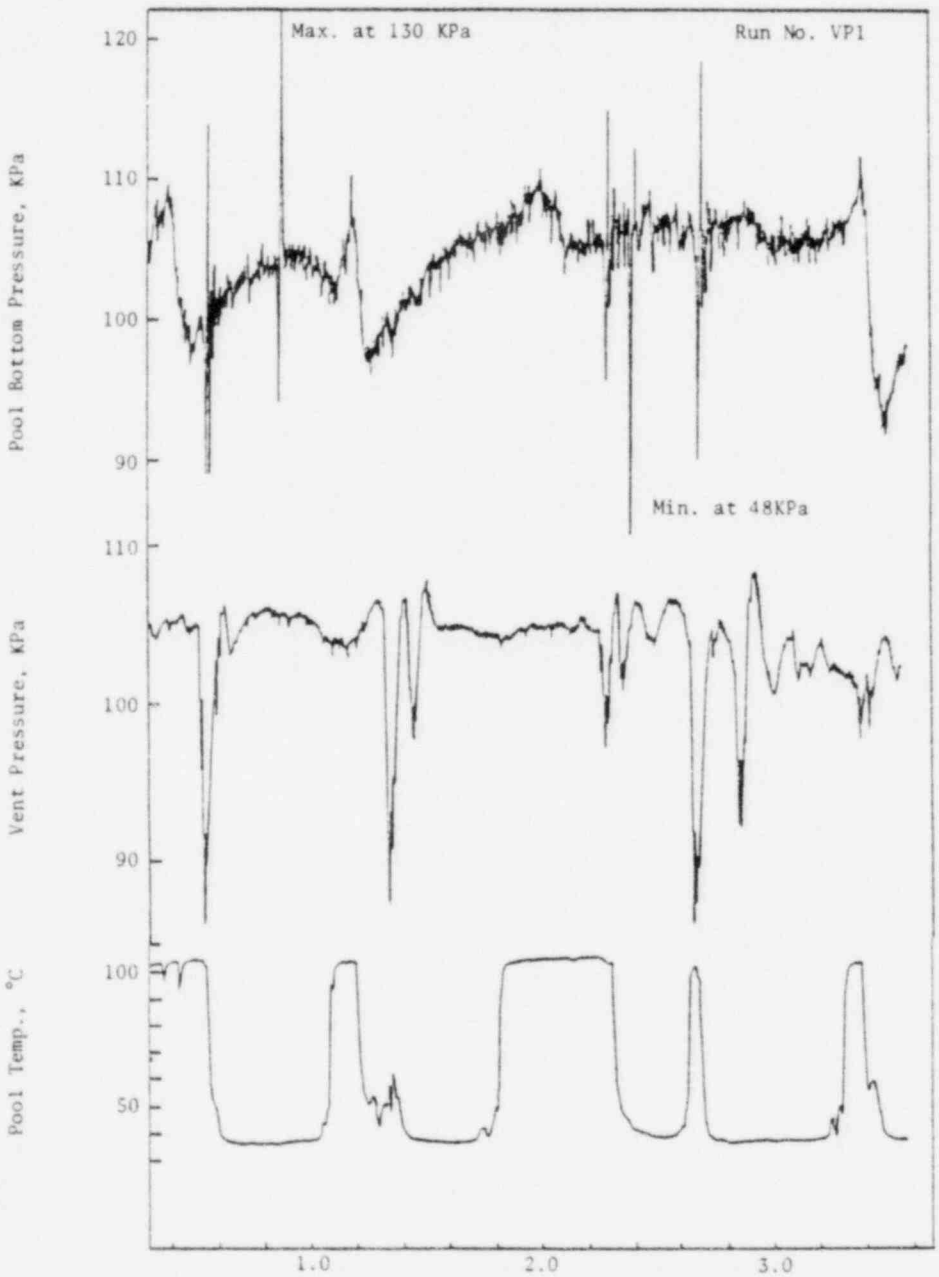
Max. at 130 KPa
Run No. VP1
Min. at 48KPa
Pool Bottom Pressure, KPa
Vent Pressure, KPa
Pool Temp., °C
120
110
100
90
110
100
90
100
50
1.0
2.0
3.0
Time, sec.

Fig. C.2

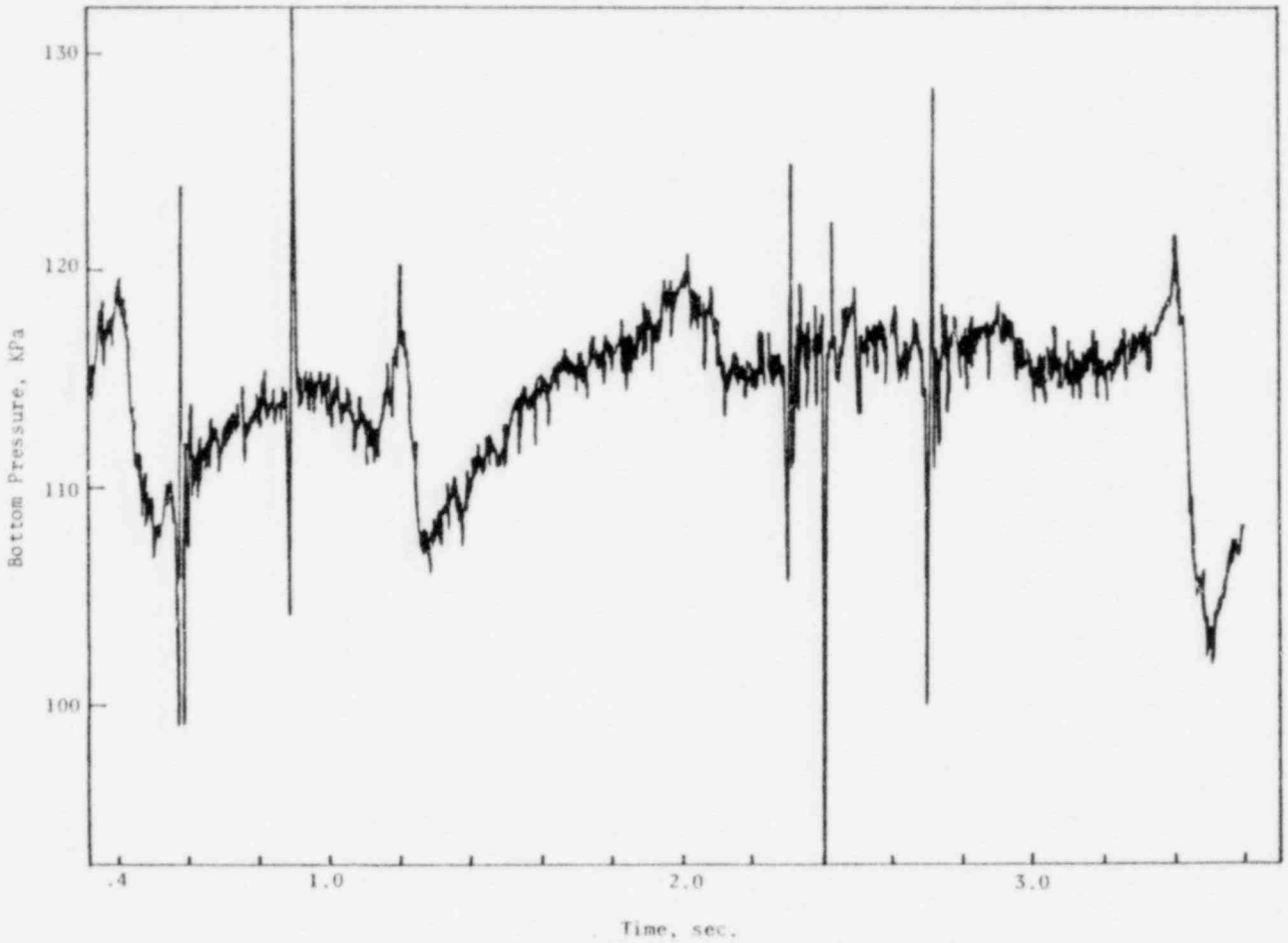


Fig. C3 Run No. VP1

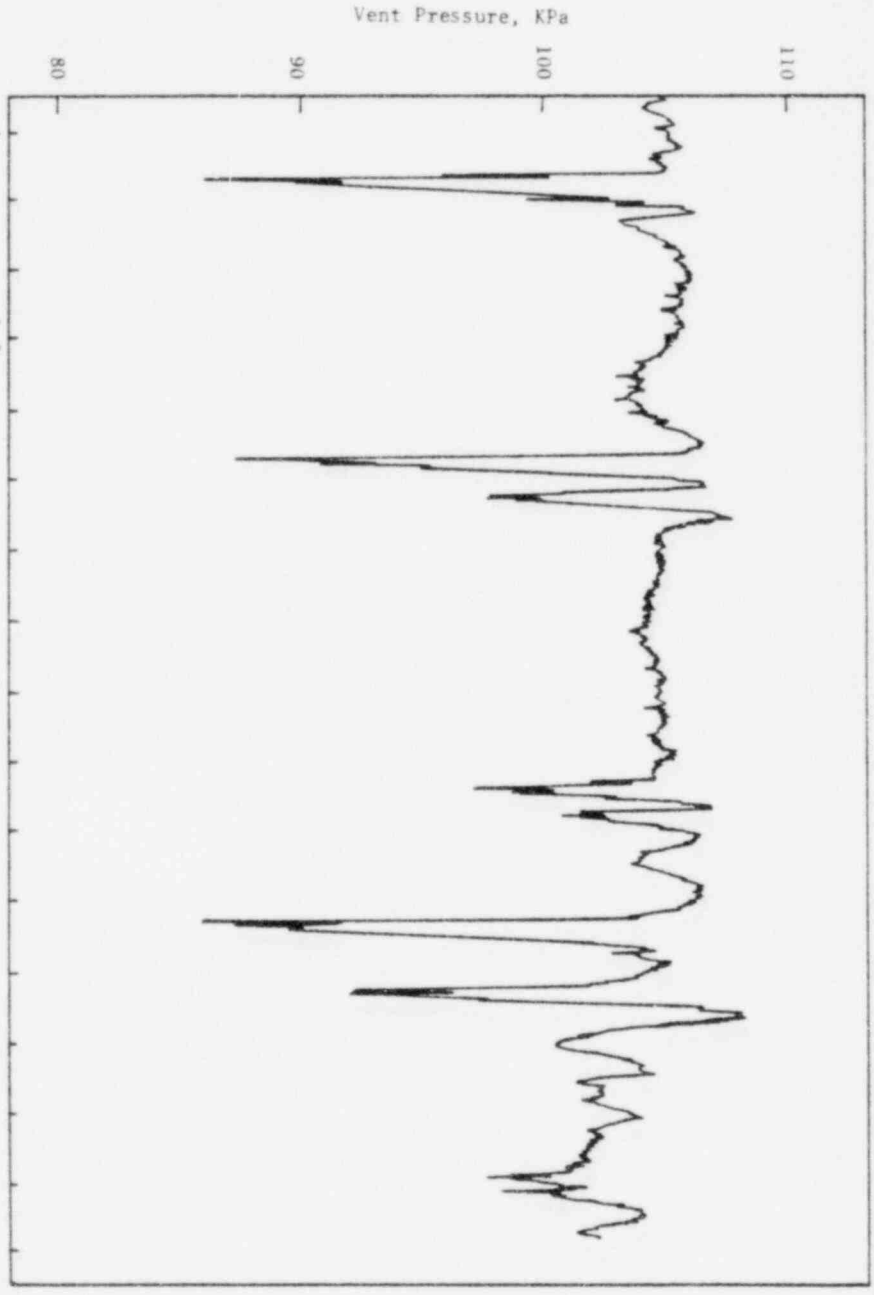


Fig. C.4 Run No. VP1

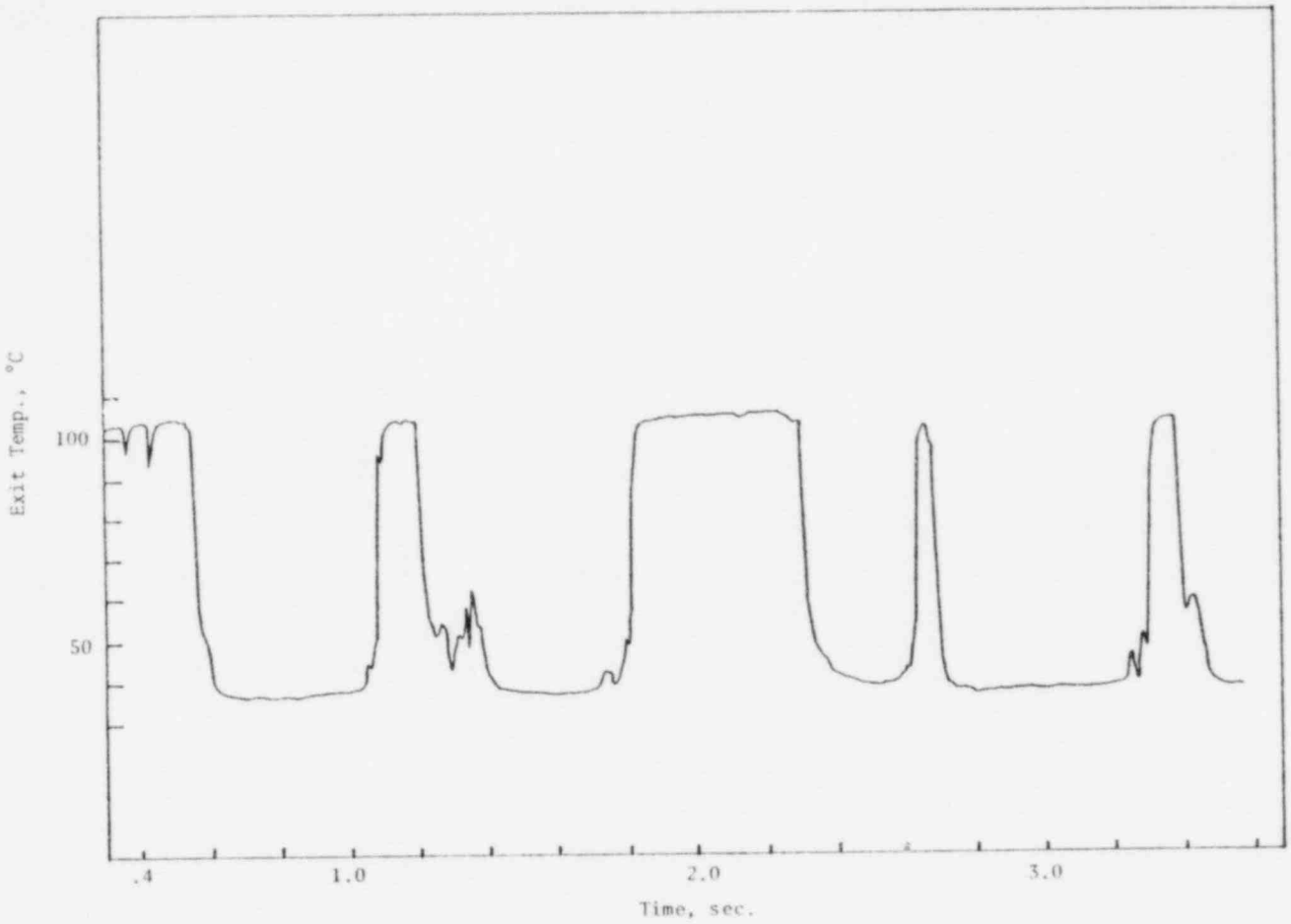


Fig. C.5 Run No. VP1

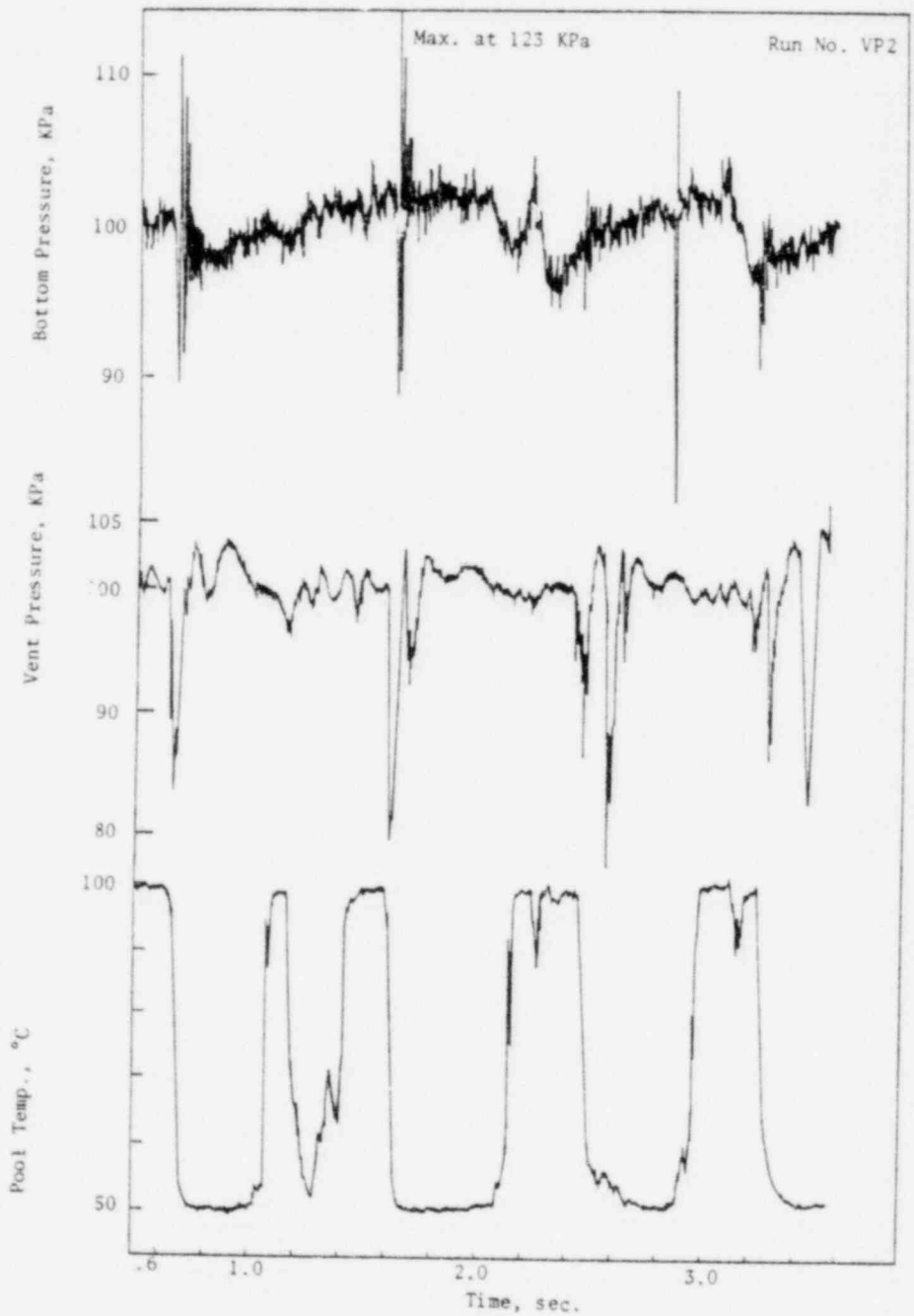
Max. at 123 KPa
Run No. VP2
Bottom Pressure, KPa
110
100
90
Vent Pressure, KPa
105
90
80
Pool Temp., °C
100
50
.6
1.0
2.0
3.0
Time, sec.

Fig. C.6

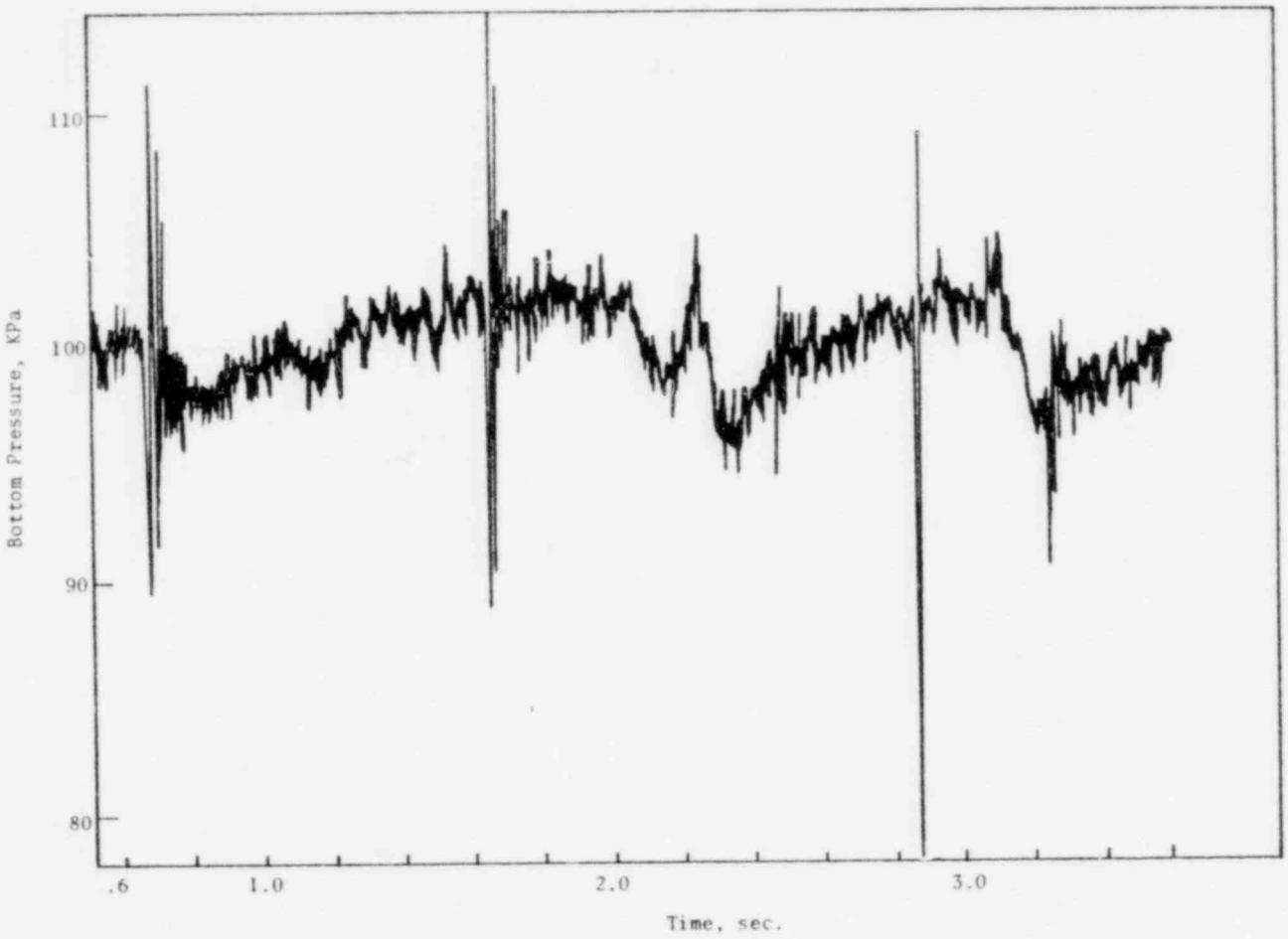


Fig. C.7 Run No. VP2

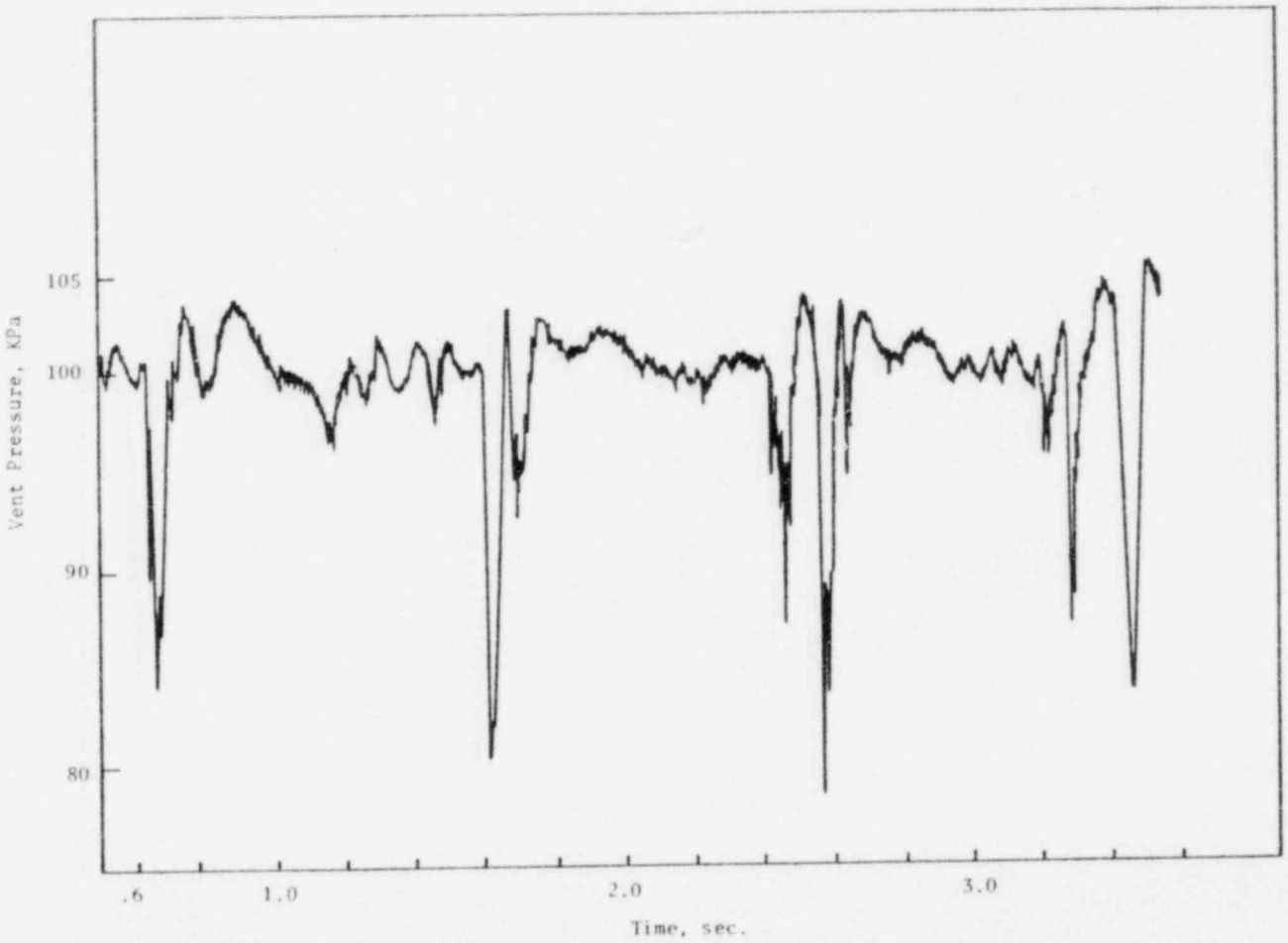


Fig. C.8 Run No. VP2

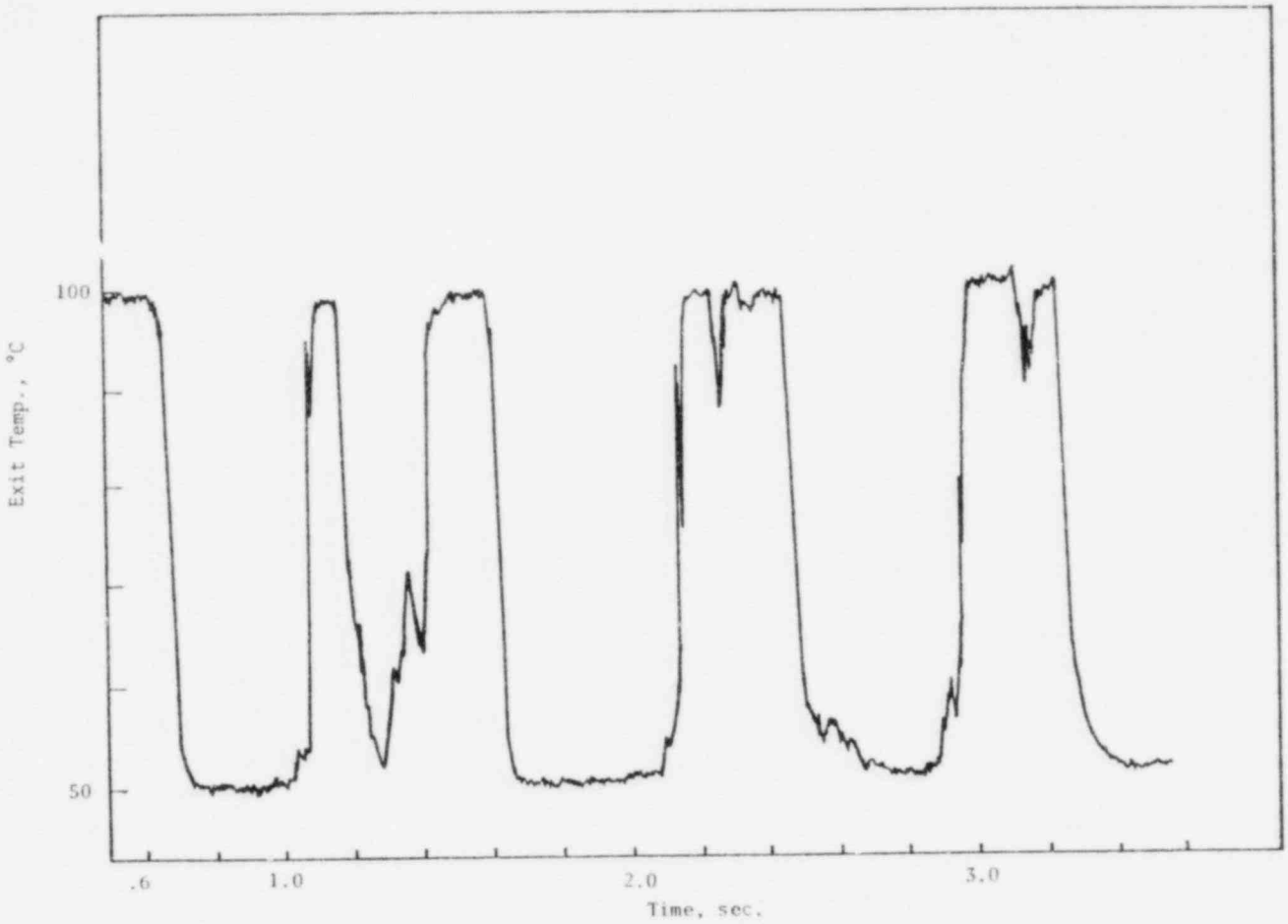


Fig. C.9 Run No. VP2

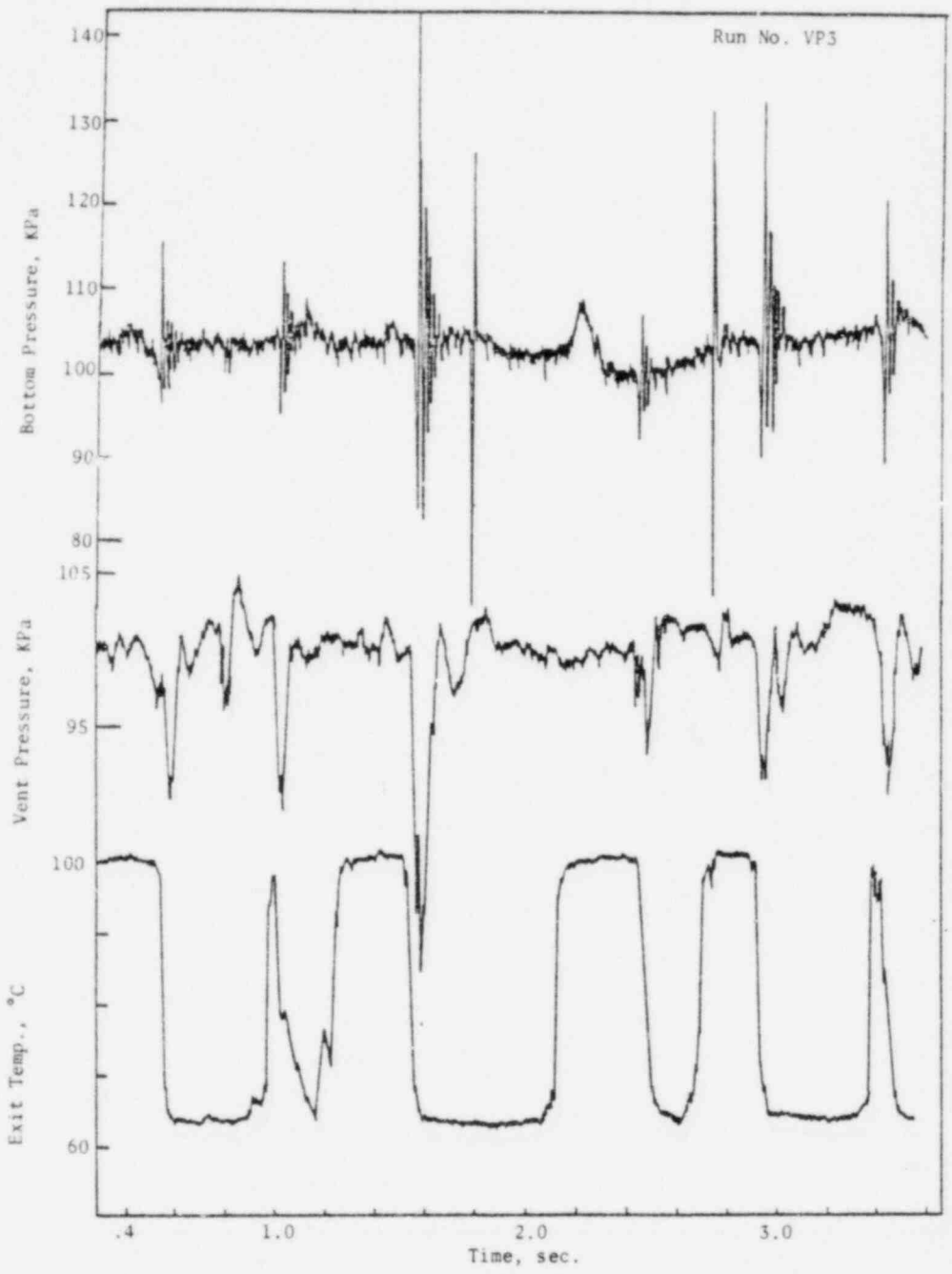


Fig. C.10 Run No. VP3

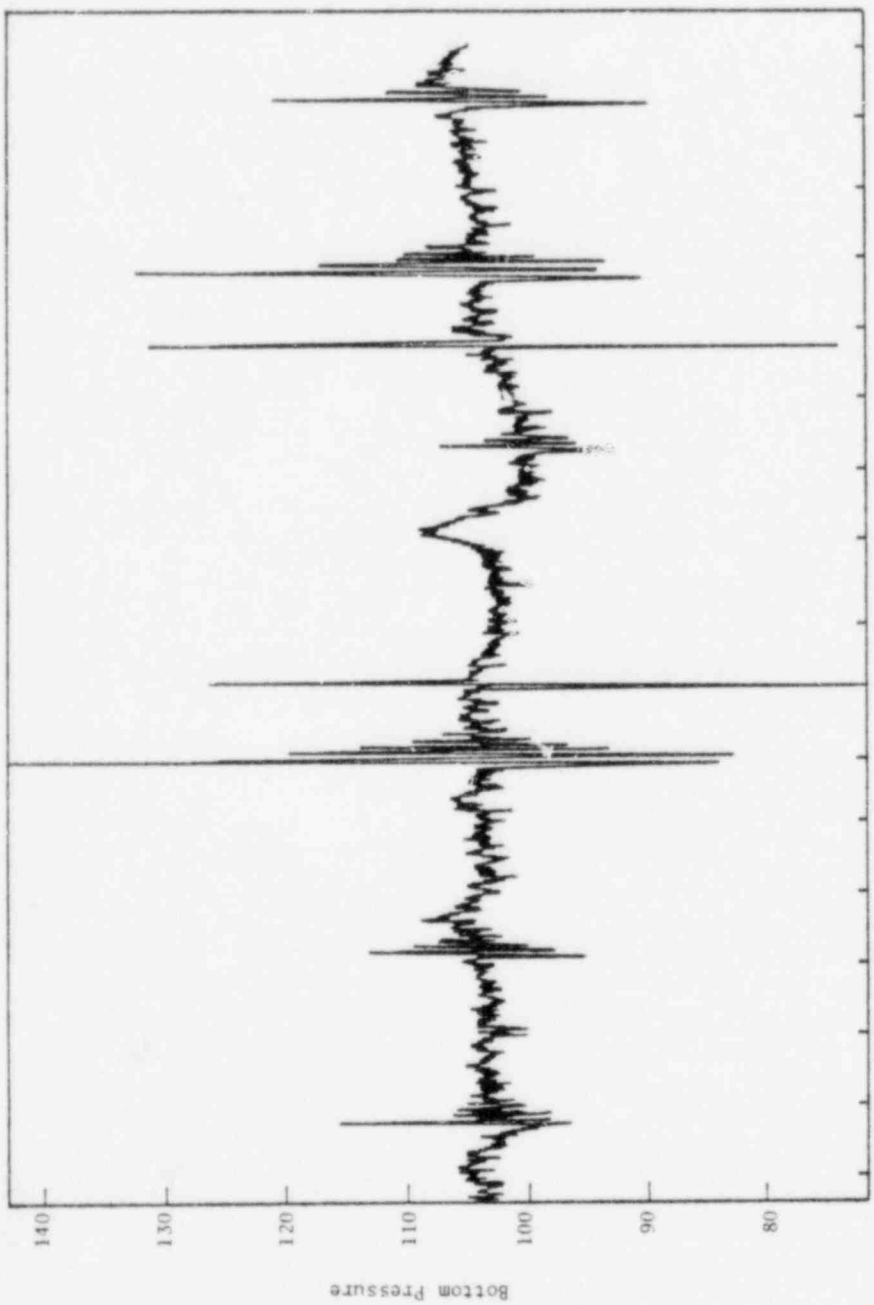


Fig. C.11 Run No. VP3

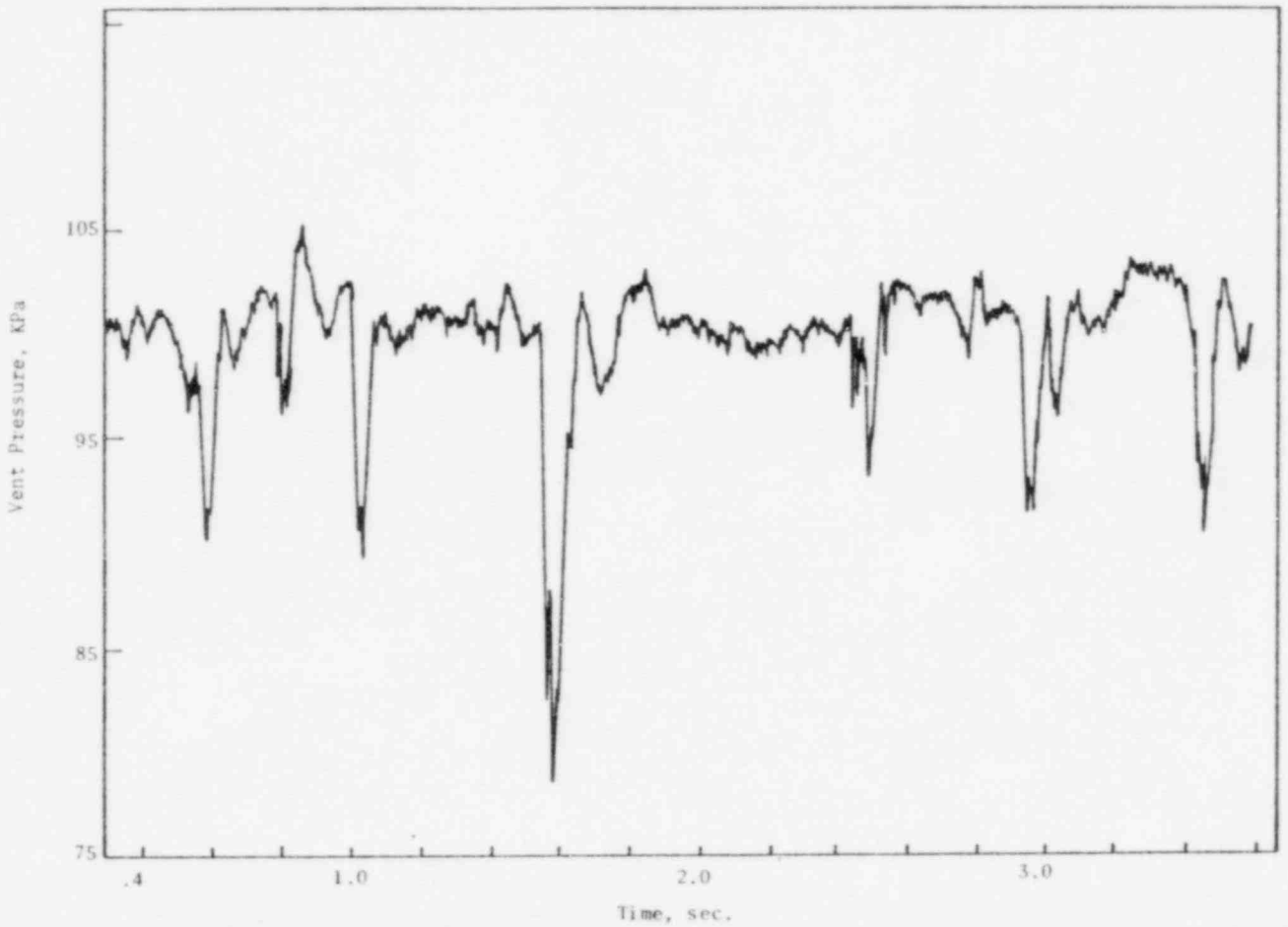


Fig. C.12 Run No. VP3

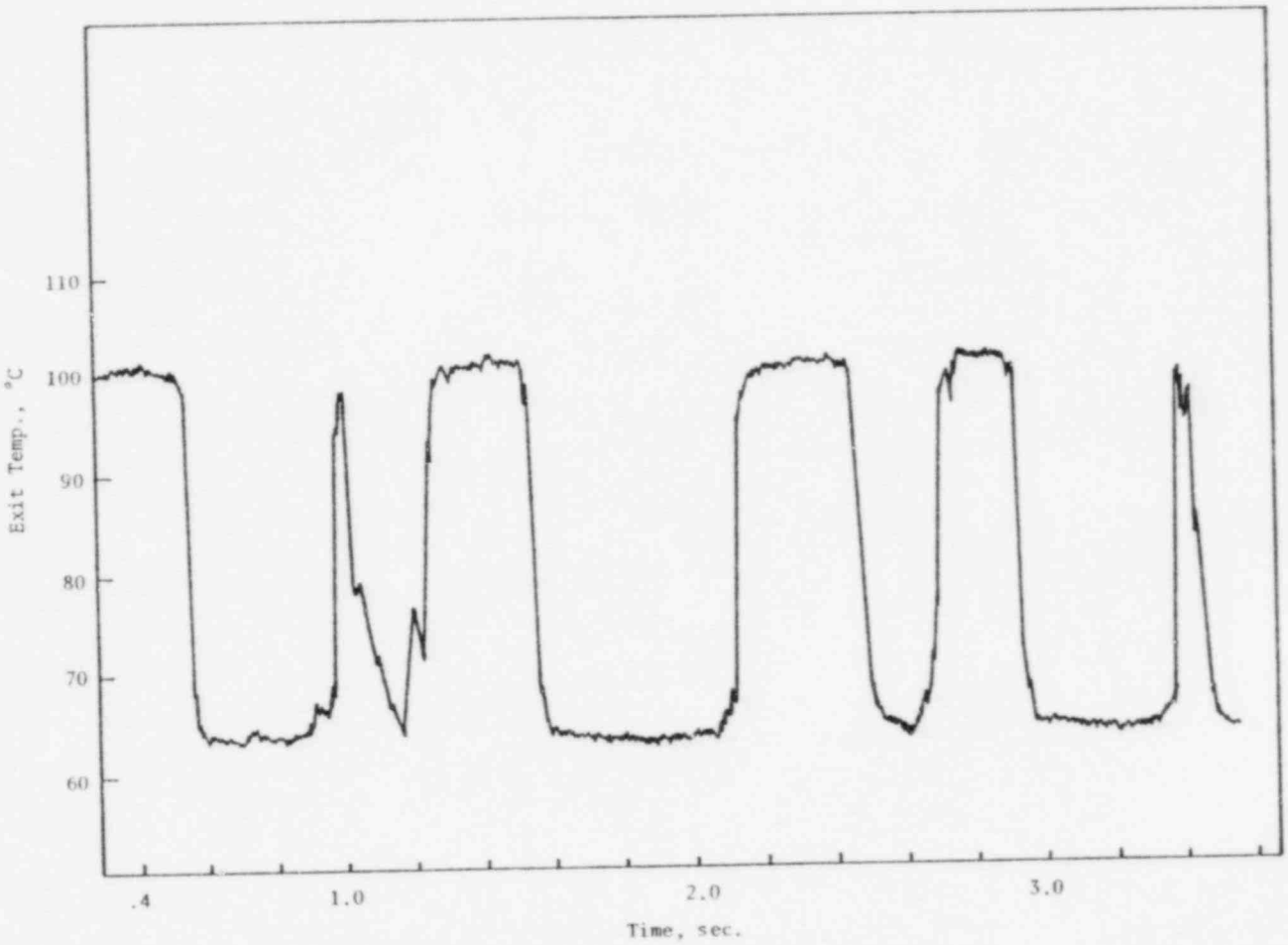


Fig. C.13 Run No. VP3

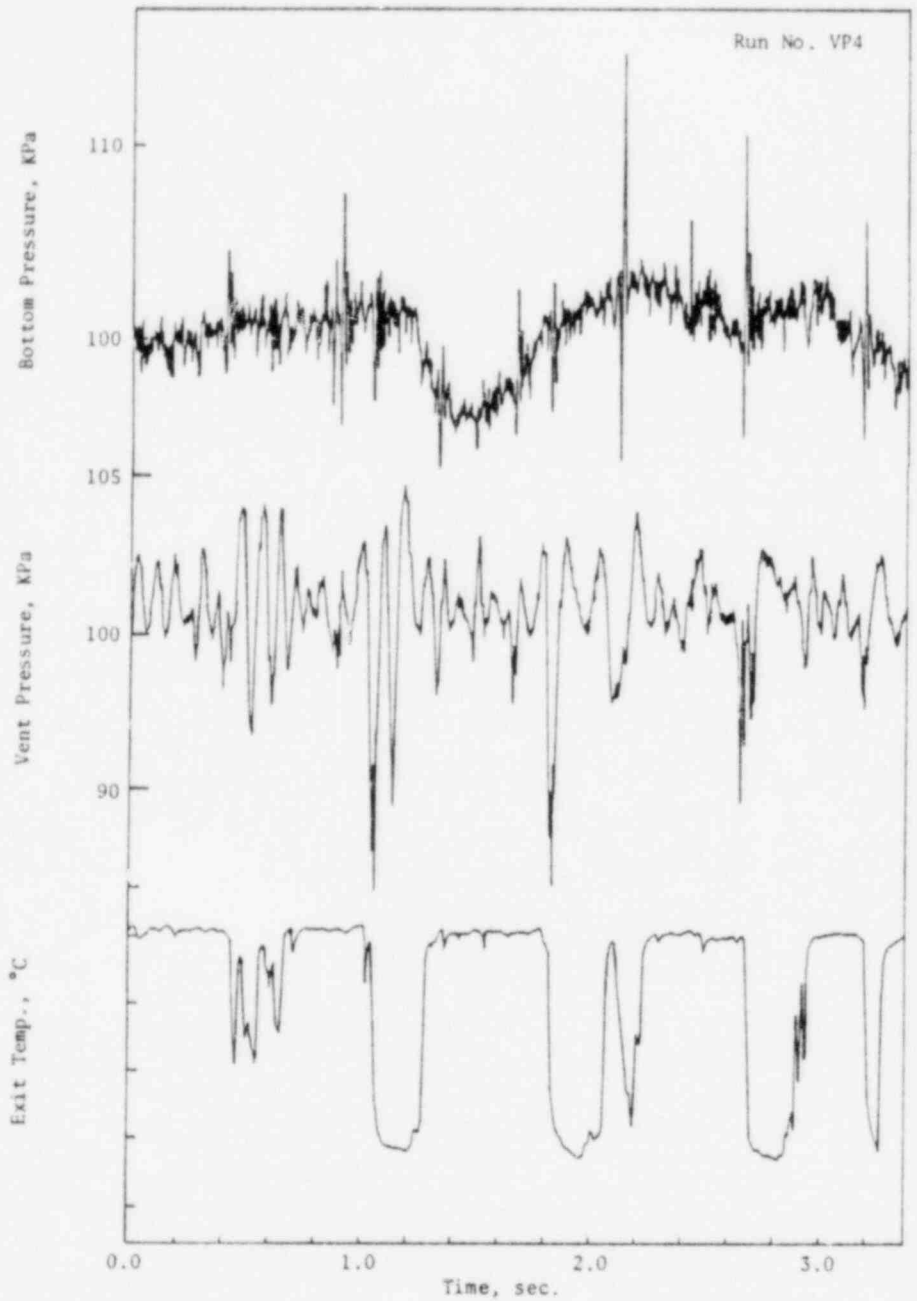


Fig. C.14 Run No. VP4

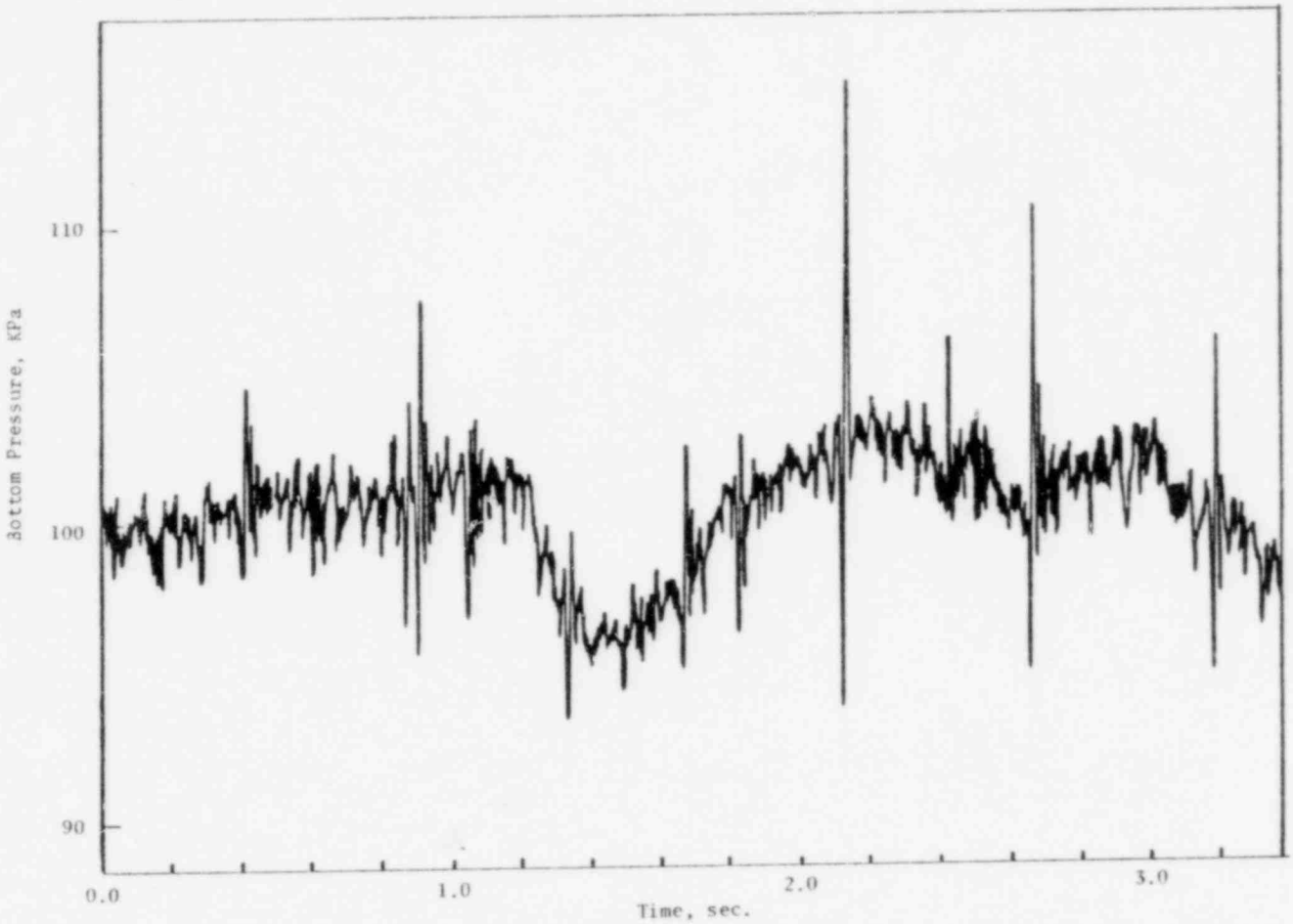


Fig. C.15 Run No. VP4

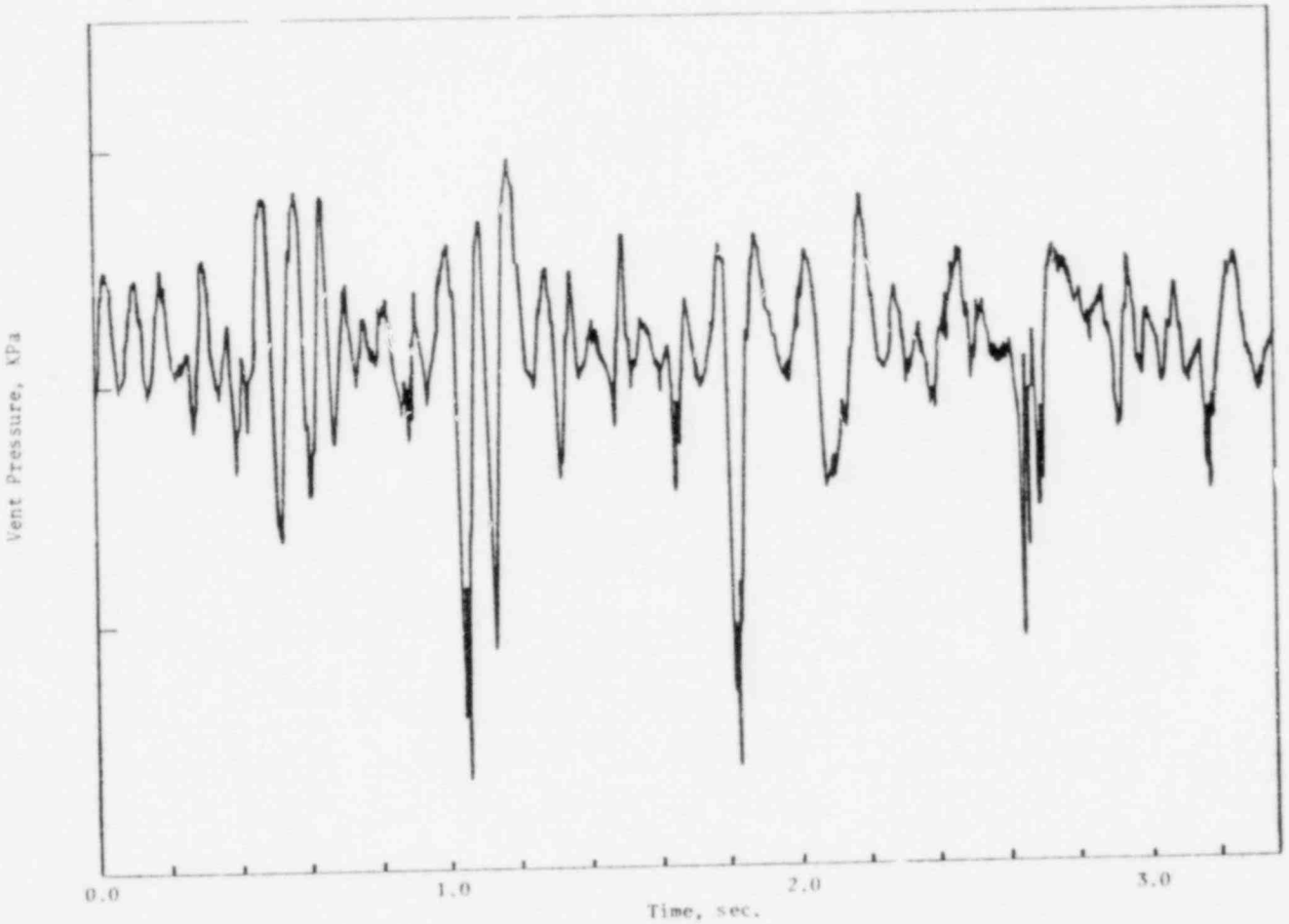


Fig. C.16 Run No. VP4

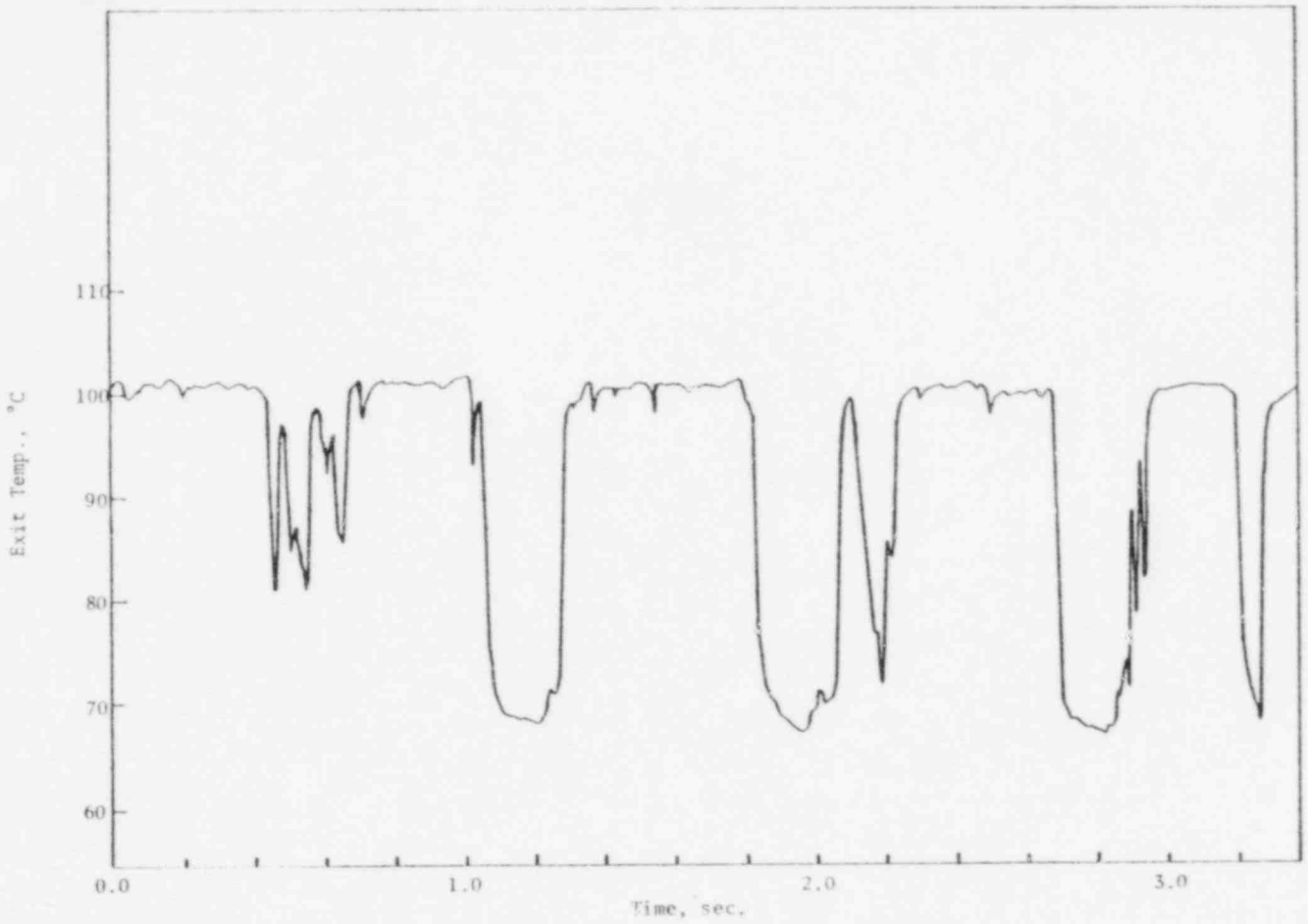


Fig. C.17 Run No. VP4

# APPENDIX D

# STEAM VELOCITY EXPERIMENTS

Flow Meter Experiments (Plastic Pipe)

| Run No. | Pool Temp., °C | Submergence Depth, cm. |
|---|---|---|
| FM1 | 53.9 | 25.4 |
| FM2 | 62.8 | 25.4 |
| FM3 | 37.2 | 50.8 |
| FM4 | 46.1 | 50.8 |
| FM5 | 62.8 | 50.8 |

(1) Steam Velocity measured by TSI-1221 hot-wire anemometer (Response time $\sim$ 100 micro-seconds).

(2) Bottom Pressure measured by Statham PL-131-TC-50 pressure transducer (error $\leqslant$ 2.58 KPa, Response Time = 0.56 ms).

(3) Side Pressure measured by Statham PL-131-TC-50 pressure transducer (error $\leqslant$ 2.58 KPa, Response Time = 0.56 ms).

(4) Exit Temperature measured by gage 36 Chromel-Alumel thermocouple.

(5) Boiler Steam Generation Rate = .00756 Kg/sec.

(6) Pipe Exit to Pool Bottom Clearance = 25.4 cm.

(7) Data sampling time = 1. ms.

Note: The exit thermocouple in these experiments was placed too close to the edge of the injection pipe; and, therefore, were measuring the temperature of the water draining off the pipe wall.

1) Upstream Pressure
2) Upstream Temperature
3) Upper Exit Thermocouple
4) Lower Exit Thermocouple (Not Used)
5) Bottom Pressure Transducer
6) Bulk Pool Temperature
7) Upstream Flow Meter
8) Side Wall Pressure Transducer

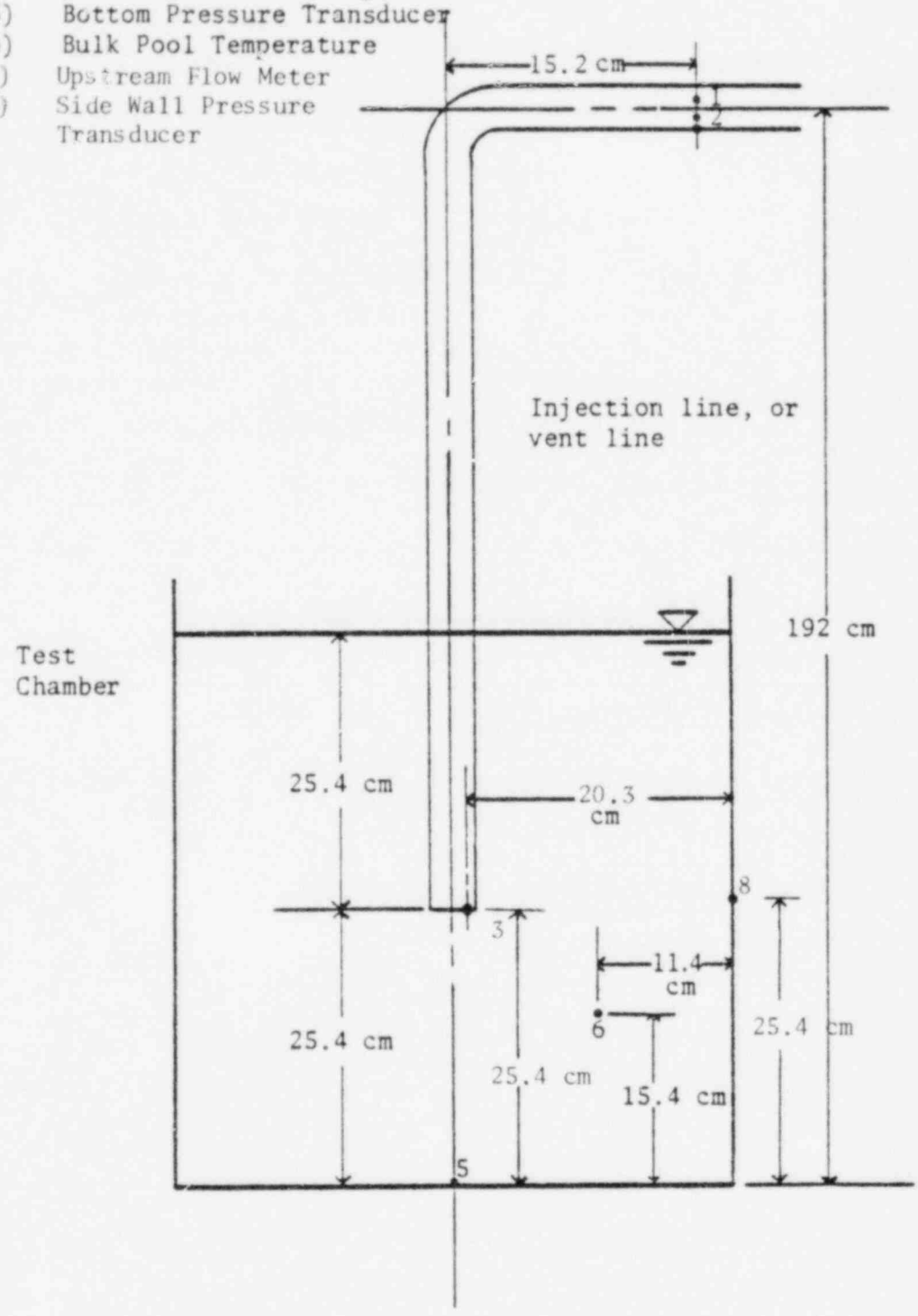


Fig. D.1 Locations of Instrumentation

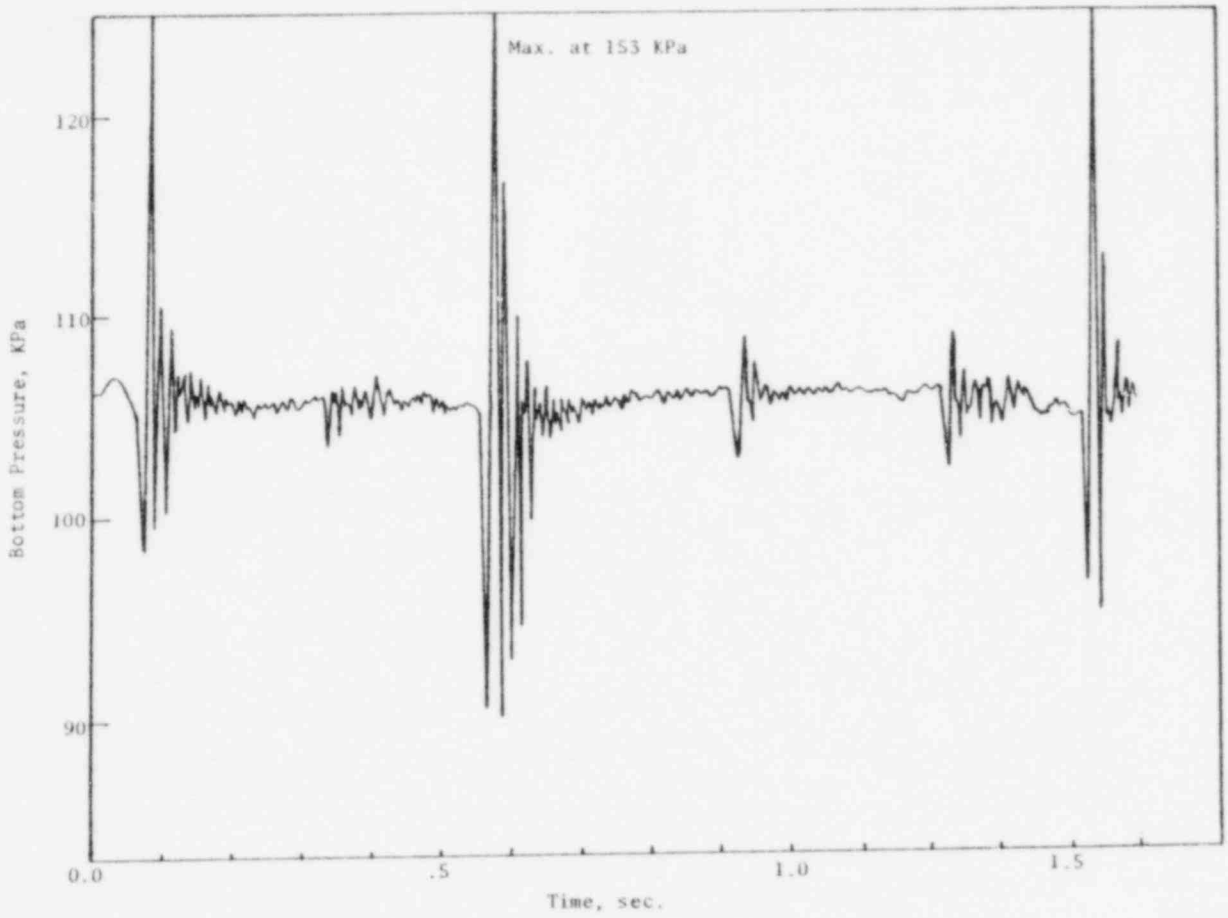


Fig. D.2 Run No. FM1

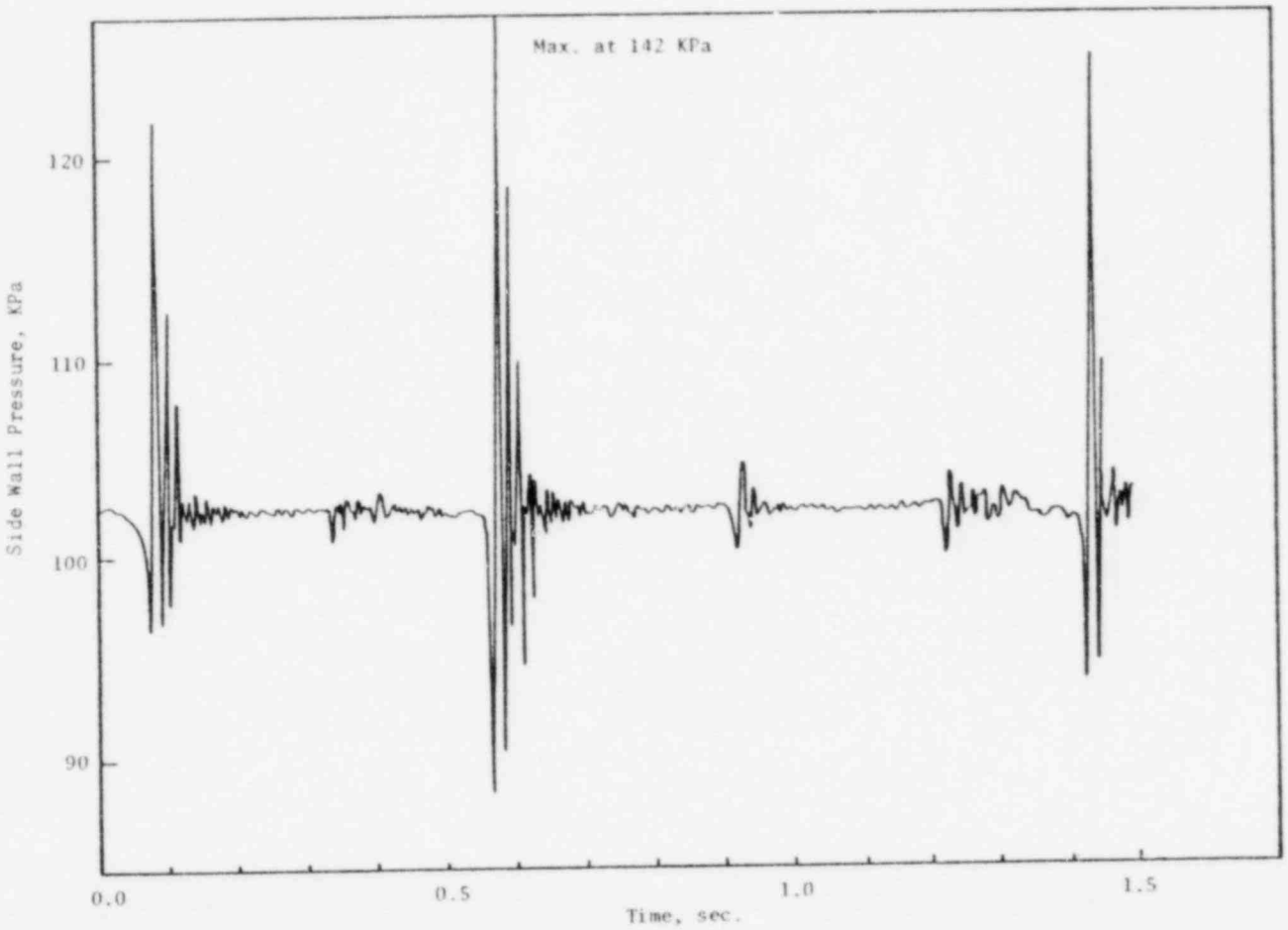


Fig. D.3 Run No. FM1

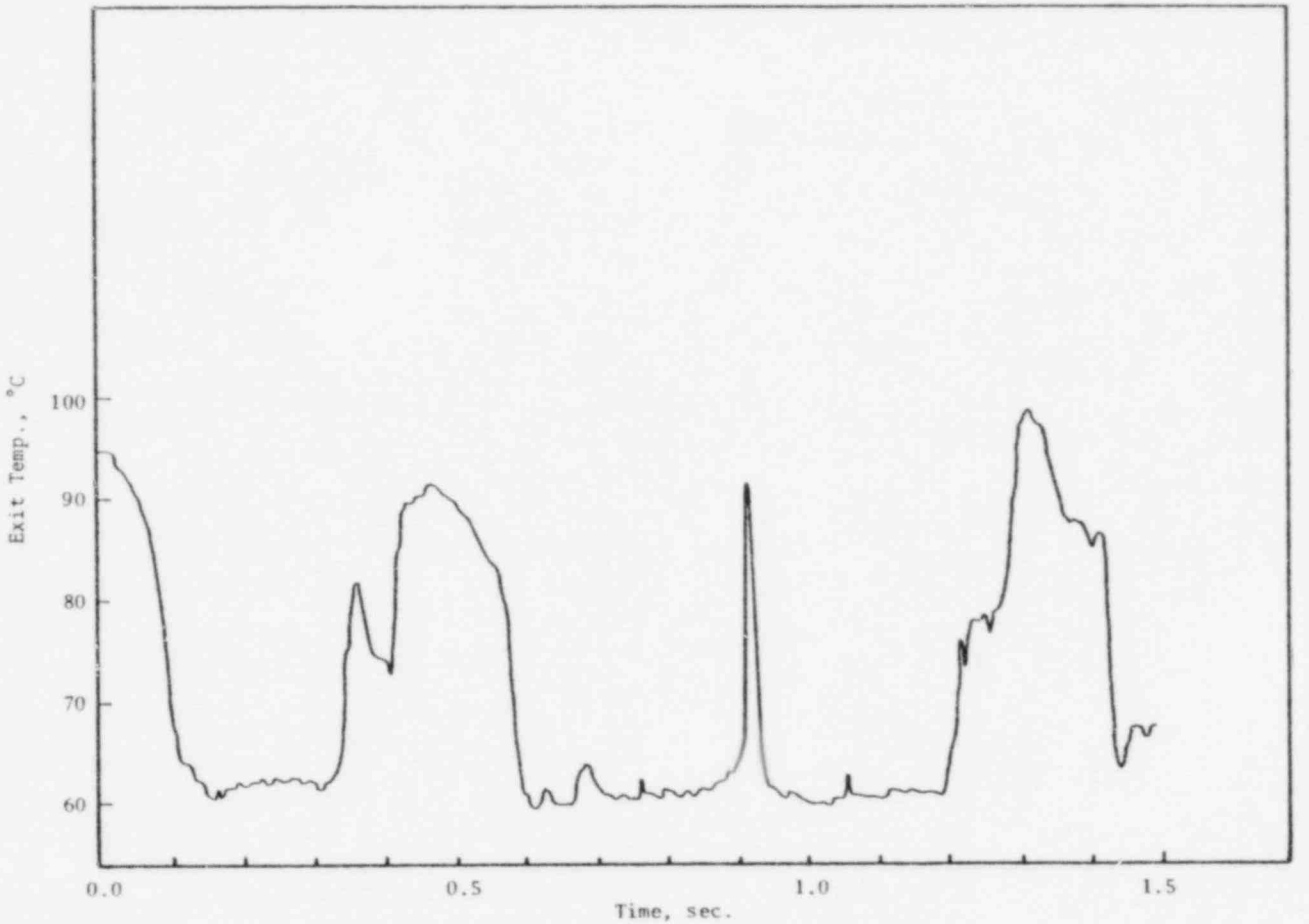


Fig. D.4 Run No. FM1

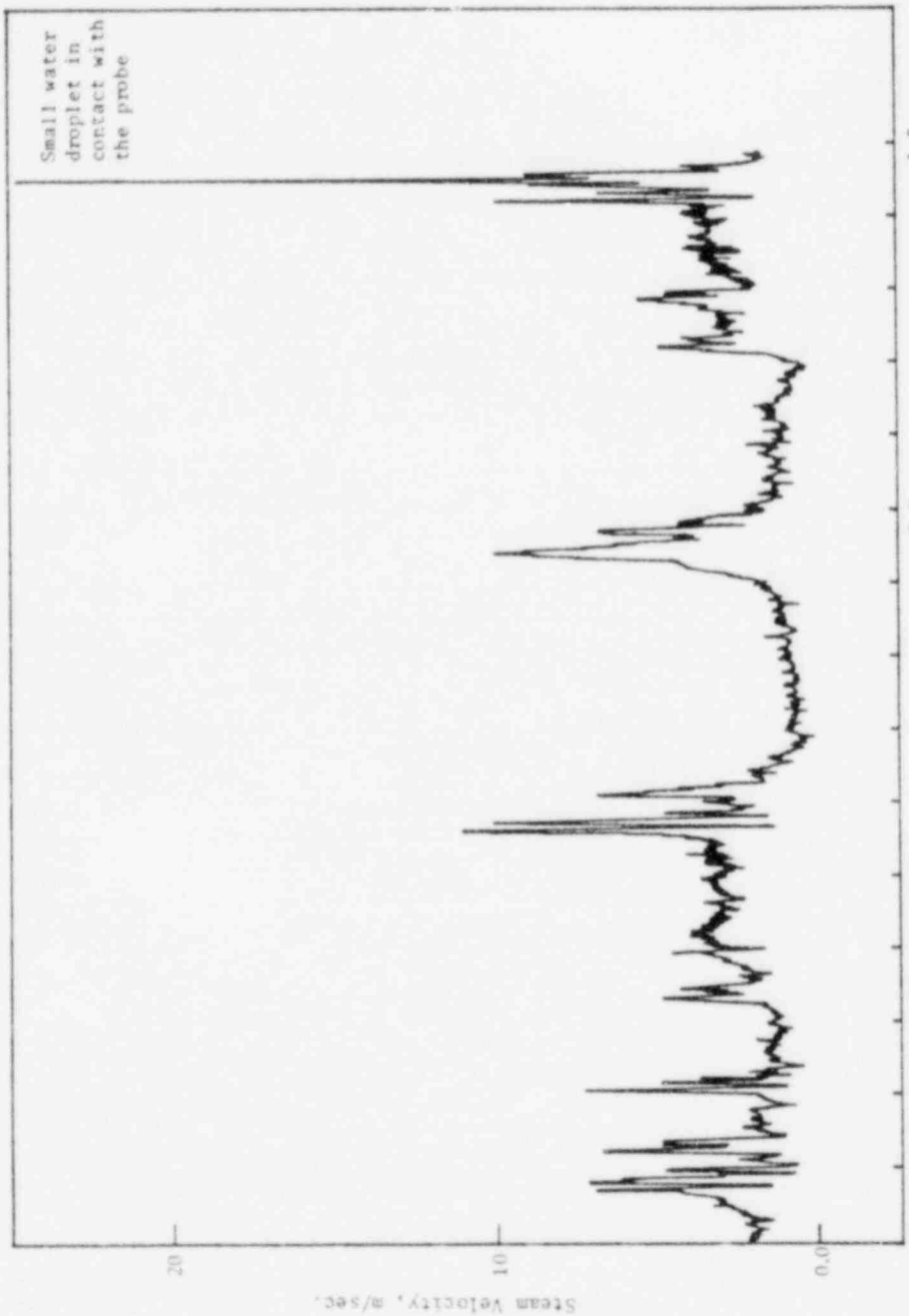


Fig. D.5 Run No. FM1

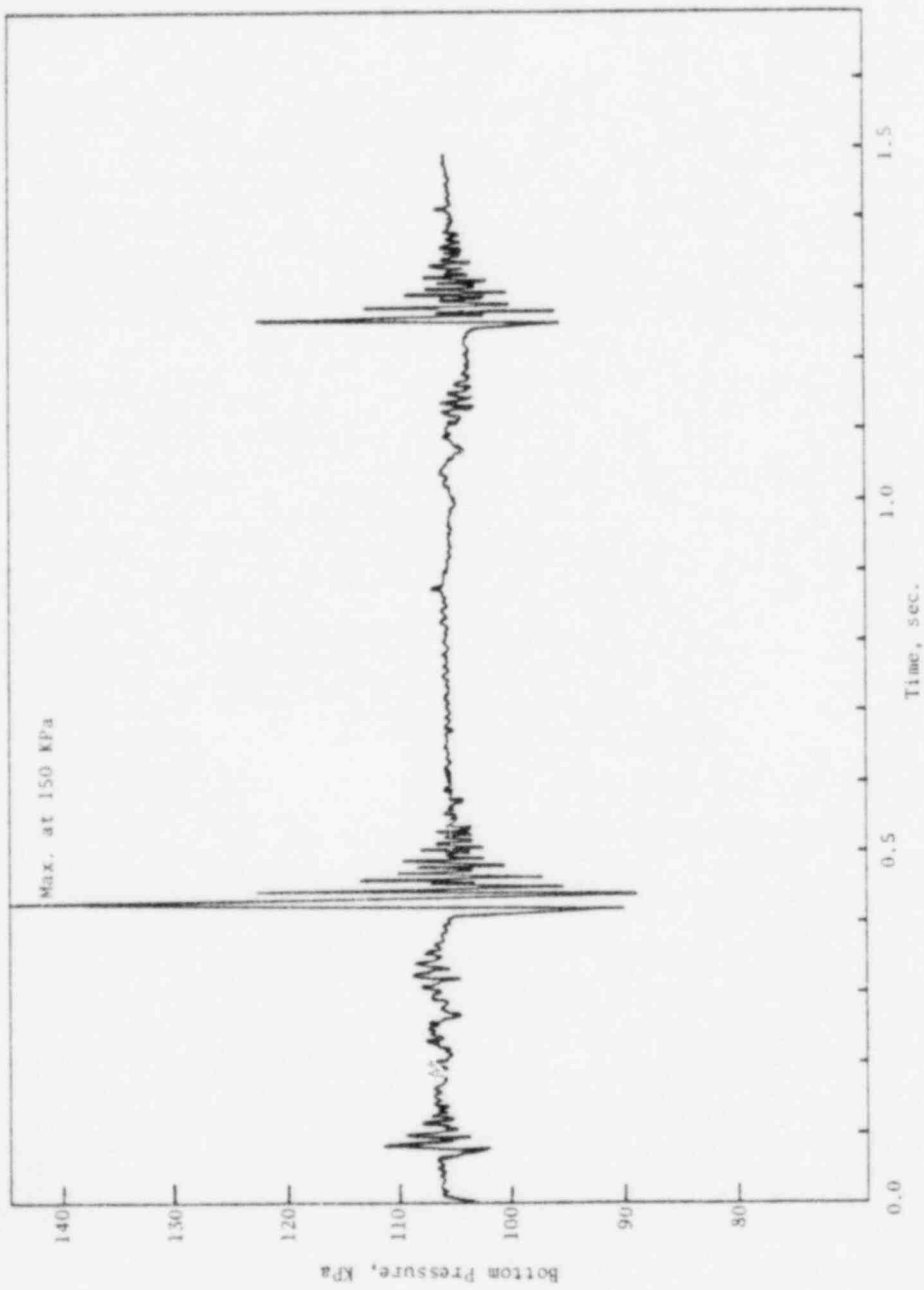


Fig. D.6 Run No. FM2

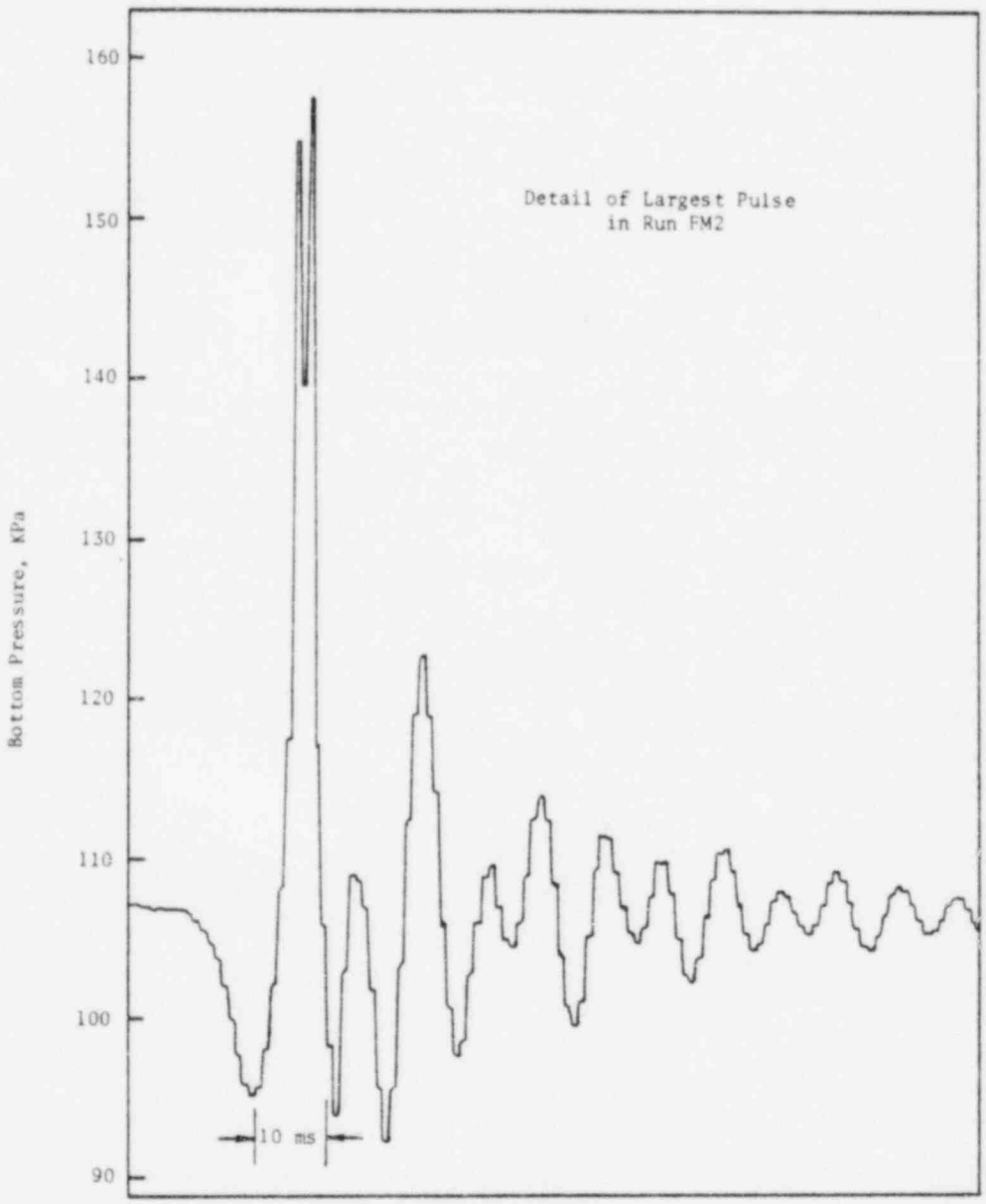


Fig. D.7 Run No. FM2

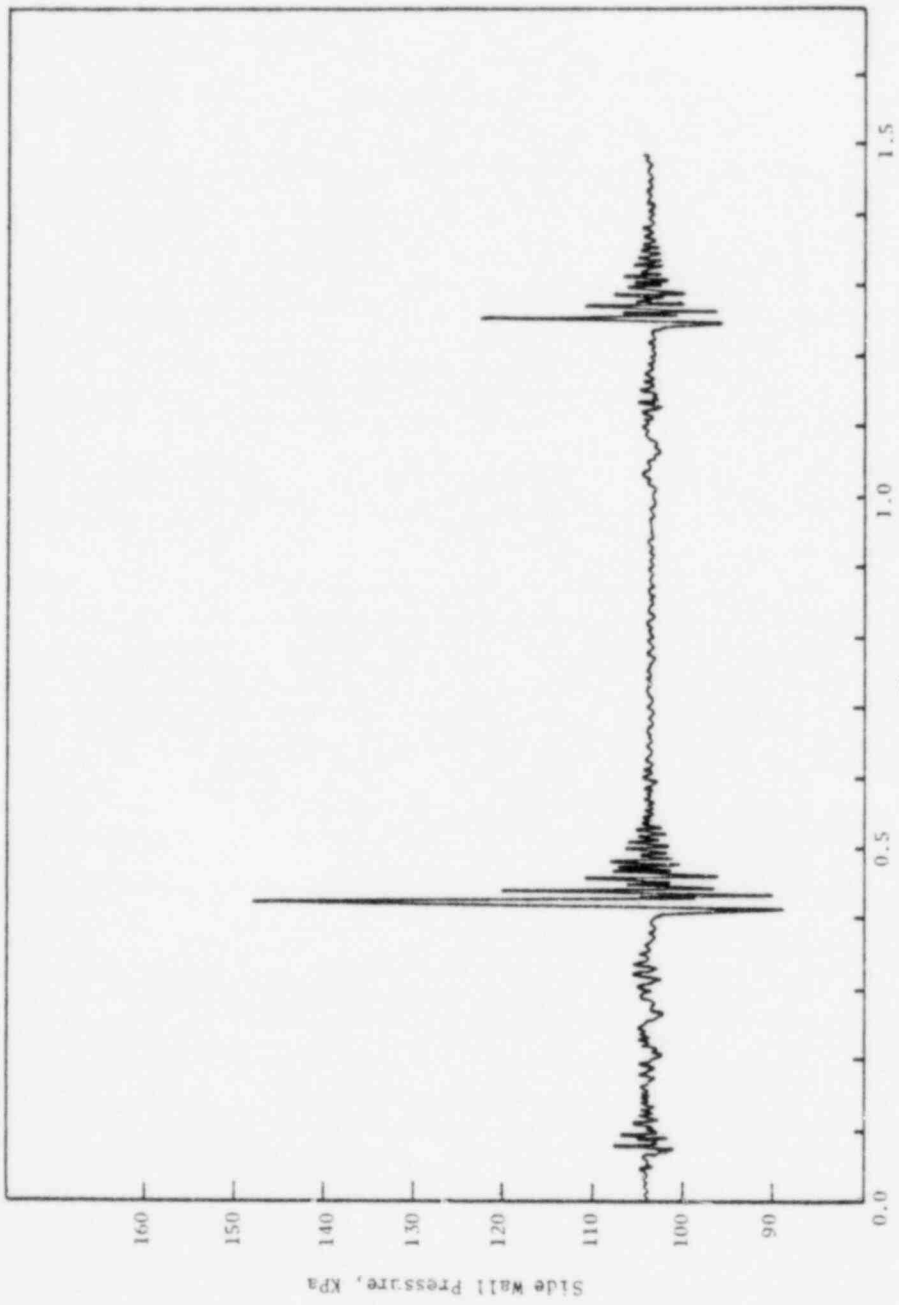


Fig. D.8 Run No. PM2

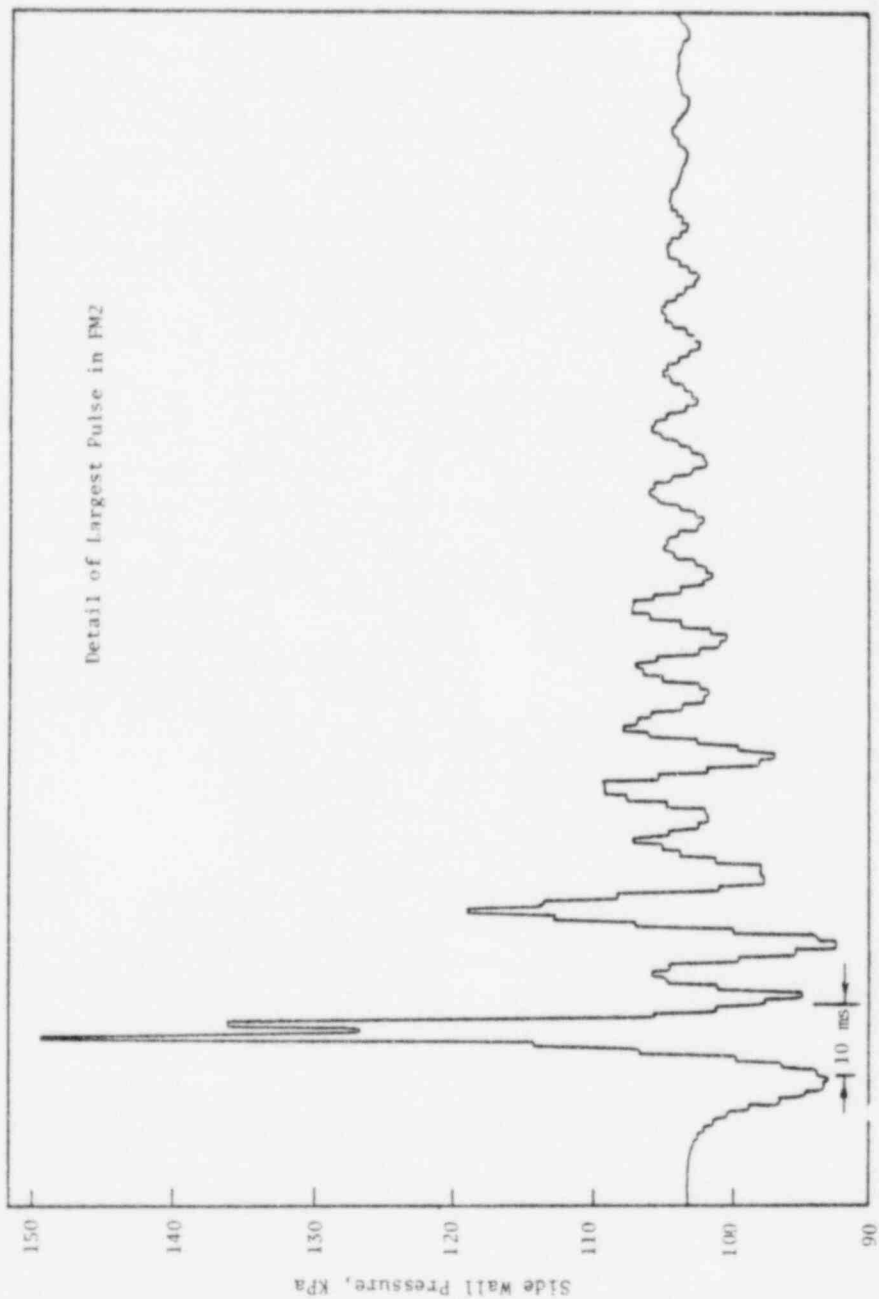


Fig. D.9 Run No. PM2

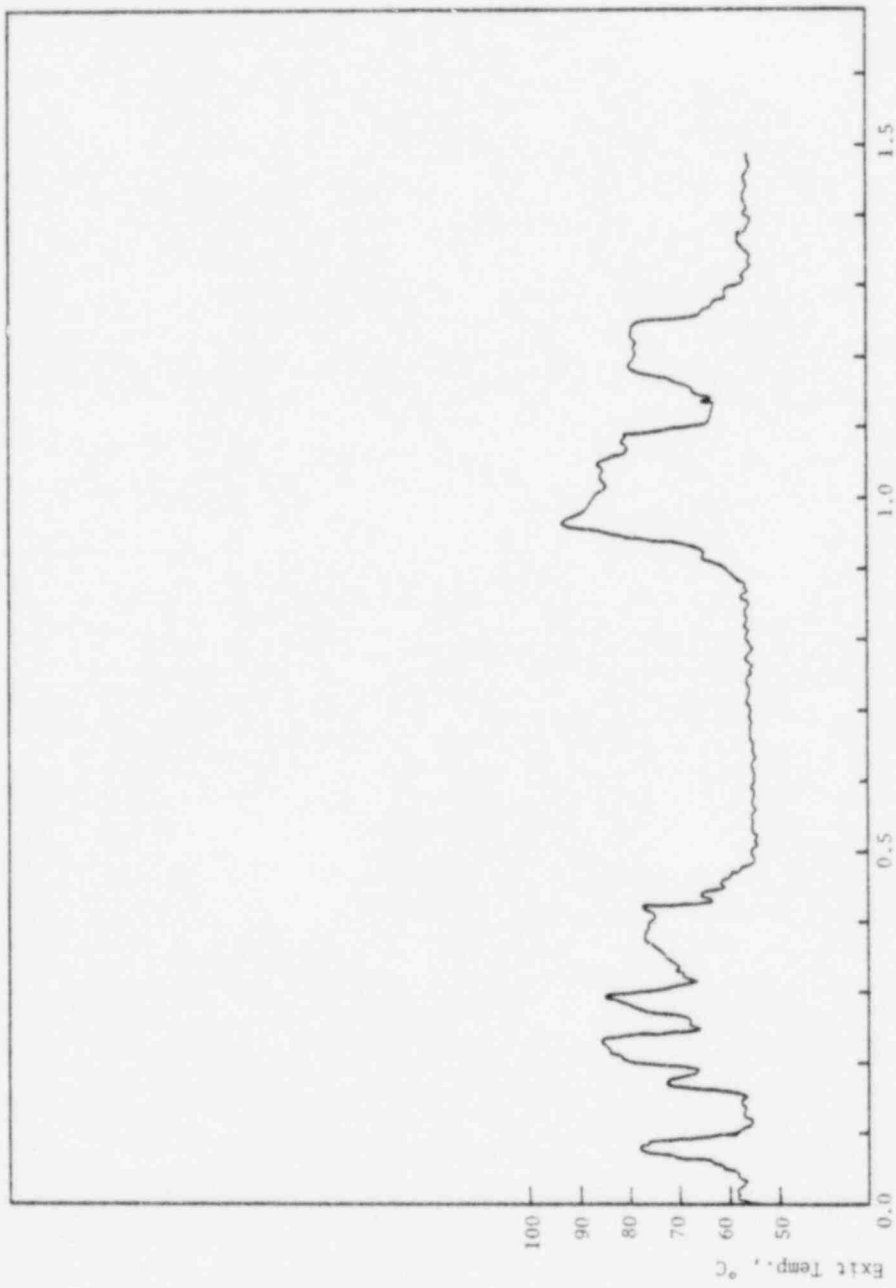


Fig. D.10 Run No. FM2

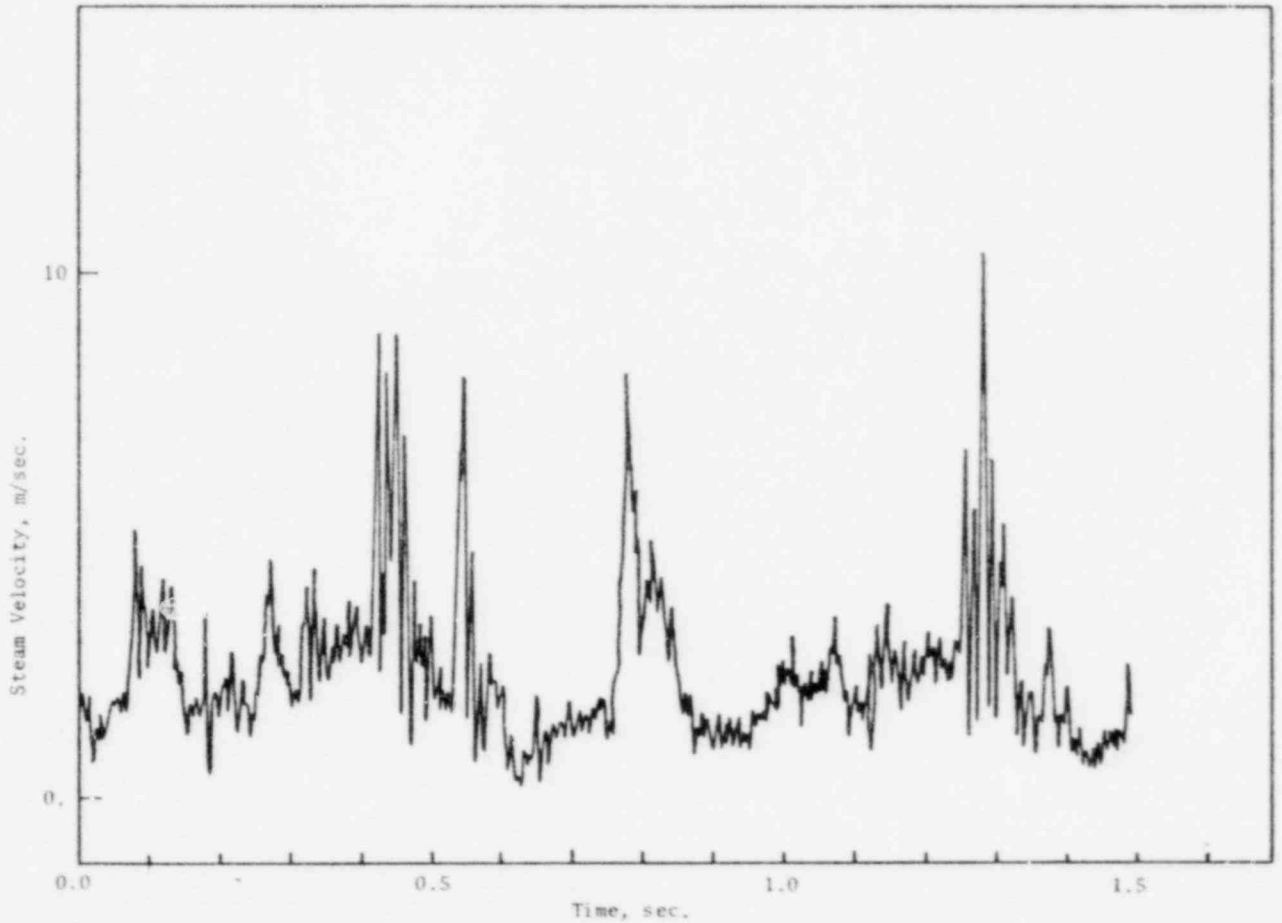


Fig. D.11 Run No. FM2

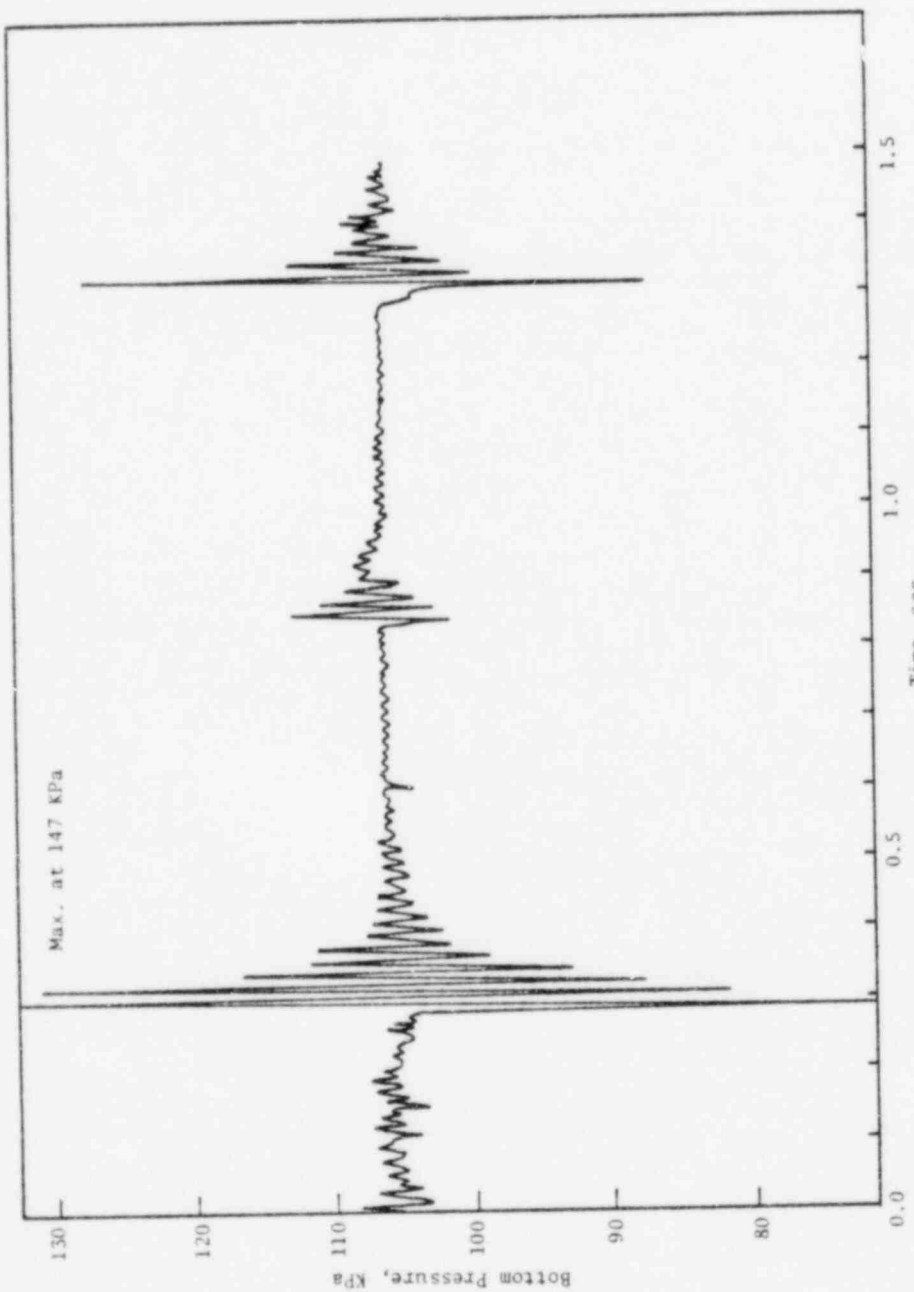


Fig. D.12 Run No. FM3

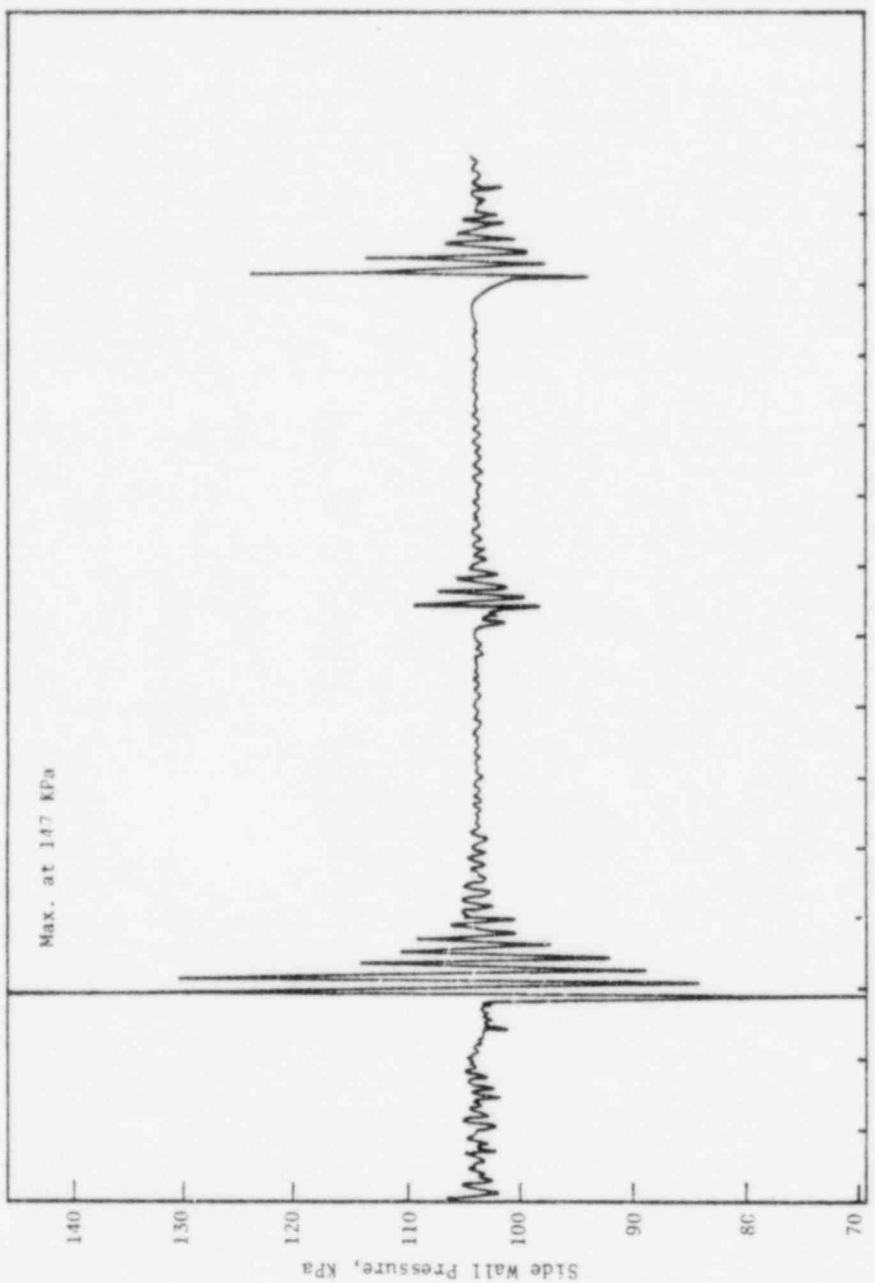


Fig. D.13 Run No. FM3

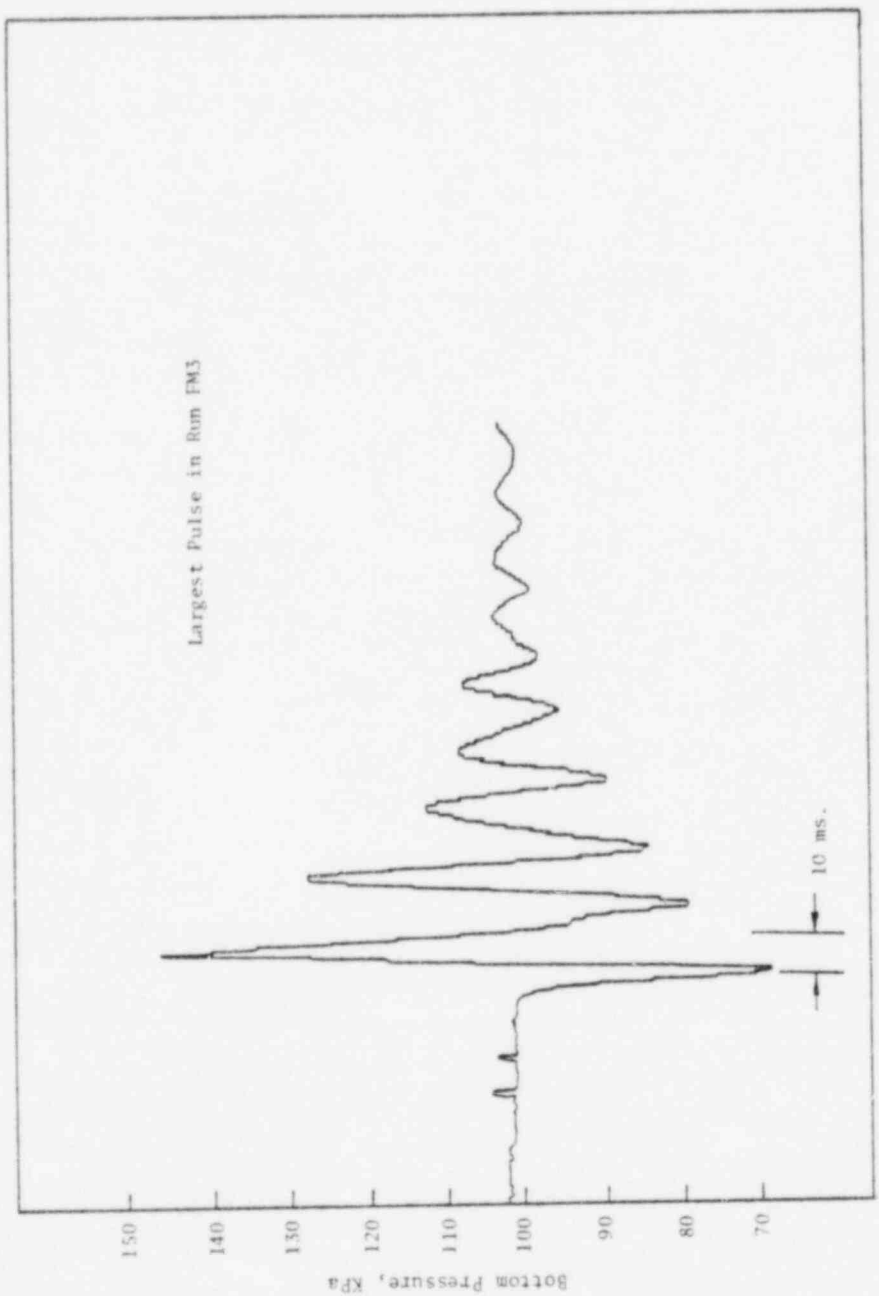


Fig. D.14 Run No. FM3

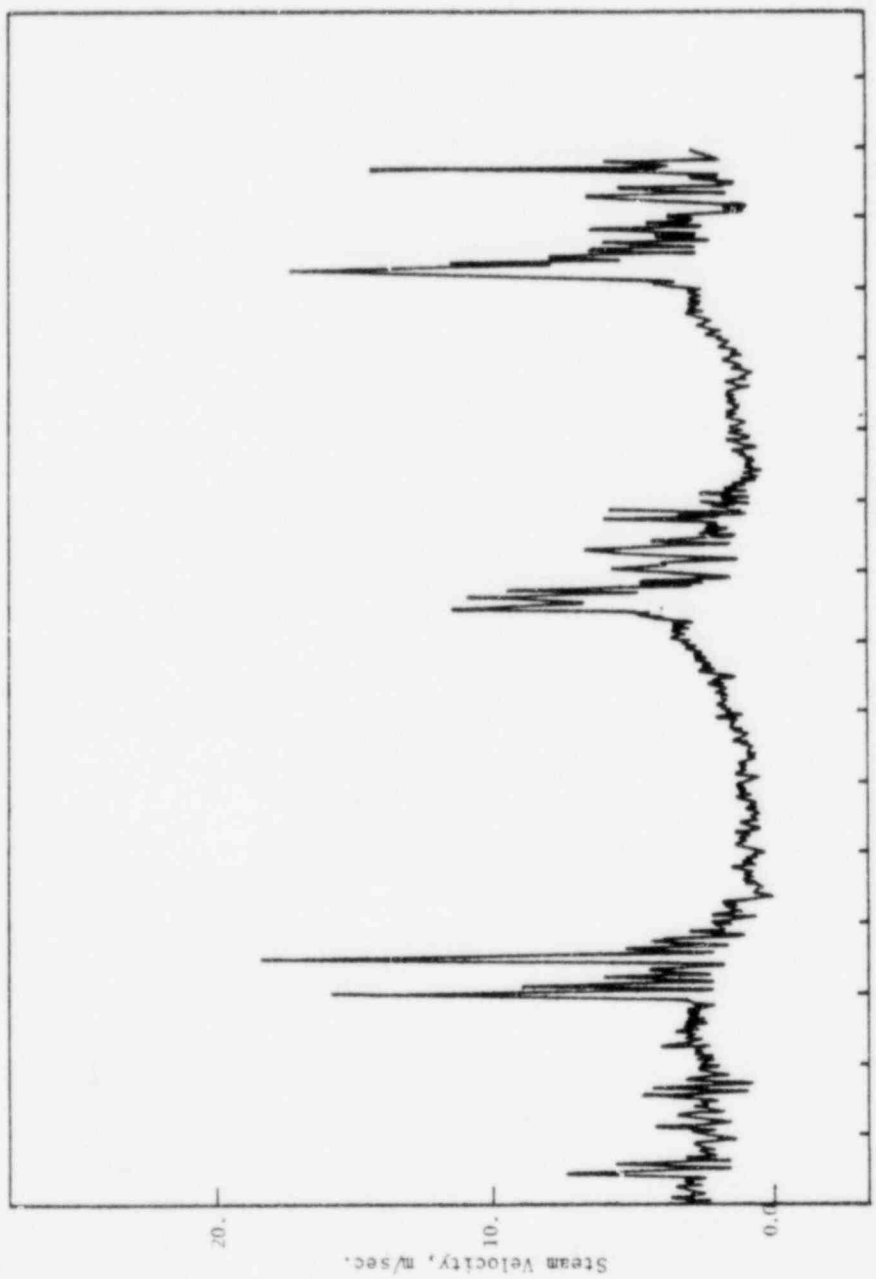


Fig. D.15 Run No. FM3

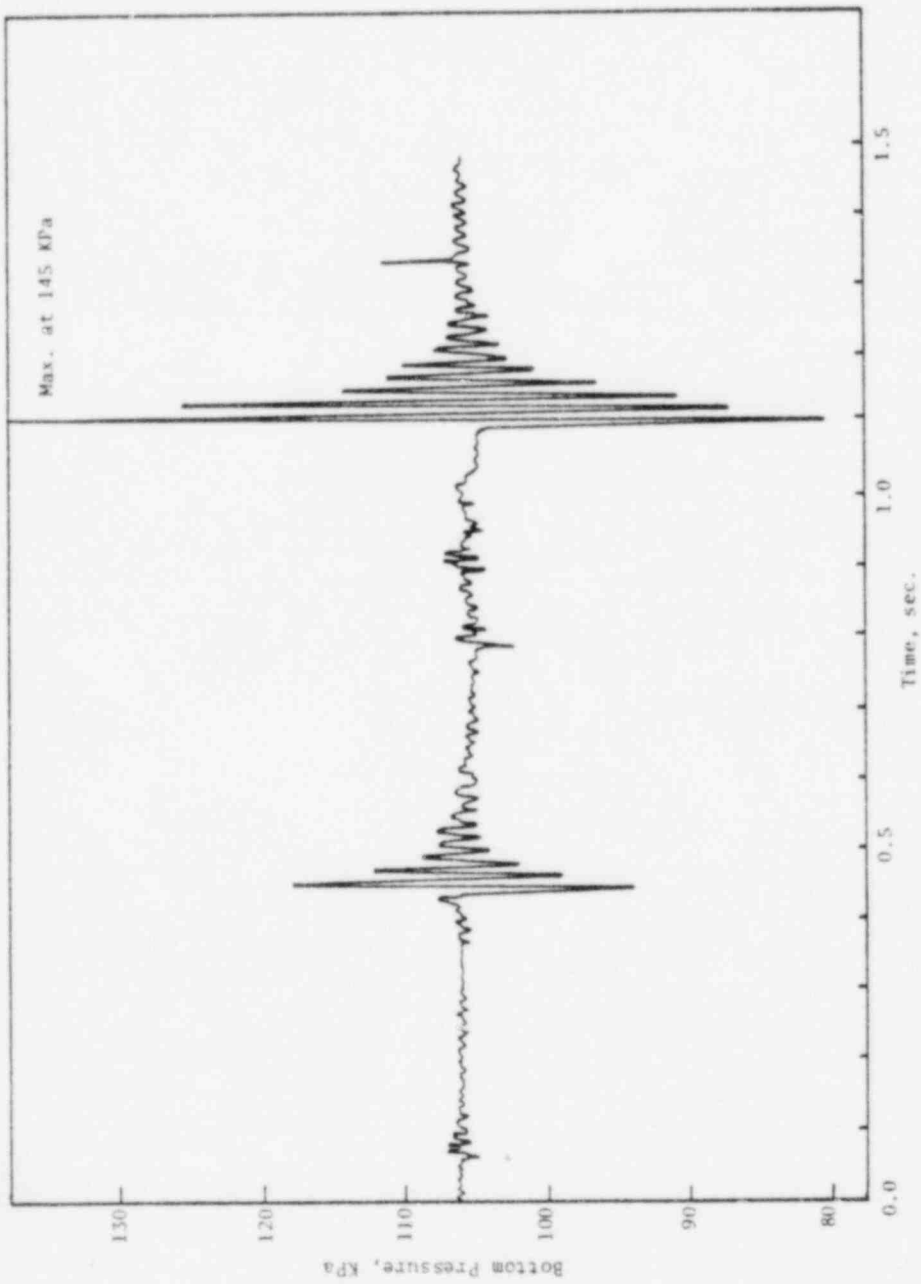


Fig. D.16 Run No. FM4

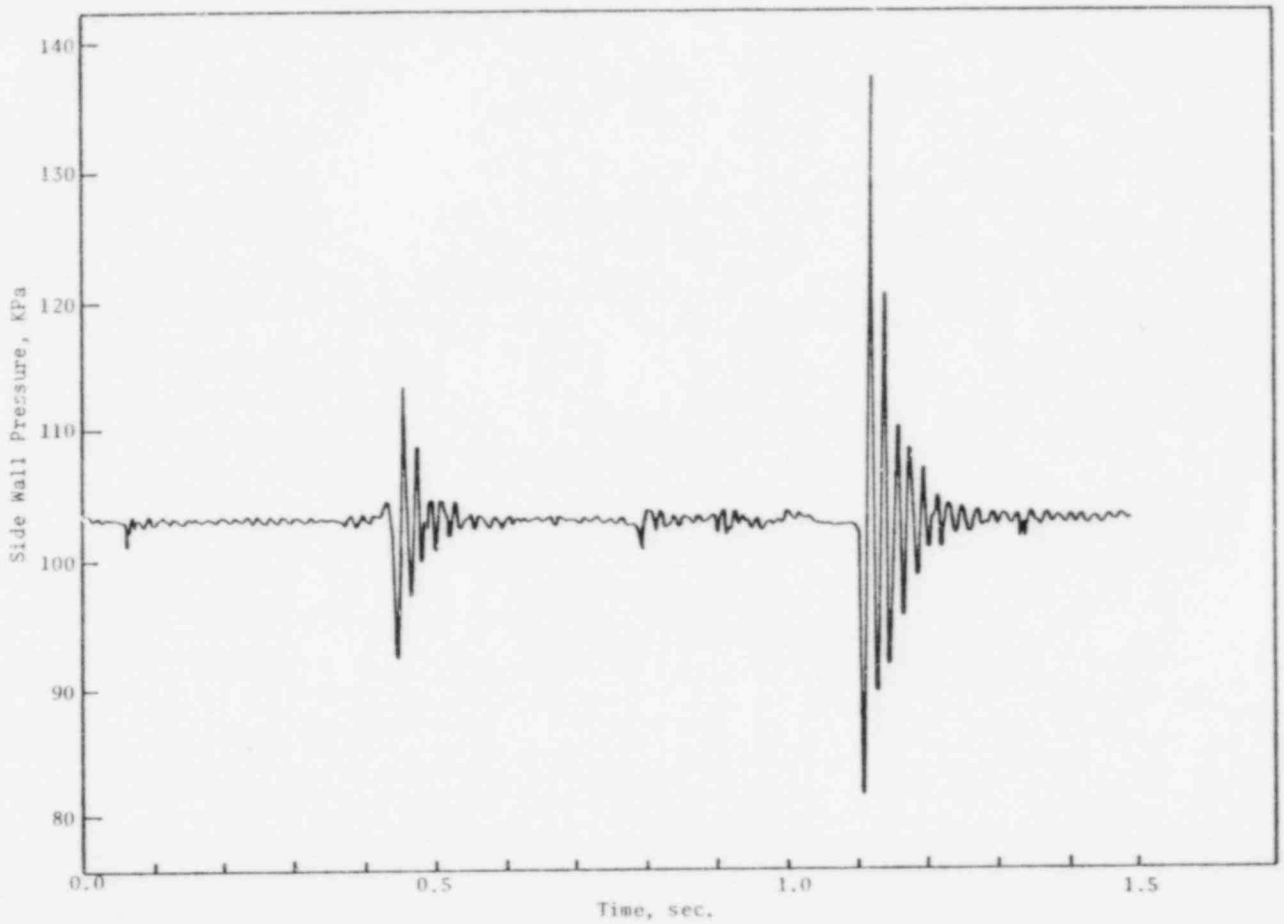


Fig. D. 17 Run No. FM4

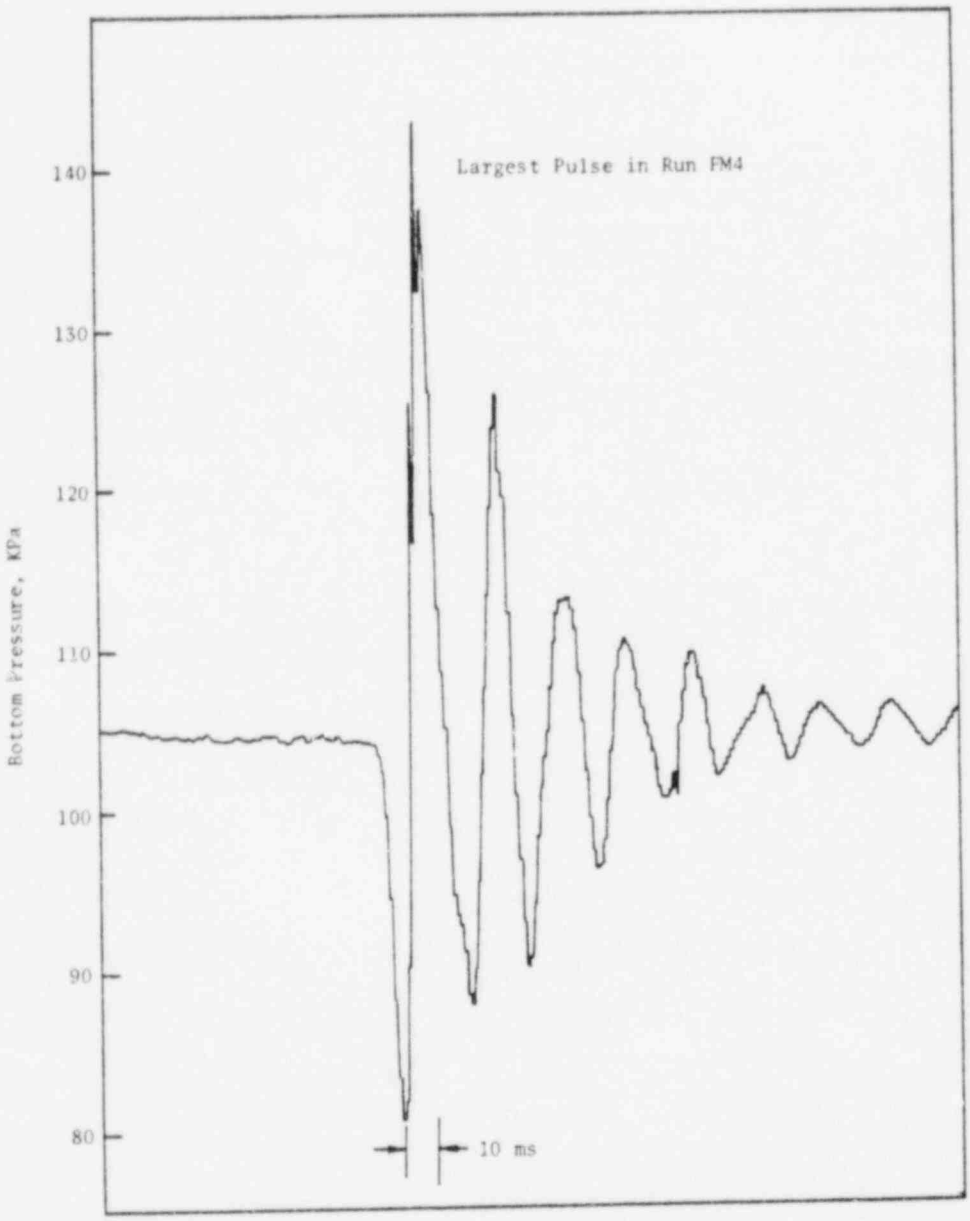


Fig. D.18 Run No. FM4

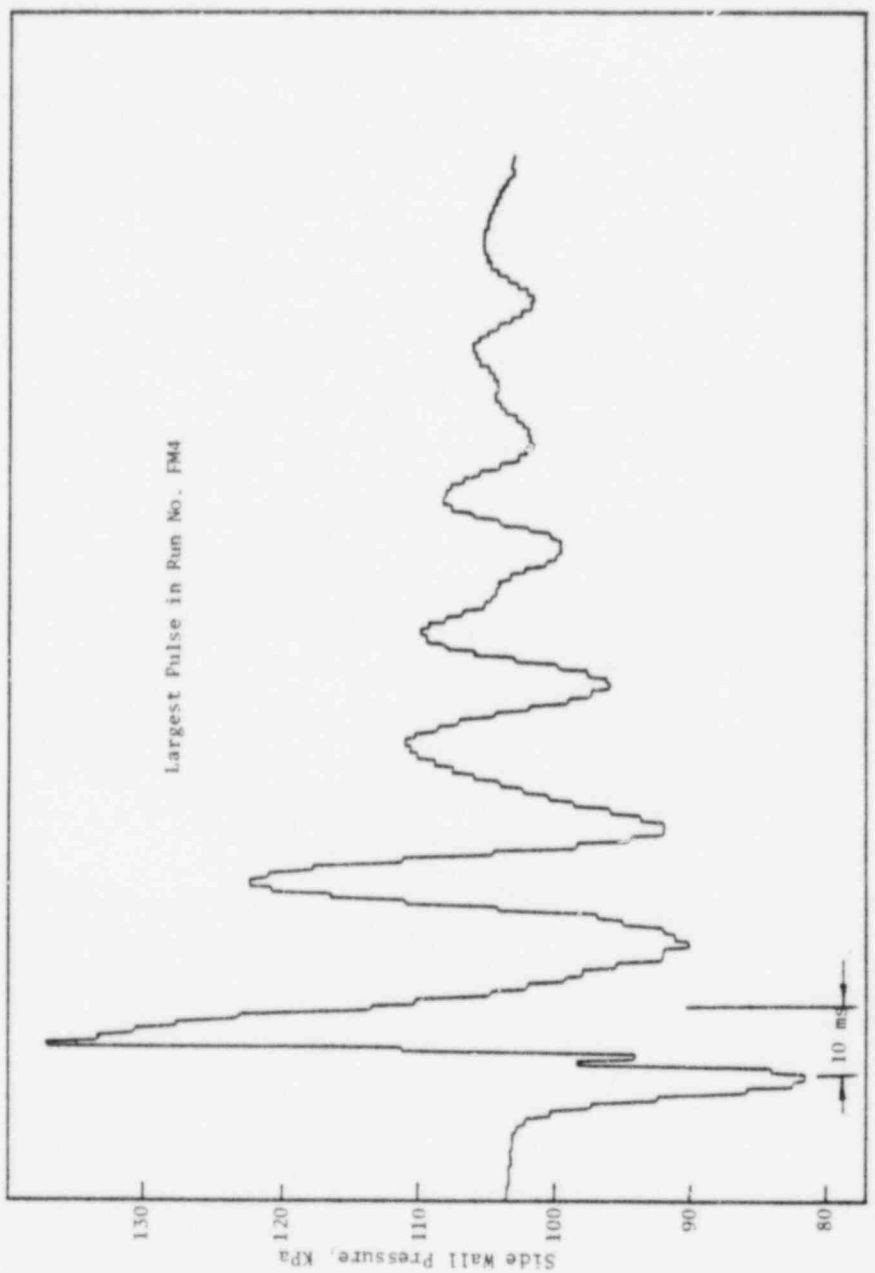


Fig. D.19 Run No. FM4

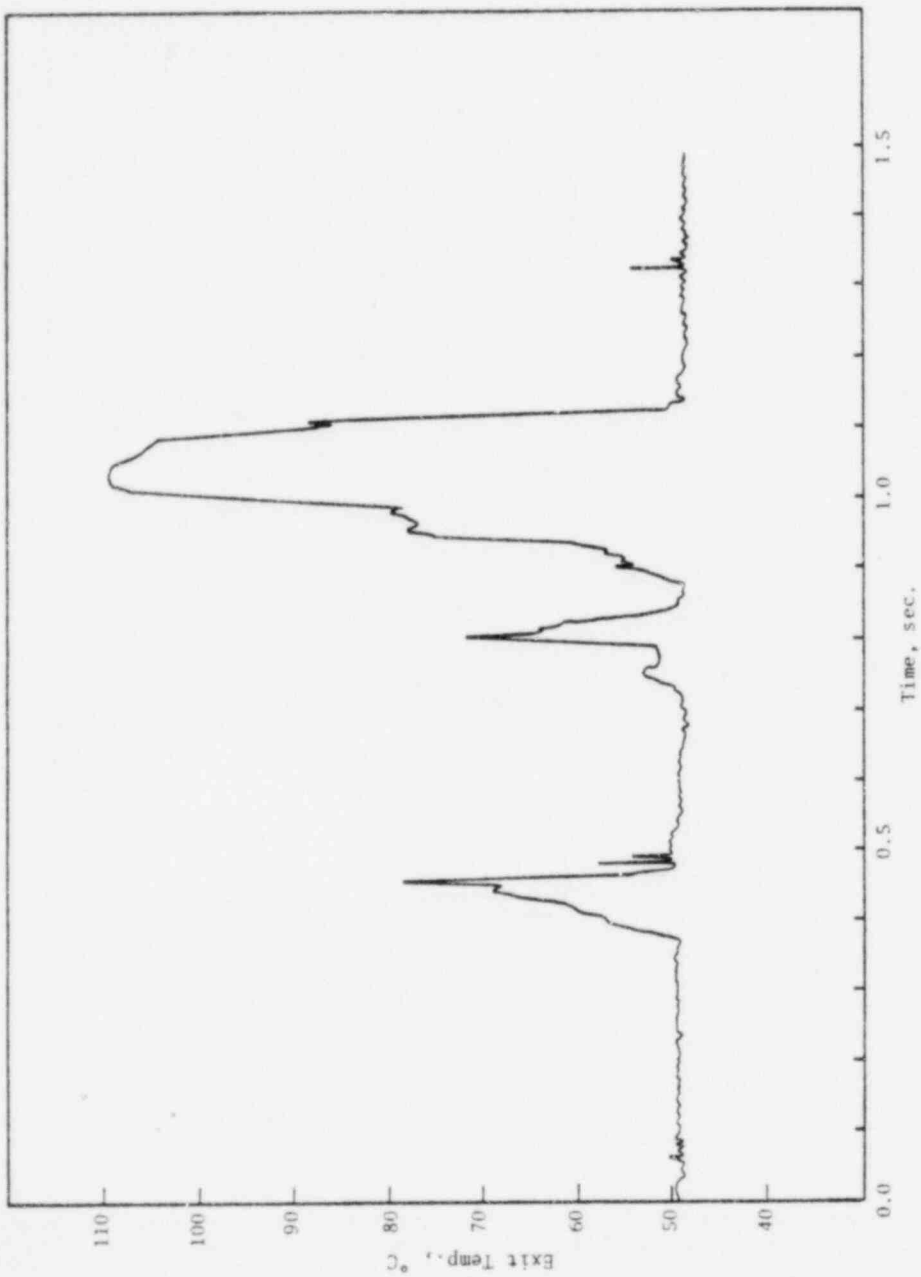


Fig. D.20 Run No. FM4

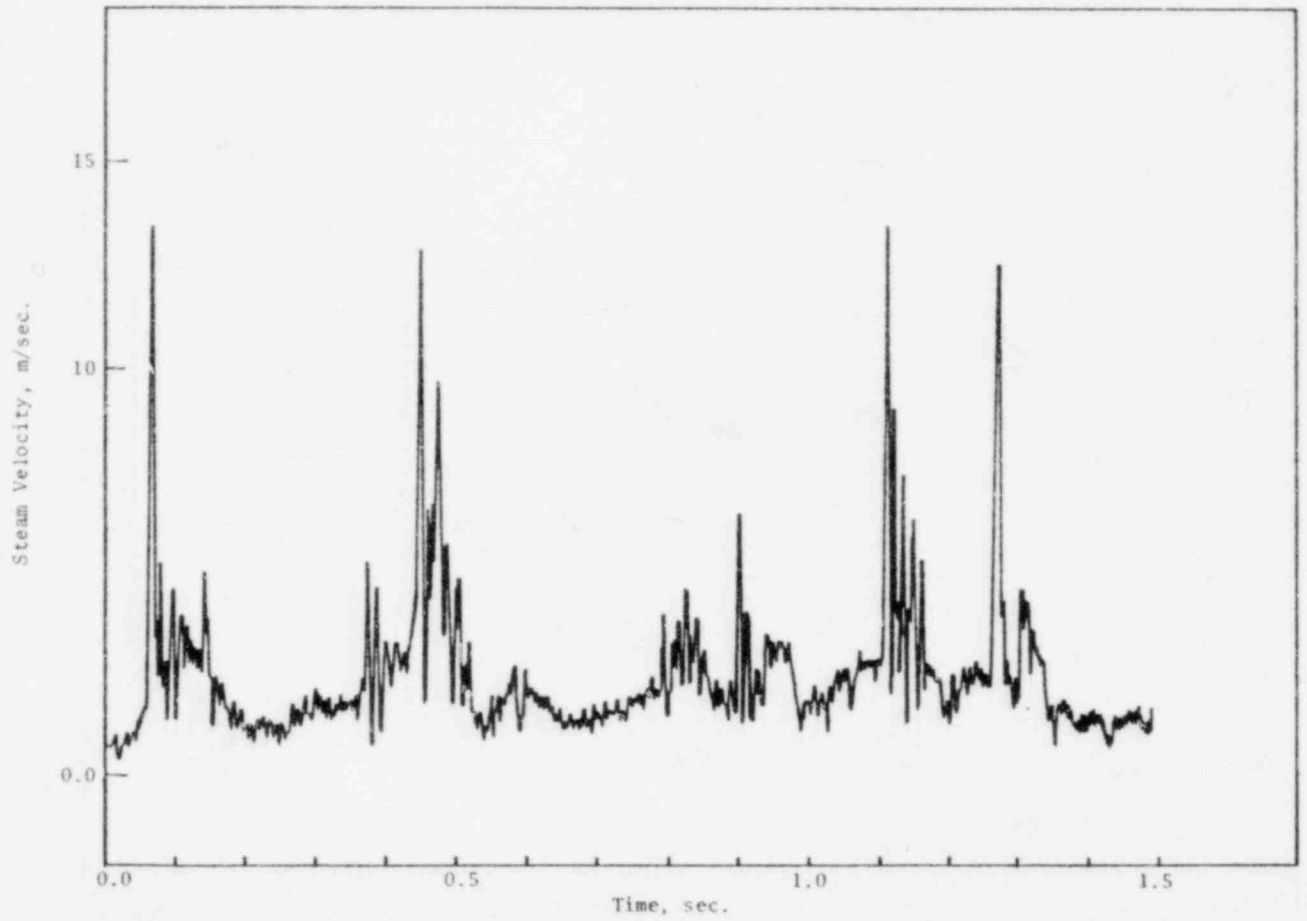


Fig. D.21 Run No. FM5

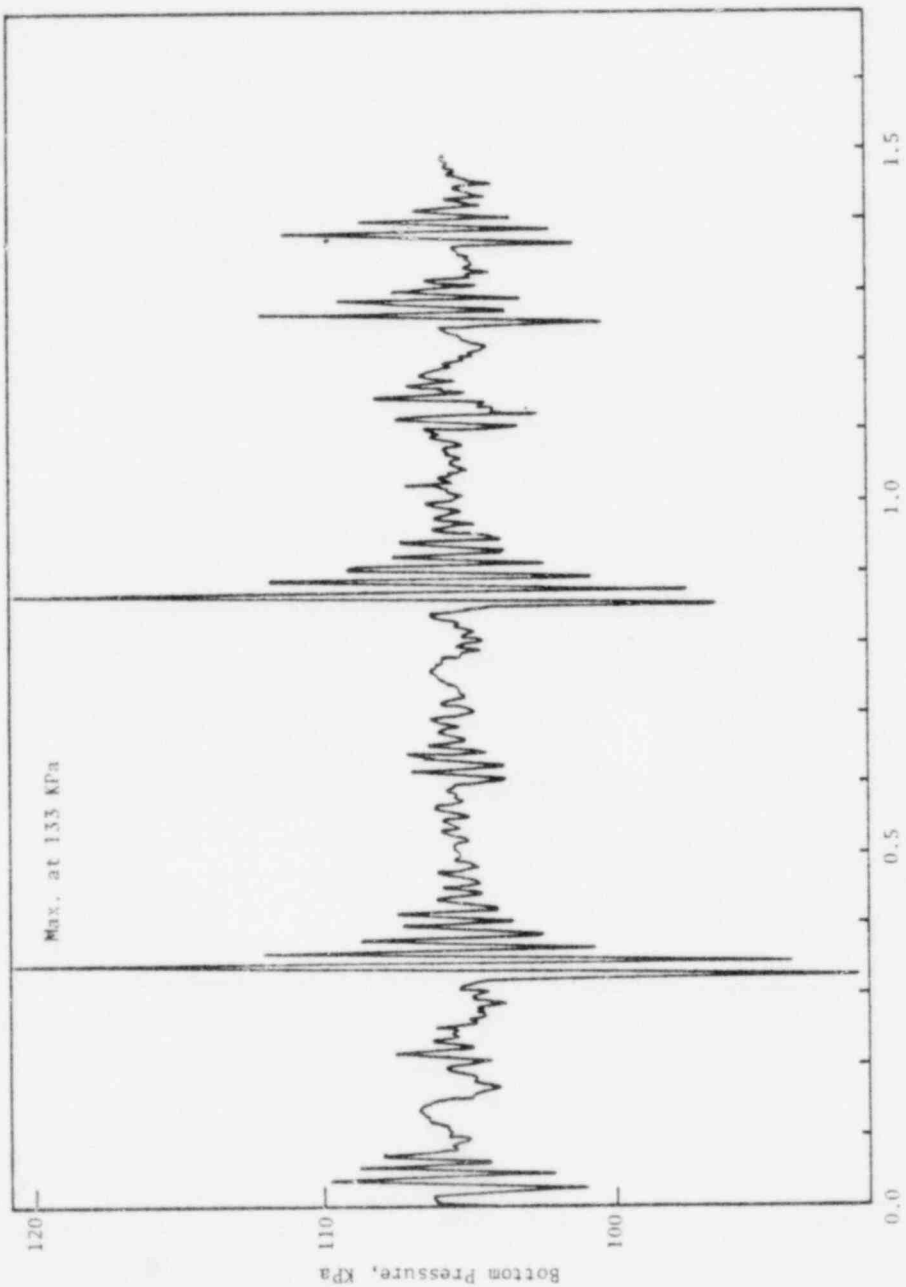


Fig. D.22 Run No. FM5

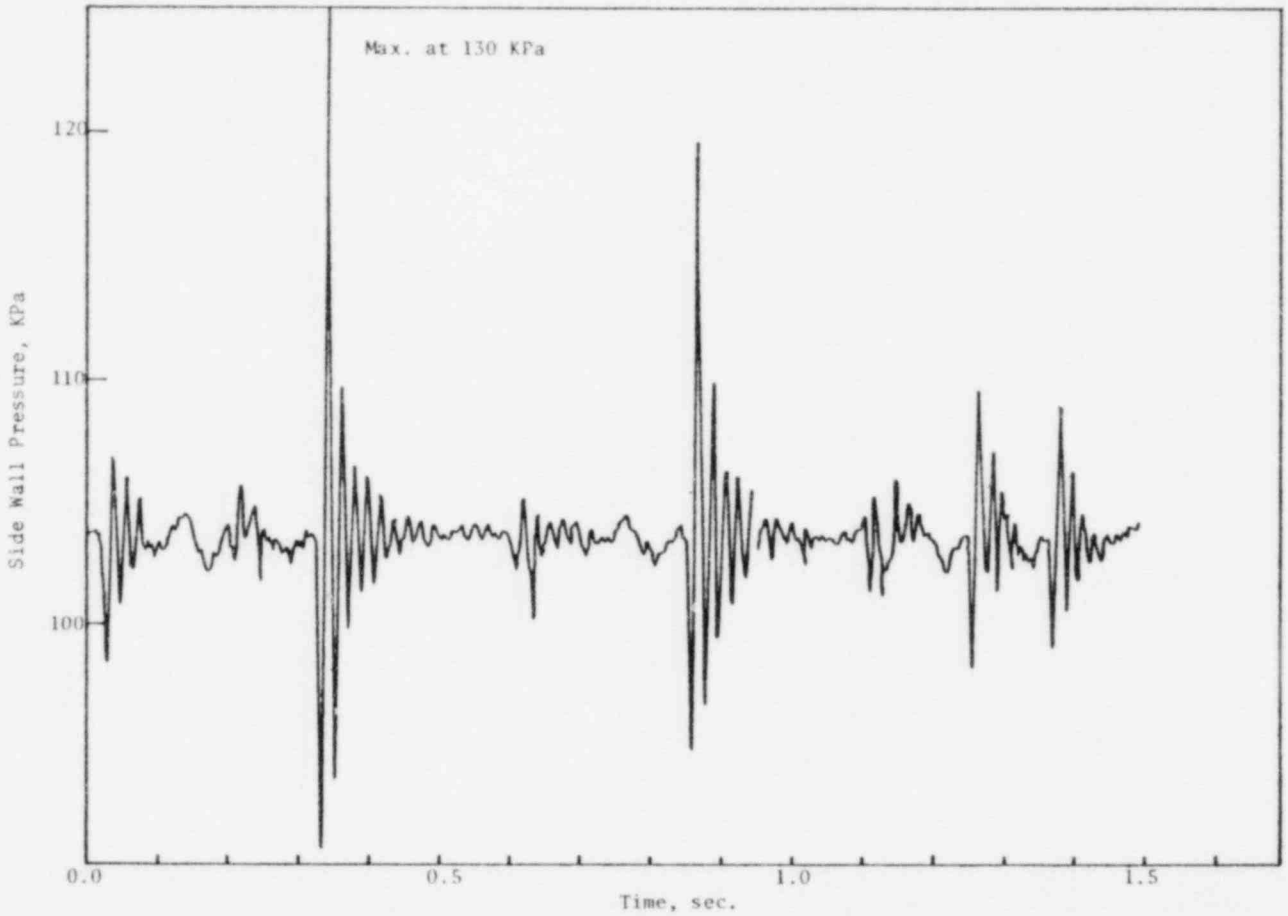


Fig. D.23 Run No. FM5

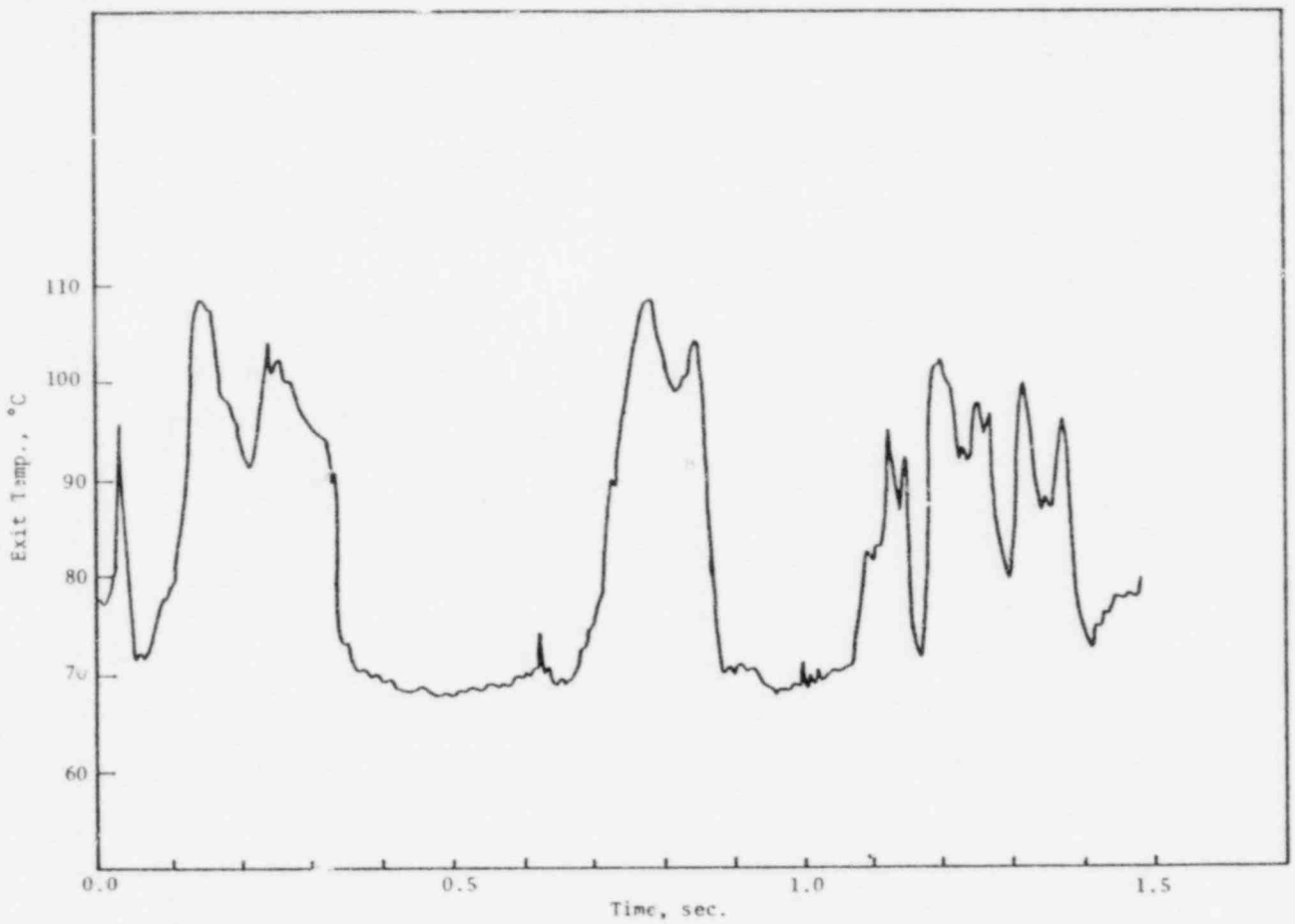


Fig. D.24 Run No. FM5

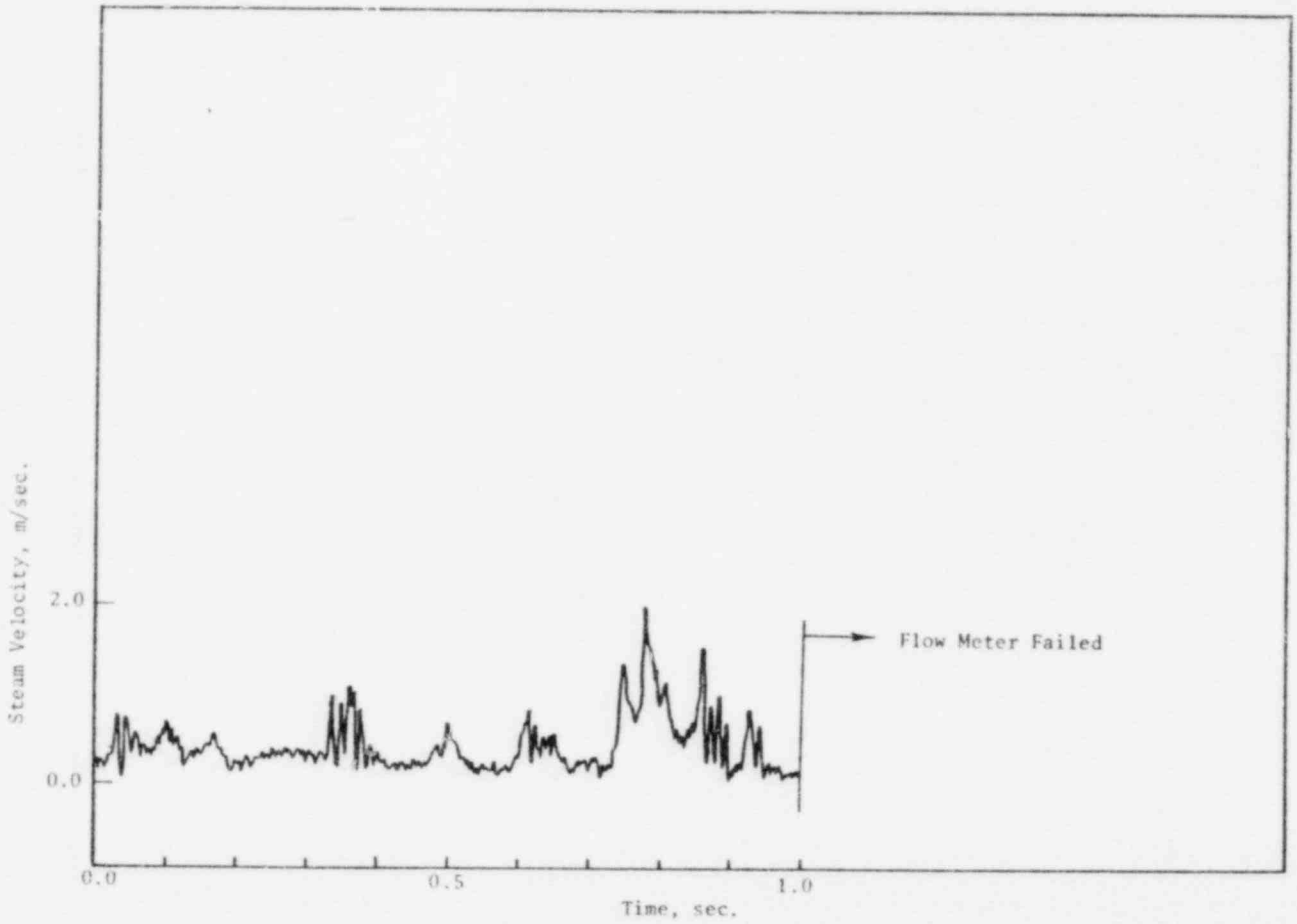


Fig. D.25 Run No. FM5

# APPENDIX E

# MIXED VENT PRESSURE AND FLOW METER EXPERIMENTS

## Mixed Vent Pressure and Flow Meter Experiments

(Steel Pipe)

| Run No. | Pool Temp., °C |
|---|---|
| MIX 1 | 57.2 |
| MIX 2 | 61.7 |

(1) Vent Pressure measured by Statham PL-131-TC-100 pressure transducer (error $\leq$ 5.17 KPa, Response Time = 0.45 ms).

(2) Bottom Pressure measured by Statham PL-131-TC-50 pressure transducer (error $\leq$ 2.58 KPa, Response Time = 0.56 ms).

(3) Steam Velocity measured by TSI-1269W ruggedized hot-film probe (Response Time $\sim$ 100 micro-seconds).

(4) Exit Temperature measured by gage 36 Chromel-Alumel thermocouple.

(5) Boiler Steam Generation Rate = .00756 Kg/sec.

(6) Pipe Exit to Pool Bottom Clearance = 25.4 cm.

(7) Submergence Depth = 25.4 cm.

1) Upstream Pressure (Not Used)
2) Upstream Temperature
3) Upper Exit Thermocouple
4) Lower Exit Thermocouple (Not Used)
5) Bottom Pressure Transducer
6) Bulk Pool Temperature
7) Vent Pressure Transducer
8) Upstream Flow Meter

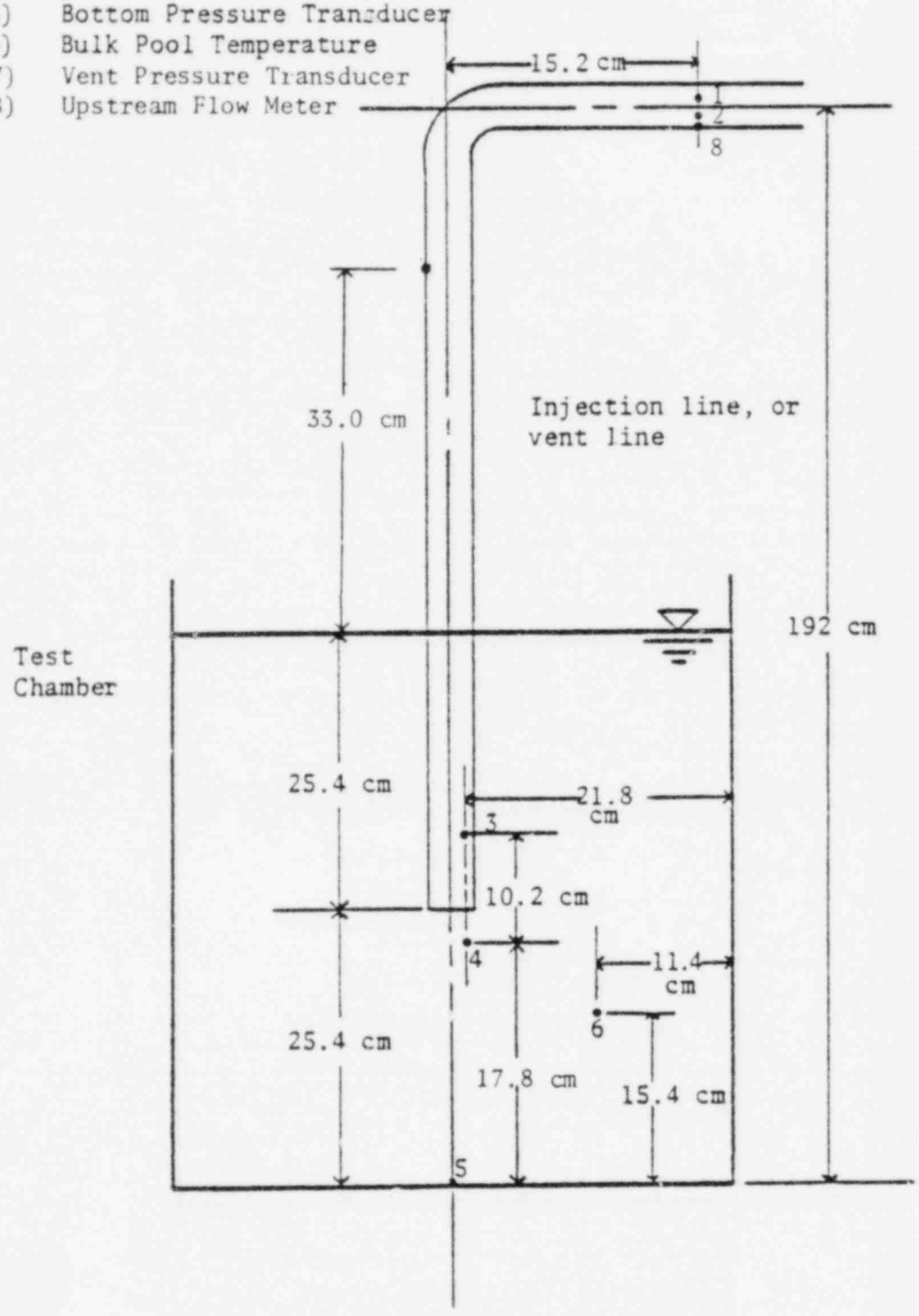


Fig. E.1 Locations of Instrumentation

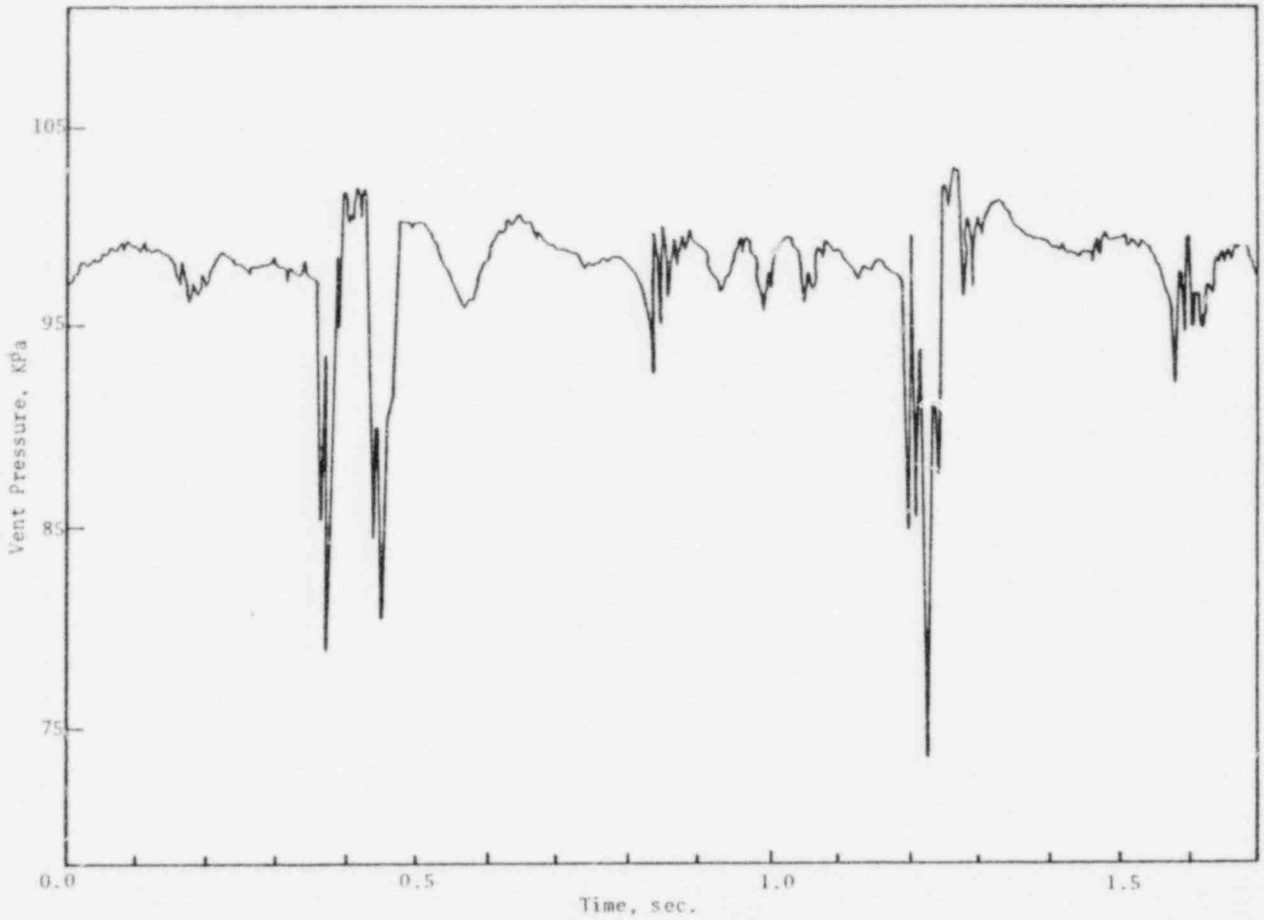


Fig. E.2 Run No. MIX1

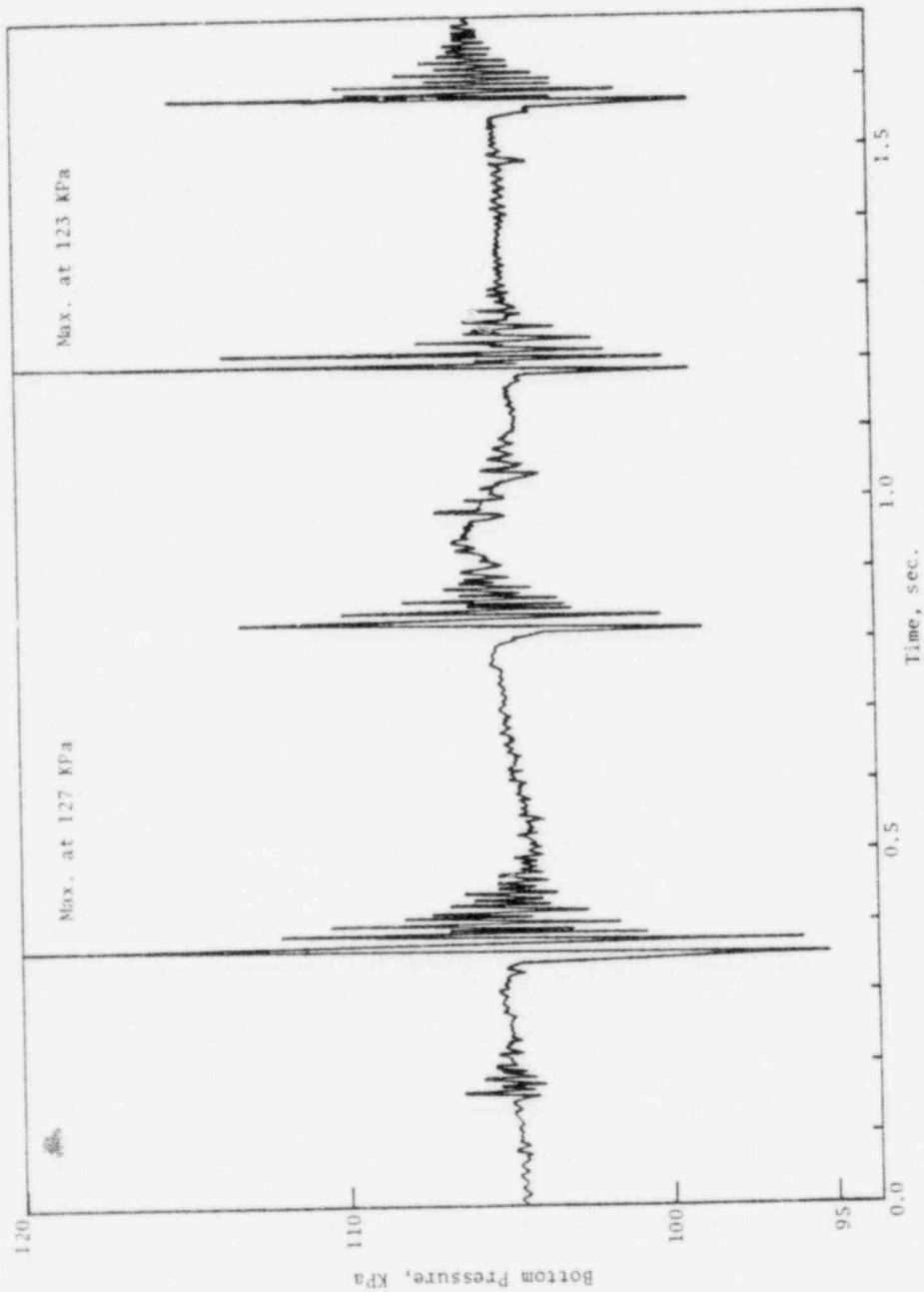


Fig. E.3 Run No. MIX1

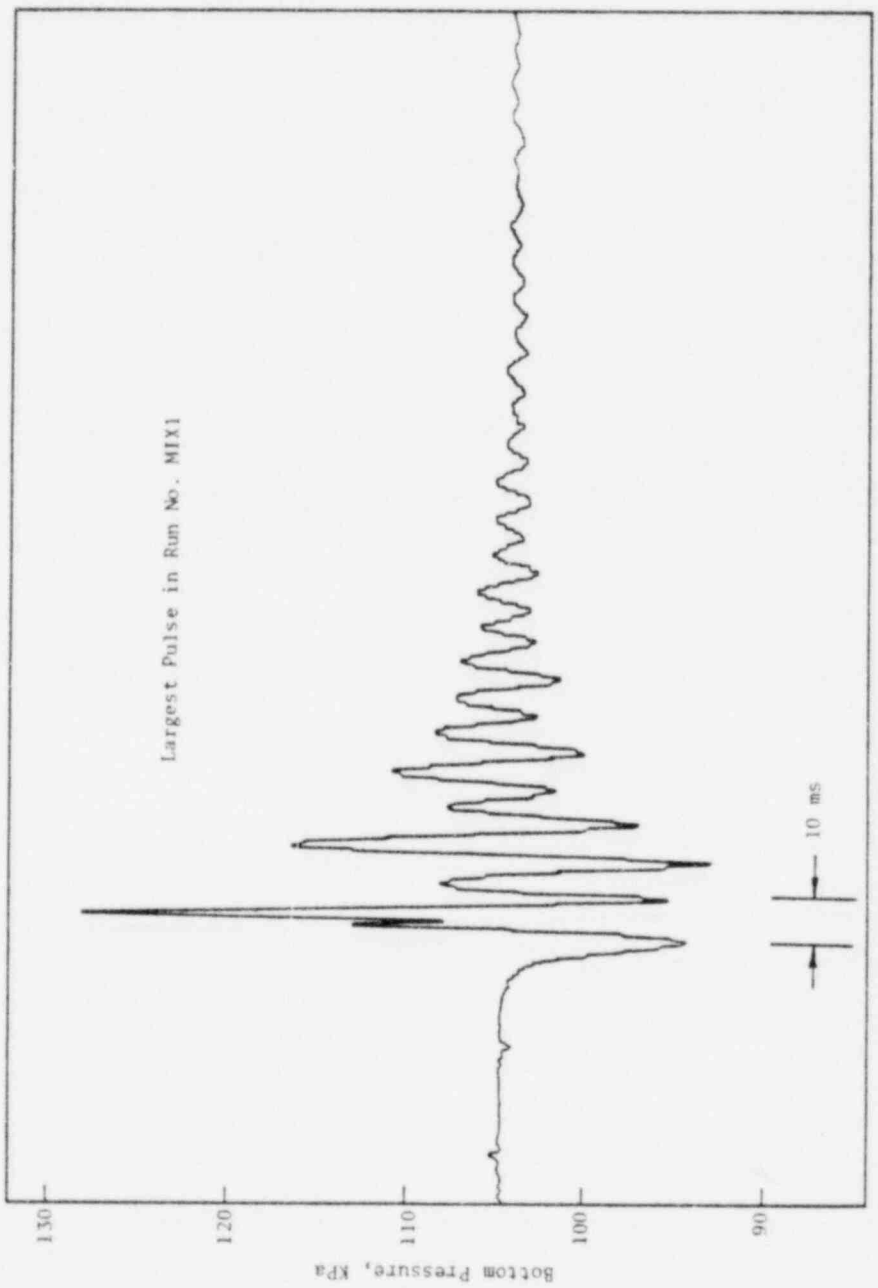


Fig. E.4 Run No. MIX1

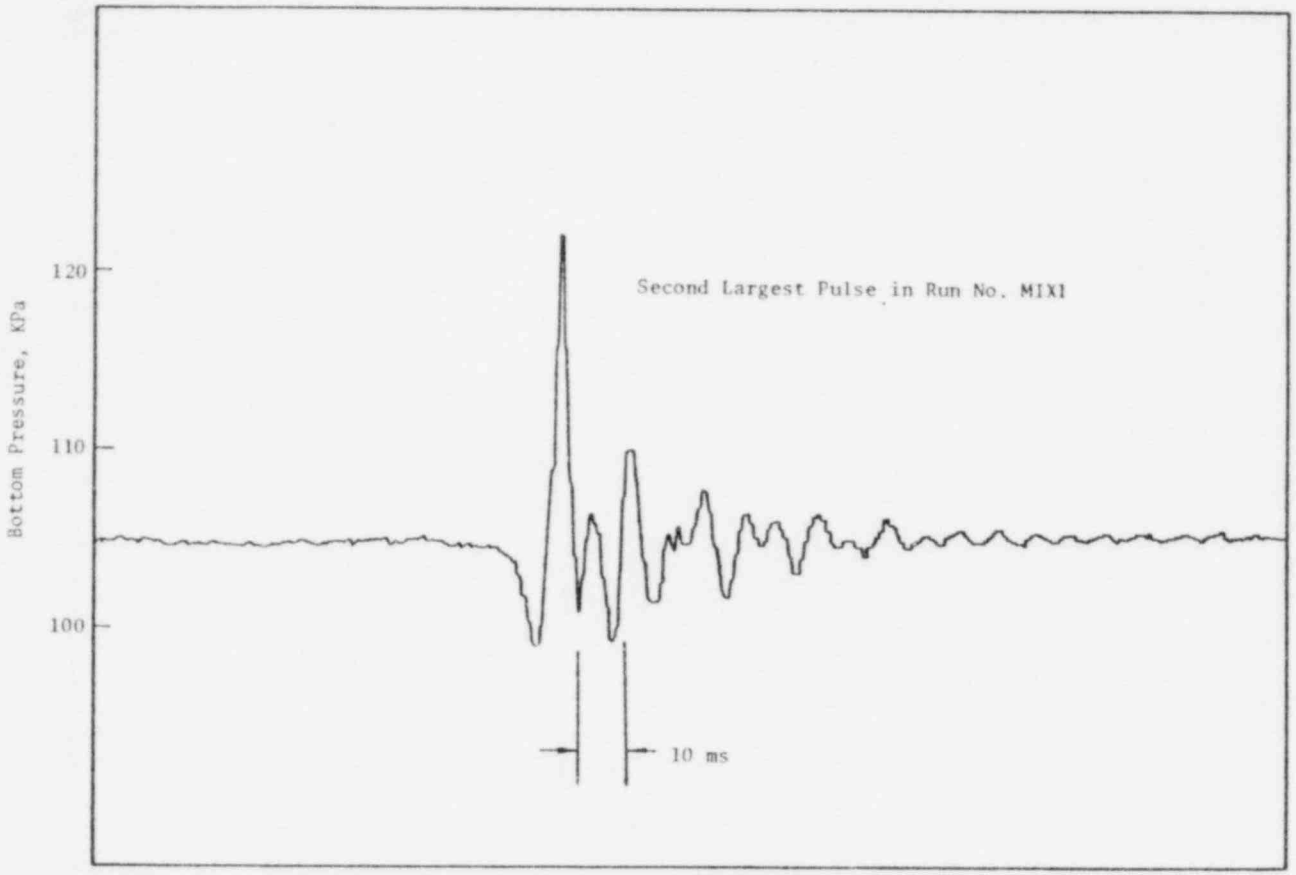


Fig. E.5 Run No. MIX1

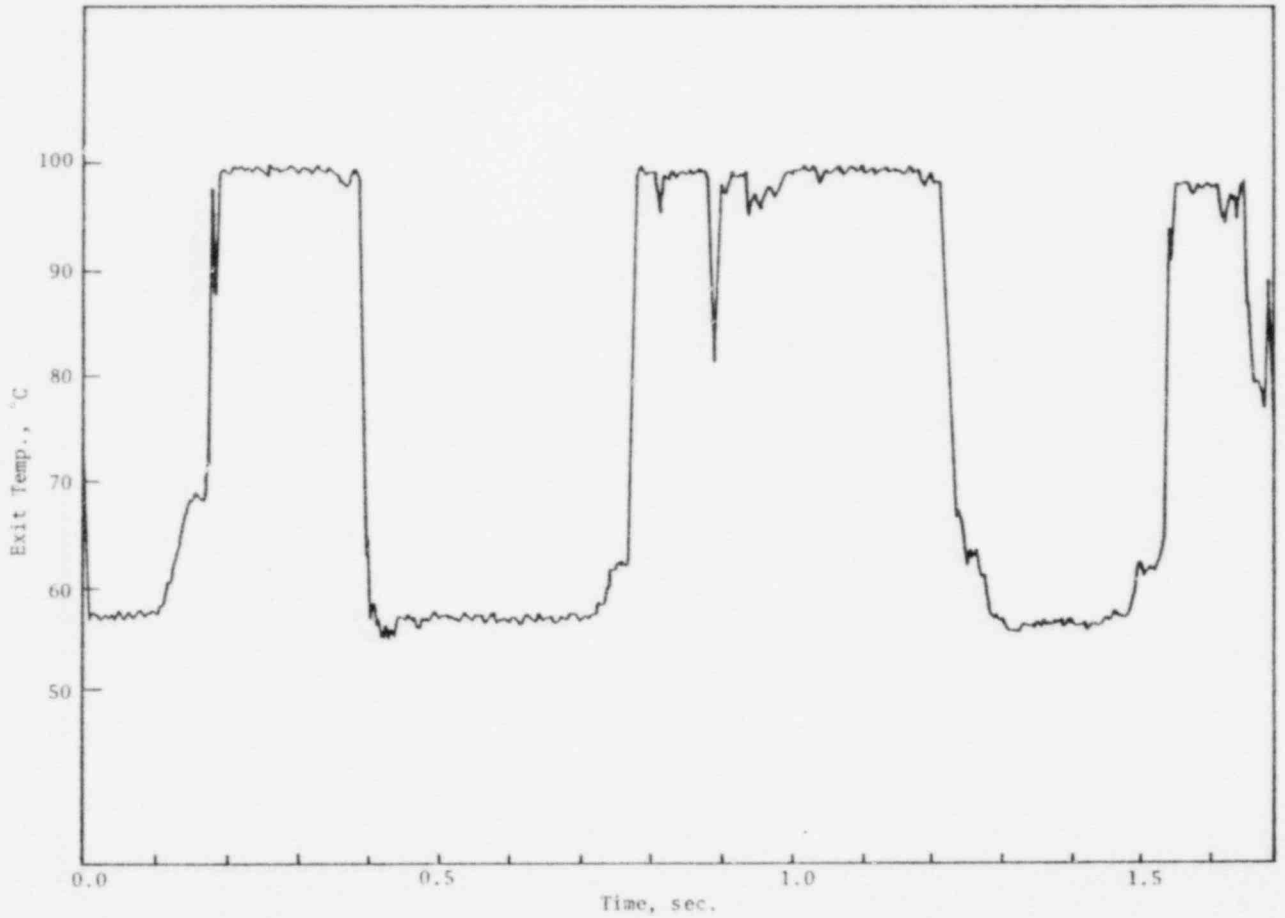


Fig. E.6 Run No. MIX 1

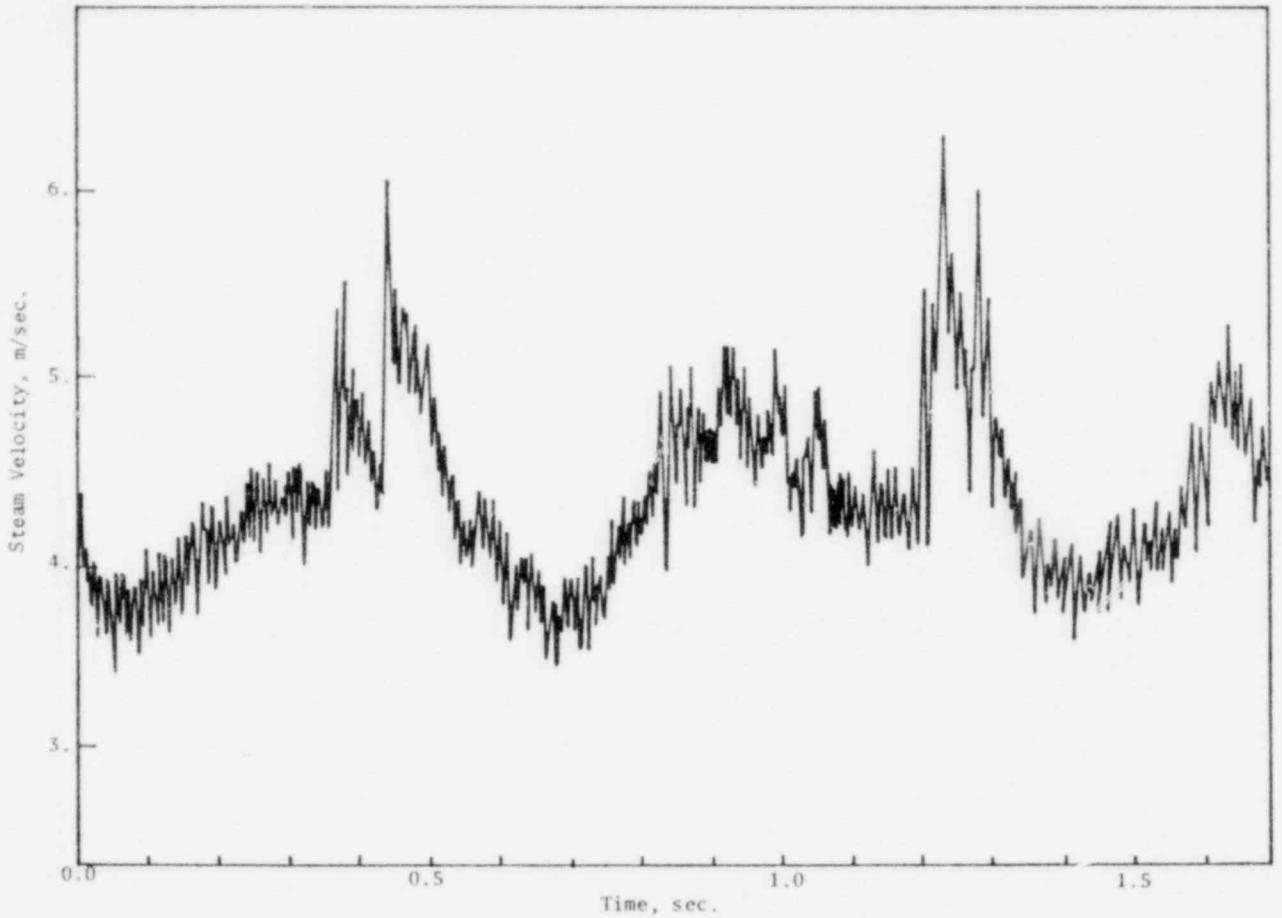


Fig. E.7 Run No. MIX1

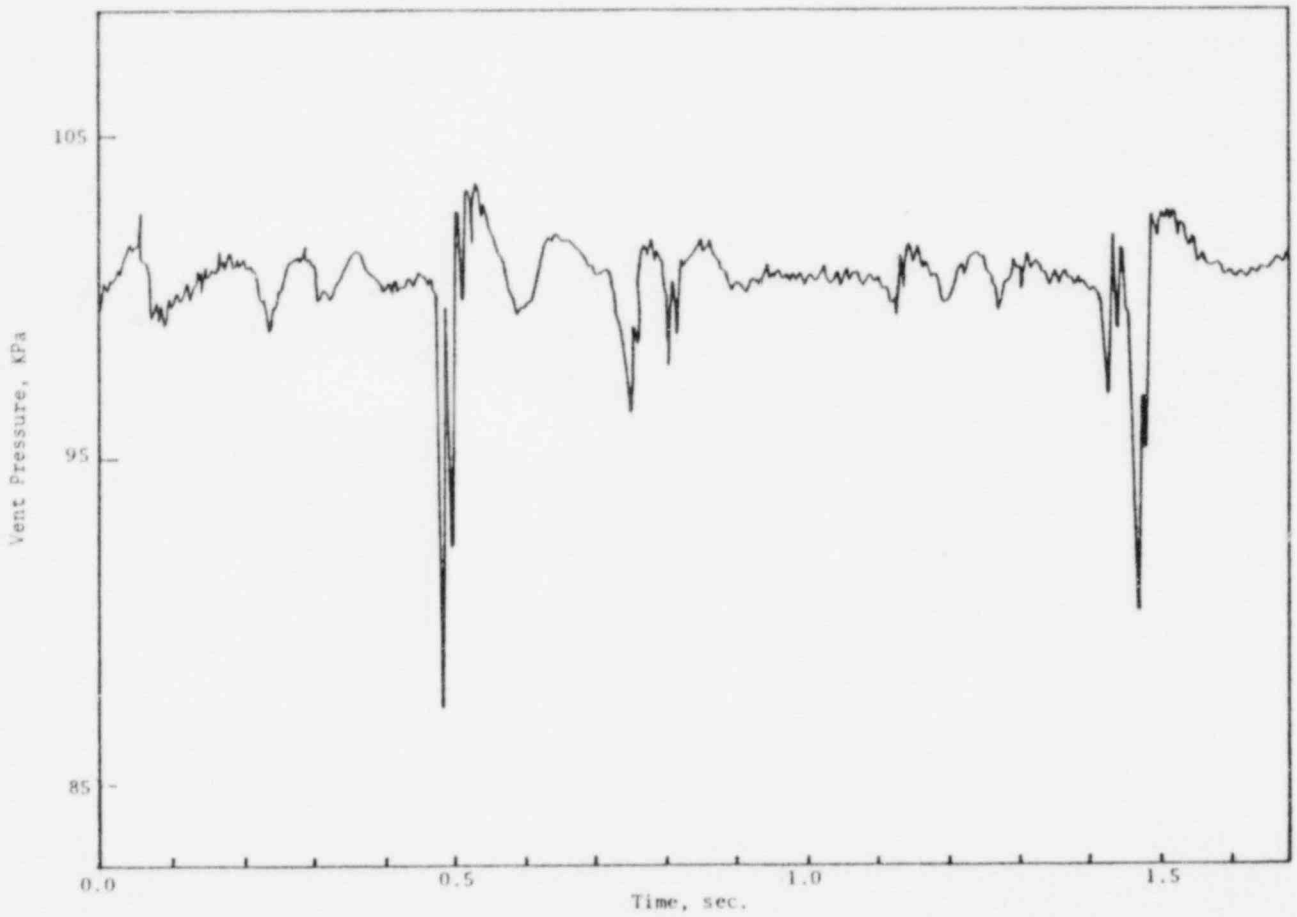


Fig. E.8 Run No. MIX2

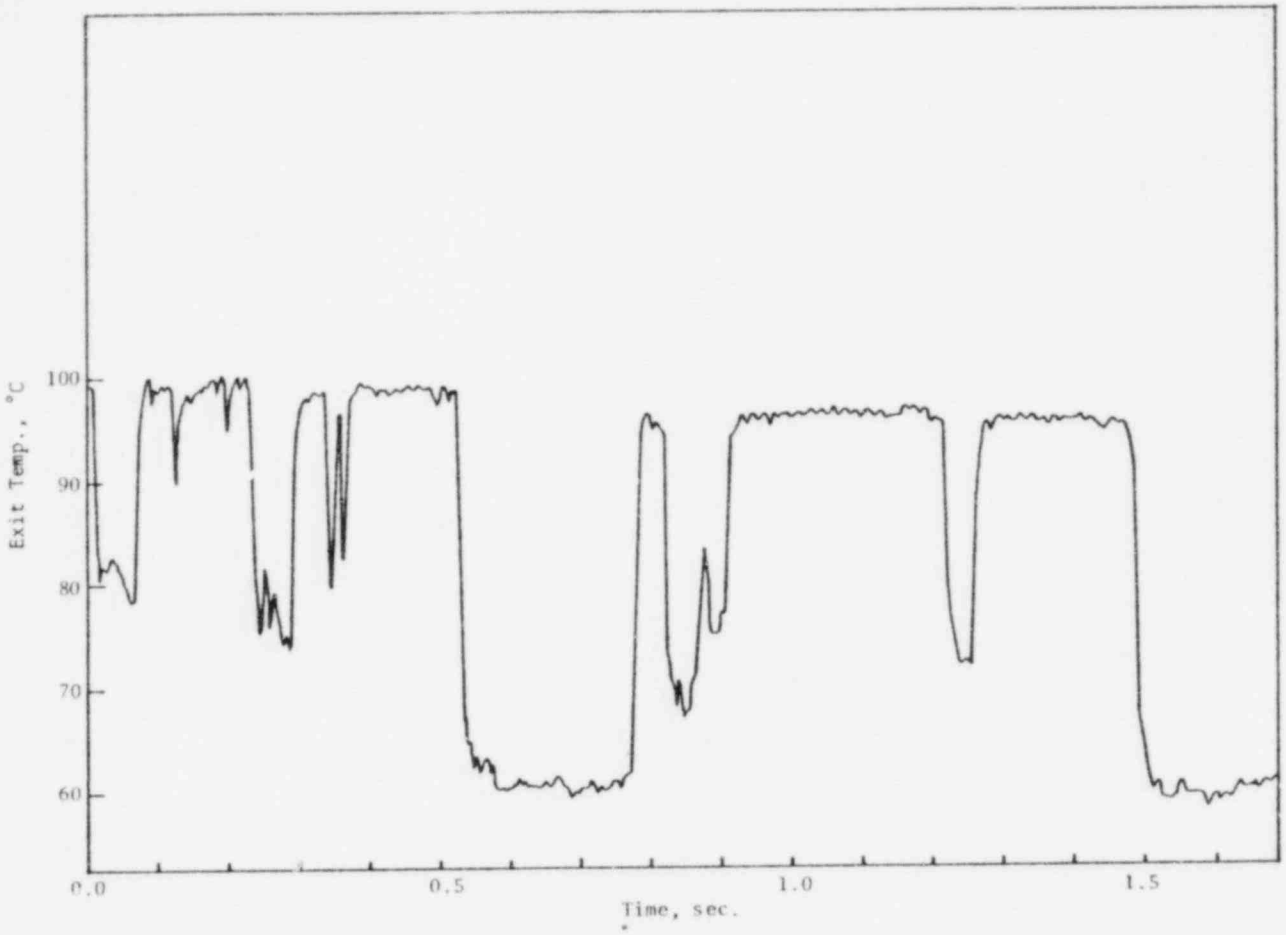


Fig. E.9 Run No. MIX2

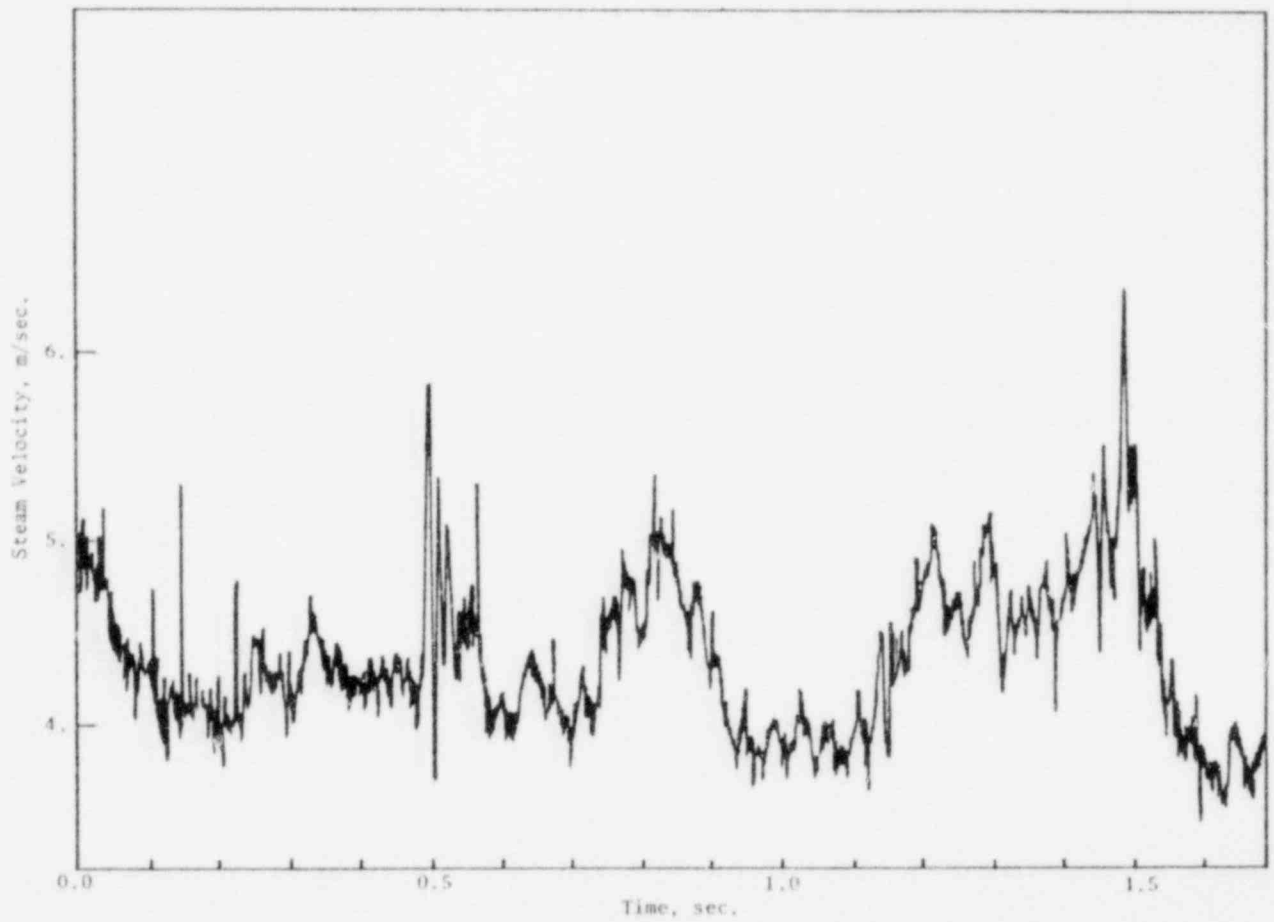


Fig. E.10 Run Nom M1X2

# APPENDIX F

# SURGE TANK PRESSURE EXPERIMENTS

## Surge Tank Pressure Experiments

(Steel Pipe)

| Run No. | Pool Temp., °C |
|---|---|
| ST1 | 40.0 |
| ST2 | 46.7 |
| ST3 | 53.3 |
| ST4 | 61.7 |

(1) Surge Tank Pressure measured by Statham PL-131-TC-15 (error $\leq$ 0.78 KPa, Response Time = 0.83 ms).

(2) Vent Pressure measured by Statham PL-131-TC-25 (error $\leq$ 1.29 KPa, Response Time = 0.63 ms).

(3) Exit Temperature measured by gage 36 Chromel-Alumel thermocouple.

(4) Boiler Steam Generation Rate = .00756 Kg/sec.

(5) Pipe Exit to Pool Bottom Clearance = 25.4 cm.

(6) Submergence Depth = 25.4 cm.

(7) Data sampling time = 2.5 ms.

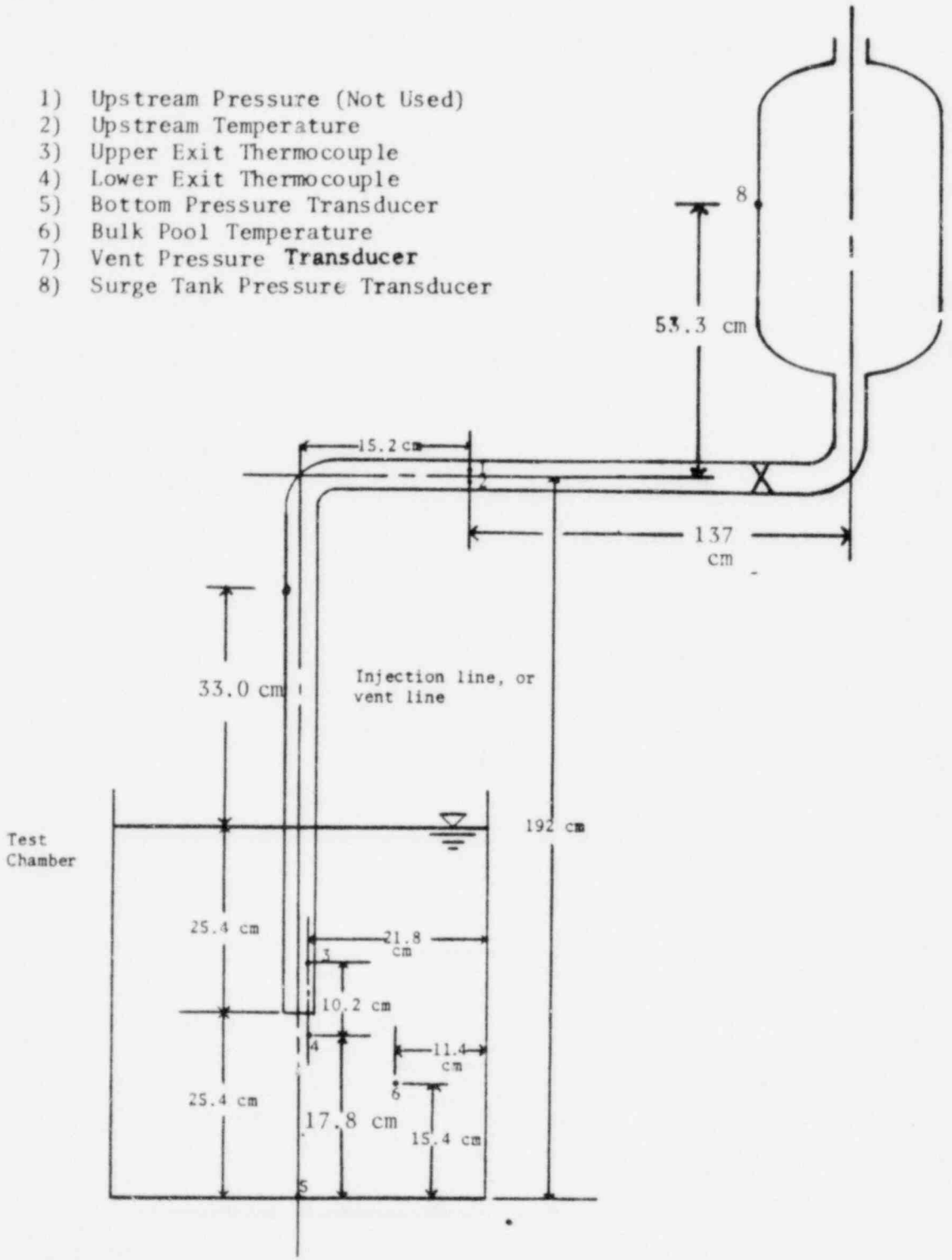


Fig. F.1 Locations of Instrumentation

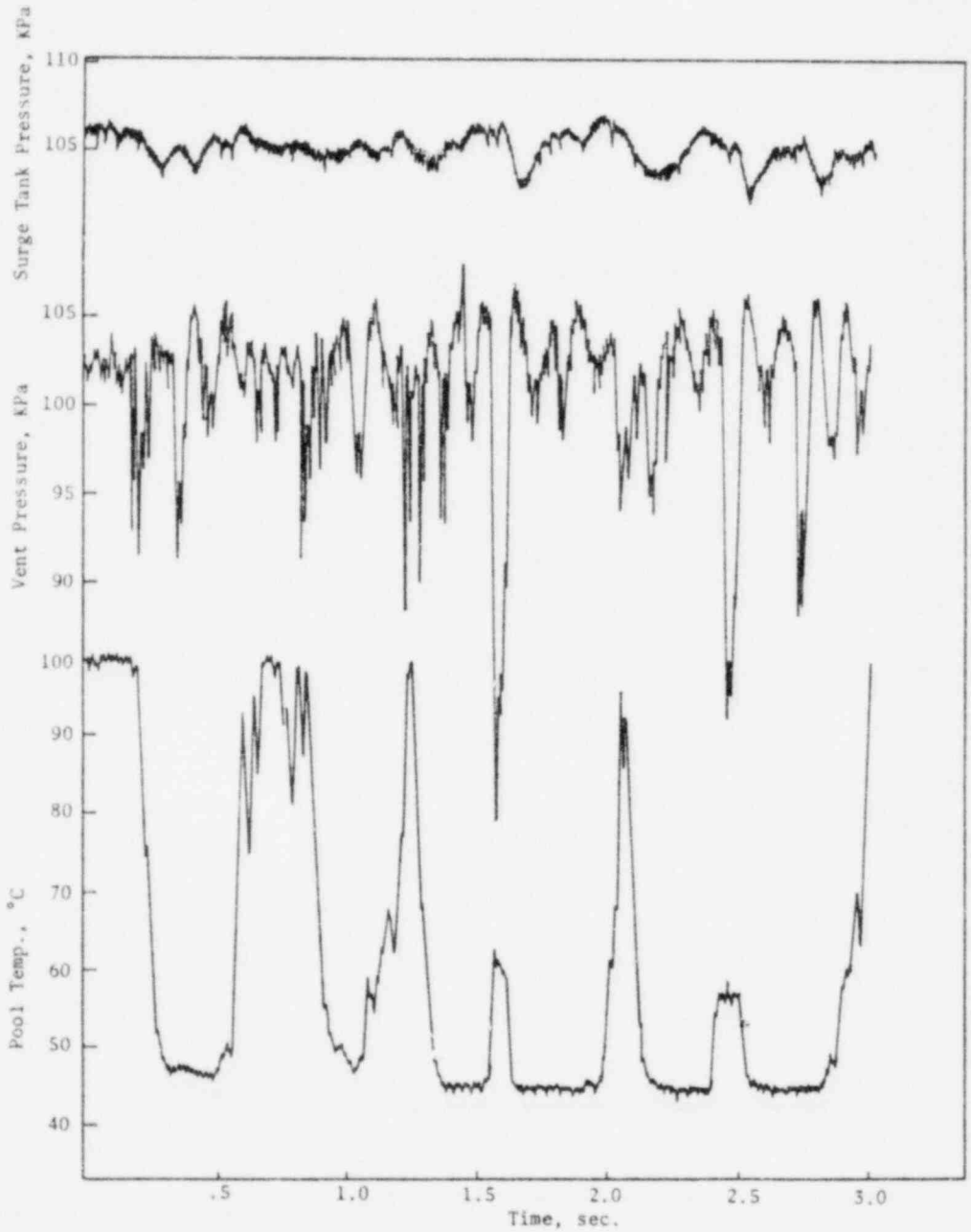


Fig. F.2 Run No. ST1

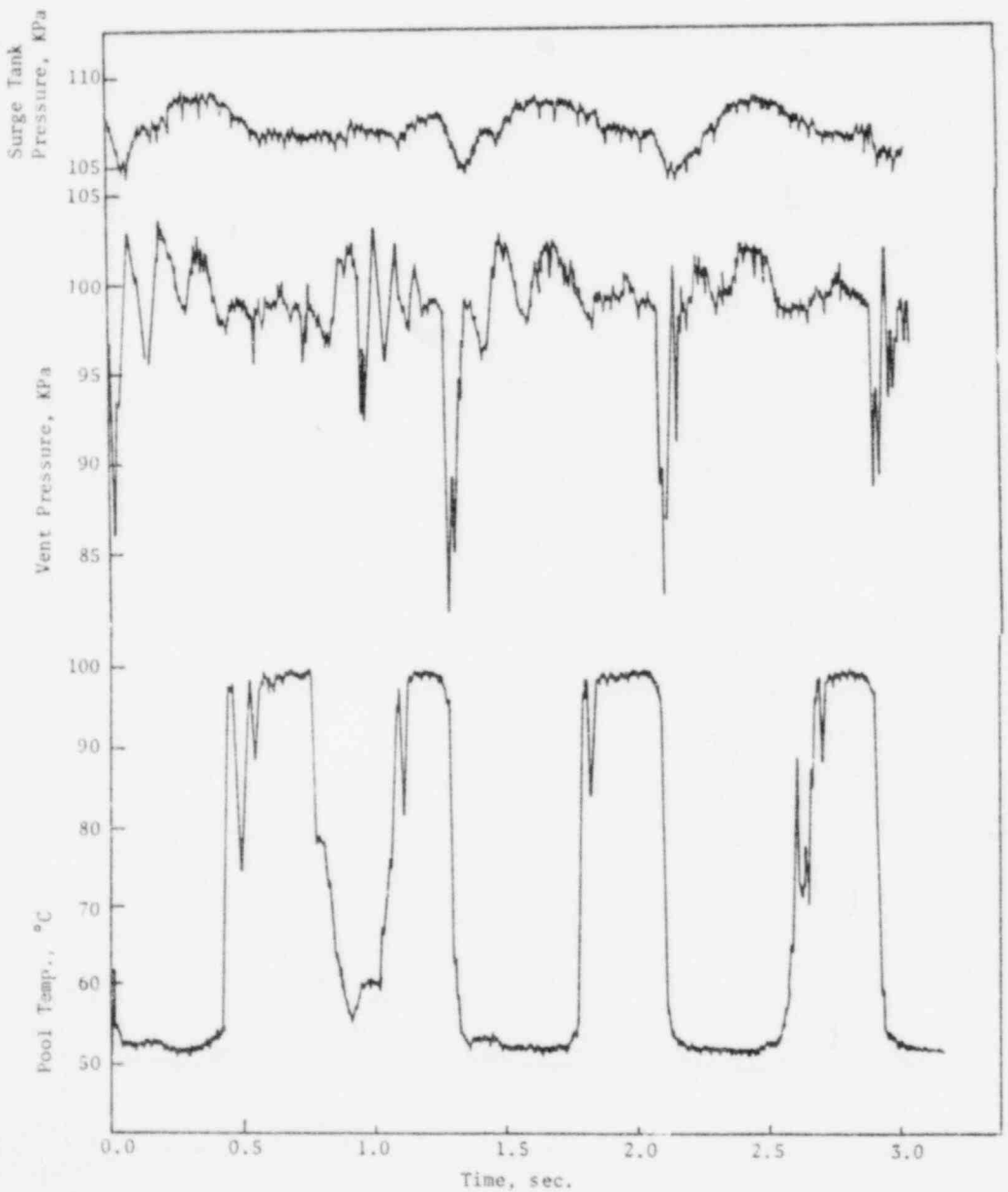


Fig. F.3 Run No. ST2

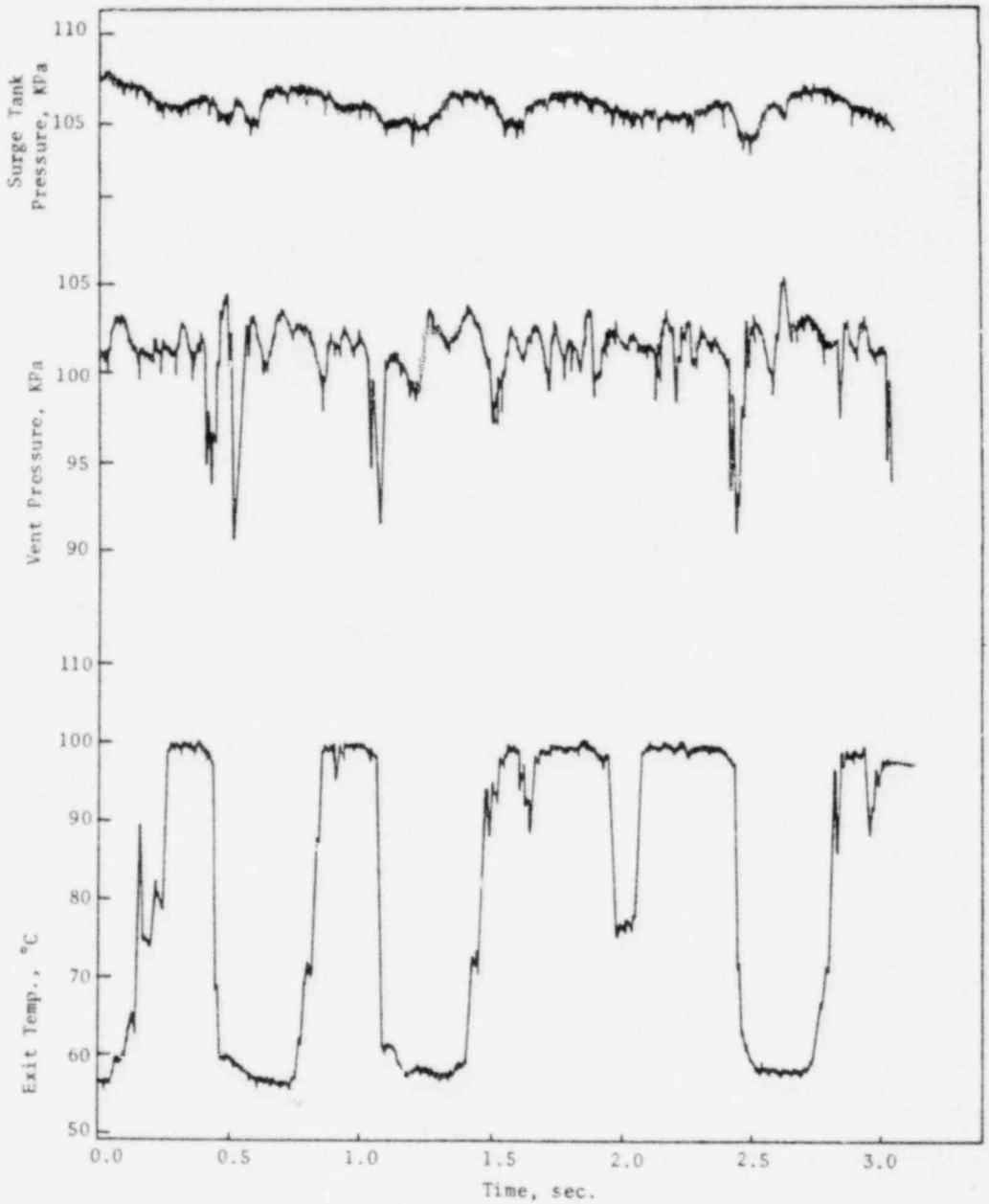


Fig. F.3 Run No. ST3

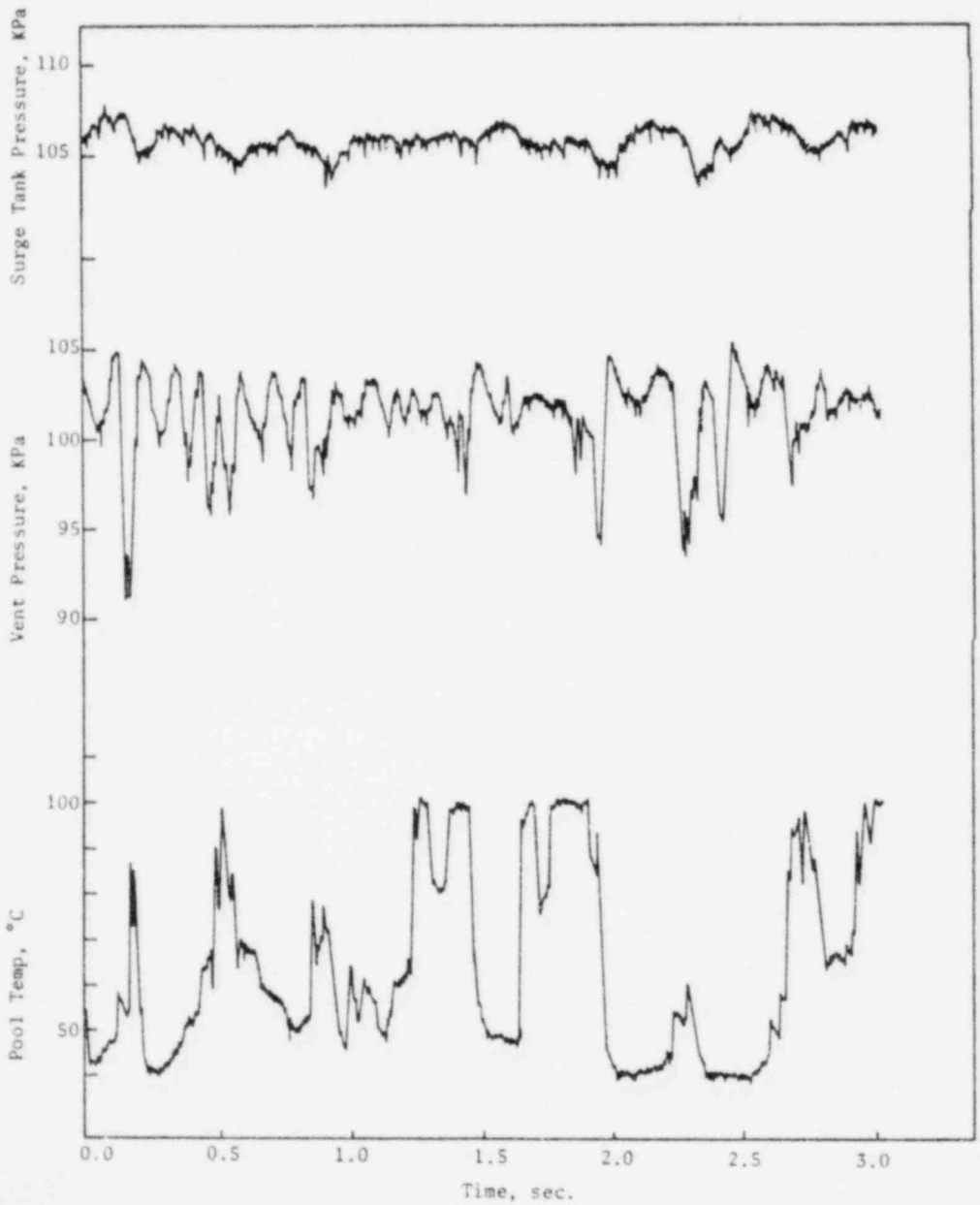


Fig. F.4 Run No. ST4

# APPENDIX G

## THE ONE-DIMENSIONAL BUBBLE DYNAMICS EQUATIONS FOR A SPHERICAL BUBBLE IN AN INFINITE POOL WITH A VAPOR SOURCE OR SINK

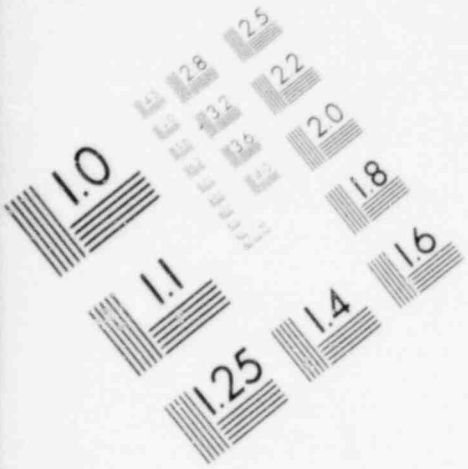


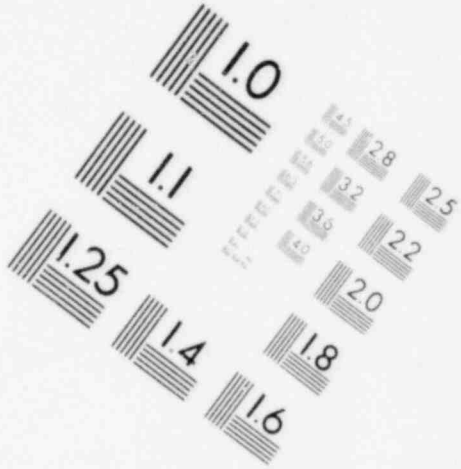


# IMAGE EVALUATION TEST TARGET (MT-3)

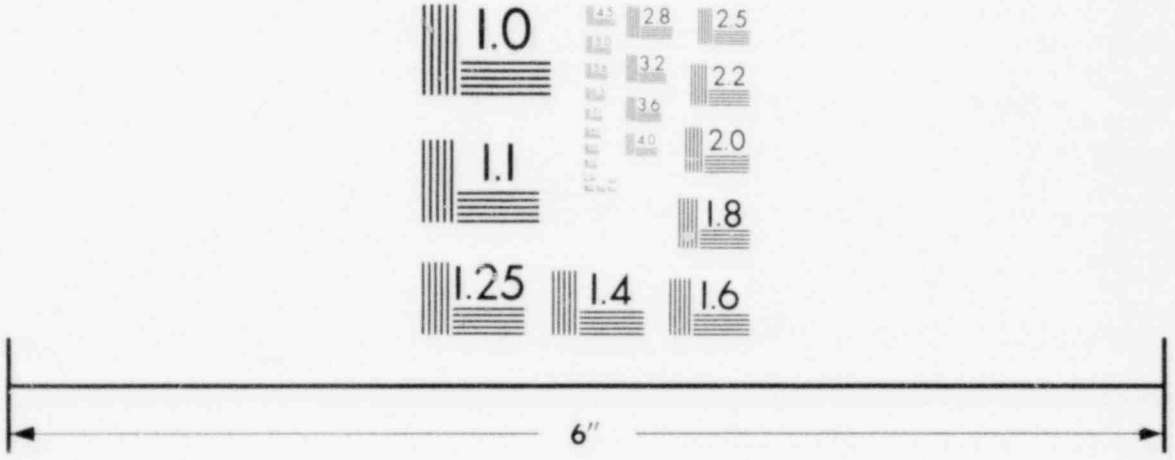


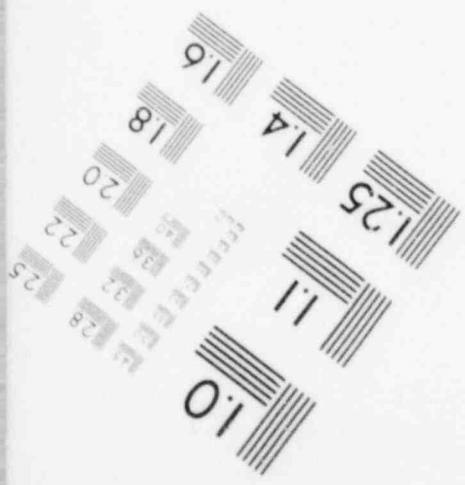


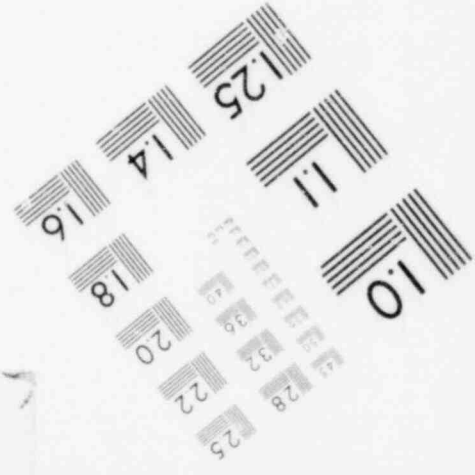

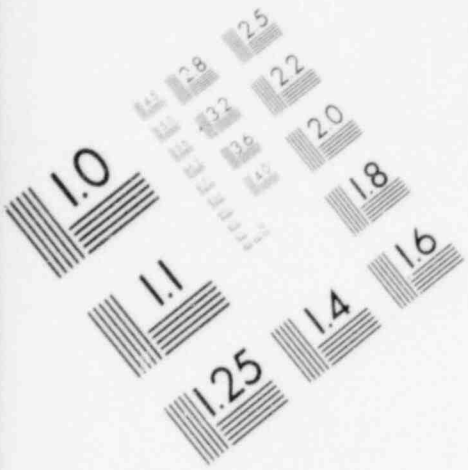


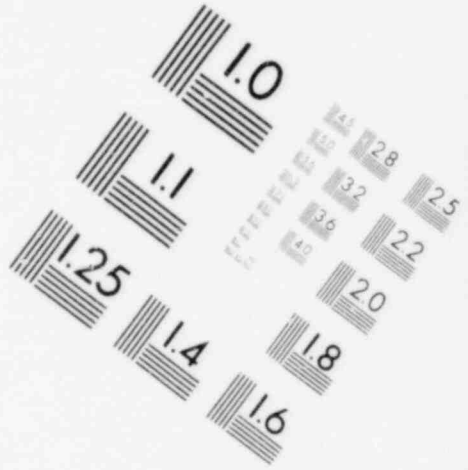


# IMAGE EVALUATION TEST TARGET (MT-3)

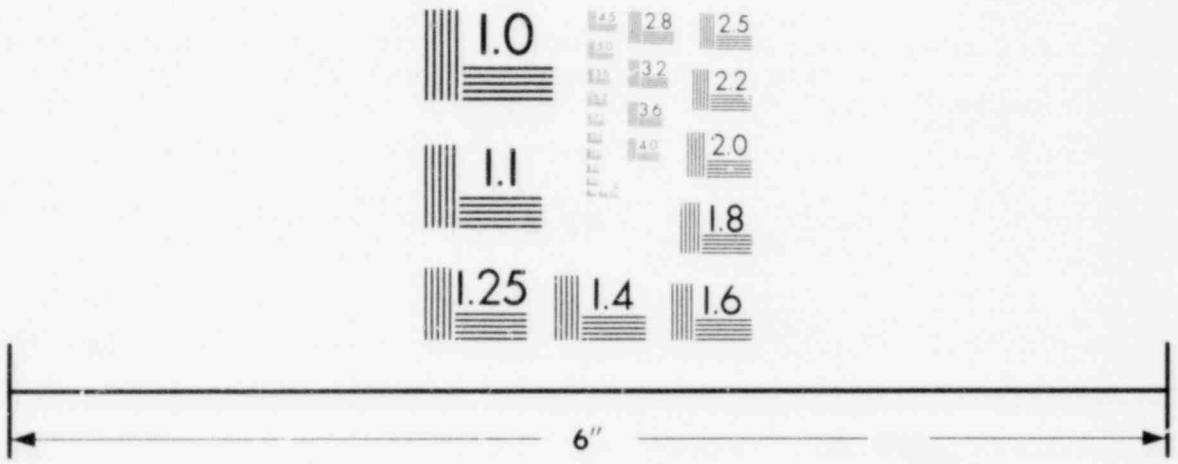


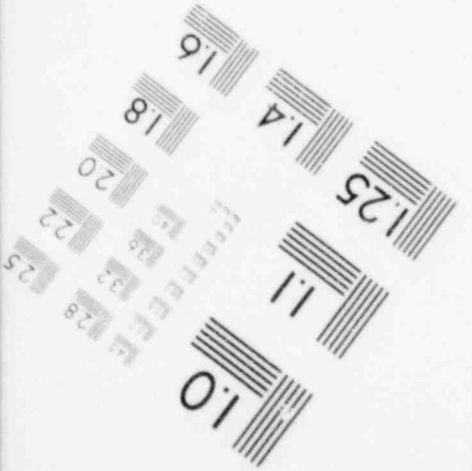


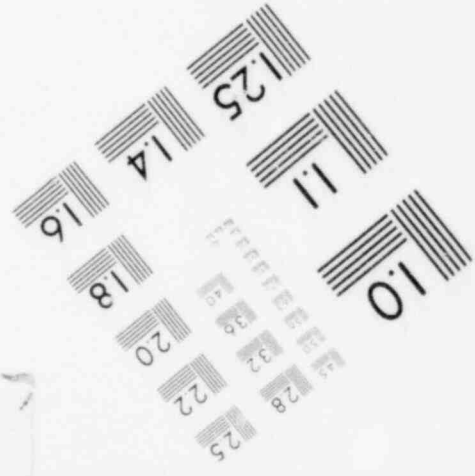

The equations describing dynamics of a vapor bubble, with a continuous vapor source or sink in an infinite pool of subcooled liquid, is presented in this appendix. Figure G.1 shows the physical model. The vapor region is assumed to have uniform pressure, temperature, and density, such that the governing equations for the vapor region are simply the mass and energy balances as well as the equation of state. These equations are presented as follows:

Mass

$$\frac{d\rho_B}{dt} = \frac{3}{r_B}\left(-m_c - \rho_B \frac{dr_B}{dt} + \frac{m_i A_i}{4\pi r_B^2}\right) \qquad (G.1)$$

Energy

$$\rho_B C_v \frac{dT_B}{dt} = \frac{3}{r_B}\left(-m_c \frac{P_B}{\rho_B} - P_B \frac{dr_B}{dt} + \frac{m_i A_i C_v (T_i - T_B)}{4\pi r_B^2}\right) \qquad (G.2)$$

Equation of State

$$\frac{1}{P_B}\frac{dP_B}{dt} = \frac{1}{\rho_B}\frac{d\rho_B}{dt} + \frac{1}{T_B}\frac{dT_B}{dt} \qquad (G.3)$$

On the liquid side, the governing equations are the one-dimensional conservation of mass, momentum and energy.

Mass

$$\frac{1}{r^2}\frac{\partial}{\partial r}\left(r^2 u_l\right) = 0 \qquad (G.4)$$

Momentum

$$\frac{\partial u_l}{\partial t} + u_l \frac{\partial u_l}{\partial r} = -\frac{1}{\rho_l}\frac{\partial P_l}{\partial r} \qquad (G.5)$$

Energy $$\frac{\partial T_g}{\partial t} + u_g \frac{\partial T_g}{\partial r} = \frac{\alpha_g}{r^2} \frac{\partial}{\partial r}\left(r^2 \frac{\partial T_g}{\partial r}\right) \qquad (G.6)$$

At the vapor-liquid interface, the conservation equations are satisfied in the limit when the interface becomes infinitesimally thin. The equations are presented as follows:

Mass $$m_c = \rho_l \left(u_l - \frac{d r_B}{dt}\right)_{r=r_B} \qquad (G.7)$$

Momentum $$P_B = (P_l)_{r=r_B} \qquad (G.8)$$

Energy $$m_c h_{fg} = -k_l \left(\frac{\partial T}{\partial r}\right)_{r=r_B} \qquad (G.9)$$

In equations (G.1) - (G.9)

$\rho$ = density

T = temperature

P = pressure

t = time

r = radius

u = velocity

$m_c$ = condensation rate

$m_s$ = steam injection rate (source or sink)

$A_s$ = flow area of injection pipe

$\Gamma$ = specific heat ratio

$C_v$ = specific heat with constant volume

$\alpha$ = thermal diffusivity

k = thermal conductivity

the subscripts $\ell$ denote liquid side and

B denotes vapor side

This set of partial differential equations could be converted to a set of ordinary differential equations. The procedure is to substitute the liquid continuity equation into the liquid momentum equation and then integrate the resulting equation from $r_B$ to infinity. This converts the momentum equation into an ordinary differential equation. In the liquid energy equation, it is convenient to approximate the temperature distribution in the liquid by a quadratic profile.

$$T = T_w + (T_\infty - T_w)(2\beta - \beta^2) \qquad (G.10)$$

where $\beta = \dfrac{r - r_B}{\delta}$

$\delta$ = thermal boundary layer thickness

$T_\infty$ = liquid temperature far away from the bubble

$T_w$ = liquid temperature at the interface.

Then, when Equation (G.10) is substituted into the liquid energy equation and the resulting equation integrated over the thermal boundary later, an ordinary differential equation involving time derivatives of $\delta$ and $T_w$ is resulted. As for the interface temperature, the assumption is made that this temperature is prescribed

by the bubble pressure based on the saturated vapor curve. Thus, a set of ordinary differential equations is derived and are listed as follows:

Vapor Side

Continuity

$$\frac{d\rho_B}{dt} = \frac{3}{4\pi r_B^3}\left(m_i A_i - m_c 4\pi r_B^2 - 4\pi r_B^2 \rho_B \frac{dr_B}{dt}\right) \quad (6.12)$$

Energy

$$\rho_B C_v \frac{dT_B}{dt} = \frac{3}{4\pi r_B^3}\left(m_i A_i C_v (T_i - T_B) - \rho_B 4\pi r_B^2 \frac{dr_B}{dt} - m_c 4\pi r_B^2 \frac{P_B}{\rho_B}\right) \quad (6.13)$$

Eqn. of State

$$\frac{1}{P_B}\frac{dP_B}{dt} = \frac{1}{\rho_B}\frac{d\rho_B}{dt} + \frac{1}{T_B}\frac{dT_B}{dt} \quad (6.14)$$

Liquid Side

Momentum & Continuity

$$\frac{d^2 r_B}{dt^2} = -\frac{1}{\rho_l}\frac{dm_c}{dt} - \frac{2u_B}{r_B}\frac{dr_B}{dt} + \frac{1}{2}\frac{u_B^2}{r_B} + \frac{g_c}{\rho_l}\frac{P_B - P_\infty}{r_B} - \frac{2\sigma}{r_B^2}\frac{g_c}{\rho_l} \quad (6.15)$$

where $P_\infty$ is the liquid pressure at infinite distance from the bubble.

Energy

$$C_1\frac{dT_w}{dt} - C_2\frac{dr_B}{dt} - C_3\frac{d\delta}{dt} = -u_B r_B^2 (T_\infty - T_w) - \alpha r_B^2 (T_\infty - T_w)\frac{2}{\delta} \quad (6.16)$$

where $$C_1 = \frac{\delta}{3}\left(\frac{\delta^2}{10} + \frac{\delta r_B}{2} + r_B^2\right)$$

$$C_2 = (T_\infty - T_w)\left(\frac{\delta^2}{6} + \frac{2\delta r_B}{3} + r_B^2\right)$$

$$C_3 = (T_\infty - T_w)\left(\frac{\delta^2}{10} + \frac{\delta r_B}{3} + \frac{r_B^2}{3}\right)$$

Interface

Continuity $$\frac{\dot{m}_c}{\rho_\ell} = u_B - \frac{dr_B}{dt} \qquad (6.17)$$

Momentum $$P_B = P_\ell(r_B) \qquad (6.18)$$

Energy $$\dot{m}_c h_{fg} = -\frac{2k_c}{\delta}(T_\infty - T_w) \qquad (6.19)$$

The initial conditions for this problem are as follows:

$$r_B(0) = r_0,$$

$$\delta(0) = 0.,$$

$$\left.\frac{dr_B}{dt}\right|_{t=0.} = 0.,$$

$$T_B(0) = T_{sat}(P_\infty),$$

$$T_w(0) = T_{sat}(P_\infty),$$

$$\dot{m}_c(0) = 0.,$$

$$P_B(0) = P_\infty,$$

$$\rho_B(0) = \rho_{v,sat}(P_\infty),$$

and the initial liquid temperature is $T_\infty$. These initial conditions correspond to the sudden transfer of a vapor bubble into a subcooled pool of stagnant liquid. The step change in the liquid temperature leads to an infinite condensation rate initially. In addition, the liquid energy equation is singular initially due to the initial condition that $\delta(0) = 0$. The latter problem was circumvented by multiplying the energy equation through by $\delta$ and then taking the limit as $\delta$ approaches zero. The resulting equation is:

$$\frac{d\delta^2}{dt} = 12\alpha \qquad (G.20)$$

Then equation (G.20) is integrated over an arbitrarily small time then

$$\delta(t_o) = \sqrt{12\,\alpha\, t_o} \qquad (G.21)$$

Eqn. (G.21) is then substituted into equation (G.19) to yield

$$m_c(t_o) = -\frac{2k_c}{h_{fg}\,\delta(t_o)}(T_\infty - T_w) \qquad (G.22)$$

It was shown in reference (14) that as long as the initial time step size and $t_o$ are of the same order ( $t_o < 10^{-6}$ ) and that

$$m_c^2(t_o)\,\Delta t < 10^{-10} \qquad (G.23)$$

the subsequent numerical solution will not be affected by the choice of $t_o$. The modified initial conditions are presented as follows:

$$r_B(0) = r_o,$$
$$\delta(0) = \delta(t_o),$$

$$\left.\frac{dr_B}{dt}\right|_{t=0.} = -\dot{m}_c(t_0),$$

$$T_B(0) = T_{sat}(P_\infty),$$

$$T_w(0) = T_{sat}(P_\infty),$$

$$m_c(0) = m_c(t_0),$$

$$P_B(0) = P_\infty,$$

$$\rho_B(0) = \rho_{v,sat}(P_\infty),$$

and the initial pool temperature is $T_\infty$.

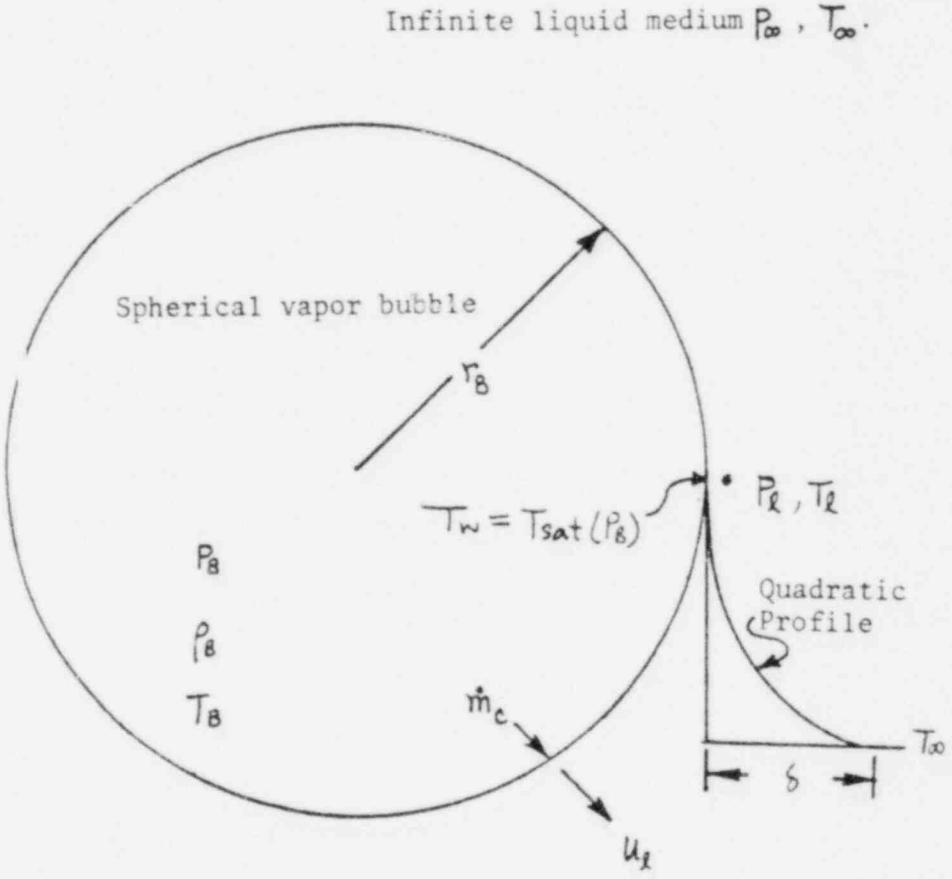


Fig.G.1 Physical Model for Vapor Bubble Dynamics

# APPENDIX H

# THE NUMERICAL PROCEDURE

# AND

# SENSITIVITY STUDIES

H.0 General Description

H.1 Sensitivity of the Choice of the Condensation Region Volume

H.2 Required Time Step for the Pipe Flow Model when Coupled to the Bubble Dynamics Model

H.3 Convergence Test on Chugging Model

H.0 General Description

The equations for the transient flow in the pipe are solved by the method of characteristics. The resulting equations for the forward and backward characteristics are

$$dP^* \pm \rho^* C^* dV^* = \frac{fL}{D} \frac{\rho^*}{k} \frac{V^*|V^*|}{2} \left(\frac{k-1}{k} V^* \mp C^*\right) dt^* \qquad \text{H.1}$$

$$\frac{dz^*}{dt^*} = \frac{V^*}{k} \mp C^* \qquad \text{H.2}$$

and the path characteristic is

$$dP^* - \frac{dP^*}{kC^{*2}} = -\frac{fL}{D}\left(\frac{k-1}{k^3}\right) \frac{\rho^*}{C^{*2}} \frac{V^{*2}}{2} |V^*| dt^* \qquad \text{H.3}$$

$$\frac{dz^*}{dt^*} = \frac{V^*}{k} \qquad \text{H.4}$$

where the starred quantities designate non-dimensionalized variables,

$\rho^*$ = dimensionless steam density

$P^*$ = dimensionless steam pressure

$V^*$ = dimensionless steam velocity

$C^*$ = dimensionless steam sound speed

$t^*$ = dimensionless time

and $f$ = friction factor

$L/D$ = length to diameter ration for the pipe

$k$ = ratio of specific heats

The boundary conditions at the pipe inlet and Region II are both the pressure prescribed conditions while the velocities at both boundaries are found from the characteristics as appropriate. The relation between the time step size and the spacial grid size which ensures a stable solution is found to be

$$\Delta t^* = \frac{\Delta z^*}{c^*(1) + v^*(1)/k} \qquad \text{H.5}$$

In the condensation region (Region II) the Euler method is used to solve the mass balance equation given in Section 4.1.2.

$$\rho_{CON}^{n+1} = \rho_{CON}^{n} + \frac{\Delta t}{V^n}\left(\dot{m}_{in}^{n} - \dot{m}_c^{n} - \rho_{CON}^{n}\left(\frac{dx}{dt}\right)^n A\right) \qquad \text{H.6}$$

where $V$ = volume of condensation region

$= (x + x_c)\, A$

$A$ = pipe cross-sectional area

$(x + x_c)$ = length of condensation region (see Figure H.1)

$\dot{m}_{in}$ = rate of steam inflow

$\dot{m}_c$ = rate of condensation

$\rho_{CON}$ = steam density

$\frac{dx}{dt}$ = interface velocity

The subscript $CON$ indicates the condensation region, superscript $n$ indicates current time step and $(n + 1)$ indicates next time step. The criteria for a stable solution for this equation is found to be (Computer Runs WCR 10, 11, 12, 13)

$$\Delta t = V^2 \qquad \text{H.7}$$

Since $V$ is a variable hence $\Delta t$ is also varied. When coupled to the method of characteristics, the largest $\Delta t$ allowed is given by Eqn. (H.5) when $\Delta t^*$ is converted to its dimensional form. As the volume of region II descreases $\Delta t$ and $\Delta t^*$ are both decreased accordingly.

The pressure in the condensation region is given by the isothermal relation for the steam, i.e.

$$\frac{P_{CON}^{n}}{\rho_{CON}^{n}} = k_1 \qquad \text{H.8}$$

where $k_1$ is given by the initial conditions in the pipe which is assumed to be saturated.

For the chugging model concerning the water slug motion, the momentum equation for the water slug is solved by the Euler method.

$$u^{n+1} = u^n + \frac{\Delta t}{\tau^n}\left\{-\alpha u^{n^2} + [(P_{cw}^n - P_b) - \rho_w x^n]A\right\} \quad \text{H.9}$$

where $\tau^n = \rho_w A(L - (1-\beta)x^n)$

$$\alpha^n = \rho_w A\beta + \rho_w f\frac{(L-x^n)}{2D}A$$

$\rho_w$ = water density

D = pipe diameter

L = submergence depth

and $\beta$ = proportionality constant for the apparent mass of the water slug

$$\beta = \begin{cases} 0.2 & \text{for slug discharge} \\ 0.0 & \text{for slug upflow} \end{cases} \quad \text{H.10}$$

For the conditions in steam chugging, the slug velocities are generally small and moderate pressure changes and are imposed by the condensation region; the stable time step for this equation is generally larger than the one chosen for the condensation region. Hence, this equation does not impose any new criteria for the choice of the time step.

As described in Chapter 4, the present model is based on two different configurations depending on whether the water slug is in the pipe or when the bubble begins to form at the exit. Hence, two different procedures are used to solve this set of equations.

During chugging, using the above set of equations, the steam conditions in the $(n+1)^{th}$ step are determined from the conditions

in the $n^{th}$ step by the procedure presented below:

Procedure A - Step (1) Using the prescribed inlet steam pressure for the $(n + 1)^{th}$ step, compute using the backward travelling and path characteristic to obtain the inlet steam velocity and density.

Step (2) Solve the characteristic equations for the steam pressure, density, and velocity at all the spacial nodes in Region I.

Step (3) Using Eqns. H.6, H.8, determine the steam density and pressure for the $(n + 1)^{th}$ step in Region II.

Step (4) Using pressure result of step (3) obtain exit steam velocity and density from Region I using forward travelling characteristic and path.

Step (5) Compute slug velocity using Eqn. H.9.

These steps are repeated until the slug is discharged out of the vent and proceeded a distance of $\frac{4Y_o}{3}$. This additional length gives the steam a volume of $\frac{4}{3}\pi Y_D^3$ serving as the initial bubble volume for the bubble dynamics model. Then the spacial grids in the pipe are reset extending Region I to cover the entire pipe. The boundary condition at the pipe exit is coupled to the steam bubble dynamics model which is solved by the Runge-Kutta method. The procedure for solving this phase of the calculation is:

Procedure B - Step (1) Same as Procedure A.

Step (2) Same as Procedure A.

Step (3) Using the bubble dynamics model described in Appendix G, determine bubble pressure at $(n + 1)^{th}$ step by Runge-Kutta method. The steam flow into the bubble is determined fr[illegible] the $n^{th}$ step.

Step (4) Using bubble pressure dete[illegible]ined at Step (3), determine steam exit velocity and density using forward travelling characteristic and path.

Step (5) Compute the condensation rate at the pipe wall using condensation model with a heat transfer surface given by the submerged surface of the vent pipe.

Step (6) Subtract the condensation rate from the steam exit flow rate to determine the actual steam flow into the bubble.

This procedure is repeated until the bubble collapse occurs and when the chugging criteria (Table 4.1) are met. Then the calculation switches back to procedure A. Note that no condensation region is used in the pipe but the condensation which occurs at the pipe wall is accounted for by subtracting it from the exit flow.

## H.1 Sensitivity to the Choice of the Condensation Region Volume

The volume of the condensation region during upflow is given by

$$V = (x + x_c) A \qquad \text{H.11}$$

TABLE H.1

| | |
|---|---|
| Vent Pipe Region I | Method of Characteristics |
| Vent Pipe Region II (Condensation Region) | Euler Method |
| Bubble Dynamics | Runge-Kutta Method |
| Bubble Collapse | Runge-Kutta Method |
| Chugging Model | Euler Method |

Initially the slug is at the exit, x is equal to the submergence depth, thus

$$V_{initial} = (L + x_c)A \qquad \text{H.12}$$

Recall from previous discussion, the time step required for the condensation region is given by Eqn. H.7.

$$\Delta t = V^2$$

Hence as the slug moves up the vent, $V$ decreases and $\Delta t$ decreases also. The choice of $x_c$ becomes critical here because if the slug approaches a height of $(L + x_c)$, the time ste, is reduced drastically due to the decrease in the volume of the condensation region. Normally, $x_c$ is chosen to be large enough such that no chugs in the given pool temperature range would exceed a ' ight of $(L + x_c)$ from the exit. However, due to the limitations by the time step, it is desirable to use a large $x_c$ to reduce the computation cost. In Runs RV5 and 6 $x_c$ is varied from 25.4 cm to 50.8 cm and the solution is compared to identify the dependence of the final solution to the choice of $x_c$. It is found that the calculated chug height and the computed time at which this maximum is attained does not differ by over 10%. Table H.2 depicts this comparison. Thus it is concluded that the dependence of the solution on the choice of $x_c$ is small.

## H.2 Required Time Step for Bubble Dynamics Model When Compled to Pipe Flow Model

Since the bubble dynamics model is solved by the Runge-Kutta method, which uses a much smaller time step than the one used in the transient pipe flow model, the coupling between the two is more complicated. The time step used in the pipe flow model is used as

TABLE H.2

| Run No. RV5 | Time, sec. | Chug Height, cm |
|---|---|---|
| $x_c$ = 25.4 cm | .006082 | .2926 |
| | .007252 | .3993 |
| | .008421 | .5029 |
| | .009591 | .5791 |
| | .01076 | .6126 |
| | .01207 | .6035 |

| Run No. RV6 | Time, sec. | Chug Height, cm. |
|---|---|---|
| $x_c$ = 50.8 cm | .006468 | .3440 |
| | .007511 | .4389 |
| | .008554 | .5242 |
| | .009597 | .5883 |
| | .01064 | .6218 |
| | .01175 | .6248 |
| | .01315 | .5913 |

Conditions for these two runs:

(1) Pipe radius = 2.54 cm

(2) Submergence depth = 25.4 cm

(3) Pipe total length = 337.8 cm

(4) Initial pipe pressure = .956 atm.

(5) Initial velocity of steam = 7.62 m/sec

(6) Steam mass flux at pipe inlet = 7.56 gm/sec

(7) Pool temperature = 53.9°C

(8) Pool surface pressure = 1.0 atm.

the time interval for the computations in the bubble dynamics model. At he end of this time interval, the computed bubble pressure is fed back to the pipe flow model. However, if the time step used in the pipe model is too large, then large changes in the bubble dynamics may have been calculated before the computed bubble pressure is fed back to the pipe flow model causing large inaccuracies in the pipe flow model and consequently large errors in the solution. Run No. WCR16A and WCR17 are made to identify the correct time step to be used in the pipe flow model. The results show that the time step in the pipe given in Eqn. H.5 has to be reduced by a factor of eight during the bubble growth period. Identical results were obtained in the two runs when in WCR17 the time step was reduced by a factor of eighty.

## H.3 Convergence Tests

A convergence test is performed by reducing the time step by a factor of two twice. The results are the same for all three runs indicating that the time step criteria given previously are adequate.

The same procedure was performed in testing the bubble collapse model. The resulting peak pressures did not differ by 1% for all three cases indicating the choice of the time step in the bubble collapse model is adequate.

TABLE H.3

COMPUTER RUN RECORD

| Run No. | Purpose/Results |
|---|---|
| RV5 | $x_c$ = 30.5 cm |
| RV6 | $x_c$ = 61. cm |
| | Solution insensitive to $x_c$ |
| WCR16A | Time step reduction factor = 8 |
| WCR17 | Time step reduction factor = 80 |
| | Solution the same, factor of 8 is adequate. |
| CONV 1, 2, 3 | Convergence Test of Chugging Model |
| SPIKE 24, 25, 26 | Convergence Test of Chugging Bubble Collapse Model |

# APPENDIX I

## THE COMPUTER PROGRAMS AND THE LISTINGS

Vent Pipe Model

| Routine Name | Calculation |
|---|---|
| MAIN | Method of Characteristics, Water Slug Model, Upstream Boundary Condition |
| XPEXP | Interpolates Surge Tank Pressure from Input |
| HTPROP | Heat Transfer Properties of Water |
| XRKGS | Runge-Kutta Procedure for Solving Bubble Bubble Growth Equations |
| INTERP | Interpolation of Steam Table Properties |
| SBUB | Bubble Growth Model and the Initial Conditions |
| FCT | Computes the Derivatives for the Runge-Kutta Procedure from the Governing Equations Given in Appendix G |
| OUTP | Output of All Calculated Quantities in the Bubble Growth Model |

Bubble Collapse Model

| Routine Name | Calculation |
|---|---|
| MAIN | Same as SBUB |
| HTPROP | Same as in Vent Pipe Model |
| RKGS | Same as XRKGS |
| INTERP | Same as in Vent Pipe Model |
| SBUB | " " |
| OUTP | " " |

```
      IMPLICIT REAL*8(A-H,O-Z)
      DOUBLE PRECISION MINF,K
      COMMON/STBUB/XPINF,XDTT,XRW,XRG,YY(8),XAIN,XR0
      COMMON/VELOC/YYY(500),CI,PP0,DD0,NPTS
      DIMENSION P(25),P0(25),V(25),V0(25),R(25),R0(25),Z(25),
     1Z0(25),C(25),C0(25)
      XP(Z,Z1,Z2)=(Z-Z1)/Z2
      F(A1,A2,A3,A4,A5,A6)=(A2-A1)/2.*A4+(1.-A2)*A3+(A2+A1)/2.*A5*A6/A6
      G(B1,B2,B3)=-2.*B3/(B1+DSQRT(B1*B1-4.*B2*B3))
C-----------------------------------------------------------------------
C----------GEOMETRIC CONDITIONS
      READ(5,444)NPTS
  444 FORMAT(I5)
      READ(5,333)(YYY(I),I=1,NPTS)
  333 FORMAT(10D8.4)
      WRITE(6,666)(YYY(I),I=1,NPTS)
  666 FORMAT(5X,10D12.4)
C-----------------------------------------------------------------------
C----------COMMON BLOCK VELOC
C-----------------------------------------------------------------------
      PP0=0.0
      DD0=.03246
C-----------------------------------------------------------------------
      RAD0=2.014/12.
      OUTR=2.25/12.
      XLS=21.65/12.
      XLA=68.11/12.
      XLSUB=XLS
      XL=XLA+XLS
      XL=XL+4.*RAD0/3.
      XLEQ=XL
      XLS=XLS+4.*RAD0/3.
      AREA=3.1416*RAD0*RAD0
      SCALER=0.875/12.
C-----------------------------------------------------------------------
C----------CONSTANTS FOR THE INLET BOUNDARY CONDITIONS
C-----------------------------------------------------------------------
      R0=.038
      P0=15.
      XM=.01666 *1.2
      COEF=125.
      TVALVE=1./COEF
      AVALVE=3.1416/144.
C-----------------------------------------------------------------------
C----------THERMAL HYDRAULIC CONDITIONS
C-----------------------------------------------------------------------
      PINF=30.67
      TSAT=252.0
      HFG=944.1
      RHOG=.07477
      RHOF=58.74
```

```
            BETA=.2
            FLD=1.615
      GC=32.2
      GGC=144.*GC/RHOW
      RW=RHOW
      PINF=PINF+XLSUB*RW/144.
            DTT=191.2
            TWATER=TSAT-DTT
            XMU=1.65-0.0122*(TWATER-100.)
            XMU=XMU/3600.
            CALL HTPROP(XKK,ALFA,SIGMA,TWATER)
                  FILMH=(GC*RW*RW*HFG/XMU/XKK/DTT)**.25*1.13*XKK
            FILMH=FILMH*14.
            RFILMH=FILMH *2.    /2.
                  WRITE(6,270)TWATER,XKK,ALFA,SIGMA,FILMH
  270       FORMAT(10X,'TEMP WATER=',E11.4,'THERMAL COND=',E11.4,
     1                  'THERMAL DIFF=',E11.4,'SURFACE TENSION=',E11.4,
     2              'WALL HT COEF=',E11.4)
C-------------------------------------------------------------------------
C----------VARIABLES IN COMMON BLOCK STBUB
C------------------------------ --------------------------------------
            XPINF=PINF
            XDTT=DTT
            XRW=RHOW
            XRG=RHOG
            XAIN=AREA
            XRO=RADO
C-------------------------------------------------------------------------
      WRITE(6,210)XLA,XLS,XLEQ,FLD,AREA
  210 FORMAT(5X,'XLA=',E11.4,'FT.  XLS=',E11.4,'FT.    XLEQ=',E11.4,
     1'FT.    FLD=',E11.4,/,5X,'AEQUI=',E11.4,' SQ.FT.',/)
C------------------------------ --------------------------------------
C----------SATURATED VAPOR CURVE NEAR ATMOSPHERIC PRESSURE
C------------------------------ --------------------------------------
            XK1=14.7/.0373
      K=1.3
      PREF=14.7
      RREF=.0373
      GRAD=.00242
C------------------------------ --------------------------------------
      CF=1.E-06
            PI=31.24
                  RI=RREF+GRAD*(PI PREF)
                  CI=DSQRT(144.*32.2*PI/RI)
            VTANK=1.57
```

```
      PTANKO=32.66
      RTANKO=RREF*GRAD*(PTANKO-PREF)
      C1=PTANKO*RTANKO**(-K)
      XMOUT=0.
      WRITE(6,213)RI,PI,CI,PINF
  213 FORMAT(5X,'INITIAL CONDITIOMS RI=',E11.4,'LBM/CU.FT.    PI=',E11.4
     1 ,'PSIA   SONIC SPEED=',E11.4,'FT/SEC    PINF=',E11.4,'PSIA',/)
      WRITE(6,214)K,RW
  214 FORMAT(5X,'SPECIFIC HEAT RATIO=',E11.4,5X,'WATER DENSITY=',E11.4,'
     1LBM/CU.FT.',/)
C-------------------------------------------------------------------------
C----------NON-DIMENSIONALIZE PARAMETERS
C-------------------------------------------------------------------------
      XMO=XM/RI/CI/AREA
      PINF=PINF/PI
      TMAX=1.
      TMAX=TMAX*CI/XL
      PREF=PREF/PI
      RREF=RREF/RI
C-------------------------------------------------------------------------
C----------CONTROL LOGIC
C----------NBUB=1 AIR BUBBLE,NBUB=2 STEAM BUBBLE
C----------NDC=TIME STEP REDUCTION FACTOR WHEN CONDENSATION OCCUR
C----------NV=0    FOR CONSTANT STAGNANT CONDITION UPSTREAM
C----------NV=1 FOR CONDITION OF CONSTANT FLOW AT VALVE
C----------NV=2 VELOCITY AT VALVE IS GIVEN
C----------NSTART=1 START FROM SLUG DISCHARGE
C----------NSTART=0 START FROM BUBBLE COLLAPSE
C----------NP=OUTPUT FREQUENCY FOR SLUG INFO,NP MUST BE MULTIPLE OF NJUMP
C----------NJUMP=OUTPUT FREQUENCY FOR VENT PIPE INFO
C----------NR=1 WHEN REVERSE FLOW OF SLUG OCCUR,ZERO OTHERWISE
C----------NOUNT FOR CONTROLLING UPWARD OR DOWNWORD FLOW OF SLUG
C----------NV=3 SURGE TANK MODEL FOR STEAM INFLOW
C----------NV=4 SURGE TANK PRESSURE GIVEN
C----------MOUNT=1 DURING REVERSE FLOW,0 OTHERWISE
C----------NDROP=1 WHEN VENT PRESSURE DROPS IN INITIAL CHUG 0 OTHERWISE
      MOUNT=0
      NBUB=2
      ND=8
          NDC=100
      N=24
      NSKIP=0
      NV=4
      NP=20
      NJUMP=80
      NMAX=200
```

```
                NR=0
                NSTART=0
          NDROP=1
C-----------------------------------------------------------------------
C----------INITIAL WATER SLUG CONDITIONS
          TCHUG=0.
          RCHUG=0.
          DELAY=0.
          WIDTH=0.040
                RMAX=0.
                ZP0=0.
                ZP=ZP0
                XBAR=ZP0*XL
       DXBAR=0.
          DZP=0.
C-----------------------------------------------------------------------
C----------LOUNT FOR AFTER VENT CLEARING STEP COUNTING
C----------KOUNT FOR BUBBLE MOTION STEP COUNTING
C----------JOUNT FOR CONDENSATION AT WALL STEP COUNTING
C----------IOUNT FOR OVERALL STEP COUNTING
       KOUNT=0
       LOUNT=0
       IOUNT=0
                ICMI=IOUNT-1
          JOUNT=1
                NOUNT=0
C-----------------------------------------------------------------------
C----------INITIAL VENT PIPE CONDITIONS
C-----------------------------------------------------------------------
          TOT1=0.
          TOT2=0.
          TOT3=0.
          TOT4=0.
          TOT5=0.
       T=0.
       TIME=0.
       NM1=N-1
       NP1=N+1
       DO 1 I=1,NP1
       P(I)=1.
       V(I)=0.
       C(I)=1.
       R(I)=1.
       PO(I)=1.
          VO(I)=25.0*K/CI
       CO(I)=1.
```

```
      RO(I)=1.
      ZO(I)=(I-1)*XLA/XL/(N-1)
      Z(I)=ZO(I)
    1 CONTINUE
C-------------------------------- ----------------------------------------
       DZ=XLA/XL/(N-1)
      SMAX=VO(1)/K+CO(1)
      DT=DZ/SMAX
      DTIME=DT*XL/CI
            IF(NSTART.EQ.0)GO TO 300
      GO TO 50
    4 CONTINUE
      IF(T.GT.TMAX) GO TO 99
      IOUNT=IOUNT+1
      DO 2 I=2,NM1
      VPCM=VO(I-1)/K+CO(I-1)
      VMCP=VO(I+1)/K-CO(I+1)
      VPCP=VO(I+1)/K+CO(I+1)
      VMCM=VO(I-1)/K-CO(I-1)
      VP=VO(I)/K
      VPC=VO(I)/K+CO(I)
      VMC=VO(I)/K-CO(I)
      DEL=DZ/DT
      AP=VPCM/2.-VPC+VPCP/2.
      BP=VPCP/2.-VPCM/2.+DEL
      AM=VMCM/2.-VMC+VMCP/2.
      BM=VMCP/2.-VMCM/2.+DEL
      APP=(VO(I-1)/2.-VO(I)-VO(I+1)/2.)/K
      BPP=(VO(I+1)/2.-VO(I-1)/2.)/K+DEL
      ZA=ZO(I)+DZ*G(BP,AP,VPC)
      ZB=ZO(I)+DZ*G(BM,AM,VMC)
      ZD=ZO(I)+DZ*G(BPP,APP,VP)
      XPZA=XP(ZA,ZO(I),DZ)
      XPZA2=XPZA*XPZA
      XPZB=XP(ZB,ZO(I),DZ)
      XPZB2=XPZB*XPZB
      XPZD=XP(ZD,ZO(I),DZ)
      XPZD2=XPZD*XPZD
      PA=F(XPZA,XPZA2,     PO(I),PO(I-1),PO(I+1),ZA)
      RA=F(XPZA,XPZA2,     RO(I),RO(I-1),RO(I+1),ZA)
      CA=F(XPZA,XPZA2,     CO(I),CO(I-1),CO(I+1),ZA)
      VA=F(XPZA,XPZA2,     VO(I),VO(I-1),VO(I+1),ZA)
      PB=F(XPZB,XPZB2,     PO(I),PO(I-1),PO(I+1),ZB)
      RB=F(XPZB,XPZB2,     RO(I),RO(I-1),RO(I+1),ZB)
      CB=F(XPZB,XPZB2,     CO(I),CO(I-1),CO(I+1),ZB)
      VB=F(XPZB,XPZB2,     VO(I),VO(I-1),VO(I+1),ZB)
```

```
      PD=F(XPZD,XPZD2,     PO(I),PO(I-1),PO(I+1),ZD)
      RD=F(XPZD,XPZD2,     RO(I),RO(I-1),RO(I+1),ZD)
      CD=F(XPZD,XPZD2,     CO(I),CO(I-1),CO(I+1),ZD)
      VD=F(XPZD,XPZD2,     VO(I),VO(I-1),VO(I+1),ZD)
      SMB=FLD*RB/K*VB*DABS(VB)/2.*((K-1.)/K*VB+CB)*DT
      SPA=FLD*RA/K*VA*DABS(VA)/2.*((K-1.)/K*VA-CA)*DT
      SRD=-FLD*(K-1.)/K/K/K*RD/CD/CD*VD*VD/2.*DABS(VD)*DT
      RCVA=RA*CA*VA
      RCVB=RB*CB*VB
      RCFAC=1./(RA*CA+RB*CB)
      P(I)=RCFAC*(RB*CB*(PA+RCVA+SPA)+RA*CA*(PB-RCVB+SMB))
      V(I)=RCFAC*(PA-PB+RCVA+RCVB+SPA-SMB)
      R(I)=RD+1./K/CD/CD*(P(I)-PD)+SRD
      C(I)=DSQRT(P(I)/R(I))
2     CONTINUE
      IF(ZP.GE.XLS/XL) GO TO 10
          BETA=.2
               IF(DXBAR.LE.0.)BETA=0.000001
      OZP=ZP
          ODZP=DZP
      PPOOL=PINF*PI
      D2XBAR=GGC*(P(N)*PI-PPOOL)-BETA*DXBAR*DXBAR+GC*(XLS-XBAR)
      D2XBAR=D2XBAR/(XLS-(1.-BETA)*XBAR)
      DXBAR=D2XBAR*DTIME+DXBAR
          IF(DXBAR.GT.0..AND.NOUNT.EQ.0)NR=0
               IF(DXBAR.GT.0..AND.NOUNT.EQ.1)ZP0=OZP
          IF(DXBAR.GT.0..AND.NOUNT.EQ.1)JOUNT=0
               IF(DXBAR.GT.0..AND.NOUNT.EQ.1)NOJNT=0
      XBAR=DXBAR*DTIME+XBAR
      ZP=XBAR/XL
      DZP=(ZP-OZP)/DT
      VW=DXBAR*K/CI
      ICM1=IOUNT-1
      IF(((ICM1/NP)*NP.EQ.ICM1)WRITE(6,230)TIME,XBAR,DXBAR
      IF(ZP.GE.XLS/XL)GO TO 9
  230 FORMAT(15X,'TIME=',E11.4,2X,'SLUG POSITION=',E11.4,2X,
     1'SLUG VELOCITY=',E11.4)
      GO TO 15
    9 CONTINUE
          LOUNT=LOUNT+1
          NDROP=0
      VCTIME=TIME-(ZP-XLS/XL)*DTIME/(ZP-OZP)
      WRITE(6,220)VCTIME,DXBAR
  220 FORMAT(/,15X,'VENT CLEARING TIME=',E11.4,/,
     110X,'VENT CLEARING VELOCITY=',E11.4,/)
```

```
C-----------------------------------------------------------------------
C----------FOR STEAM BUBBLE AFTER VENT CLEAR RESET ALL NODE POINTS
C-----------------------------------------------------------------------
      IF(NBUB.EQ.1)GO TO 21
      DO 401 I=1,N
      WRITE(6,888)I,ZO(I),PO(I),VO(I),RO(I),CO(I)
  401  CONTINUE
      TIME=VCTIME
      DZO=DZ
      DZ=1./DFLOAT(N-1)
      M=(XLA/XL+ZP0)/DZ
      DO 20 I=1,N
      Z(I)=DZ*DFLOAT(I-1)
   20 CONTINUE
      DO 22 I=2,M
      DO 23 J=1,N
      DIF=Z(I)-ZO(J)
      IF(DIF.LE.0.)GO TO 24
   23 CONTINUE
   24 CONTINUE
      PARAM=(Z(I)-ZO(J-1))/DZO
      P(I)=PO(J-1)+PARAM*(PO(J)-PO(J-1))
      V(I)=VO(J-1)+PARAM*(VO(J)-VO(J-1))
      R(I)=RO(J-1)+PARAM*(RO(J)-RO(J-1))
      C(I)=CO(J-1)+PARAM*(CO(J)-CO(J-1))
   22 CONTINUE
      P(1)=PO(1)
      V(1)=VO(1)
      R(1)=RO(1)
      C(1)=CO(1)
      MP1=M+1
      AAA=ZO(N)
      888=1.-AAA
      DO 25 I=MP1,N
      P(I)=PCOND/PI
      R(I)=RCON/RI
      C(I)=DSQRT(P(I)/R(I))
      V(I)=(Z(I)-AAA)*(VW-VO(N))/888 +VO(N)
   25 CONTINUE
      DO 26 I=1,N
      PO(I)=P(I)
      VO(I)=V(I)
      RO(I)=R(I)
      CO(I)=C(I)
      ZO(I)=Z(I)
```

```
      WRITE(6,888)I,ZO(I),PO(I),VO(I),RO(I),CO(I)
   26 CONTINUE
   21 CONTINUE
C-----------------------------------------------------------------------
      VWO=0.
      RADO=RADO
      RHOBO=R(N)*RI
      PBO=P(N)*PI
      TCHUG=0.
      PCHUG=P(N)
      WRITE(6,250)TIME,RADO,VWO,RHOBO,PBO
      DT=DZ/SMAX*0.8/DFLOAT(ND)
      DTIME=DT*XL/CI
      GO TO 15
   10 CONTINUE
      KOUNT=KOUNT+1
      IF(NSUB.EQ.1)GO TO 17
      TIN=PO(N)*PI*144./RO(N)/RI/85.76
C-----------------------------------------------------------------------
C----------VARIABLES IN ARGUMENT IN CALL SBUB
C-----------------------------------------------------------------------
      XPEND=PO(N)*PI
      X11=XLS-4.*RADO/3.
      QTOT1=FILMH*3.1416*RADO*2.*DTT*(X11)**.75
      X22=2.*RADO-4.*RADO/3.
      IF(X22.LT.0.)X22=0.
      QTOT2=FILMH*3.1416*OUTR*2.*DTT*(X22)**.75
      QTOT1=QTOT1+QTOT2
      XMCOND=QTOT1*DTIME/HFG
      XMCW=XMCOND/DTIME/AREA
      XMDOT=RO(N)*RI*VO(N)*CI/K-XMCW
      IF(XMDOT.LT.0.)XMCOND=(XMDOT+XMCW)*DTIME*AREA
      IF(XMDOT.LT.0.)XMDOT=0.
      TOT4=TOT4+XMDOT*AREA*DTIME
      TOT5=TOT5+XMCOND
      XTIN=TIN
      XVW=VWO
      XTIME=TIME
      XDTIME=DTIME
      XRG=RO(N)*RI
      CALL SBUB(XPEND,XMDOT,XTIN,XVW,XPB,XTIME,XDTIME,LOUNT)
      PB=XPB
      VW=XVW
      RHOB=YY(2)*RHOW
      RAD=YY(7)*RADO
```

```
            IF(RMAX.LT.RAD)RMAX=RAD
          SUMP=0.
          DO 404 I=1,N
          SUMP=SUMP+PO(I)
404       CONTINUE
          PBAR=SUMP/DFLOAT(N)
          TWOR=1.5*RADO
          TCHUG=TCHUG+DTIME
          FACT=0.5*RMAX
          IF(PCHUG.LT.PINF)FACT=0.9*RMAX
          IF(RAD.GT.TWOR)FACT=0.983*RMAX
          IF(RAD.LT.FACT.AND.PBAR.LT.PINF)GO TO 300
          LOUNT=LOUNT+1
          GO TO 18
 17       CONTINUE
      VW=VWO+(-3.*VWO*VWO/2.+(P(N)*PI-PINF)*GGC)*DTIME/RADO
      RAD=RADO+VWO*DTIME
      RHOB=RHOBO-RHOBO*VWO*DTIME/RADO
      RHOB=RHOB+3.*R(N)*RI*V(N)*CI/K*RO*RO*DTIME/4.
      PB=PBO+XKI*(RHOB-RHOBO)
 18       CONTINUE
      P(N)=PB/PI
111       CONTINUE
      VCN=VO(N)/K+CO(N)
      VCNM1=VO(N-1)/K+CO(N-1)
      ZA=ZO(N)-VCN*DT/(1.+(VCN-VCNM1)/DZ*DT)
      ZX=(ZO(N)-ZA)/DZ
      PA=PO(N)-(PO(N)-PO(N-1))*ZX
      RA=RO(N)-(RO(N)-RO(N-1))*ZX
      VA=VO(N)-(VO(N)-VO(N-1))*ZX
      CA=CO(N)-(CO(N)-CO(N-1))*ZX
      FMC=FLD*RA/K*VA*DABS(VA)*((K-1.)/K*VA-CA)*DT/2.
          V(N)=VA-(P(N)-PA)/RA/CA+FMC/RA/CA
      I=N
      FACC=(VO(I)-VO(I-1))*DT/DZ/K
      ZD=ZO(N)-(DZ*VO(N))/(VO(N)-VO(N-1)+DZ/DT)
      VD=VO(I-1)+(VO(I)-VO(I-1))*(ZD-ZO(I-1))/DZ
      RD=RO(I-1)+(RO(I)-RO(I-1))*(ZD-ZO(I-1))/DZ
      PD=PO(I-1)+(PO(I)-PO(I-1))*(ZD-ZO(I-1))/DZ
      CD=CO(I-1)+(CO(I)-CO(I-1))*(ZD-ZO(I-1))/DZ
      SRD=-FLD*(K-1.)/K/K/K*RD/CD/CD*VD*VD/2.*DABS(VD)*DT
      R(I)=RD+1./K/CD/CD*(P(I)-PD)+SRD
      C(N)=DSQRT(P(N)/R(N))
          IF(NBUB.EQ.2.AND.LOUNT.LT.2)GO TO 222
```

300

```
            VWO=VW
            RADO=RAD
            RHOBO=RHOB
            PBO=PB
                IF((ICM1/NP)*NP.NE.ICM1)GO TO 1555
            WRITE(6,789)XMCOND
  789       FORMAT(5X,'CONDEN=',D15.8)
            WRITE(6,250)TIME,RADO,VWO,RHOBO,PBO
  250 FORMAT(5X,'TIME=',D15.9,'BUB RAD=',E11.4,'BUB VEL=',E11.4,
     1'BUB DEN=',E11.4,'END PRES=',E11.4)
 1555           CONTINUE
C-------------------------------------------------------------------
       GO TO 16
   15 CONTINUE
                IF(NR.EQ.1)GO TO 302
C-------------------------------------------------------------------
C----------ASSUME NO CONDENSATION UNTIL SLUG HAS MOVED BY XLENGT
C-------------------------------------------------------------------
            XLENGT=0.1*XLS/XL
                 ZZZ=OZP-ZP0
                  IF(NBUB.EQ.2.AND.ZZZ.GT.XLENGT)GO TO 19
C----------SLUG END CONDITION FOR CHARACTERISTICS =OR NO CONDENSATION
C-------------------------------------------------------------------
       V(N)=V(N-1)+DZ/(DZP*DT+DZ)*(VW-V(N-1))
       IF(ZP.GE.XLS/XL)V(N)=VW*4.
       VCN=VO(N)/K+CO(N)
       VCNM1=VO(N-1)/K+CO(N-1)
       ZA=ZO(N)-VCN*DT/(1.+(VCN-VCNM1)/DZ*DT)
       ZX=(ZO(N)-ZA)/DZ
       PA=PO(N)-(PO(N)-PO(N-1))*ZX
       RA=RO(N)-(RO(N)-RO(N-1))*ZX
       VA=VO(N)-(VO(N)-VO(N-1))*ZX
       CA=CO(N)-(CO(N)-CO(N-1))*ZX
       FMC=FLD*RA/K*VA*DABS(VA)*((K-1.)/K*VA-CA)*DT/2.
       P(N)=PA-RA*CA*(V(N)-VA)+FMC
       I=N
       FACC=(VO(I)-VO(I-1))*DT/DZ/K
       ZD=ZO(N)-(DZ*VO(N))/(VO(N)-VO(N-1)+DZ/DT)
       VD=VO(I-1)+(VO(I)-VO(I-1))*(ZD-ZO(I-1))/DZ
       RD=RO(I-1)+(RO(I)-RO(I-1))*(ZD-ZO(I-1))/DZ
       PD=PO(I-1)+(PO(I)-PO(I-1))*(ZD-ZO(I-1))/DZ
       CD=CO(I-1)+(CO(I)-CO(I-1))*(ZD-ZO(I-1))/DZ
       SRD=-FLD*(K-1.)/K/K/K*RD/CD/CD*VD*VD/2.*DABS(VD)*DT
```

```
      R(I)=RO+1./K/CO/CO*(P(I)-PO)+SRO
      C(N)=DSQRT(P(N)/R(N))
      GO TO 16
   19      CONTINUE
C-----------------------------------------------------------------------
C----------CONDENSATION REGION BOUNDARY CONDITION
C-----------------------------------------------------------------------
           IF(JOUNT.EQ.1)RCONO=R(N)*RI
           IF(JOUNT.EQ.1)PCONDO=P(N)*PI
           IF(JOUNT.EQ.1)DT=DT/DFLOAT(NDC)
           IF(JOUNT.EQ.1)DTIME=DTIME/DFLOAT(NDC)
           IF(JOUNT.EQ.1)XK1=P(N)*PI/R(N)/RI
           JOUNT=JOUNT+1
                XLN=(OZP-ZPO)*XL
                 QTOT=FILMH*3.1416*RADO*2.*DTT*(X_N)**.75
                QTOT=QTOT*DTIME
           XMCOND=QTOT/HFG
           TOT1=TOT1+XMCOND
           XMIC=RO(N)*RI*VO(N)*CI/K*DTIME*AREA
                VOLC=AREA*XLN
           RCON=RCONO+(XMIC-XMCOND-RCONO*ODZP*DT*XL*AREA)/VOLC
           PCOND=PCONDO+XK1*(RCON-RCONO)
           P(N)=PCOND/PI
           IF((JOUNT/200)*200.EQ.JOUNT)DTIME=VOLC*0.001
           DT=DTIME*CI/XL
           GO TO 111
  222      CONTINUE
           RCONO=RCON
           PCONDO=PCOND
           IF(DXBAR.GT.0..AND.MOUNT.EQ.1)GO TO 7
  777      CONTINUE
       IF((ICM1/NP)*NP.NE.ICM1)GO TO 16
           WRITE(6,260)PCOND,RCON,XMCOND,XMIC,VOLC,JOUNT
  260      FORMAT(5X,'CONDENSATION REGION',/,15X,'PRES=',E11.4,'DEN=',
     1             E11.4,'CONDEN=',E11.4,'INFLOW=',E11.4,'VOLUME=',E11.4,
     2             I5)
           GO TO 16
C-----------------------------------------------------------------------
C----------REVERSE FLOW OF SLUG CONDENSATION REGION
C-----------------------------------------------------------------------
  302           CONTINUE
           MOUNT=1
           TREV=TREV+DTIME
           JOUNT=JOUNT+1
           XLL=XCH+OZP*XL
           XCONL=OZP*XL
           TERM=DELAY+WIDTH
           QTOT=0.
           IF(TREV.GT.DELAY.AND.TREV.LT.TERM)QTOT=2.3*DTT*RADO/SCALER
```

```
      IF(NDROP.EQ.1.AND.QTOT.GT.0.0)GO TO 405
      IF(OZP.LT.0.)XCONL=0.
      QTOT=RFILMH*3.1416*RADO**2.*DTT*(XCONL)**.75
      IF(TREV.GT.0.106.AND.TREV.LT.0.163)GO TO 406
      IF(TREV.GT.0.057)GO TO 405
406   CONTINUE
      TWOR=1.5*RADO
      IF(TCHUG.GT.0.025.AND.RCHUG.GT.TWOR)QTOT=2.3*DTT *RADO/SCALER
405   CONTINUE
      QTOT=QTOT*DTIME
      XMCOND=QTOT/HFG
      TOT2=TOT2+XMCOND
      XMIC=RO(N)*RI*VO(N)*CI/K*DTIME*AREA
      VOLC=AREA*XLL
      RCON=RCONO+(XMIC-XMCOND-RCONO*ODZP*DT*X_*AREA)/VOLC
      PCOND=PCONDO+XK1*(RCON-RCONO)
      P(N)=PCOND/PI
      GO TO 111
C-------------------------------- ----------------------------------------
   16 CONTINUE
      DO 3 I=1,N
      PO(I)=P(I)
      VO(I)=V(I)
      CO(I)=C(I)
      RO(I)=R(I)
    3 CONTINUE
      IF(IOUNT.LT.NSKIP)GO TO 6
            IF((ICM1/NJUMP)*NJUMP.NE.ICM1)GO TO 6
      WRITE(6,402)TIME,TOT1,TOT2,TOT3,TOT4,TOT5
402   FORMAT(2X,'MASS BALANCE',5X,5D15.8)
      WRITE(6,107)
      WRITE(6,110)
      DO 5 I=1,N
      OC=CO(I)*CI
      OV=CI*VO(I)/K
      OP=PO(I)*PI
      OZ=XL*ZO(I)
      OR=RI*RO(I)
            IF(DABS(VO(I)).LT..00001)OV=0.
      WRITE(6,106)I,OZ,OP,OV,OR,OC
    5 CONTINUE
    6 CONTINUE
      IF(ZP.GE.XLS/XL) GO TO 50
C----------NO SHIFTING OF NODES IF CONDENSATION IN PIPE EXISTS
      IF(NBUB.EQ.2)GO TO 50
```

```
C-------------------------------------------------------------------------
C----------NR=1 WATER SLUG CHUGS UP THE PIPE,ZERO OTHERWISE
C----------SHIFTING OF NODES DUE TO SLUG MOTION
C-------------------------------------------------------------------------
    7 CONTINUE
      DZO=DZ
      DZ=(XLA/XL+ZP)/(N-1)
      NM1=N-1
       DO 8 I=1,NM1
      Z(I)=(I-1)*DZ
      ZO(I)=Z(I)
    8 CONTINUE
      ZO(N)=(N-1)*DZ
                DT=DZ/SMAX*.8
                DTIME=DT*XL/CI
           MOUNT=0
           GO TO 777
   50 IF(VO(2)/K.GE.CO(2)) GO TO 52
                IF(T.GT.TMAX)GO TO 99
      TIME=TIME+DTIME
      T=T+DT
      ASTAR=COEF*AVALVE*TIME
      IF(ASTAR.GT.AVALVE)ASTAR=AVALVE
      XM=XMO*ASTAR/AVALVE
      VMC1=VO(1)/K-CO(1)
      VMC21=VO(2)/K-CO(2)-VMC1
      ZB=VMC1*DT/(1.+VMC21/DZ*DT) *(-1.)
      PB=PO(1)+(PO(2)-PO(1))*ZB/DZ
      VB=VO(1)+(VO(2)-VO(1))*ZB/DZ
      RB=RO(1)+(RO(2)-RO(1))*ZB/DZ
      CB=CO(1)+(CO(2)-CO(1))*ZB/DZ
      IF(NV.EQ.1)GO TO 53
                IF(NV.EQ.2)GO TO 56
           IF(NV.EQ.3)GO TO 57
           IF(NV.EQ.4)GO TO 58
      A=XM*PO*K/PI
      B=XM*RO/RI*(K-1.)/2./K
      S=RB*CB
      D=PB-S*VB+FLD*RB/K*VB*DABS(VB)/2.*((K-1.)/K*VB+CB)*DT
      CPB=S+B
      DCB=D/CPB
      V(1)=(-DCB+DSQRT(DCB*DCB+4.*A/CPB))/2.
      P(1)=S*V(1)+D
      R(1)=P(1)/(PO/PI*RI/RO-(K-1.)/2./K/K*V(1)*V(1))
```

```
      C(1)=DSQRT(P(1)/R(1))
      IF(V(1).LT.C(1)*K) GO TO 4
      GO TO 52
   53 CONTINUE
      VV=VO(1)
      S=RB*CB
      D=PB-S*VB+FLD*RB/K*VB*DABS(VB)/2.*((K-1.)/K*VB+CB)*DT
   55 CONTINUE
      PV=D+S*VV
                 RV=RREF*(PV/PREF)**(1./K)
      VVN=XM*K/RV
      IF(DABS(VVN-VV).LE.CF)GO TO 54
      VV=VVN
      GO TO 55
   54 CONTINUE
      P(1)=PV
      V(1)=VV
      R(1)=RV
      C(1)=DSQRT(P(1)/R(1))
      IF(V(1).LT.C(1)*K)GO TO 4
   56              CONTINUE
      S=RB*CB
      D=PB-S*VB+FLD*RB/K*VB*DABS(VB)/2.*((K-1.)/K*VB+CB)*DT
                 V(1)=XV *K
      P(1)=S*V(1)+D
      R(1)=P(1)/(P0/PI*RI/R0-(K-1.)/2./K/K*V(1)*V(1))
      C(1)=DSQRT(P(1)/R(1))
      IF(V(1).LT.C(1)*K) GO TO 4
   57    CONTINUE
      S=RB*CB
      D=PB-S*VB+FLD*RB/K*VB*DABS(VB)/2.*((K-1.)/K*VB+CB)*DT
         XMOUT=RO(1)*VO(1)*AREA *RI*CI/K
         RTANK=RTANKO+(XM-XMOUT)/VTANK *DTIME
         RTANKO=RTANK
         PTANK=RTANK**K*C1
   58    CONTINUE
      S=RB*CB
      D=PB-S*VB+FLD*RB/K*VB*DABS(VB)/2.*((K-1.)/K*VB+CB)*DT
         IF(NV.EQ.4)CALL XPEXP(PTANK,TIME)
         P(1)=PTANK/PI
         V(1)=(P(1)-D)/S
      R(1)=P(1)/(P0/PI*RI/R0-(K-1.)/2./K/K*V(1)*V(1))
      C(1)=DSQRT(P(1)/R(1))
         TOT3=TOT3+RO(1)*RI*VO(1)*CI/K*AREA*DTIME
         ICM1=ICOUNT-1
         IF((ICM1/NP)*NP.EQ.ICM1)WRITE(6,555)TIME,PTANK,R(1),V(1),D
```

```
 550          FORMAT(2X,5D12.4)
      IF(V(1).LT.C(1)*K) GO TO 4
   52 CONTINUE
      WRITE(6,240)TIME
  106 FORMAT(5X,I5,5E15.4)
  240 FORMAT(15X,'CHOKING AT VALVE AT TIME =',E11.4)
      V(1)=K*DSQRT(2./(K+1.)*RI/R0*P0/PI)
      P(1)=XM*DSQRT(2./(K+1.)*P0/PI*R0/RI)
      R(1)=XM*R0/RI*DSQRT((K+1.)/2.*PI/P0*R0/RI)
      C(1)=DSQRT(2./(K+1.)*P0/PI*RI/R0)
      GO TO 4
C-----------------------------------------------------------------------
C----------PREPARE CONDITIONS FOR REVERSE FLOW OF SLUG
C-----------------------------------------------------------------------
  300          CONTINUE
               NOUNT=1
               XBAR=XLS-RAD0*4./3.-1.D-05
          TREV=0.
          RCHUG=RMAX
               RMAX=0.
               DXBAR=0.
               DZP=0.
               ZP0=XBAR/XL
               ZP=ZP0
          XCH=2.
               NP1=N+1
               DO 301 I=1,NP1
           Z(I)=DFLOAT(I-1)*(XLA-XCH)/XL/DFLOAT(N-1)
  301          CONTINUE
          DO 400 I=1,N
          WRITE(6,888)I,Z0(I),P0(I),V0(I),R0(I),C0(I)
  400     CONTINUE
          DZ0=1./DFLOAT(N-1)
          IF(TIME.EQ.0.)DZ0=XLA/XLS/DFLOAT(N-1)
          DO 304 I=1,N
          DO 305 J=1,N
          ZZ=Z(I)-Z0(J)
          IF(ZZ.LT.0.)GO TO 306
  305     CONTINUE
  306     CONTINUE
          CHANGE=-ZZ/DZ0
          P(I)=P0(J)-CHANGE*(P0(J)-P0(J-1))
          V(I)=V0(J)-CHANGE*(V0(J)-V0(J-1))
          R(I)=R0(J)-CHANGE*(R0(J)-R0(J-1))
          C(I)=C0(J)-CHANGE*(C0(J)-C0(J-1))
          WRITE(6,888)I,Z0(I),P0(I),V0(I),R0(I),C0(I)
```

```
  888 FORMAT(2X,I5,5D15.8)
  304       CONTINUE
            MM=(ZO(N)-Z(N))/DZO
            PSUM=0.
            RSUM=0.
            DO 308 I=1,MM
            KK=N+1-I
            PSUM=PSUM+PO(KK)
            RSUM=RSUM+RO(KK)
  308       CONTINUE
            PCONDO=PSUM*PI/DFLOAT(MM)
            RCONO=RSUM*RI/DFLOAT(MM)
            DO 307 I=1,N
            PO(I)=P(I)
            VO(I)=V(I)
            RO(I)=R(I)
            CO(I)=C(I)
            ZO(I)=Z(I)
  307       CONTINUE
       WRITE(6,107)
       WRITE(6,110)
                 DO 303 I=1,N
       OC=CO(I)*CI
       OV=CI*VO(I)/K
       OP=PO(I)*PI
       OZ=XL*ZO(I)
       OR=RI*RO(I)
       IF(DABS(VO(I)).LT..001) OV=0.
       WRITE(6,106)I,OZ,OP,OV,OR,OC
  303            CONTINUE
                 WRITE(6,230)TIME,XBAR,DXBAR
                  LOUNT=0
                  NR=1
                  JOUNT=1
                  KOUNT=0
            DZ=(XLA-XCH)/XL/DFLOAT(N-1)
                  DT=DZ/SMAX*0.8
            DT=DT/2.
                  DTIME=DT*XL/CI
       WRITE(6,999)TIME,PCONDO,RCONO,DZ,DZO
  999  FORMAT(2X,5D15.8)
                  IF(TIME.EQ.0.)GO TO 50
                  GO TO 4
C-------------------------------- ----------------------------------------
    99 CONTINUE
   110 FORMAT(17X,'FEET',11X,'PSIA',9X,'FEET/SEC',6X,'LBM/CU.FT',9X,'FEET
      1/SEC',/)
   107 FORMAT(7X    ,'NODE',4X,'DISTANCE',7X,'PRESSURE',7X,'VELOCITY',7X,'
      1 DENSITY',8X,'SONIC SPEED')
       STOP
       END
```

```
      SUBROUTINE HTPROP(XKC,ALFA,SIGMA,TSAT)
      IMPLICIT REAL*8(A-H,O-Z)
      TSTAR=TSAT-32.
      XKC=.319+.0007*TSTAR-.15D-05*TSTAR**2.+.25D-09*TSTAR**3.
      XKC=XKC/3600.
      ALFA=5.07+.014*TSTAR-.32D-04*TSTAR**2.+.13D-07*TSTAR**3.
      ALFA=ALFA/1000./3600.
      TSTAR=TSTAR*5./9.
      SIGMA=75.62-.1391*TSTAR-.0003*TSTAR**2.+.25D-06*TSTAR**3.
      SIGMA=SIGMA*6.85D-05
      RETURN
      END

      SUBROUTINE XPEXP(XP,TIME)
      IMPLICIT REAL*8(A-H,O-Z)
          COMMON/VELOC/YYY(500),CI,PP0,DD0,NPTS
      P0=PP0
      DD=DD0
      DO 1 I=1,NPTS
      XX=TIME-DD*DFLOAT(I-1)
      IF(XX.LT.0.)GO TO 2
1     CONTINUE
      WRITE(6,3)
3     FORMAT(5X,'DATA TIME EXCEEDED',/)
      STOP
2     CONTINUE
      XP=YYY(I-1)+(DD+XX)/DD*(YYY(I)-YYY(I-1))
      XP=XP+P0
      RETURN
      END

      SUBROUTINE DERI(W1,W2, W3,W4,U1,U2,U3,U4,DUDW)
      IMPLICIT REAL*8(A-H,O-Z)
      D21=(U2-U1)/(W2-W1)
      D32=(U3-U2)/(W3-W2)
      D43=(U4-U3)/(W4-W3)
      D31=(D32-D21)/(W3-W1)
      D42=(D43-D32)/(W4-W2)
      D41=(D42-D31)/(W4-W1)
      DUDW=D21+(W1-W2)*D31+(W1-W2)*(W1-W3)*D41
      RETURN
      END
```

```
      SUBROUTINE OUTP(X,Y,DERY,IHLF,NDIM,PRMT)
      IMPLICIT REAL*8(A-H,O-Z)
      COMMON/PROP/XK,XMP,R,XKC,ALFA,RHOW,SIGMA,CV,CP,XJA
      COMMON/COEFF/A1,A2,A3,A4,A5,A6,A7,A8,A9,
     1             C1,C2,C3,C4,C5,C6,C7,
     2             D1,D2,D3,D4,D5,X0,DEL0
      COMMON/PRINT/DTB1,DTB2,DTB3,DDEL1,DDEL2,DDEL3,DDEL4,TSTAR,U0,
     1             DXMC1,DXMC2,DXMC3,D2RB1,D2RB2,N,N0
     2             ,KKKX
      COMMON/CONST/RO,CO,PO,TO,UO,PI,PIP,GC,XJ,G,CDEF,TINO ,PINF
     1             ,XMIN,AIN,TINF
      DIMENSION PRMT(5),Y(8),DERY(8)
        IF(X.EQ.X0)RETURN
      N0=N
      N=N+1
        KKK=KKKX
      DEL=Y(4)
      DEL0=DEL
      X0=X
      NJUMP=1000
      NP=200
                IF(N.LT.3500000)RETURN
                IF(KKK.GT.1)NP=10
      IF(N.EQ.2)PRMT(5)=1.
      IF(N.LE.10)GO TO 2
      IF((N/NP)*NP.NE.N)RETURN
    2 CONTINUE
      TIME=X0*RO/CO/TSTAR
      SPEED=DERY(7)/U0*CO
      WRITE(6,10,X0,DEL0,N ,TIME,SPEED
      REALT=X0*RO/CO
      RADIUS=RO*Y(7)*12.
      VELOC=DERY(7)*CO
      WRITE(6,20)REALT,RADIUS,VELOC,A3,A6
   20 FORMAT(10X,10HREAL TIME=,D15.8,5H SEC ,7HRADIUS=,D15.8,
     15H IN  ,9HVELOCITY=,D15.8,7H FT/SEC,2D15.8)
      WRITE(6,1)(Y(I),I=1,8)
      WRITE(6,1)(DERY(I),I=1,8)
    1 FORMAT(5X,8D 4.7)
   10 FORMAT(5X,2HX=,D15.8,5X,4HDEL=,D15.8,5X,2HN=,I6,20X,5HTIME=,
     1D15.8,7HSPEED =,D15.8)
        IF(KKK.GT.1)RETURN
      IF((N/NJUMP)*NJUMP.EQ.N)PRMT(5)=1.
      RETURN
      END
```

```
      SUBROUTINE STEAM(P,T,HLV,DH,DX,NN)
      IMPLICIT REAL*8(A-H,O-Z)
      COMMON/TABLE/PP(120),TT(120),HFG(120),VFG(120)
      DIMENSION F(120),G(120),X(120),V(120)
C------NN=2 GIVEN T GET PSAT
C----------NN=1 GIVEN P GET TSAT
C----------PP  TT  IN ASCENDING ARDERS
      IF(NN.GT.1)GO TO 200
      XX=P
      DO 1 I=1,120
      X(I)=PP(I)
      F(I)=TT(I)
      G(I)=HFG(I)
      V(I)=VFG(I)
    1 CONTINUE
      GO TO 500
  200 CONTINUE
      XX=T
      DO 2 I=1,120
      X(I)=TT(I)
      F(I)=PP(I)
      G(I)=HFG(I)
      V(I)=VFG(I)
    2 CONTINUE
  500 CONTINUE
      DO 10 I=1,120
      D=XX-X(I)
      IF(D.LT.0.)GO TO 20
   10 CONTINUE
      WRITE(6,900)NN
  900 FORMAT(/,45X,21HFAIL IN INTERPOLATION,I5,/)
      STOP
   20 CONTINUE
      IP1=I
      I=I-1
      IM1=I-1
      C=(X(I)-X(IM1))*(F(I)-F(IP1))-(X(I)-X(IP1))*(F(I)-F(IM1))
      DENOM=(X(I)-X(IM1))*(X(I)**2-X(IP1)**2)-
     1      (X(I)-X(IP1))*(X(I)**2-X(IM1)**2)
      C=C/DENOM
      B=(F(I)-F(IP1))/(X(I)-X(IP1))-C*(X(I)+X(IP1))
      A=F(I)-B*X(I)-C*X(I)*X(I)
      FF=A+B*XX+C*XX*XX
      C=(X(I)-X(IM1))*(G(I)-G(IP1))-(X(I)-X(IP1))*(G(I)-G(IM1))
      C=C/DENOM
      B=(G(I)-G(IP1))/(X(I)-X(IP1))-C*(X(I)+X(IP1))
```

```
      A=G(I)-B*X(I)-C*X(I)*X(I)
      GG=A+B*XX+C*XX*XX
      C=(X(I)-X(IM1))*(V(I)-V(IP1))-(X(I)-X(IP1))*(V(I)-V(IM1))
      C=C/DENOM
      B=(V(I)-V(IP1))/(X(I)-X(IP1))-C*(X(I)+X(IP1))
      A=V(I)-B*X(I)-C*X(I)*X(I)
      VV=A+B*XX+C*XX*XX
      X1=XX
```

:========== P A G E  S K I P  S U P P R E S S E D ========:



```
      X2=X(IP1)
      X3=X(I+2)
      X4=X(I+3)
      G1=GG
      G2=G(IP1)
      G3=G(I+2)
      G4=G(I+3)
      CALL DERI(X1,X2,X3,X4,G1,G2,G3,G4,DGDX)
      IF(NN.GT.1)GO TO 201
      T=FF
      HLV=GG
      DH=DGDX
      DXDF=GG/VV/(FF+460.)/144.*778.
      DX=1./DXDF
      RETURN
  201 CONTINUE
      P=FF
      HLV=GG
      DH=DGDX
      DFDX=GG/VV/(XX+460.)/144.*778.
      RETURN
      END
```

```
      SUBROUTINE SBUB(XPEND,XMDOT,XTIN,XVW,XPB,XTIME,XDTIME,KKK)
      IMPLICIT REAL*8(A-H,O-Z)
      EXTERNAL FCT,OUTP
      DIMENSION PRMT(5),AUX(8,8),Y(8),DERY(8)
      COMMON/STBUB/XPINF,XDTT,XRW,XRG,YY(8),XAIN,XRO
      COMMON/DTIME/H
      COMMON/PROP/XK,XKP,R,XKC,ALFA,RHOW,SIGMA,CV,CP,XJA
      COMMON/CONST/RO,CO,PO,TO,UO,PI,PIP,GC,XJ,G,COEF,TINO ,PINF
     1            ,XMIN,AIN,TINF
      COMMON/COEFF/A1,A2,A3,A4,A5,A6,A7,A8,A9,
     1            C1,C2,C3,C4,C5,C6,C7,
     2            D1,D2,D3,D4,D5,X0,DEL0
      COMMON/PRINT/DTB1,DTB2,DTB3,DDEL1,DDEL2,DDEL3,DDEL4,TSTAR,U0,
     1            DXMC1,DXMC2,DXMC3,D2RB1,D2RB2,N,N0
     2            ,KKKX
C----------READ IN STEAM TABLE
      COMMON/TABLE/PP(120),TT(120),HFG(120),VFG(120)
C----------ARGUMENTS IN SUBROUTINE
      PINI=XPEND
      XMIN=XMDOT
      TIN=XTIN
      TIME=XTIME
      TMAX=XDTIME
      KKKX=KKK
      VINI=XVW
C-----------------------------------------------------------------------
      IF(KKK.GT.1)GO TO 7
        IF(NT.EQ.120)GO TO 103
      READ(5,99)NT
   99 FORMAT(I5)
      READ(5,100)(TT(I),I=1,NT)
      READ(5,100)(PP(I),I=1,NT)
      READ(5,100)(HFG(I),I=1,NT)
      READ(5,100)(VFG(I),I=1,NT)
  100 FORMAT(1008.4)
      WRITE(6,102)
  102 FORMAT(//25X,'STEAM TABLE T P HFG',//)
      WRITE(6,101)(TT(I),I=1,NT)
      WRITE(6,101)(PP(I),I=1,NT)
      WRITE(6,101)(HFG(I),I=1,NT)
      WRITE(6,101)(VFG(I),I=1,NT)
  101 FORMAT(5X,10D12.4)
  103          CONTINUE
C----------INPUT CONSTANTS
      N=0
      N0=0
```

```
      PI=3.14159
      PIP=4.*PI
      XK=1.3
      R=85.76
      XJ=778.
      COEF=1.
      GC=32.2
      G=DSQRT(GC/2./PI/R)*COEF
      CV=.335
      CP=.445
      CPW=1.
      NEQUIL=0
C----------PARAMETERS FROM COMMON STBUB
           PINF=XPINF
           DTT=XDTT
           RHOG=XRG
           AIN=XAIN
           RHOW=XRW
           RO=XRO
C-------------------------------------------------------------------------------
    5 CONTINUE
C----------COLLAPSE
C----------COLLAPSE
      CALL STEAM(PINF,TSAT,HFGP,DHFGDP,DTDP,1)
      CALL HTPROP(XKC,ALFA,SIGMA,TSAT)
      TINF=TSAT-DTT+460.
      TIN1=TINF-460.
      CALL STEAM(PB,TIN1,HFGB,DHFGB,DTDPB,2)
      UO=DSQRT(2.*GC*144.*(PINF-PB)/3./RHOW)
      FO=ALFA/RO/UO
      TSTAR=FO*RO*RO/ALFA
      DELP=PINF-PB
      XJA=RHOW*CPW*DTT/RHOG/HFGP
      BFC=XJA*XJA*ALFA/RO*DSQRT(RHOW/GC/DELP)/12.
    6 CONTINUE
      WRITE(6,98)XKC,ALFA,SIGMA,TIN1
   98 FORMAT(5X,'XKC=',E11.4,'ALFA=',E11.4,'SIGMA=',E11.4,'TIN1=',
     1 E11.4)
      WRITE(6,95)RHOG,XJA,BFC,DTT
   95 FORMAT(15X,5HRHOG=,E15.8,5X,4HXJA=,E15.8,5X,4HBFC=,E15.8,
     14HDTT=,E15.8)
      CO=DSQRT(144.*GC*PINF/RHOW)
      PO=PINF
```

```
      PB=PINI
      TQ=TINF
      TIN0=TIN/TINF
      U0=DSQRT(GC*PINF*144./RHOW)
      A1=GC*PINF*144./RHOW/CO/CO
      A2=2.*SIGMA*GC/RO/CO/CO/RHOW
      A3=XMIN*AIN/CO/RHOW/(PIP/3.*RO*RO)
      A4=3.*PINF*144./CV/RHOW/TINF/XJ
      A5=.5/XKC/TINF
      A6=A3
      A7=.16666667
      A8=.33333333
      A9=12.*ALFA/RO/CO
      C1=2.*XKC*TINF/RHOW/CO/HFGP/RO
      T1=1.D-07*U0/RO
      X0=0.
      DEL0=0.
      H=0.
      WRITE(6,97)PB,RO,CO,G
   97 FORMAT(1X,3HPB=,D15.8,5X,3HRO=,D15.8,5X,3HCO=,D15.8,5X,2HG=,D15.8)
C----------INITIAL CONDITIONS USING NORMALIZED PARAMETERS
      TB=TINF
      RHOB=RHOG/RHOW
      TB=(TSAT+460.)/TINF
      TW=TB
      PB=PINI/PINF
      DEL=0.
      XMC=0.
      DRB=VINI/CO
      RB=1.
      NDIM=8
      Y(1)=TB
      Y(2)=RHOB
      Y(3)=PB
      Y(4)=DEL
      Y(5)=XMC
      Y(6)=DRB
      Y(7)=RB
      Y(8)=TW
      PRMT(5)=0.
      DO 4 I=1,NDIM
      AUX(1,I)=Y(I)
```

```
    4 CONTINUE
        DDD=1.2
      KOUNT=0
    2 CONTINUE
        IF(KOUNT.GT.5)DDD=1.5
      DT=.000005*RO/UO
      IF(BFC.EQ.0.)DT=DT/10./5.
      IF(BFC.NE.0..AND.PINF.LT.5.)DT=DT/10.
      XKOUNT=KOUNT
      DO 1 I=1,NDIM
      Y(I)=AUX(1,I)
      DERY(I)=1./DFLOAT(NDIM)
    1 CONTINUE
      PBB=Y(3)*PINF
      CALL STEAM(PBB,TSAT,HFGP,DHFGDP,DTDP,1)
      Y(8)=(TSAT+460.)/TINF
C-----------FOR ZERO INITIAL DRIVING PRESSURE FINITE TEMP DIFFERENCE
      IF(KOUNT.EQ.1)Y(5)=C1*(Y(8)-1.)/Y(4)
      IF(KOUNT.EQ.1)Y(6)=-Y(5)
      IF(KOUNT.EQ.1)DELTAT=.01*C1*C1*(Y(8)-1.)**2/A9/Y(5)**2
      IF(KOUNT.GE.1)DT=DELTAT*RO/UO/4.
      PRMT(1)=XO+H
      PRMT(2)=TMAX*UO/RO
      PRMT( 3)=DT*UO/RO*DDD**(XKOUNT)
      PRMT(4)=.0001
      CALL XRKGS(PRMT,Y,DERY,NDIM,IHLF,FCT,OUTP,AUX)
      IF(XO.GE.PRMT(2))GO TO 3
      KOUNT=KOUNT+1
      GO TO 2
    7     CONTINUE
          KOUNT=KOUNT+1
      XKOUNT=DFLOAT(KOUNT)
          ND=10
      IF(KOUNT.GT.5)DDD=1.5
      DT=.000005*RO/CO
      A3=XMIN*AIN/CO/RHOW/(PIP/3.*RO*RO)
      A6=A3
   10 CONTINUE
      PRMT(5)=0.
      DO 8 I=1,NDIM
      Y(I)=YY(I)
      DERY(I)=1./DFLOAT(NDIM)
    8 CONTINUE
```

```
      PBB=Y(3)*PINF
      CALL  STEAM(PBB,TSAT,HFGP,DHFGDP,DTDP,1)
      Y(8)=(TSAT+460.)/TINF
      PRMT(1)=TIME*CO/RO
      PRMT(2)=PRMT(1)+TMAX*CO/RO
      IF(KOUNT.GT.200)XKOUNT=200.
      PRMT(3)=DT*CO/RO*DDD**XKOUNT
      DIV=(PRMT(2)-PRMT(1))/FLOAT(ND)
      IF(PRMT(3).GT.DIV)PRMT(3)=DIV
      PRMT(4)=.0001
      CALL  XRKGS(PRMT,Y,DERY,NDIM,IHLF,FCT,OUTP,AUX)
3 CONTINUE
      DO 9 I=1,NDIM
      YY(I)=Y(I)
9     CONTINUE
      XPB=Y(3)*PINF
      XVW=Y(6)*CO
      RETURN
  END
```

```
      SUBROUTINE XRKGS(PRMT,Y,DERY,NDIM,IHLF,FCT,OUTP,AUX)
      IMPLICIT REAL*8(A-H,O-Z)
      DIMENSION Y(8),DERY(8),AUX(8,8),A(4),B(4),C(4),PRMT(5)
      COMMON/DTIME/H
      DO 1 I=1,NDIM
    1 AUX(8,I)=.06666667*DERY(I)
      X=PRMT(1)
      XEND=PRMT(2)
      H=PRMT(3)
      IF(PRMT(5).EQ.1.)GO TO 201
      PRMT(5)=0.
      CALL FCT(X,Y,DERY)
      GO TO 202
  201 CONTINUE
      PRMT(5)=0.
      DO 203 I=1,NDIM
  203 DERY(I)=AUX(2,I)
  202 CONTINUE
C
C     ERROR TEST
      IF(H*(XEND-X))38,37,2
C
C     PREPARATIONS FOR RUNGE-KUTTA METHOD
    2 A(1)=.5
      A(2)=.2928932
      A(3)=1.707107
      A(4)=.1666667
      B(1)=2.
      B(2)=1.
      B(3)=1.
      B(4)=2.
      C(1)=.5
      C(2)=.2928932
      C(3)=1.707107
      C(4)=.5
C
C     PREPARATIONS OF FIRST RUNGE-KUTTA STEP
      DO 3 I=1,NDIM
      AUX(1,I)=Y(I)
      AUX(2,I)=DERY(I)
      AUX(3,I)=0.
    3 AUX(6,I)=0.
      IREC=0
      H=H+H
      IHLF=-1
      ISTEP=0
```

```
      IEND=0
C
C
C     START OF A RUNGE-KUTTA STEP
    4 IF((X+H-XEND)*H)7,6,5
    5 H=XEND-X
    6 IEND=1
C     RECORDING OF INITIAL VALUES OF THIS STEP
    7 CALL OUTP(X,Y,DERY,IREC,NDIM,PRMT)
      IF(PRMT(5))40,8,40
    8 ITEST=0
    9 ISTEP=ISTEP+1
C
C
C     START OF INNERMOST RUNGE-KUTTA LOOP
      J=1
   10 AJ=A(J)
      BJ=B(J)
      CJ=C(J)
      DO 11 I=1,NDIM
      R1=H*DERY(I)
      R2=AJ*(R1-BJ*AUX(6,I))
      Y(I)=Y(I)+R2
      R2=R2+R2+R2
   11 AUX(6,I)=AUX(6,I)+R2-CJ*R1
      IF(J-4)12,15,15
   12 J=J+1
      IF(J-3)13,14,13
   13 X=X+.5*H
   14 CALL FCT(X,Y,DERY)
      GOTO 10
C     END OF INNERMOST RUNGE-KUTTA LOOP
C
C
C     TEST OF ACCURACY
   15 IF(ITEST)16,16,20
C
C     IN CASE ITEST=0 THERE IS NO POSSIBILITY FOR TESTING OF ACCURACY
   16 DO 17 I=1,NDIM
   17 AUX(4,I)=Y(I)
      ITEST=1
      ISTEP=ISTEP+ISTEP-2
   18 IHLF=IHLF+1
      X=X-H
```

```
      H=.5*H
      DO 19 I=1,NDIM
      Y(I)=AUX(1,I)
      DERY(I)=AUX(2,I)
   19 AUX(6,I)=AUX(3,I)
      GOTO 9
C
   20 IMOD=ISTEP/2
      IF(ISTEP-IMOD-IMOD)21,23,21
   21 CALL FCT(X,Y,DERY)
      DO 22 I=1,NDIM
      AUX(5,I)=Y(I)
   22 AUX(7,I)=DERY(I)
      GOTO 9
C
C     COMPUTATION OF TEST VALUE DELT
   23 DELT=0.
      DO 24 I=1,NDIM
   24 DELT=DELT+AUX(8,I)*DABS(AUX(4,I)-Y(I))
      IF(DELT-PRMT(4))28,28,25
C
C     ERROR IS TOO GREAT
   25 IF(IHLF-10)26,36,36
   26 DO 27 I=1,NDIM
   27 AUX(4,I)=AUX(5,I)
      ISTEP=ISTEP+ISTEP-4
      X=X-H
      IEND=0
      GOTO 18
C
C     RESULT VALUES ARE GOOD
   28 CALL FCT(X,Y,DERY)
      DO 29 I=1,NDIM
      AUX(1,I)=Y(I)
      AUX(2,I)=DERY(I)
      AUX(3,I)=AUX(6,I)
      Y(I)=AUX(5,I)
   29 DERY(I)=AUX(7,I)
```

```
      CALL OUTP(X-H,Y,DERY,IHLF,NDIM,PRMT)
      IF(PRMT(5))40,30,40
   30 DO 31 I=1,NDIM
      Y(I)=AUX(1,I)
   31 DERY(I)=AUX(2,I)
      IREC=IHLF
      IF(IEND)32,32,39
C
C     INCREMENT GETS DOUBLED
   32 IHLF=IHLF-1
      ISTEP=ISTEP/2
      H=H+H
      IF(IHLF)4,33,33
   33 IMOD=ISTEP/2
      IF(ISTEP-IMOD-IMOD)4,34,4
   34 IF(DELT-.02*PRMT(4))35,35,4
   35 IHLF=IHLF-1
      ISTEP=ISTEP/2
      H=H+H
      GOTO 4
C
C
C     RETURNS TO CALLING PROGRAM
   36 IHLF=11
      CALL FCT(X,Y,DERY)
      GOTO 39
   37 IHLF=12
      GOTO 39
   38 IHLF=13
   39 CALL OUTP(X,Y,DERY,IHLF,NDIM,PRMT)
   40 RETURN
      END
```

```
      SUBROUTINE FCT(X,Y,DERY)
      IMPLICIT REAL*8(A-H,O-Z)
      DIMENSION Y(8),DERY(8)
      COMMON/PRINT/DTB1,DTB2,DTB3,DDEL1,DDEL2,DDEL3,DDEL4,TSTAR,U0,
     1             DXMC1,DXMC2,DXMC3,D2RB1,D2RB2,N,N0
     2             ,KKKX
      COMMON/COEFF/A1,A2,A3,A4,A5,A6,A7,A8,A9,
     1             C1,C2,C3,C4,C5,C6,C7,
     2             D1,D2,D3,D4,D5,X0,DEL0
      COMMON/CONST/RO,CO,PO,TO,UO,PI,PIP,GC,XJ,G,COEF,TINO   ,PINF
     1,XMIN,AIN,TINF
      COMMON/PROP/XK,XKP,R,XKC,ALFA,RHOW,SIGMA,CV,CP ,XJA
      PAR1=1.D-03
      PAR2=1.
      NC=100
C----------IDENTIFY VARIABLES
      TB=Y(1)
      RHOB=Y(2)
      PB=Y(3)
      DEL=Y(4)
      XMC=Y(5)
      DRB=Y(6)
      RB=Y(7)
      TW=Y(8)
      UB=DRB+XMC
      DEL2=DEL*DEL
C----------CALCULATE ALL COEFFICIENTS
C----------ALL COEFFICIENTS ARE DIMENSIONLESS
      BR=1./RB
      BOHR=1./RHOB
      PBB=PB*PINF
      IF((N/NC)*NC.EQ.N)CALL STEAM(PBB,TSAT,HFGP,DHFGDP,DTDP,1)
      HFG=HFGP
      D1=DEL*A8*(DEL2*.1+DEL*RB*.5+RB*RB)
      D2=-(1.-TW)*(DEL2*A7+2.*DEL*RB*A8+RB*RB)
      D3=RB*RB*(1.-TW)
      D4=-(1.-TW)*(DEL2*.1+DEL*RB*A8+RB*RB*A8)
      D5=A9
      F0=PINF*DTDP/TINF
      F1=HFG*RHOW*CO*RO*DEL*A5
      F2=HFG*RHOW*CO*RO*XMC*A5
      F3=RHOW*CO*RO*DEL*XMC*DHFGDP*PINF*A5
      IF(X.GE.PAR1)D5=-A9*A7*(1.-TW)*RB*RB/DEL
      DTB1=A3*(XK*TINO-TB)*BOHR*BR*BR*BR-XMC*PB*A9*BOHR*BOHR*BR
      DTB3=-A4*PB*BOHR*BR*DRB
      DTB=DTB1+DTB3
```

```
      DRHOB=-3.*RHOB*DRB*BR+A6*BR*BR*BR-3.*XMC*BR
      DPB=PB*(DTB/TB+DRHOB*BOHR)
      DTW=F0*DPB
      IF(X.LT.PAR1)GO TO 1
      DDEL1=1./D4
      DDEL2=D5-D3*UB
      DDEL3=-D1*DTB-D2*DRB
      DDEL=DDEL1*(DDEL2+DDEL3)

1**********PAGE  SKIP  SUPPRESSED ********

; LEVEL  21                FCT              DATE = 79123          00/53/0

      GO TO 2
    1 CONTINUE
      DELOLD=DEL
      DELNEW=DSQRT(D5*(X-X0)+DELOLD*DELOLD)
      IF(X.EQ.0.)GO TO 3
      DDEL=(DELNEW-DELOLD)/(X-X0)
      GO TO 4
    3 DDEL=0.
    4 CONTINUE
    2 CONTINUE
      IF(DEL.EQ.0.)DXMC=0.
      IF(DEL.EQ.0.)GO TO 5
      DXMC=(DTW-F2*DDEL-F3*DPB)/F1
    5 CONTINUE
      D2RB1=-DXMC-2.*UB*DRB*BR+.5*UB*BR*UB
      D2RB2=A1*(PB-PAR2)*BR-A2*BR*BR
      D2RB=D2RB1+D2RB2
C-----------INSERT DERIVATIVES
      DERY(1)=DTB
      DERY(2)=DRHOB
      DERY(3)=DPB
      DERY(4)=DDEL
      DERY(5)=DXMC
      DERY(6)=D2RB
      DERY(7)=DRB
      DERY(8)=DTW
      RETURN
      END
```

```
      IMPLICIT REAL*8(A-H,O-Z)
      EXTERNAL FCT,OUTP
      DIMENSION PRMT(5),AUX(8,8),Y(8),DERY(8)
      COMMON/DTIME/H
      COMMON/PROP/XK,XKP,R,XKC,ALFA,RHOW,SIGMA,CV,CP,XJA
      COMMON/CONST/RO,CO,PC,TO,UO,PI,PIP,GC,XJ,G,COEF,TINO ,PINF
     1            ,XMIN,AIN,TINF
      COMMON/COEFF/A1,A2,A3,A4,A5,A6,A7,A8,A9,
     1             C1,C2,C3,C4,C5,C6,C7,
     2             D1,D2,D3,D4,D5,X0,DEL0
      COMMON/PRINT/DTB1,DTB2,DTB3,DDEL1,DDEL2,DDEL3,DDEL4,TSTAR,U0,
     1             DXMC1,DXMC2,DXMC3,D2RB1,D2RB2,N,N0
C----------READ IN STEAM TABLE
      COMMON/TABLE/PP(120),TT(120),HFG(120),VFG(120)
      READ(5,99)NT
   99 FORMAT(I5)
      READ(5,100)(TT(I),I=1,NT)
      READ(5,100)(PP(I),I=1,NT)
      READ(5,100)(HFG(I),I=1,NT)
      READ(5,100)(VFG(I),I=1,NT)
  100 FORMAT(10D8.4)
      WRITE(6,102)
  102 FORMAT(//25X,'STEAM TABLE T P HFG',//)
      WRITE(6,101)(TT(I),I=1,NT)
      WRITE(6,101)(PP(I),I=1,NT)
      WRITE(6,101)(HFG(I),I=1,NT)
      WRITE(6,101)(VFG(I),I=1,NT)
  101 FORMAT(5X,10D12.4)
C----------INPUT CONSTANTS
      N=0
      N0=0
      PI=3.14159
      PIP=4.*PI
      XK=1.3
      R=85.76
      XJ=778.
      COEF=1.
           RPIPE=2.25/12.
           SCALER=1./12.
           XMIN=0.
           AIN=.046 *RPIPE/SCALER
           TIN=212.+460.
      RHOW=62.4
      GC=32.2
      G=DSQRT(GC/2./PI/R)*COEF
      CV=.335
      CP=.445
      CPW=1.
```

```
      NEQUIL=0
C----------IF NEQUIL=1 GROWTH
C----------IF NEQUIL=0 COLLAPSE
      IF(NEQUIL.NE.1)GO TO 5
C----------GROWTH
      PINF=1.47
      CALL STEAM(PINF,TSAT,HFGP,DHFGDP,DTDP,1)
      CALL HTPROP(XKC,ALFA,SIGMA,TSAT)
      DTT=2.
      TINF=TSAT+DTT  +460.
      TINI=TINF-460.
      WRITE(6,98)TSAT,TINF,TINI
   98 FORMAT(15X,3D15.8)
      CALL STEAM(PSAT,TINI,HFGT,DHFGDT,DPDT,2)
      PB=PSAT
      F0=.0366372194
      RHOW=61.789
      RHOG=.00431
      U0=DSQRT(2.*GC*144.*(PSAT-PINF)/3./RHOW)
      R0=ALFA/F0/U0
      TSTAR=F0*R0*R0/ALFA
      XJA=RHOW*CPW*DTT/RHOG/HFGP
      BFC=0.
      GO TO 6
    5 CONTINUE
C----------COLLAPSE
C----------COLLAPSE
          PINF=24.57
      CALL STEAM(PINF,TSAT,HFGP,DHFGDP,DTDP,1)
      CALL HTPROP(XKC,ALFA,SIGMA,TSAT)
          DTT=145.
      TINF=TSAT-DTT+460.
      TINI=TINF-460.
      CALL STEAM(PB,TINI,HFGB,DHFGB,DTDPB,2)
          PB=19.56
          RHOW=59.08
          RHOG=0.0612
      U0=DSQRT(2.*GC*144.*(PINF-PB)/3./RHOW)
          RC=0.2894
      F0=ALFA/RC/U0
      TSTAR=F0*R0*R0/ALFA
      DELP=PINF-PB
      XJA=RHOW*CPW*DTT/RHOG/HFGP
      BFC=XJA*XJA*ALFA/RC*DSQRT(RHOW/GC/DELP)/12.
    6 CONTINUE
      WRITE(6,98)XKC,ALFA,SIGMA
```

```
      WRITE(6,95)RHOG,XJA,BFC,DTT
   95 FORMAT(15X,5HRHOG=,E15.8,5X,4HXJA=,E15.8,5X,4HBFC=,E15.8,
     14HDTT=,E15.8)
      CO=DSQRT(144.*GC*PINF/RHOW)
      PO=PINF
      TO=TINF
      TINO=TIN/TINF
      UO=DSQRT(GC*PINF*144./RHOW)
      A1=GC*PINF*144./RHOW/CO/CO
      A2=2.*SIGMA*GC/RC/CO/CO/RHOW
      A3=XMIN*AIN/CC/RHOW/(PI*3.*RO*RO)
      A4=3.*PINF*144./CV/RHOW/TINF/XJ
      A5=.5/XKC/TINF
      A6=A3
      A7=.16666667
      A8=.33333333
      A9=12.*ALFA/RC/CO
      C1=2.*XKC*TINF/RHOW/CO/HFGP/RO
      T1=1.D-07*UO/RO
      XO=0.
      DELO=0.
      H=0.
      TMAX=1.D+04
      WRITE(6,97)PB,RO,CC,G
   97 FORMAT(1X,3HPB=,D15.8,5X,3HRO=,D15.8,5X,3HCO=,D15.8,5X,2HG=,D15.8
C----------INITIAL CONDITIONS USING NORMALIZED PARAMETERS
      TB=TINF
      RHOB=RHOG/RHOW
      TB=(TSAT+460.)/TINF
      TW=TB
          PB=PB/PINF
      DEL=0.
      XMC=0.
      DRB=0.
      RB=1.
      NDIM=8
      Y(1)=TB
      Y(2)=RHOB
      Y(3)=PB
      Y(4)=DEL
      Y(5)=XMC
      Y(6)=DRB
      Y(7)=RB
      Y(8)=TW
```

```
      PRMT(5)=0.
      DO 4 I=1,NDIM
      AUX(1,I)=Y(I)
    4 CONTINUE
      DDD=1.1
      IF(BFC.GT..2)DDD=1.1
      KOUNT=0
    2 CONTINUE
      DT=.000005*RC/UO
      IF(BFC.EQ.0.)DT=DT/10./5.
      IF(BFC.NE.0..AND.PINF.LT.5.)DT=DT/10.
      XKOUNT=KOUNT
      DO 1 I=1,NDIM
      Y(I)=AUX(1,I)
      DERY(I)=1./DFLOAT(NDIM)
    1 CONTINUE
      PBB=Y(3)*PINF
      CALL STEAM(PBB,TSAT,HFGP,DHFGDP,DTDP,1)

      Y(8)=(TSAT+460.)/TINF
C----------FOR ZERO INITIAL DRIVING PRESSURE FINITE TEMP DIFFERENCE
      IF(KOUNT.EQ.1)Y(5)=C1*(Y(8)-1.)/Y(4)
      IF(KOUNT.EQ.1)Y(6)=-Y(5)
      IF(KOUNT.EQ.1)DELTAT=.01*C1*C1*(Y(8)-1.)**2/A9/Y(5)**2
      IF(KOUNT.GE.1)DT=DELTAT*RC/UO/4.
      PRMT(1)=XO+H
      PRMT(2)=TMAX*UO/RO
      PRMT( 3)=DT*UO/RC*DDD**(XKOUNT)
      PRMT(4)=.0001
      CALL XRKGS(PRMT,Y,DERY,NDIM,IHLF,FCT,OUTP,AUX)
      IF(XO.GE.PRMT(2))GO TO 3
      KOUNT=KOUNT+1
          IF(Y(7).LT.0.91)KOUNT=KOUNT-2
      WRITE(6,96)KOUNT
      GO TO 2
   96 FORMAT(//,5X,6HKOUNT=,I5,//)
    3 CONTINUE
      STOP
      END
```

```
      SUBROUTINE OUTP(X,Y,DERY,IHLF,NDIM,PRMT)
      IMPLICIT REAL*8(A-H,O-Z)
      COMMON/PROP/XK,XKP,R,XKC,ALFA,RHOW,SIGMA,CV,CP,XJA
      COMMON/COEFF/A1,A2,A3,A4,A5,A6,A7,A8,A9,
     1             C1,C2,C3,C4,C5,C6,C7,
     2             D1,D2,D3,D4,D5,X0,DEL0
      COMMON/PRINT/DTB1,DTB2,DTB3,DDEL1,DDEL2,DDEL3,DDEL4,TSTAR,U0,
     1             DXMC1,DXMC2,DXMC3,D2RB1,D2RB2,N,N0
      COMMON/CONST/RO,CO,PO,TO,UO,PI,PIP,GC,XJ,G,COEF,TINO ,PINF
     1            ,XMIN,AIN,TINF
      DIMENSION PRMT(5),Y(8),DERY(8)
      N0=N
      N=N+1
      DEL=Y(4)
      DEL0=DEL
      X0=X
      NJUMP=1000
      NP=200
      IF(N.EQ.2)PRMT(5)=1.
      IF(N.LE.10)GO TO 2
      IF((N/NP)*NP.NE.N)RETURN
    2 CONTINUE
      TIME=X0*RO/CO/TSTAR
      SPEED=DERY(7)/U0*CO
      WRITE(6,10)X0,DEL0,N ,TIME,SPEED
      REALT=X0*RO/CO
      RADIUS=RO*Y(7)*12.
      VELOC=DERY(7)*CO
      WRITE(6,20)REALT,RADIUS,VELOC,A3,A6
   20 FORMAT(10X,10HREAL TIME=,D15.8,5H SEC ,7HRADIUS=,D15.8,
     15H IN  ,9HVELOCITY=,D15.8,7H FT/SEC,2D15.8)
      WRITE(6,1)(Y(I),I=1,8)
      WRITE(6,1)(DERY(I),I=1,8)
    1 FORMAT(5X,8D14.7)
   10 FORMAT(5X,2HX=,D15.8,5X,4HDEL=,D15.8,5X,2HN=,I6,20X,5HTIME=,
     1D15.8,7HSPEED =,D15.8)
      IF((N/NJUMP)*NJUMP.EQ.N)PRMT(5)=1.
      RETURN
      END
```

```
      SUBROUTINE DERI(W1,W2, W3,W4,U1,U2,U3,U4,DUDW)
      IMPLICIT REAL*8(A-H,O-Z)
      D21=(U2-U1)/(W2-W1)
      D32=(U3-U2)/(W3-W2)
      D43=(U4-U3)/(W4-W3)
      D31=(D32-D21)/(W3-W1)
      D42=(D43-D32)/(W4-W2)
      D41=(D42-D31)/(W4-W1)
      DUDW=D21+(W1-W2)*D31+(W1-W2)*(W1-W3)*D41
      RETURN
      END

      SUBROUTINE KTPROP(XKC,ALFA,SIGMA,TSAT)
      IMPLICIT REAL*8(A-H,O-Z)
      TSTAR=TSAT-32.
      XKC=.319+.0007*TSTAR-.15D-05*TSTAR**2.+.25D-09*TSTAR**3.
      XKC=XKC/3600.
      ALFA=5.07+.014*TSTAR-.32D-04*TSTAR**2.+.13D-07*TSTAR**3.
      ALFA=ALFA/1000./3600.
      TSTAR=TSTAR*5./9.
      SIGMA=75.62-.1391*TSTAR-.0003*TSTAR**2.+.25D-06*TSTAR**3.
      SIGMA=SIGMA*6.85D-05
      RETURN
      END
```

```
      SUBROUTINE XRKGS(PRMT,Y,DERY,NDIM,IHLF,FCT,OUTP,AUX)
      IMPLICIT REAL*8(A-H,O-Z)
      DIMENSION Y(8),DERY(8),AUX(8,8),A(4),B(4),C(4),PRMT(5)
      COMMON/DTIME/H
      WRITE(6,200)
  200 FORMAT(//,40X,13HREACHED XRKGS,//)
      DO 1 I=1,NDIM
    1 AUX(8,I)=.06666667*DERY(I)
      X=PRMT(1)
      XEND=PRMT(2)
      H=PRMT(3)
      IF(PRMT(5).EQ.1.)GO TO 201
      PRMT(5)=0.
      CALL FCT(X,Y,DERY)
      GO TO 202
  201 CONTINUE
      PRMT(5)=0.
      DO 203 I=1,NDIM
  203 DERY(I)=AUX(2,I)
  202 CONTINUE
C
C     ERROR TEST
      IF(H*(XEND-X))38,37,2
C
C     PREPARATIONS FOR RUNGE-KUTTA METHOD
    2 A(1)=.5
      A(2)=.2928932
      A(3)=1.707107
      A(4)=.1666667
      B(1)=2.
      B(2)=1.
      B(3)=1.
      B(4)=2.
      C(1)=.5
      C(2)=.2928932
      C(3)=1.707107
      C(4)=.5
C
C     PREPARATIONS OF FIRST RUNGE-KUTTA STEP
      DO 3 I=1,NDIM
      AUX(1,I)=Y(I)
      AUX(2,I)=DERY(I)
      AUX(3,I)=0.
    3 AUX(6,I)=0.
      IREC=0
      H=H+H
      IHLF=-1
      ISTEP=0
      IEND=0
```

```
C       START OF A RUNGE-KUTTA STEP
      4 IF((X+H-XEND)*H)7,6,5
      5 H=XEND-X
      6 IEND=1
C
C       RECORDING OF INITIAL VALUES OF THIS STEP
      7 CALL OUTP(X,Y,DERY,IREC,NDIM,PRMT)
        IF(PRMT(5))40,8,40
      8 ITEST=0
      9 ISTEP=ISTEP+1
C
C
C       START OF INNERMOST RUNGE-KUTTA LOOP
        J=1
     10 AJ=A(J)
        BJ=B(J)
        CJ=C(J)
        DO 11 I=1,NDIM
        R1=H*DERY(I)
        R2=AJ*(R1-BJ*AUX(6,I))
        Y(I)=Y(I)+R2
        R2=R2+R2+R2
     11 AUX(6,I)=AUX(6,I)+R2-CJ*R1
        IF(J-4)12,15,15
     12 J=J+1
        IF(J-3)13,14,13
     13 X=X+.5*H
     14 CALL FCT(X,Y,DERY)
        GOTO 10
C       END OF INNERMOST RUNGE-KUTTA LOOP
C
C
C       TEST OF ACCURACY
     15 IF(ITEST)16,16,20
C
C       IN CASE ITEST=0 THERE IS NO POSSIBILITY FOR TESTING OF ACCURACY
     16 DO 17 I=1,NDIM
     17 AUX(4,I)=Y(I)
        ITEST=1
        ISTEP=ISTEP+ISTEP-2
     18 IHLF=IHLF+1
        X=X-H
        H=.5*H
        DO 19 I=1,NDIM
        Y(I)=AUX(1,I)
        DERY(I)=AUX(2,I)
     19 AUX(6,I)=AUX(3,I)
        GOTO 9
```

```
C
   20 IMOD=ISTEP/2
      IF(ISTEP-IMOD-IMOD)21,23,21
   21 CALL FCT(X,Y,DERY)
      DO 22 I=1,NDIM
      AUX(5,I)=Y(I)
   22 AUX(7,I)=DERY(I)
      GOTO 9
C
C     COMPUTATION OF TEST VALUE DELT
   23 DELT=0.
      DO 24 I=1,NDIM
   24 DELT=DELT+AUX(8,I)*DABS(AUX(4,I)-Y(I))
      IF(DELT-PRMT(4))28,28,25
C
C     ERROR IS TOO GREAT
   25 IF(IHLF-10)26,36,36
   26 DO 27 I=1,NDIM
   27 AUX(4,I)=AUX(5,I)
      ISTEP=ISTEP+ISTEP-4
      X=X-H
      IEND=0
      GOTO 18
C
C     RESULT VALUES ARE GOOD
   28 CALL FCT(X,Y,DERY)
      DO 29 I=1,NDIM
      AUX(1,I)=Y(I)
      AUX(2,I)=DERY(I)
      AUX(3,I)=AUX(6,I)
      Y(I)=AUX(5,I)
   29 DERY(I)=AUX(7,I)
      CALL OUTP(X-H,Y,DERY,IHLF,NDIM,PRMT)
      IF(PRMT(5))40,30,40
   30 DO 31 I=1,NDIM
      Y(I)=AUX(1,I)
   31 DERY(I)=AUX(2,I)
      IREC=IHLF
      IF(IEND)32,32,39
C
C     INCREMENT GETS DOUBLED
   32 IHLF=IHLF-1
      ISTEP=ISTEP/2
      H=H+H
      IF(IHLF)4,33,33
```

```
   33 IMOD=ISTEP/2
      IF(ISTEP-IMOD-IMOD)4,34,4
   34 IF(DELT-.02*PRMT(4))35,35,4
   35 IHLF=IHLF-1
      ISTEP=ISTEP/2
      H=H+H
      GOTO 4
C
C
C     RETURNS TO CALLING PROGRAM
   36 IHLF=11
      CALL FCT(X,Y,DERY)
      GOTO 39
   37 IHLF=12
      GOTO 39
   38 IHLF=13
   39 CALL OUTP(X,Y,DERY,IHLF,NDIM,PRMT)
   40 RETURN
      END
```

```
      SUBROUTINE FCT(X,Y,DERY)
      IMPLICIT REAL*8(A-H,O-Z)
      DIMENSION Y(8),DERY(8)
      COMMON/PRINT/DTB1,DTB2,DTB3,DDEL1,DDEL2,DDEL3,DDEL4,TSTAR,U0,
     1            DXMC1,DXMC2,DXMC3,D2RB1,D2RB2,N,NO
      COMMON/COEFF/A1,A2,A3,A4,A5,A6,A7,A8,A9,
     1            C1,C2,C3,C4,C5,C6,C7,
     2            D1,D2,D3,D4,D5,X0,DEL0
      COMMON/CONST/RO,CO,PO,TO,UO,PI,PIP,GC,XJ,G,COEF,TINO   ,PINF
     1,XMIN,AIN,TINF
      COMMON/PROP/XK,XKP,R,XKC,ALFA,RHOW,SIGMA,CV,CP  ,XJA
      PAR1=1.D-03
      PAR2=1.
      NC=100
C----------IDENTIFY VARIABLES
      TB=Y(1)
      RHOB=Y(2)
      PB=Y(3)
      DEL=Y(4)
      XMC=Y(5)
      DRB=Y(6)
      RB=Y(7)
      TW=Y(8)
      UB=DRB+XMC
      DEL2=DEL*DEL
C----------CALCULATE ALL COEFFICIENTS
           ACTIME=X*RO/CO
           HTC=50.
           IF(ACTIME.GT.1.D-06)XMIN=HTC*(TB-1.)*TINF/954.8
           XAIN=AIN
           IF(Y(7).LT.0.5)XAIN=AIN*Y(7)**3.
           A3=-XMIN*XAIN/CO/RHOW/(PIP/3.*RO*RO)
           A6=A3
C----------ALL COEFFICIENTS ARE DIMENSIONLESS
      BR=1./RB
      BOHR=1./RHOB
      PBB=PB*PINF
      IF((N/NC)*NC.EQ.N)CALL STEAM(PBB,TSAT,HFGP,DHFGDP,DTDP,1)
      HFG=HFGP
      D1=DEL*A8*(DEL2*.1+DEL*RB*.5+RB*RB)
      D2=-(1.-TW)*(DEL2*A7+2.*DEL*RB*A8+RB*RB)
      D3=RB*RB*(1.-TW)
      D4=-(1.-TW)*(DEL2*.1+DEL*RB*A8+RB*RB*A8)
      D5=A9
      FO=PINF*DTDP/TINF
      F1=HFG*RHOW*CO*RC*DEL*A5
      F2=HFG*RHOW*CO*RC*XMC*A5
      F3=RHOW*CO*RO*DEL*XMC*DHFGDP*PINF*A5
      IF(X.GE.PAR1)D5=-A9*A7*(1.-TW)*RB*RB/DEL
```

```
      DTB1=A3*(XK*TINO-TB)*BOHR*BR*BR*BR-XMC*PB*A4*BOHR*BOHR*BR
      DTB3=-A4*PB*BOHR*BR*DRB
      DTB=DTB1+DTB3
      DRHOB=-3.*RH(B*DRB*BR+A6*BR*BR*BR-3.*XMC*BR
      DPB=PB*(DTB/TB+DRHOB*BOHR)
      DTW=FO*DPE
      IF(X.LT.PAR1)GO TO 1
      DDEL1=1./D4
      DDEL2=D5-D3*UB
      DDEL3=-D1*DTB-D2*DRB
      DDEL=DDEL1*(DDEL2+DDEL3)
      GO TO 2
    1 CONTINUE
      DELOLD=DEL
      DELNEW=DSQRT(D5*(X-X0)+DELOLD*DELOLD)
      IF(X.EQ.0.)GO TO 3
      DDEL=(DELNEW-DELOLD)/(X-X0)
      GO TO 4
    3 DDEL=0.
    4 CONTINUE
    2 CONTINUE
      IF(DEL.EQ.0.)DXMC=0.
      IF(DEL.EQ.0.)GO TO 5
      DXMC=(DTW-F2*DDEL-F3*DPB)/F1
    5 CONTINUE
      D2RB1=-DXMC-2.*UB*DRB*BR+.5*UB*BR*UB
      D2RB2=A1*(PB-PAR2)*BR-A2*BR*BR
      D2RB=D2RB1+D2RB2
C-----------INSERT DERIVATIVES
      DERY(1)=DTB
      DERY(2)=DRHOB
      DERY(3)=DPB
      DERY(4)=DDEL
      DERY(5)=DXMC
      DERY(6)=D2RB
      DERY(7)=DRB
      DERY(8)=DTW
      RETURN
      END
```

```
      SUBROUTINE STEAM(P,T,HLV,CP,DX,NN)
      IMPLICIT REAL*8(A-H,O-Z)
      COMMON/TABLE/PP(120),TT(120),HFG(120),VFG(120)
      DIMENSION F(120),G(120),X(120),V(120)
C------NN=2 GIVEN T GET PSAT
C----------NN=1 GIVEN P GET TSAT
C----------PP   TT   IN ASCENDING ARDERS
      IF(NN.GT.1)GO TO 200
      XX=P
      DO 1 I=1,120
      X(I)=PP(I)
      F(I)=TT(I)
      G(I)=HFG(I)
      V(I)=VFG(I)
    1 CONTINUE
      GO TO 500
  200 CONTINUE
      XX=T
      DO 2 I=1,120
      X(I)=TT(I)
      F(I)=PP(I)
      G(I)=HFG(I)
      V(I)=VFG(I)
    2 CONTINUE
  500 CONTINUE
      DO 10 I=1,120
      D=XX-X(I)
      IF(D.LT.0.)GO TO 20
   10 CONTINUE
      WRITE(6,900)NN
  900 FORMAT(/,45X,21HFAIL IN INTERPOLATION,I5,/)
      STOP
   20 CONTINUE
      IP1=I
      I=I-1
      IM1=I-1
      C=(X(I)-X(IM1))*(F(I)-F(IP1))-(X(I)-X(IP1))*(F(I)-F(IM1))
      DENOM=(X(I)-X(IM1))*(X(I)**2-X(IP1)**2)-
     1      (X(I)-X(IP1))*(X(I)**2-X(IM1)**2)
      C=C/DENOM
      B=(F(I)-F(IP1))/(X(I)-X(IP1))-C*(X(I)+X(IP1))
      A=F(I)-B*X(I)-C*X(I)*X(I)
      FF=A+B*XX+C*XX*XX
      C=(X(I)-X(IM1))*(G(I)-G(IP1))-(X(I)-X(IP1))*(G(I)-G(IM1))
      C=C/DENOM
      B=(G(I)-G(IP1))/(X(I)-X(IP1))-C*(X(I)+X(IP1))
      A=G(I)-B*X(I)-C*X(I)*X(I)
      GG=A+B*XX+C*XX*XX
      C=(X(I)-X(IM1))*(V(I)-V(IP1))-(X(I)-X(IP1))*(V(I)-V(IM1))
```

```
      C=C/DENCM
      B=(V(I)-V(IP1))/(X(I)-X(IP1))-C*(X(I)+X(IP1))
      A=V(I)-B*X(I)-C*X(I)*X(I)
      VV=A+B*XX+C*XX*XX
      X1=XX
      X2=X(IP1)
      X3=X(I+2)
      X4=X(I+3)
      G1=GG
      G2=G(IP1)
      G3=G(I+2)
      G4=G(I+3)
      CALL  DERI(X1,X2,X3,X4,G1,G2,G3,G4,DGDX)
      IF(NN.GT.1)GO TO 201
      T=FF
      HLV=GG
      DH=DGDX
      DXDF=GG/VV/(FF+460.)/144.*778.
      DX=1./DXDF
      RETURN
  201 CONTINUE
      P=FF
      HLV=GG
      DH=DGDX
      DFDX=GG/VV/(XX+460.)/144.*778.
      RETURN
      END
```

RC FORM 335 (7-77) U.S. NUCLEAR REGULATORY COMMISSION

**BIBLIOGRAPHIC DATA SHEET**

1. REPORT NUMBER (Assigned by DDC): NUREG/CR-1562

2. (Leave blank)

3. RECIPIENT'S ACCESSION NO.

TITLE AND SUBTITLE (Add Volume No., if appropriate)

Steam Chugging in Pressure Suppression Containment

5. DATE REPORT COMPLETED: MONTH August YEAR 1979


AUTHOR(S)

J.K.B. Lee and C. K. Chan

PERFORMING ORGANIZATION NAME AND MAILING ADDRESS (Include Zip Code)

Chemical, Nuclear and Thermal Engineering Dept.
University of California, Los Angeles
Los Angeles, California 90024


DATE REPORT ISSUED: MONTH September YEAR 1979

6. (Leave blank)

8. (Leave blank)


SPONSORING ORGANIZATION NAME AND MAILING ADDRESS (Include Zip Code)

Analysis Development Branch
Division of Reactor Safety Research
Nuclear Regulatory Commission
Washington, D. C. 20555


10. PROJECT/TASK/WORK UNIT NO.

11. CONTRACT NO.: AT (48-24)-0342

TYPE OF REPORT: Topical

PERIOD COVERED (Inclusive dates): July 1, 1976-July 31, 1979

13. SUPPLEMENTARY NOTES

14. (Leave blank)


ABSTRACT (200 words or less)

The condensation-induced hydrodynamic loads during low flow vapor injection (steam chugging) is studied. Qualitative visual experiments in a small scale single vent system indicate that the interfacial motion admits certain characteristic patterns in various ranges of pool temperatures and steam mass fluxes. Systematic classification of these characteristic patterns based on these two parameters resulted in a condensation regime map.

Steam chugging occurs at the low mass flux (below 75 $Kg/m^2$-sec) and low pool temperature (below 80°C) region of the map. Three different modes of chugging are identified: the internal chug where all condensation takes place in the vent; the detached bubble chug where the bubble is detached from the vent during formation; and the encapsulating bubble chug where the bubble grows to encapsulate the vent exit following formation. The hydrodynamic loads measured at the pool bottom show mild oscillations (~0.1 atm.) for internal chugs; moderate oscillations (~.3 atm) for detached bubble chugs; and large spiky oscillations (~0.5 atm.) for encapsulating bubble chugs.

A theoretical model is proposed as a first step in the analytical approach to this complicated phenomenon. Comparison with the experimental results, however, indicates that further improvement in the theoretical model is needed.


17. KEY WORDS AND DOCUMENT ANALYSIS

17a. DESCRIPTORS

17b. IDENTIFIERS/OPEN-ENDED TERMS

18. AVAILABILITY STATEMENT

19. SECURITY CLASS (This report)

21. NO. OF PAGES

20. SECURITY CLASS (This page)

22. PRICE $